

Modeling Gas Burner Fires in Ranch and Colonial Style Structures

Mark McKinnon
Craig Weinschenk
Daniel Madrzykowski

UL Firefighter Safety Research Institute
Columbia, MD 21045

This publication is available free of charge from:
<https://dx.doi.org/10.54206/102376/MWJE4818>

UNDERWRITERS
LABORATORIES™



Modeling Gas Burner Fires in Ranch and Colonial Style Structures

Mark McKinnon
Craig Weinschenk
Daniel Madrzykowski

UL Firefighter Safety Research Institute
Columbia, MD 21045

June 25, 2020

This publication is available free of charge from:
<https://dx.doi.org/10.54206/102376/MWJE4818>

UNDERWRITERS
LABORATORIES™



Underwriters Laboratories Inc.
Terrence Brady, President

UL Firefighter Safety Research Institute
Steve Kerber, Director

In no event shall UL be responsible to anyone for whatever use or non-use is made of the information contained in this Report, and in no event shall UL, its employees, or its agents incur any obligation or liability for damages including, but not limited to, consequential damage arising out of or in connection with the use or inability to use the information contained in this Report. Information conveyed by this Report applies only to the specimens actually involved in these experiments. UL has not established a factory Follow-Up Service Program to determine the conformance of subsequently produced material, nor has any provision been made to apply any registered mark of UL to such material. The issuance of this Report in no way implies Listing, Classification or Recognition by UL, and does not authorize the use of UL Listing, Classification or Recognition Marks or other reference to UL on or in connection with the product or system.

Contents

List of Figures	iii
List of Tables	vii
List of Abbreviations	viii
1 Background	1
1.1 The Use of Fire Models in Fire Investigation	1
1.2 Fire Dynamics Simulator	2
1.2.1 Previous Validation Exercises	3
2 Objectives	5
3 Experimental Configuration	6
3.1 Single-Story Structure	6
3.2 Two-Story Structure	8
3.3 Instrumentation	12
3.3.1 Measurement Uncertainty	13
3.4 Single-Story Structure	14
3.5 Two-Story Structure	15
3.6 Fire Source	17
4 Modeling	18
4.1 Materials	18
4.2 Model Parameters	18
4.2.1 Simulation Mode	19
4.2.2 Spatial Resolution	22
4.2.3 Pressure Zones	24
4.2.4 Definition of Leaks	26
4.3 Device Parameter Uncertainty	28
5 Single-Story Results	30
5.1 Single-Story: Experiment 1	30
5.1.1 Experiment 1: Temperature	30
5.1.2 Experiment 1: Pressure	35
5.1.3 Experiment 1: Velocity	39
5.2 Single-Story: Experiment 2	41

5.2.1	Experiment 2: Temperature	41
5.2.2	Experiment 2: Pressure	46
5.2.3	Experiment 2: Velocity	50
5.3	Single-Story: Experiment 3	53
5.3.1	Experiment 3: Temperature	53
5.3.2	Experiment 3: Pressure	58
5.3.3	Experiment 3: Velocity	62
6	Two-Story Results	65
6.1	Two-Story: Experiment 4	65
6.1.1	Experiment 4: Temperature	65
6.1.2	Experiment 4: Pressure	73
6.1.3	Experiment 4: Velocity	79
6.2	Two-Story: Experiment 5	82
6.2.1	Experiment 5: Temperature	82
6.2.2	Experiment 5: Pressure	89
6.2.3	Experiment 5: Velocity	95
6.3	Two-Story: Experiment 6	96
6.3.1	Experiment 6: Temperature	96
6.3.2	Experiment 6: Pressure	103
6.3.3	Experiment 6: Velocity	108
7	Discussion	111
7.1	Experimental Uncertainty	111
7.2	Accuracy of Predictions	112
8	Conclusions	120
9	Summary	122
	References	123
	Appendix A Metrics to Assess Agreement Between Measured Data and Predictions	127
	Appendix B FDS Input Files	136

List of Figures

3.1	Single-Story Structure Dimensioned Floorplan	7
3.2	Dimensioned Layout of the First Story of the two-story structure	9
3.3	Dimensioned Layout of the Second Story of the two-story structure	10
3.4	Single-Story Structure Dimensioned Instrument Plan	14
3.5	Two-Story Structure Dimensioned Instrument Plan of First Story	16
3.6	Two-Story Structure Dimensioned Instrument Plan of Second Story	17
4.1	Comparison of Typical Temperature Predictions from Each Simulation Mode . . .	20
4.2	Comparison of Typical Pressure Predictions from Each Simulation Mode	21
4.3	Comparison of Typical Velocity Predictions form Each Simulation Mode	21
4.4	Comparison of Typical Temperature Predictions from Coarse and Moderate Res- olution Simulations	23
4.5	Comparison of Typical Pressure Predictions from Coarse and Moderate Resolu- tion Simulations	23
4.6	Comparison of Typical Velocity Predictions from Coarse and Moderate Resolu- tion Simulations	24
4.7	Comparison of Model Pressure Predictions with Three Different Zones Definitions	26
4.8	Comparison of Model Pressure Predictions with Different Definitions of Zones . .	28
5.1	Temperatures in the living room of the single-story structure during Experiment 1	31
5.2	Temperatures in the hallway of the single-story structure during Experiment 1 . .	31
5.3	Temperatures in bedroom 1 of the single-story structure during Experiment 1 . . .	32
5.4	Temperatures in bedroom 2 of the single-story structure during Experiment 1 . . .	32
5.5	Temperatures in bedroom 3 of the single-story structure during Experiment 1 . . .	33
5.6	Temperatures in the kitchen of the single-story structure during Experiment 1 . . .	33
5.7	Temperatures in the breakfast area of the single-story structure during Experiment 1	34
5.8	Temperatures in the dining room of the single-story structure during Experiment 1	34
5.9	Pressures in the living room of the single-story structure during Experiment 1 . . .	36
5.10	Pressures in bedroom 1 of the single-story structure during Experiment 1	36
5.11	Pressures in bedroom 2 of the single-story structure during Experiment 1	37
5.12	Pressures in bedroom 3 of the single-story structure during Experiment 1	37
5.13	Pressures in the kitchen of the single-story structure during Experiment 1	38
5.14	Pressures in the dining room of the single-story structure during Experiment 1 . .	38
5.15	Velocities measured in the hallway of the single-story structure during Experiment 1	39
5.16	Velocities measured in the front door of the single-story structure during Experi- ment 1	40
5.17	Velocities measured in window E of the single-story structure during Experiment 1	41

5.18	Temperatures in the living room of the single-story structure during Experiment 2	42
5.19	Temperatures in the hallway of the single-story structure during Experiment 2 . . .	42
5.20	Temperatures in bedroom 1 of the single-story structure during Experiment 2 . . .	43
5.21	Temperatures in bedroom 2 of the single-story structure during Experiment 2 . . .	43
5.22	Temperatures in bedroom 3 of the single-story structure during Experiment 2 . . .	44
5.23	Temperatures in the kitchen of the single-story structure during Experiment 2 . . .	44
5.24	Temperatures in the breakfast area of the single-story structure during Experiment 2	45
5.25	Temperatures in the dining room of the single-story structure during Experiment 2	45
5.26	Pressures in the living room of the single-story structure during Experiment 2 . . .	47
5.27	Pressures in bedroom 1 of the single-story structure during Experiment 2	47
5.28	Pressures in bedroom 2 of the single-story structure during Experiment 2	48
5.29	Pressures in bedroom 3 of the single-story structure during Experiment 2	48
5.30	Pressures in the kitchen of the single-story structure during Experiment 2	49
5.31	Pressures in the dining room of the single-story structure during Experiment 2 . . .	49
5.32	Velocities measured in the hallway of the single-story structure during Experiment 2	50
5.33	Velocities measured in window E of the single-story structure during Experiment 2	51
5.34	Velocities measured in the front door of the single-story structure during Experiment 2	52
5.35	Temperatures in the living room of the single-story structure during Experiment 3	53
5.36	Temperatures in the living room of the single-story structure during Experiment 3	54
5.37	Temperatures in bedroom 1 of the single-story structure during Experiment 3 . . .	54
5.38	Temperatures in bedroom 2 of the single-story structure during Experiment 3 . . .	55
5.39	Temperatures in bedroom 3 of the single-story structure during Experiment 3 . . .	55
5.40	Temperatures in the kitchen of the single-story structure during Experiment 3 . . .	56
5.41	Temperatures in the breakfast area of the single-story structure during Experiment 3	56
5.42	Temperatures in the dining room of the single-story structure during Experiment 3	57
5.43	Pressures in the living room of the single-story structure during Experiment 3 . . .	59
5.44	Pressures in bedroom 1 of the single-story structure during Experiment 3	59
5.45	Pressures in bedroom 2 of the single-story structure during Experiment 3	60
5.46	Pressures in bedroom 3 of the single-story structure during Experiment 3	60
5.47	Pressures in the kitchen of the single-story structure during Experiment 3	61
5.48	Pressures in the dining room of the single-story structure during Experiment 3 . . .	61
5.49	Velocities measured in the hallway of the single-story structure during Experiment 3	63
5.50	Velocities measured in window E of the single-story structure during Experiment 3	63
6.1	Temperatures in the center of the family room of the two-story structure during Experiment 4	66
6.2	Temperatures in the foyer of the two-story structure during Experiment 4	66
6.3	Temperatures under the hallway of the two-story structure during Experiment 4 . . .	67
6.4	Temperatures in the kitchen of the two-story structure during Experiment 4	67
6.5	Temperatures in the middle of the second story hallway in the two-story structure during Experiment 4	68
6.6	Temperatures in the master bedroom of the two-story structure during Experiment 4	68
6.7	Temperatures in bedroom 2 of the two-story structure during Experiment 4	69
6.8	Temperatures in bedroom 3 of the two-story structure during Experiment 4	69

6.9	Temperatures in bedroom 4 of the two-story structure during Experiment 4	70
6.10	Pressures in the family room of the two-story structure during Experiment 4	73
6.11	Pressures next to the front door of the two-story structure during Experiment 4	74
6.12	Pressures in the living room of the two-story structure during Experiment 4	74
6.13	Pressures in the den of the two-story structure during Experiment 4	75
6.14	Pressures in the master bedroom of the two-story structure during Experiment 4	75
6.15	Pressures in bedroom 2 of the two-story structure during Experiment 4	76
6.16	Pressures in bedroom 3 of the two-story structure during Experiment 4	76
6.17	Pressures in bedroom 4 of the two-story structure during Experiment 4	77
6.18	Velocities in the front door of the two-story structure during Experiment 4	79
6.19	Velocities in window K of the two-story structure during Experiment 4	80
6.20	Velocities in window L of the two-story structure during Experiment 4	80
6.21	Temperatures in the center of the family room of the two-story structure during Experiment 5	82
6.22	Temperatures in the foyer of the two-story structure during Experiment 5	83
6.23	Temperatures under hallway of the two-story structure during Experiment 5	83
6.24	Temperatures in kitchen of the two-story structure during Experiment 5	84
6.25	Temperatures in middle of second story hallway in the two-story structure during Experiment 5	84
6.26	Temperatures in the master bedroom of the two-story structure during Experiment 5	85
6.27	Temperatures in the bedroom 2 of the two-story structure during Experiment 5	85
6.28	Temperatures in the bedroom 3 of the two-story structure during Experiment 5	86
6.29	Temperatures in the bedroom 4 of the two-story structure during Experiment 5	86
6.30	Pressures in the family room of the two-story structure during Experiment 5	89
6.31	Pressures next to the front door of the two-story structure during Experiment 5	90
6.32	Pressures in the living room of the two-story structure during Experiment 5	90
6.33	Pressures in den of the two-story structure during Experiment 5	91
6.34	Pressures in the master bedroom of the two-story structure during Experiment 5	91
6.35	Pressures in bedroom 2 of the two-story structure during Experiment 5	92
6.36	Pressures in bedroom 3 of the two-story structure during Experiment 5	92
6.37	Pressures in bedroom 4 of the two-story structure during Experiment 5	93
6.38	Velocities in the front door of the two-story structure during Experiment 5	95
6.39	Temperatures in the center of the family room of the two-story structure during Experiment 6	96
6.40	Temperatures in the foyer of the two-story structure during Experiment 6	97
6.41	Temperatures under hallway of the two-story structure during Experiment 6	97
6.42	Temperatures in the kitchen of the two-story structure during Experiment 6	98
6.43	Temperatures in the middle of the second story hallway in the two-story structure during Experiment 6	98
6.44	Temperatures in the master bedroom of the two-story structure during Experiment 6	99
6.45	Temperatures in bedroom 2 of the two-story structure during Experiment 6	99
6.46	Temperatures in bedroom 3 of the two-story structure during Experiment 6	100
6.47	Temperatures in bedroom 4 of the two-story structure during Experiment 6	100
6.48	Pressures in the family room of the two-story structure during Experiment 6	103
6.49	Pressures next to the front door of the two-story structure during Experiment 6	104

6.50	Pressures in the living room of the two-story structure during Experiment 6	104
6.51	Pressures in the master bedroom of the two-story structure during Experiment 6 .	105
6.52	Pressures in bedroom 2 of the two-story structure during Experiment 6	105
6.53	Pressures in bedroom 3 of the two-story structure during Experiment 6	106
6.54	Pressures in bedroom 4 of the two-story structure during Experiment 6	106
6.55	Velocities in window K of the two-story structure during Experiment 6	108
6.56	Velocities in window A of the two-story structure during Experiment 6	109
6.57	Velocities in the front door of the two-story structure during Experiment 6	109
7.1	Comparison between Temperature Measurements and Predictions	113
7.2	Comparison between Pressure Measurements and Predictions	115
7.3	Comparison between Velocity Measurements and Predictions	116

List of Tables

3.1	Single-Story Structure Window Sizes	8
3.2	Two-Story Structure, First Story Window Sizes	11
3.3	Two-Story Structure, Second Story Window Sizes	11
3.4	Sequence of Events for Single-Story Structure Experiments	12
3.5	Sequence of Events for Two-Story Structure Experiments	12
4.1	Gypsum Board Material Properties Defined in FDS Models	18
A.1	Model Agreement Metrics for Single-Story Experiment 1 Temperatures	129
A.2	Model Agreement Metrics for Single-Story Experiment 1 Pressures	129
A.3	Model Agreement Metrics for Single-Story Experiment 1 Velocities	129
A.4	Model Agreement Metrics for Single-Story Experiment 2 Temperatures	130
A.5	Model Agreement Metrics for Single-Story Experiment 2 Pressures	130
A.6	Model Agreement Metrics for Single-Story Experiment 2 Velocities	130
A.7	Model Agreement Metrics for Single-Story Experiment 3 Temperatures	131
A.8	Model Agreement Metrics for Single-Story Experiment 3 Pressures	131
A.9	Model Agreement Metrics for Single-Story Experiment 3 Velocities	131
A.10	Model Agreement Metrics for Two-Story Experiment 4 Temperatures	132
A.11	Model Agreement Metrics for Two-Story Experiment 4 Temperatures	132
A.12	Model Agreement Metrics for Two-Story Experiment 4 Pressures	132
A.13	Model Agreement Metrics for Two-Story Experiment 4 Pressures	132
A.14	Model Agreement Metrics for Two-Story Experiment 4 Velocities	133
A.15	Model Agreement Metrics for Two-Story Experiment 5 Temperatures	133
A.16	Model Agreement Metrics for Two-Story Experiment 5 Temperatures	133
A.17	Model Agreement Metrics for Two-Story Experiment 5 Pressures	133
A.18	Model Agreement Metrics for Two-Story Experiment 5 Pressures	134
A.19	Model Agreement Metrics for Two-Story Experiment 5 Velocities	134
A.20	Model Agreement Metrics for Two-Story Experiment 6 Temperatures	134
A.21	Model Agreement Metrics for Two-Story Experiment 6 Temperatures	134
A.22	Model Agreement Metrics for Two-Story Experiment 6 Pressures	134
A.23	Model Agreement Metrics for Two-Story Experiment 6 Pressures	135
A.24	Model Agreement Metrics for Two-Story Experiment 6 Velocities	135

List of Abbreviations

AF	Above floor
ATF	Bureau of Alcohol, Tobacco and Firearms
BC	Below ceiling
BDP	Bi-directional probe
CFI	Certified Fire Investigator
HVAC	Heating, Ventilation, and Air Conditioning
IAAI	International Association of Arson Investigators
NASFM	National Association of State Fire Marshals
NFPA	National Fire Protection Association
NIJ	National Institute of Justice
NIST	National Institute of Standards and Technology
OSAC	Overseas Security Advisory Council
PUF	Polyurethane Foam
TC	Thermocouple
UL FSRI	UL Firefighter Safety Research Institute
VTT	Technical Research Centre of Finland

Acknowledgments

This project was supported by Award No. 2015-DN-BX-K052, awarded by the National Institute of Justice, Office of Justice Programs, U.S. Department of Justice. The opinions, findings, and conclusions or recommendations expressed in this publication/program/exhibition are those of the author(s) and do not necessarily reflect those of the Department of Justice.

To ensure the research results are of use to the fire investigation community, UL FSRI assembled a technical panel of national fire investigation experts that represent a range of forensic specialties in both the public, private, academic, and research sectors. The individuals below provided direction for the project by assisting in planning the experiments, witnessing the testing, and reviewing the results.

Fire Service Technical Panel

Name	Affiliation
Robert Byrnes	Fire Department City of New York (ret.)
Steve Carman	Carman & Associates Fire Investigation, Inc
Paul Claffin	Bureau of ATF, Fire Investigation & Arson Enforcement Division
Chris Connealy	Texas State Fire Marshal, TDI Deputy Insurance Commissioner
Richard Dyer	Dyer Fire Consulting
John Golder	Forensic Investigation and Consultation, LLC
Mark Goodson	Goodson Engineering
David Icove	University of Tennessee, Knoxville
Thomas Kane	Fire Department City of New York
John Lentini	Scientific Fire Analysis, LLC
Thomas Lichtenstein	UL LLC
Jeffrey Lyle	Chicago Fire Department
Kevin McGrattan	National Institute of Standards and Technology
Robert Pyzyna	Northbrook Fire Department

The authors acknowledge Kelly Opert and the technical staff of the UL Large Fire Lab for their assistance in preparing, documenting, and conducting the full-scale experiments, especially Paul Courtney, Andres Sarmineto, Rommel Royster, Jeff Mlyniec, Colin Grimon, Eric Anderson, Derek Dziekonski, Kyle Hunter, Cordelro Black, and Mauricio Cigarroa. These experiments would not have been possible without support of the UL FSRI team. The UL FSRI team instrumented, conducted, and collected data from these experiments. The authors thank Robin Zevotek, Keith Stakes, Jack Regan, Joshua Crandall, Steve Kerber, Sarah Huffman, Sean DeCrane, Robert James, and especially Roy McLane of Thermal Fabrications, Cathy Madrzykowski of Rendered Useful Studio, and Andrea Chen of the codex club.

In remembrance of Michael Murphy, Chicago Fire Department and Jaime Novak, St. Paul Fire Department.

1 Background

Structure fires accounted for approximately 38% of the 1.32 million fires reported in the U.S. in 2017 [1]. A similar percentage (37.3%) was reported as the mean ratio of structure fires to total fires for 22 countries mostly from Europe and Asia [2]. According to the United States Fire Administration (USFA), of the approximately 500,000 structure fires, there were an estimated 371,500 residential fires resulting in 2,695 civilian deaths and 10,825 civilian injuries in the U.S. in 2017 [3]. In addition to the high cost of life from residential fires, it was also estimated that total property loss in the U.S. due to these fires amounted to \$7.8 billion in 2017. The majority of these losses were attributed to single- and two-family residential structure fires.

Fire investigations are an integral part of a holistic fire protection strategy that has been developed with the goal of improving the safety of the built environment. Investigations provide a means to identify the cause of a fire as well as collect a set of data that can provide insight about the development and spread of the fire. By determining the cause of a fire and identifying consumer products, materials, and phenomena that contributed to fire growth, valuable insight is gained that may inform the fire protection and safety community in future designs, effectively reducing the losses from fires. Data such as the room of fire origin, the influence of ventilation, the possibility of changing flow paths on the developing fire-induced flow dynamics, and the ultimate cause of the fire are critical to understanding and reducing the number and severity of fires.

Fire models are increasingly relied upon in fire investigations as well as scientific studies to test hypotheses and improve scientists', engineers', and investigators' understanding of fire dynamics. The most detailed fire models that are currently available are in a class called field models, and also commonly referred to as computational fluid dynamics (CFD) models. NFPA 921 *Guide for Fire and Explosion Investigations* states that fire dynamic analyses conducted with field models may be used to predict gas temperatures, gas and smoke concentrations, flow rates of gases and unburned fuel, temperatures of the walls and ceilings, and the effects of opening or closing doors and windows, among other important fire phenomena [4]. NFPA 921 emphasizes the importance of rigorous verification and validation (V&V) of fire models to ensure physical phenomena are accurately represented and suggests that the entire body of V&V work that has been compiled for a given model be evaluated for suitability prior to utilizing the model in an investigation.

1.1 The Use of Fire Models in Fire Investigation

This study was conducted to support rigorous validation of computational fire models, specifically regarding the prediction of fire-induced flow dynamics within a residential structure using a field model. Further, several of the fire and arson investigation research issues identified by the NIJ-supported Fire and Arson Investigation Technology Working Group Operational Requirements (December 2016) were incorporated into this project to some extent. Specifically identified needs

include: 1) understanding of the effects of ventilation on fire damage and patterns; 2) repeatability and reproducibility of test measurements of large-scale structure fires; and 3) development of materials property data for accurate computer model inputs [5].

Fires involve a complex combination of physical phenomena that are represented by governing equations in CFD models. Verification conducted on a set of equations that define a model ensures the equations yield the expected numerical values while validation ensures that the equations adequately represent the physics of a scenario. The standard process for conducting V&V on a fire model is described in ASTM E 1355 *Standard Guide for Evaluating the Predictive Capability of Deterministic Fire Models* [6]. Verification generally requires analytical solutions to equations that describe fundamental physics experiments. Validation of a CFD fire model generally consists of comparing model predictions to experimental data to ensure the necessary physics are properly represented. Validation of fire models using full-scale fire test data is rare due to the safety concerns, logistical limitations, and the high cost of full-scale fire experiments. This relative scarcity of full-scale fire data has created a gap in the V&V suite which has resulted in uncertainty about the use of fire models for specific applications, particularly in fire investigations.

1.2 Fire Dynamics Simulator

The Fire Dynamics Simulator (FDS) is a CFD model used to simulate fire-driven fluid flow that has been developed by a multi-national team led by the National Institute of Standards and Technology (NIST) and the Technical Research Centre of Finland (VTT) [7, 8]. The model numerically solves a form of the Navier-Stokes equations appropriate for low-speed, thermally-driven flow. The partial derivatives of the conservation equations of mass, momentum, and energy are approximated as finite differences, and the solution is updated in time on a three-dimensional, rectilinear grid. FDS typically uses the Large Eddy Simulation (LES) approach, which presumes that the grid resolution is sufficient to resolve the dominant eddy structures and the Deardorff submodel is used for unresolved turbulence.

FDS applies a lumped species approach to model combustion where three lumped species which represent fuel, air, and combustion products are tracked. Reaction rates are mixing-controlled [9] with a simple extinction model based on a critical flame temperature [10] by default. Thermal radiation is computed through solution of the radiation transport equation for a gray gas using the Finite Volume Method on the same grid as the flow solver. A companion program, Smokeview [11, 12], is used for visualizing the results of the FDS computations. FDS has undergone extensive V&V [13–15], and the experiments and simulations described here are intended to provide further validation to the model.

1.2.1 Previous Validation Exercises

FDS has undergone extensive verification and validation and the results of many of the validation studies have been published by NIST [14], including several multi-compartment experiments. A set of experiments conducted by the Bureau of Alcohol, Tobacco, Firearms, and Explosives (ATF), known as the ATF Corridors series, featured a two-story structure with long hallways and a single stairwell with a natural gas fire source supplying well-defined heat release rates ranging from 50 kW to 500 kW [15]. Simulations were compared to experimental data to validate gas temperature and velocity predictions from FDS. Hadjisophocleous and Wang simulated smoke movement and predicted gas temperatures in a simple ten-story facility designed to simulate the central core of a high rise building with fire sources that included a propane gas burner [16,17] and combustible product fuel packages [17].

The PRISME Door series involved a hydrocarbon pool fire in a compartment in which the smoke propagation from the fire to adjacent compartments through an open doorway was characterized [18]. The PRISME Door experiments were modeled to validate hot gas layer thicknesses, ceiling jet temperature, gas velocity, and pressure predictions in multi-compartment configurations [19]. Each of the aforementioned experimental series were ideal for fire model validation because the geometry was easily represented in rectilinear coordinates and all fire sources and boundary conditions were well-characterized. These multi-compartment experimental series have contributed to validation and widespread acceptance of FDS as a tool available to the fire protection community, but each study focused specifically on simple industrial-style occupancies and, beyond stairs and doorways, did not incorporate any features that are found in modern residential occupancies that may complicate the dynamics of fire-induced flow.

The Dalmarnock fire experiments were conducted in a typical high-rise apartment and the data collected were used to evaluate FDS fire modeling techniques in an international round-robin format. Gas temperature, smoke obscuration, gas velocity, and heat flux to the walls were measured in two experiments that were conducted in fully-furnished apartments in a high-rise building while ventilation conditions were modified during in a well-defined manner [20]. The fire source and fuel packages in the experiments were typical furniture items, most of which had not been independently characterized to determine the contribution to fire development. As a result of this complication, a comparison of a priori modeling results from the round-robin provided an important commentary on the disparity of modeling methodologies among practitioners rather than a true fire model validation exercise.

An experimental series conducted at NIST that involved the evaluation of smoke alarm response in a single-story manufactured home has been used to validate FDS [21]. Experiments that involved either an upholstered chair or a mattress as a flaming ignition source were modeled to validate ceiling jet temperature as well as fire and smoke detection device activation predictions in FDS. These experiments involved well-characterized fuel sources, but these fuels were necessarily highly sooting for the purpose of studying smoke alarm activation, which may complicate fire modeling and make the cases less desirable for model validation.

Recently, a set of experiments conducted in a three-story 1970s-era apartment building allowed

researchers to study the effect of fire on pressures measured in the apartment and ventilation system [22]. Vents in the apartment were alternated between open and closed while the fan for the exhaust system was alternated between on and off. Pressure, temperature, gas concentrations, and velocity were measured in the exhaust ducts and the pressure between the apartment and the surrounding atmosphere was also measured. FDS simulations of these experiments were intended to validate the pressure and velocity predictions made using the Heating, Ventilation, and Air Conditioning (HVAC) submodel. Although these experiments were conducted in a typical residential occupancy, the apartment did not feature a modern design or modern construction techniques and the investigation was focused specifically on the HVAC submodel within FDS.

A review of the available literature and validation repositories indicates a lack of experiments conducted in modern residential structures. This lack of available data has created a need to validate fire model predictions of fluid flow through the complicated geometries typical of modern open-concept residential designs. An additional goal of this work was to provide several data sets from full-scale experiments with well-defined ventilation scenarios to provide unique validation cases for the fire modeling community.

2 Objectives

The primary objectives of this series of experiments include:

1. To measure the environment within the structures that result from a well-defined, stationary fire source.
2. To provide a discussion of basic buoyancy-driven fluid dynamics in structures, specifically with regard to the impact of ventilation on the resulting fluid dynamics.
3. To provide several unique validation cases for the Fire Dynamics Simulator (FDS) and the fire modeling community at large.
4. To provide a baseline for comparisons of FDS simulations with data collected in furniture-fueled experiments conducted in the same structures.

FDS is perpetually under development with the source code constantly changing as technology improves, new features are proposed, and additional validation data are made available. Currently, the sixth major release of FDS is available and publication of the seventh major release is imminent. Additional objectives of this report were to provide a discussion about the process of conducting a validation study for FDS as well as to provide a benchmark for the model agreement with these experimental data against which predictions made with future releases of FDS may be compared.

3 Experimental Configuration

All experiments described in this report were conducted at full scale in purpose-built residential-style structures with variable ventilation configurations. The design of the structures, fuel loads, and types of experiments were planned during a workshop with the technical panel assembled for this study. The structures included an approximately 111 m² single-story ranch structure and a 297 m² two-story colonial structure. The colonial structure had a two-story family room and open foyer. The structures were designed by a residential architectural company to represent a popular legacy design and a popular modern design. These designs have been used in several previous UL FSRI firefighting ventilation research studies [23, 24].

The single-story, traditional ranch-style structure was designed to represent a home constructed in the mid-twentieth century with walls and doorways separating all of the rooms and 2.44 m ceilings. Ranch-style homes were first built in the 1920s, and by the 1950s comprised nine out of ten houses built in U.S.. Ranch homes are still the most popular style of home in 34 states across the United States. [25]. The two-story, contemporary colonial-style structure was designed to represent a more modern design that incorporated an open plan arrangement, a two-story foyer, a two-story family room, and four bedrooms. According to the U.S. Census Bureau, 50% of the single family houses built in 2017 were two-story houses, 45% had four bedrooms, and 37% of the two-story houses had an open two-story foyer [26].

All experiments featured a 0.6 m x 0.6 m natural gas burner as the fire source to provide control of the fire and hot gas plume. Each ventilation scenario consisted of opening windows and doors to the homes in a distinct sequence to generate flow paths that connected the fires with remote intake and exhaust vents. In total, three unique experiments were conducted in the single-story structure and three unique experiments were conducted in the two-story structure. Some of the experiments were repeated and the data collected in these replicates has been analyzed to evaluate repeatability of the experiments. All experiments were conducted at UL's Large Fire Laboratory in Northbrook, IL.

3.1 Single-Story Structure

The single-story, ranch-style structure had overall interior dimensions of 13.9 m by 7.7 m. The layout of the structure included three bedrooms, a living room, a dining room, and a kitchen. The space continuous with the kitchen between the kitchen and the dining room was designated as the breakfast area. There were also areas, normally designed as a bathroom and closets, that were walled-off from the rest of the structure to provide protection to the installed instrumentation. Figure 3.1 shows a dimensioned plan view drawing of the ranch structure indicating major dimensions.

The walls were constructed from dimensional lumber, 38 mm by 89 mm (nominally 2 in. by 4 in.).

The studs were lined with two layers of gypsum board. The base layer was 16 mm (5/8 in.) thick regular gypsum wallboard. The top layer was 13 mm (1/2 in.) thick light gypsum wallboard. The ceiling supports were constructed from engineered lumber I-joists and were covered with gypsum wallboard in the same manner as the walls. The floor was constructed from dimensional lumber, 38 mm by 89 mm (nominally 2 in. by 4 in.) and covered with a 18 mm (3/4 in.) thick plywood subfloor. On top of the plywood was 13 mm (1/2 in.) cement board.

The single-story structure had two exterior doors (front and back), three bedroom doors, and a doorway that led to the kitchen. All doors/doorways had a height of approximately 2.0 m. The interior doors were hollow-core wood frame doors. To repeatably control ventilation (i.e., size and timing of opening), the exterior vent enclosures (windows) were purpose-built as side-hinged shutters. Each shutter was wood-framed and finished with a layer of insulation on the inside and a layer of 13 mm (1/2 in.) plywood on the outside. The shutters were affixed to the exterior of the framed window openings. For windows greater than 1.0 m in width, shutters were installed on each side of the opening and met in the middle when closed. One of the two shutters had a lip installed to overlap the gap where the two shutters met. These shutters allowed for the windows to be manipulated open and closed as many times as needed during the experimental series. The ability of the shutter to open fully at a designated time was a particular benefit to this design. This functionality is not possible with a standard glass window insert. Window shutters like this are common in fire service training props. Table 3.1 shows the sizes of the windows.

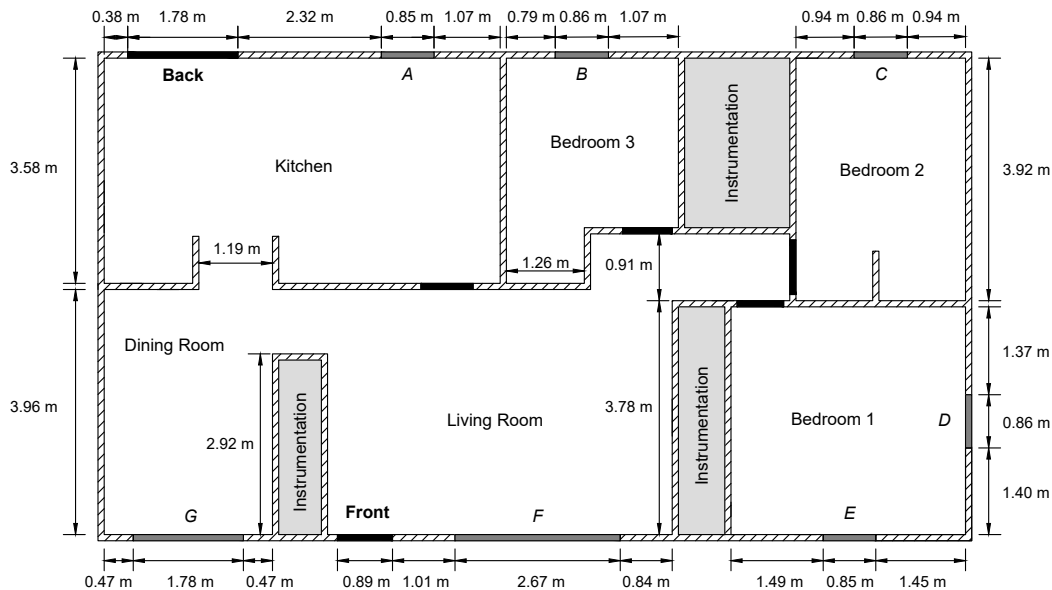


Figure 3.1: Dimensioned plan view drawing of the single-story structure

To characterize ventilation within the single-story structure, a leakage test was conducted with all exterior vents closed. The standard test method described in ASTM E 779 *Standard Test Method for Determining Air Leakage Rate by Fan Pressurization* was followed to determine the air changes per hour and the equivalent leakage area [27]. The leakage in the structure was 4 air changes per hour (ACPH) at 50 Pa with an equivalent leakage area of 0.08 m² at 10 Pa. Equivalent leakage area

Table 3.1: Single-story structure window sizes and sill heights

Window	Size (W x H)	Sill Height
A	0.85 m x 1.02 m	1.07 m
B	0.86 m x 1.46 m	0.61 m
C	0.86 m x 1.46 m	0.61 m
D	0.86 m x 1.46 m	0.61 m
E	0.85 m x 1.46 m	0.61 m
F	2.67 m x 1.46 m	0.61 m
G	1.78 m x 1.46 m	0.61 m

is defined as the area of a sharp-edged hole that would have the same leakage flow rate as the building if both were subjected to a 10 Pa pressure difference. For a single-story residential structure, a tight house would have 3.5 ACPH50, a moderately tight house would have 8.8 ACPH50, a typical house would have 17.5 ACPH50, and a leaky house would have 35 ACPH50 [28]. Considering the uncertainty in typical pressure measurements, the structure fell between a tight and moderately tight structure.

3.2 Two-Story Structure

The two-story, colonial-style structure had overall interior dimensions of 15.05 m by 10.13 m. The layout of the first story included a living room, den, family room, kitchen, laundry room, dining room, closet, and entrance foyer. The first story included two areas that were walled-off from the rest of the structure that provided protection for the installed instrumentation. Figure 3.2 shows a dimensioned plan view drawing of the first story of the two-story structure indicating major dimensions.

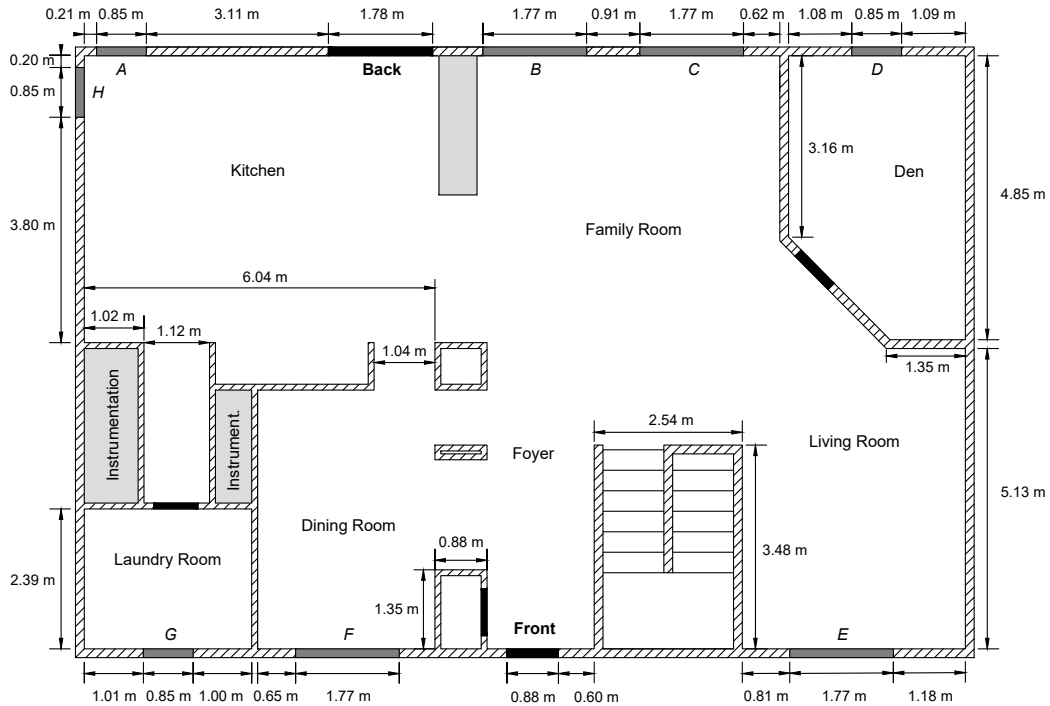


Figure 3.2: Dimensioned plan view drawing of the first story of the two-story structure

The second story had the same interior dimensions as the first story, with four bedrooms and three areas that were walled-off from the structure that provided protection to the installed instrumentation (these instrumentation areas included the hall bath, the bedroom 4 closet, and a combination of the master bath and closet). The areas above the first story family room and above the foyer were open to the second story. Figure 3.3 shows a dimensioned plan view drawing of the second story of the two-story structure indicating major dimensions and the areas open to the story below.

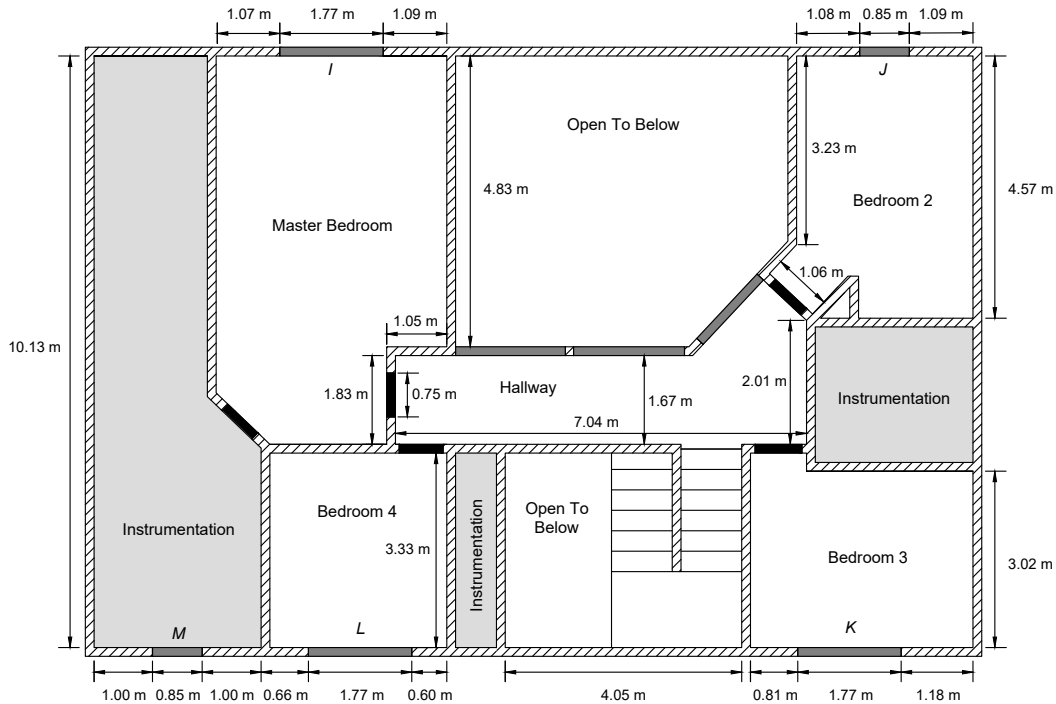


Figure 3.3: Dimensioned plan view drawing of the second story of the two-story structure

Similar to the single-story structure, the walls were constructed from dimensional lumber, 38 mm by 89 mm (nominally 2 in. by 4 in.). The studs were lined with two layers of gypsum board. The base layer was 16 mm (5/8 in.) thick regular gypsum wallboard. The top layer was 13 mm (1/2 in.) thick light gypsum wallboard. The ceiling supports for the upper story were constructed from engineered lumber I-joists and were covered with gypsum wallboard in the same manner as the walls. The floor for the upper story was supported by dimensional joists, 38 mm by 286 mm (nominally 2 in. by 12 in.) and covered with 18 mm (3/4 in.) thick plywood subfloor. The floor of the lower level was constructed from dimension lumber, 38 mm by 89 mm (nominally 2 in. by 4 in.) and covered with 18 mm (3/4 in.) thick plywood sub floor. On top of the plywood was 13 mm (1/2 in.) cement board.

The two-story structure had two exterior doors (front and back) and six interior doors (four bedrooms, laundry room, and den). All doors had a height of approximately 2.0 m. The interior doors were hollow-core wood frame doors. To repeatably control ventilation size and timing of opening, the exterior vents (doors and windows) were purpose built in the same fashion as the single-story structure. Table 3.2 shows the size of the windows. All interior doors were open for all experiments, with the exception of the door to the den, which was closed in the experiment that is labeled as "Experiment 6" in this report.

Table 3.2: Two-Story Structure, First Story Window Sizes and Sill Heights

Window	Size (W x H)	Sill Height
A	0.85 m x 0.85 m	1.22 m
B	1.77 m x 1.45 m	0.61 m
C	1.77 m x 1.45 m	0.61 m
D	0.85 m x 1.46 m	0.61 m
E	1.77 m x 1.46 m	0.61 m
F	1.77 m x 1.46 m	0.61 m
G	0.85 m x 1.46 m	0.61 m
H	0.85 m x 0.85 m	1.22 m

Table 3.3 shows the size of the windows on the second story of the two-story structure. For the second story hallway, the height of the interior wall that opened to the first story was 0.95 m as shown in rows N, O, and P in Table 3.3.

Table 3.3: Two-Story structure, Second Story Window Sizes and Sill Heights

Window	Size (W x H)	Sill Height
I	1.77 m x 1.46 m	1.22 m
J	0.85 m x 1.46 m	0.61 m
K	1.77 m x 1.46 m	0.61 m
L	1.77 m x 1.46 m	0.61 m
M	0.85 m x 1.46 m	0.61 m
N	1.88 m x 1.26 m	0.95 m
O	1.90 m x 1.26 m	0.95 m
P	1.51 m x 1.26 m	0.95 m

Tables 3.4 and 3.5 summarize the sequence of events for the three experiments conducted in the single-story structure and the three experiments conducted in the two-story structure. In each table, times are referenced from ignition and a dash indicates that the vent was closed throughout the entire experiment. All interior doors were open for all experiments, with the exception of the door to the den in the two-story structure, which was closed in the experiment that is labeled "Two-Story Experiment 6" in this report.

Table 3.4: Sequence of Events for Single-Story Structure Experiments

Event	Experiment 1	Experiment 2	Experiment 3
Front Door Open	300 s	1200 s	-
Back Door Open	-	-	300 s
Window C Open	-	900 s	-
Window E Open	600 s	600 s	600 s
Burner Off	900 s	1500 s	900 s

Table 3.5: Sequence of Events for Two-Story Structure Experiments

Event	Experiment 4	Experiment 5	Experiment 6
Front Door Open	600 s	600 s	1200 s
Window A Open	-	-	900 s
Window B Open	-	900 s	-
Window K Open	900 s	-	600 s
Window L Open	1200 s	-	-
Burner Off	1500 s	1200 s	1500 s

ASTM E 779 tests were conducted for the two-story structure to estimate the air leakage in terms of air changes per hour and the equivalent leakage area [27]. The leakage in the two-story structure was 4 ACPH50 with an equivalent leakage area of 0.18 m² at 10 Pa. As with the single-story structure, the two-story structure leakage values fell between a tight house and a moderately tight house.

3.3 Instrumentation

Instrumentation was installed to measure gas temperature, gas pressure, and gas velocity within the structures. Gas temperatures were measured with bare-bead Chromel-Alumel (type-K) thermocouples made from 1.3 mm diameter wire as well as 1.6 mm bead diameter inconel sheathed thermocouples. Sheathed thermocouples were used in conjunction with the bi-directional probes for gas velocity measurements. The bare bead thermocouples were welded by laboratory personnel specifically for this series. Pressure measurements were made using differential pressure sensors to determine pressure changes relative to ambient conditions (outside of the structure). Differential pressure sensors were also used to determine gas velocity magnitude using the bi-directional probes. The differential pressure sensor was a Setra Model 264 with a range of ± 125 Pa.

All numerical data was recorded with a National Instruments data acquisition system that incorporated a SCXI-1001 chassis with eight SCXI-1102C 32-Channel modules each connected to a TC-2095 end terminal with built-in cold junction compensation for thermocouple measurements. The TC-2095 also accepted 0-10 V DC for non-thermocouple measurements. The system was

configured for a total of 256 channels with a 1 Hz sample rate. A separate system was used for each structure.

3.3.1 Measurement Uncertainty

Thermocouple measurements may be affected by imperfect weldments between the dissimilar metals, radiative heat transfer from the fire source or hot gas layer, and small variations in orientation along the thermocouple array. Theoretical error as high as approximately 11% for upper layer temperatures and significantly higher for lower layer temperatures (calculated with Celsius temperatures) measured using bare-bead type-K thermocouples (diameters ranging from 1 mm to 1.5 mm) have been reported by researchers at NIST [29,30]. The total expanded relative uncertainty ($k = 2$) of the temperature measurements from these experiments is estimated to be $\pm 24\%$.

The relative uncertainty in pressure transducer measurements is usually low, but the total expanded uncertainty of the measurement incorporates uncertainty in leakage area, ventilation rate, total heat release rate (HRR), etc. The total expanded uncertainty of differential pressure measurements in a test series with a mean maximum pressure increase of approximately 150 Pa was calculated as ± 40 Pa [31]. Drawing from the results of this past research, the total expanded relative uncertainty ($k = 2$) associated with pressure measurements is estimated as $\pm 23\%$.

Bi-directional probe measurements may be affected by variations in orientation of the probe relative to the flow velocity direction and potential fouling of the probe lines due to sooty conditions. A constant calibration factor of 1.08 was assumed to calculate velocity from differential pressure and temperature measurements made using the bi-directional probes. McCaffrey and Heskestad showed that this is generally a good estimate of the calibration factor for uniform flows with Reynolds numbers ranging from approximately 1000 to 3800, which resulted in a maximum error of 8% from the known velocity in those situations. The error between the actual velocity and the measurements calculated using a calibration factor of 1.08 increased significantly for Reynolds numbers below 1000 [32]. Kent and Schneider found uncertainty of approximately $\pm 15\%$ in the calibration constant for flows with Reynolds numbers below 400 [33]. The angle of orientation of the bi-directional probe relative to the flow direction is an additional source of uncertainty. McCaffrey and Heskestad found a relative uncertainty of $\pm 10\%$ when the angle of orientation relative to the flow direction was modified by $\pm 50^\circ$ using a probe with a diameter of 22 mm in a flow with a Reynolds number of 3400, and Kent and Schneider confirmed this uncertainty over the same range when using a 25.4 mm diameter probe in a uniform flow with a Reynolds number of 900 [32, 33].

A gas velocity measurement study examining flow through doorways in pre-flashover compartment fires yielded expanded uncertainties ranging from $\pm 14\%$ to $\pm 22\%$ for measurements from bi-directional probes similar to those used during this series of experiments to measure velocity magnitudes [34]. Due to the relatively low velocity magnitudes measured in the experiments presented in this work as well as the scatter in measurements made in replicate experiments, the total expanded relative uncertainty ($k = 2$) associated with velocity measurements for this work is estimated to be $\pm 22\%$.

3.4 Single-Story Structure

The locations of the instrumentation and the natural gas burner in the ranch-style structure are displayed in Figure 3.4. The wall and ceiling immediately adjacent to the burner were reinforced with cement board to minimize excessive thermal damage to the structure. Each thermocouple array consisted of eight type-K thermocouples. The highest elevation thermocouple in each array was located 2.5 cm below the ceiling with the remaining seven spaced at approximately 30.5 cm intervals (30.5 cm below ceiling, 61 cm below ceiling, ... , 213 cm below ceiling). Three pressure taps were installed at each location at elevations of 30.5 cm, 122 cm, and 213 cm below ceiling.

Bi-directional velocity probes were installed in relevant doorways, windows, and the interior hallway. In each case, the five probes in the array were evenly spaced along the centerline of the opening. See Table 3.1 for the heights of the exterior vents. The probes in the windows were spaced 0.24 m apart. Therefore the probe in the window at the highest elevation was 0.61 m below the ceiling and the lowest elevation probe in the windows was approximately 1.6 m below the ceiling. The probes in the front door opening were spaced 0.33 m apart. The probe in the front door opening at the highest elevation was 0.73 m below the ceiling and the lowest elevation probe was approximately 2.07 m below the ceiling. The probes in the hallway were spaced 0.4 m apart. The probe in the hallway at the highest elevation was 0.4 m below the ceiling and the lowest elevation probe was approximately 2.0 m below the ceiling. The temperature and gas velocity measurements at the front door and each of the windows were only utilized for experiments where the front door or the particular window of interest was opened.

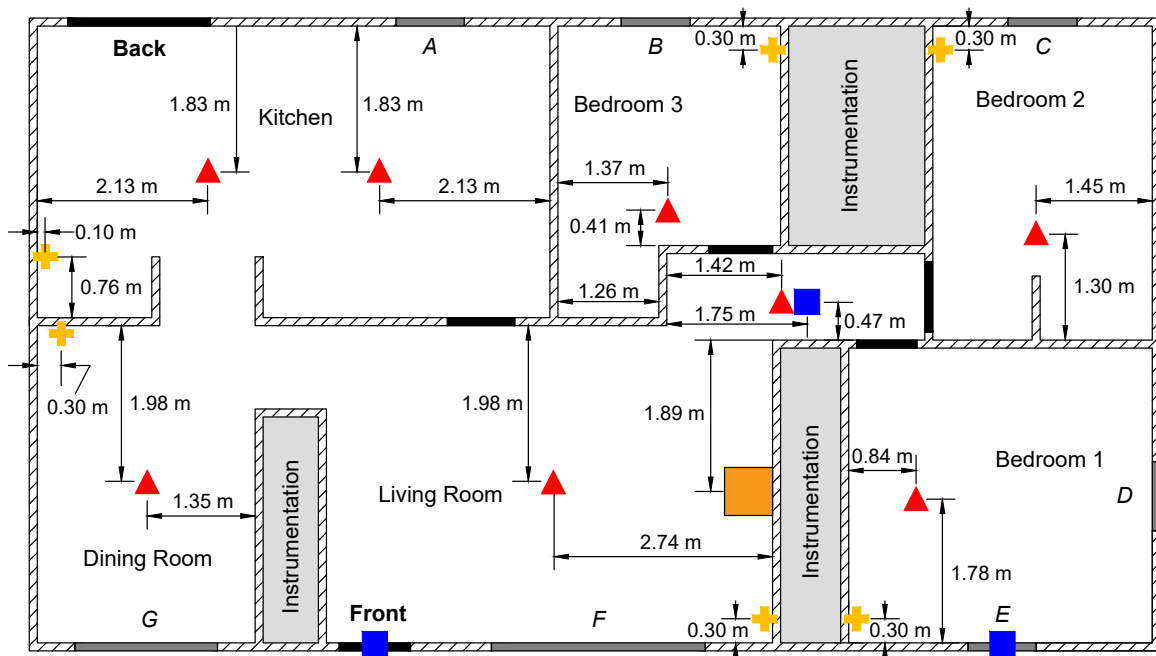






Figure 3.4: Dimensioned plan view drawing of instrumentation in the single-story structure

Icon	Instrumentation
	Thermocouple Array
	Gas Velocity Array
	Pressure Tap Array
	Natural Gas Burner

3.5 Two-Story Structure

Figures 3.5 and 3.6 show the dimensioned locations of instrumentation and the gas burner on the first and second story of the structure, respectively. The wall immediately adjacent to the burner was reinforced with cement board to minimize excessive thermal damage to the structure. In similar fashion to the single-story structure, instrumentation in the two-story structure remained constant throughout the three experiments. Thermocouple arrays consisted of either eight or 16 type-K thermocouples. There were two 16-thermocouple arrays installed in the two-story structure: one in the family room and one in the foyer. The remainder of the thermocouple arrays had eight probes. In all cases, the highest elevation thermocouple in each array was located 2.5 cm below the ceiling with the remaining thermocouples spaced at 30.5 cm intervals. The lowest elevation thermocouples in the eight-thermocouple arrays were approximately 213 cm below the ceiling and the lowest elevation thermocouples in the 16-thermocouple arrays were approximately 460 cm below the ceiling. Three pressure taps were installed at each location at elevations of 30.5 cm, 122 cm, and 213 cm below the ceiling in all locations except the family room. Because the family room was open to the second story, the three elevations at which pressures were measured were 30.5 cm, 244 cm, and 460 cm below the ceiling. Bi-directional velocity probes were installed in relevant doorways and windows. In each case, the five probes in the array were evenly spaced within the respective location.

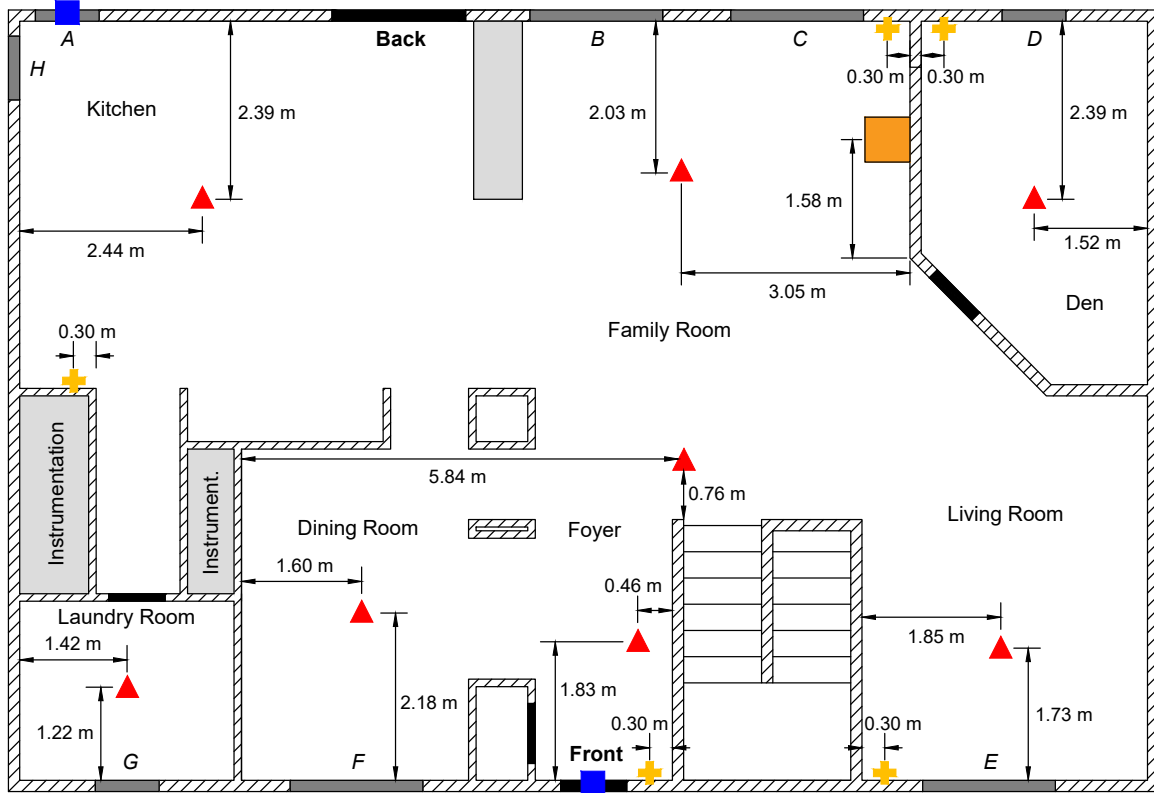






Figure 3.5: Dimensioned plan view drawing of instrumentation of the first story of the two-story structure

Icon	Instrumentation
	Thermocouple Array
	Gas Velocity Array
	Pressure Tap Array
	Natural Gas Burner

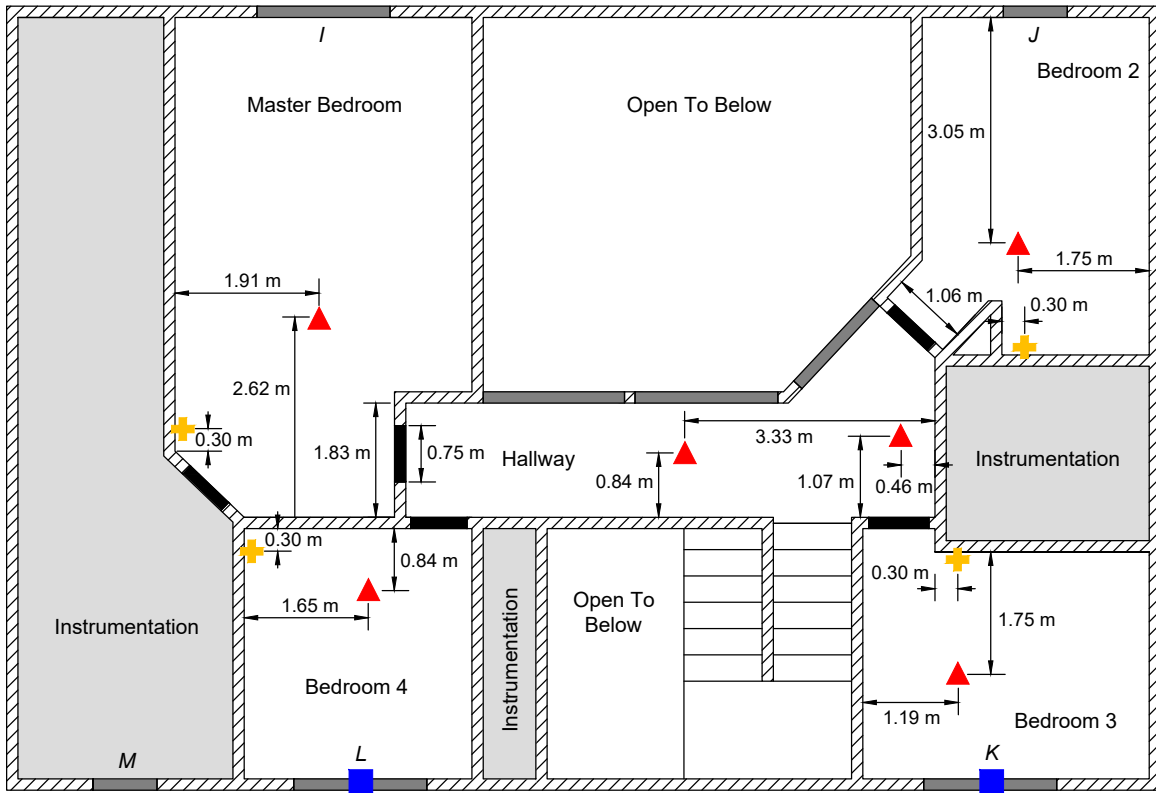


Figure 3.6: Dimensioned plan view drawing of instrumentation of the second story of the two-story structure

3.6 Fire Source

A single natural gas burner was the sole fire source within the unfurnished structures for all experiments. The burner had dimensions of 0.6 m by 0.6 m and the surface of the burner was located approximately 0.6 m above the floor. The burner was calibrated under a ventilation hood instrumented with an oxygen-depletion calorimeter. The calibration yielded a heat of combustion of approximately 45 MJ/kg for the natural gas that supplied the burner. An Alicat MCRH-5000 SLPM mass flow controller was used to ensure the mass flow rate to the burner matched the desired heat release rate. The total heat release rate for the single-story structure was 250 kW (flow rate set point of approximately 400 standard liters per minute (SLPM) with a reference temperature of 0°C), and 500 kW (flow rate set point of approximately 800 SLPM with a reference temperature of 0°C) for the two-story structure. In the single-story structure, the burner was positioned in the center of the far right wall in the living room. In the two-story structure, the burner was positioned approximately at the center of the wall in the family room that was common between the family room and the den.

4 Modeling

FDS (Version 6.7.1) was used to simulate the effect of ventilation on buoyancy-driven fluid flow in the single-story ranch-style and two-story colonial-style homes. The geometry of the structures was defined in the models as closely as possible to the constructed structures while adhering to the underlying rectilinear grid. The ambient temperature was assumed to be 20°C in all simulations. The initial temperature on the first story of the two-story structure in Experiment 6 was assumed to be 26°C and the initial temperature on the second story was assumed to be 35°C to provide the best agreement with the experimental data for that experiment. The initial temperature throughout the structure for all other experiments was assumed to be 20°C.

FDS devices and control logic were utilized to remove obstructions representing windows and exterior doors at predefined times in the simulations that matched the experimental timeline. The gas burner was represented in each model as an inlet vent attached to a solid obstruction with a predefined total HRR that matched the set point HRR in the experiments. FDS input files for Single-Story Experiment 1 and Two-Story Experiment 4 have been included in Appendix B.

4.1 Materials

The structures were built with non-combustible gypsum wallboard construction with non-combustible cement board on surfaces in close proximity to the burner. It was expected that the relatively small difference in properties between the cement board and the gypsum wallboard would not affect the results of the simulations so the only material defined for the models was gypsum board with the thermo-physical properties shown in Table 4.1.

Table 4.1: Gypsum Board Material Properties Defined in FDS Models [35, 36]

Property	Value
Specific Heat Capacity	1.0 kJ/kg/K
Thermal Conductivity	0.16 W/m/K
Density	480.0 kg/m ³

4.2 Model Parameters

The following sections describe an investigation conducted to determine the set of model parameters that provided the best predictions of the experimental data with consideration also given to the computational cost of each modification of the parameters. Each section describes a parameter

or set of parameters that was independently investigated to determine the effect of the parameter on the model predictions. The effect of changing more than one parameter at a time on the model predictions was not investigated in this work.

4.2.1 Simulation Mode

Due to the large number of parameters that control the mathematics and numerical stability of a simulation, FDS incorporates four distinct simulation modes. The modes include Direct Numerical Simulation (DNS), Large Eddy Simulation (LES), Very Large Eddy Simulation (VLES), and Simplified Very Large Eddy Simulation (SVLES), listed in order of decreasing computational expense. Each LES mode provides simplifying assumptions for: 1) the representation of the baroclinic torque, 2) the method of calculation for the Courant-Friedrichs-Lewy (CFL) constraint, 3) whether the the Von Neumann constant is evaluated during the simulation, 4) the method of defining the specific heats of gas species, 5) the number of iterations for the pressure solver, and 6) the near-wall turbulence model.

Baroclinic torque is responsible for generating vorticity due to misalignment of the pressure and density gradients. Inclusion of the baroclinic torque in a calculation may have an effect on the puffing behavior of a buoyant diffusion flame due to the large density gradients expected within a flame [7]. The SVLES simulation mode neglects the baroclinic torque and all other simulation modes include it in the pressure term of the momentum transport equation.

The CFL constraint limits the timestep size due to the advection velocity, ensuring that a fluid element does not traverse more than one cell width during a time step. Determining the timestep to fulfill the CFL constraint requires calculation of the norm of the velocity vector. The norm of the velocity vector for the LES mode is the L_1 norm, which is most restrictive and most expensive in terms of computational resources and time. The L_∞ norm is used in the VLES mode, which also includes a representation of the divergence of the velocity vector, which is an added measure to ensure stability of the simulation. The L_∞ norm without the divergence of the velocity vector is used to calculate the CFL constraint for the SVLES mode, which is the least restrictive form of the velocity norm. These simplifications to calculation of the norm are not expected to affect the results, but may influence the stability of the simulations [7].

The Von Neumann constraint is a stability measure that is analogous to the CFL constraint applied to diffusive transport instead of advection. The Von Neumann constraint ensures that variations in scalar fields do not lead to spurious oscillations that may result in simulation instabilities. The Von Neumann constraint is checked in all LES modes except for the SVLES mode [7].

The ratio between the constant volume specific heat and the constant pressure specific heat is assumed constant in the SVLES mode. In reality this ratio is a function of temperature, but it has been suggested that the assumption of a constant ratio may be suitable for a compartment that does not approach flashover conditions. This assumption improves the speed of the simulation because calculating temperature-dependent properties for each gas species increases the computational cost of several routines. All other simulation modes involve the calculation of temperature-dependent

gas properties [7].

The pressure solver in FDS enforces an imperfect no-flux boundary condition at solid obstructions within the computational domain. This imperfect representation results in a non-zero normal velocity at these boundaries that is not physically accurate. The magnitude of this error may be reduced through additional iterations of the pressure solver. The LES and VLES modes include a maximum of 10 pressure solver iterations and the SVLES includes 3 iterations per half of the time step in an attempt to decrease the error to below the defined velocity tolerance [7].

FDS uses a Deardorff turbulent viscosity model throughout the domain that is not well-defined near the wall. To improve the model representation of the local physics near the wall, FDS utilizes a near-wall model to resolve the eddy viscosity in the first cell away from the wall. The LES mode uses the wall-adapting local eddy-viscosity model (WALE) in this region that causes the eddy viscosity to approach zero at a rate proportional to the cube of the distance from the wall. A less expensive solution is used in the VLES and SVLES modes that utilizes a constant-coefficient Smagorinsky model with an explicit damping function applied to force the eddy viscosity to zero at the proper rate [7].

Preliminary simulations were conducted to investigate the effect of the simulation mode on the model predictions. Figure 4.1 displays the temperature measured approximately 2.5 cm below the ceiling of the family room in Two-Story Experiment 4 as well as model predictions made using the SVLES, VLES, and LES simulation modes. The discrete data points in the figure represent experimental data and the curves represent model predictions. It is evident in the figure that the SVLES mode captured the rising edge of the experimental data and the maximum temperatures measured in the experiment more accurately than the other simulation modes. All simulation modes produced predictions that were approximately equivalent after 900 s into the experiment.

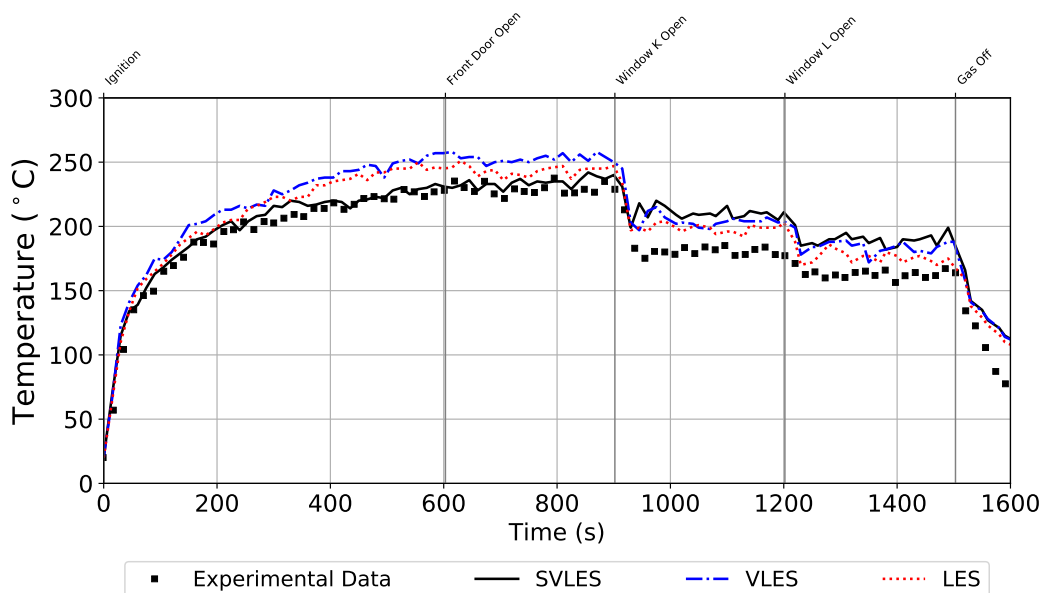


Figure 4.1: Comparison of typical temperature predictions from each simulation mode

Model predictions are compared to the pressure measured approximately 0.3 m below the ceiling in the front door corridor in Two-Story Experiment 4 in Figure 4.2 and to the velocity measured at the highest elevation in the front door opening in Figure 4.3. In both figures, the discrete data points represent experimental data and the curves represent model predictions. The pressure and velocity predictions were not as sensitive to the simulation mode as the temperature predictions, with little variation between the curves produced from models that employed each mode.

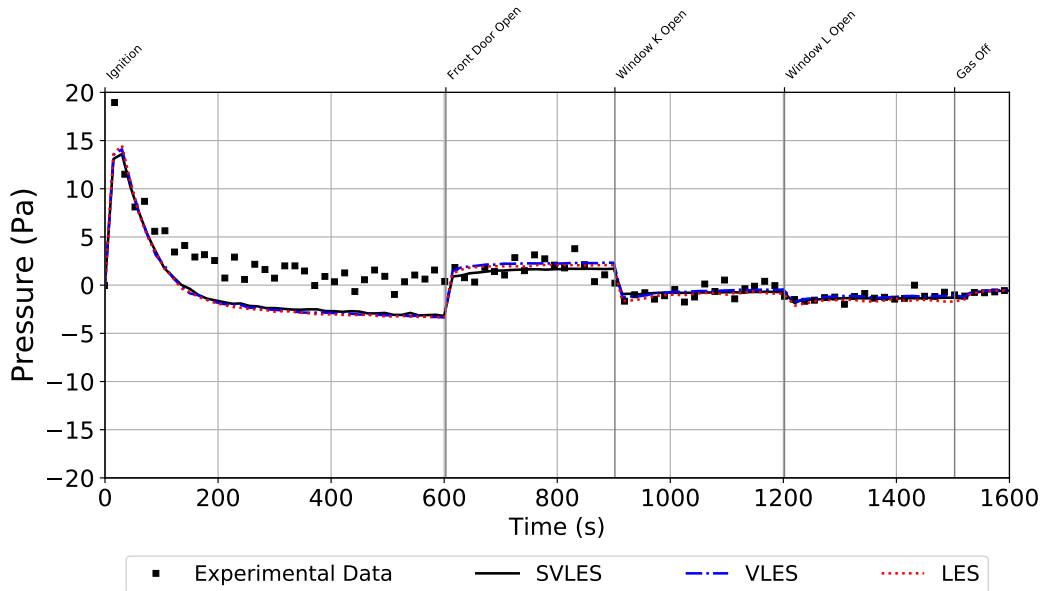


Figure 4.2: Comparison of typical pressure predictions from each simulation mode

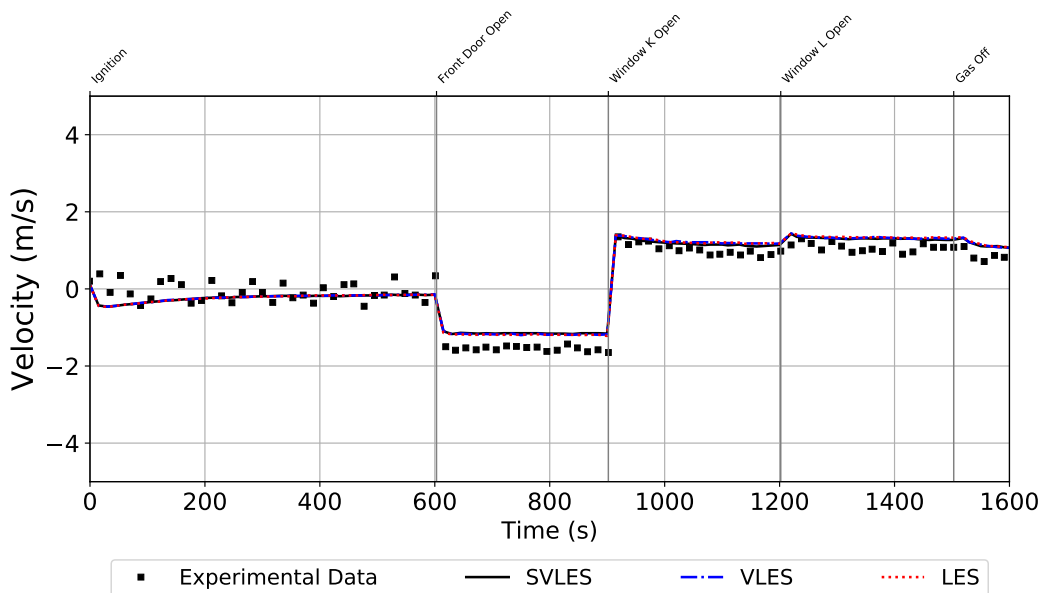


Figure 4.3: Comparison of typical velocity predictions from each simulation mode

The trends in the comparison of simulation predictions against experimental data shown in Figure 4.1, Figure 4.2, and Figure 4.3 are representative of all measurement locations throughout both structures. Temperatures measured at high elevation were most accurately represented with the SVLES mode during the initial increase after ignition of the burner and all simulation modes predicted consistent temperatures after several ventilation events resulted in an overall decrease in temperatures. The velocity and pressure predictions were generally equivalent regardless of the simulation mode. The VLES mode required approximately 30% more computation time than the SVLES mode and the LES mode required approximately 100% more computation time than the SVLES mode. After analysis of these preliminary simulations, it was determined that the data for each measurand and measurement location were predicted with comparable accuracy regardless of simulation mode, although the SVLES mode had the lowest computational cost. The SVLES mode was used to simulate all of the experiments that are presented in the following sections.

4.2.2 Spatial Resolution

The model geometries were defined as closely as possible to the constructed homes while adhering to the underlying rectilinear grid. Preliminary simulations of the two-story structure were conducted to determine the sensitivity of the simulation results to the spatial resolution. The fire size in the two-story structure was 500 kW, which corresponded to an effective fire diameter, $D^* = 0.727$ [37]. Two levels of resolution were investigated with both simulated using the SVLES simulation mode. The grid was defined to be uniform throughout the computational domain with all cubic elements and cell sizes of 0.1 m and 0.05 m. These resolutions corresponded to $D^*/dx = 7.3$ (coarse resolution) and $D^*/dx = 14.6$ (moderate resolution).

Figure 4.4 provides a comparison of temperature data collected approximately 2.5 cm below the ceiling of the Foyer in Two-Story Experiment 4 as well as model predictions made using the coarse resolution and moderate resolution simulations. The discrete data points in the figure represent experimental data and the curves represent model predictions. The relative agreement between predictions and data for each resolution simulation are representative of all measurement locations for each structure. It is evident in the figure that the temperature prediction is not sensitive to the model resolution.

Figure 4.5 provides a comparison of the pressures measured approximately 0.3 m below the ceiling in the front door corridor in Two-Story Experiment 4 and Figure 4.6 provides a comparison of the velocity measured at the highest elevation in the front door opening against predictions in Two-Story Experiment 4. In both figures, the discrete data points represent experimental data and the curves represent model predictions. The relative agreement between model predictions for each resolution simulation are representative of all measurement locations for each structure. It is evident in these figures that the pressure and velocity predictions are not significantly affected by an increase in resolution from coarse to moderate.

The grid in the coarse resolution simulations of the experiments conducted in the two-story structure had a total of 1,205,280 elements split evenly into 48 meshes and the grid in the moderate resolution simulations had a total of 9,216,000 elements split evenly into 144 meshes. A computa-

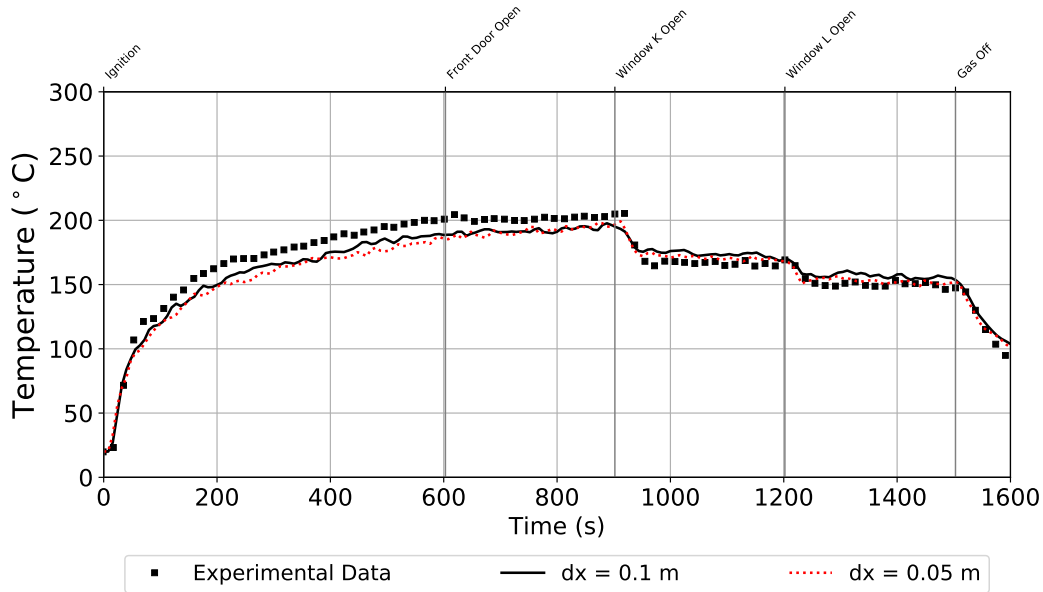


Figure 4.4: Comparison of typical temperature predictions from coarse and moderate resolution simulations

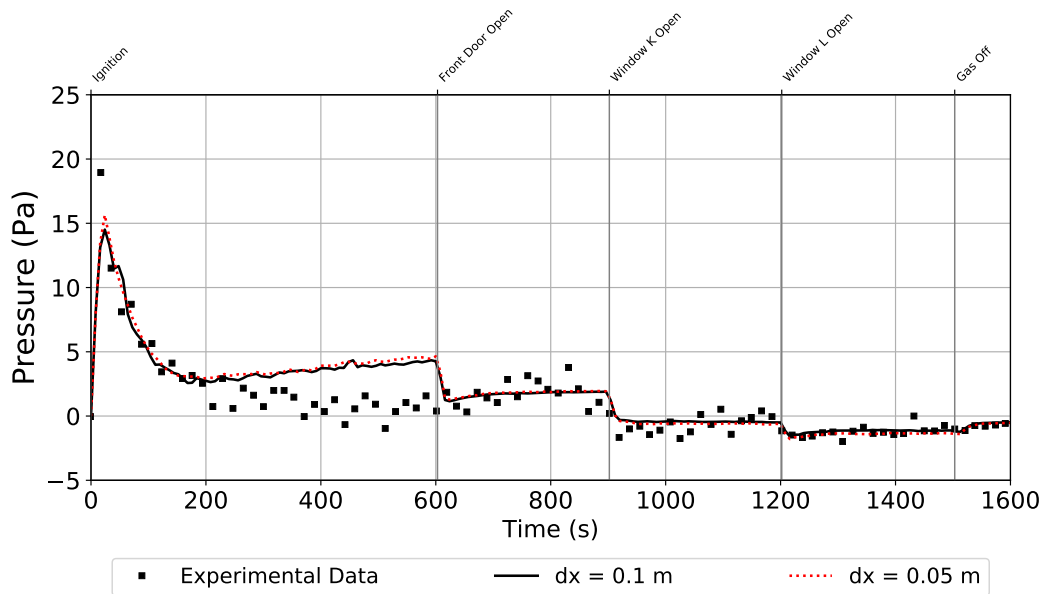


Figure 4.5: Comparison of typical pressure predictions from coarse and moderate resolution simulations

tional cluster comprised of individual nodes with a total of 48 2nd generation Intel Xeon Platinum 8000 series processor cores and a sustained clock speed of 3.6 GHz was used to perform the simulations. The coarse resolution models required 48 cores, which utilized one full node in this cluster and the moderate resolution simulations required 144 cores, which utilized three full nodes in the

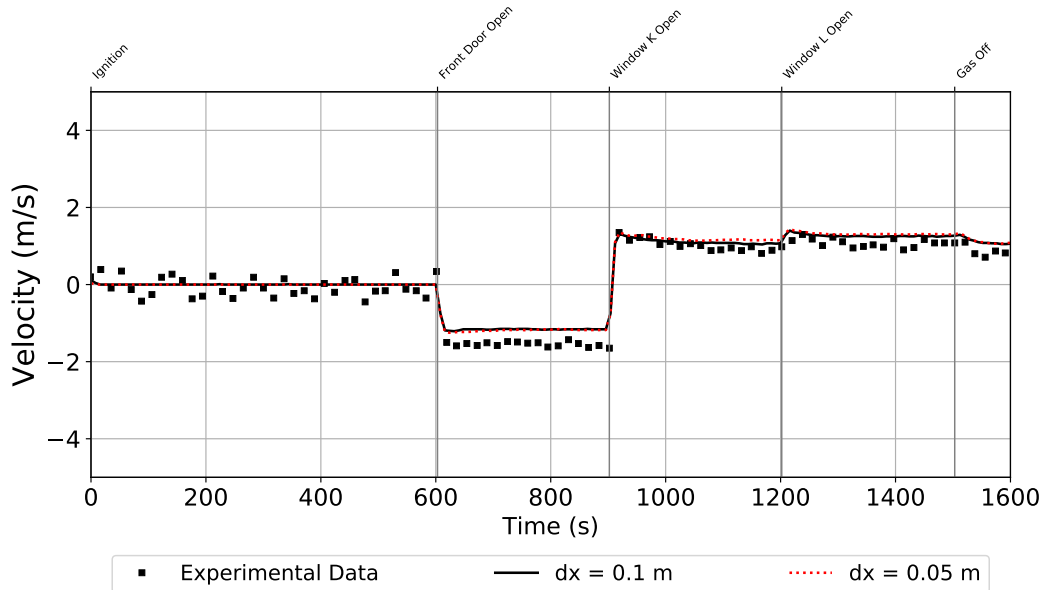


Figure 4.6: Comparison of typical velocity predictions from coarse and moderate resolution simulations

cluster. The coarse resolution simulation required approximately 16 hours on a single 48-core node for a total of 1800 s of simulation time and the moderate resolution simulation required approximately 116 hours on three 48-core nodes for the same simulation duration. A review of the time allocated to each FDS routine indicated that 18% of the time spent running the coarse resolution simulation was dedicated to communications whereas 48% of the time spent running the moderate resolution simulation was dedicated to communications, which represents a significant decrease in simulation efficiency.

An increase in model resolution for the model that represented the two-story structure resulted in a significant increase in computational cost without much change in the predicted quantities. This result led to adoption of a coarse resolution model for each structure to represent each distinct experiment. The resulting models had a total of 414,720 elements defined for the single-story domain and 1,205,280 elements for the two-story domain.

4.2.3 Pressure Zones

The experimental effort presented in this work is one of the few sets of experiments in which static pressures were measured throughout a residential structure containing a well-defined fire source. This unique aspect of the experiments made them ideal for validation of the inherent functionality of FDS specifically related to pressure predictions. Although a detailed discussion of the technical details related to solution of the governing equations for pressure throughout the domain in FDS and the theory behind and implementation of pressure zones is left to the developers of FDS [7, 8], a brief explanation is provided in this section.

FDS relies on a low Mach number approximation, first presented by Rehm and Baum [38], in which pressure is represented as a linear combination of a background pressure and a perturbation pressure. The background pressure is variant in elevation and time within a given volume, and the perturbation pressure varies spatially and temporally and is responsible for driving fluid flow within a continuous volume. Decomposition of the pressure into background and perturbation components simplifies representation and solution of the governing equations. The solution procedure consists of a phase in which all thermodynamic quantities, velocities, and species mass fractions are estimated to ensure the time step is adequately small to retain stability, followed by a phase in which these estimated quantities are corrected. In the correction phase, the densities of the gas species and each unique background pressure are corrected first, followed by all other quantities and source terms which are dependent on the pressure and density. The perturbation pressure and the corrected velocity are calculated last in each time step. Almost all of the quantities predicted by FDS rely on an accurate representation of pressure, including temperatures and gas velocities [8].

Pressure zones allow the model practitioner to define a unique background pressure for a sealed compartment within the model (a space completely enclosed by solid obstructions). Pressure zones also facilitate the definition of leakage paths between compartments with different background pressures. The background pressure may change due to many phenomena, but the changes in background pressure that are pertinent to this work derive from a fire source within the zone. When an obstruction that separates two pressure zones is removed, the two zones effectively become a single zone. To account for pressure equilibration between the two zones, a volumetric flow rate is assigned to the gases in each zone that causes the background pressures to quickly change to match each other. The characteristic time for the pressures to come into equilibrium is generally on the order of seconds [8].

Preliminary simulations were conducted to investigate the sensitivity of the model to the definition of pressure zones to differentiate the structure from the exterior, as well as the sealed instrumentation areas throughout the structure from the instrumented volume of the structure. Figure 4.7 presents pressure data measured approximately 213 cm below the ceiling in the living room of the single-story structure as well as model predictions produced with three different definitions of pressure zones. The discrete data points in the figure represent experimental data and the curves represent model predictions. One simulation was conducted with no pressure zones defined, one simulation was conducted with a single pressure zone that encompassed the entire interior volume of the structure, and one simulation was conducted with pressure zones defined for each specific continuous volume that was isolated for at least part of the experiment. For the single-story structure, the isolated volumes that were defined as pressure zones corresponded to the three instrumentation areas shaded in Figure 3.4.

As shown in the figure, the simulation with no zones defined displayed a different rate of increase in the initial pressure rise immediately after ignition as well as a lower maximum pressure than the simulations with pressure zones defined. The pressure curves predicted with the simulations that included a single and multiple pressure zones were indistinguishable from each other. After the first ventilation event (front door open at 300 s), the predicted pressure curves from all of the simulations displayed the same behavior. The computational cost for implementing the single zone

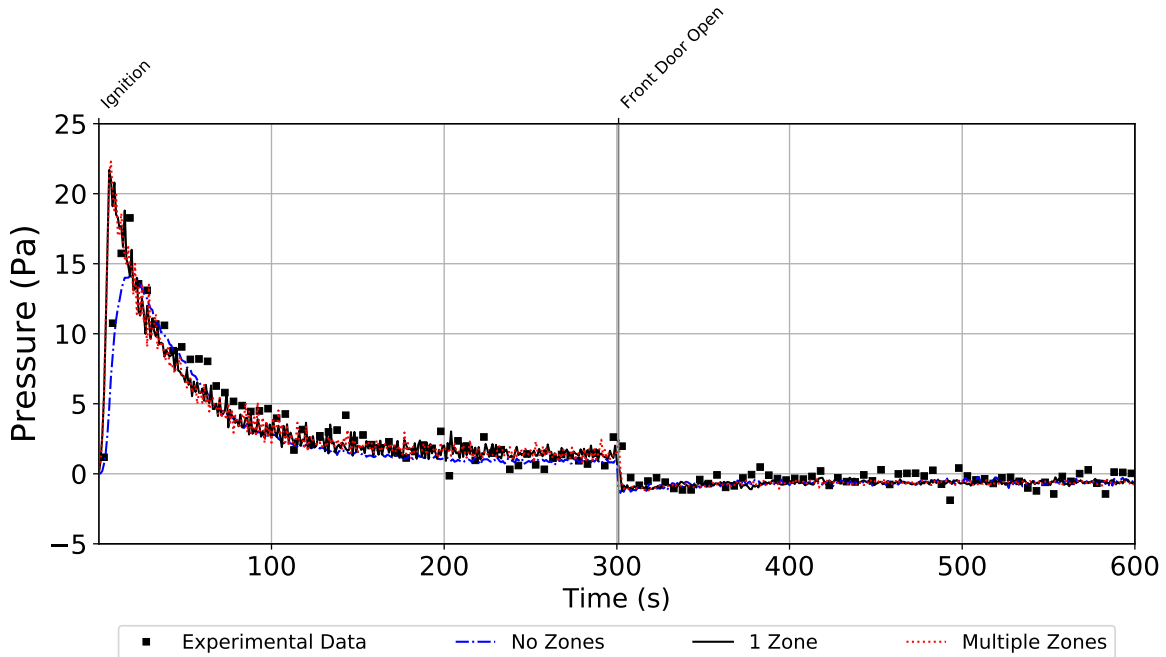


Figure 4.7: Comparison of model pressure predictions with three different zones definitions

representation was approximately 6% higher and the multiple zone representation was approximately 24% higher than the representation without zones defined in the single-story simulations. To maintain simplicity and reduce computational costs, it was determined that a single pressure zone would be defined in each model that incorporated the volume within the exterior envelope of each structure. It is acknowledged that definition of pressure zones is the best practice in CFD fire modeling and it is recommended that a similar exercise to investigate the sensitivity of results to the definition of pressure zones be conducted when residential fire scenarios are simulated.

4.2.4 Definition of Leaks

With few exceptions, no modern structure is constructed to be airtight, due, in part, to the prohibitive cost of such construction. To ensure the most accurate representation of the validation experiments, it is important to define the model to represent the construction as closely as reasonably possible to the structures in which the physical experiments were conducted. FDS provides functionality to define leaks to simulate sub-grid resolution gas flows into and out of a compartment. This functionality uses the HVAC submodel in FDS, and eliminates the need to explicitly resolve the physical dimensions of the leak.

There are two methods to define leaks in FDS that largely depend on the pressures that are used to calculate the flow rate through the leak. The first approach is referred to as "Pressure Zone Leakage" in the FDS literature and was formulated to primarily represent bulk leakage due to imperfect seals at walls, windows, and doors. The pressures used to determine the flow rate through

the leak in the first method are the mean background pressures of each zone defined in the leak assignment. To define a leak using this method requires definition of the two zones on either side of the leak as well as assignment of a leakage area to surfaces within one of the pressure zones [7].

The second method to define leaks in FDS is referred to in the FDS literature as "Localized Leakage" and was formulated to represent flow through a specific leak in the geometry. This method uses the local pressures at the leak to calculate the flow rate through the leak. To define a leak using this method requires linking two vents within the model that represent the two sides of the leak as well as definition of a leakage area [7]. The results of simulations that utilize this method of defining leaks are dependent on the locations of the vents that are defined to represent the leaks due to the use of the local pressure to calculate flow through the leaks. Preliminary simulations showed that defining vents on the walls resulted in lower pressure magnitude predictions at all locations and defining a vent on the ceiling of the two-story structure resulted in lower pressure magnitudes as well as lower temperature predictions.

Preliminary simulations were conducted to investigate the sensitivity of the model to the two methods of defining leaks. To test the "Pressure Zone Leakage" method, a surface that was assigned to the doors was defined with the effective leakage area measured as described in Section 3. To test the "Localized Leakage" method, a fictitious vent was defined at the floor level of each structure. Using the HVAC namelist group, the fictitious vent was specified to transport gases from the interior to the exterior of the structure through an orifice with the effective leakage area measured as described in Section 3. Figure 4.8 presents pressure data measured approximately 213 cm below the ceiling in the living room of the single-story structure as well as model predictions produced with each leakage method implemented. The discrete data points in the figure represent experimental data and the curves represent model predictions.

The figure indicates that the "Pressure Zone Leakage" method of defining leaks predicted a pressure below atmospheric at this elevation prior to the first ventilation event. Negative pressures were not observed in any of the experiments prior to the first ventilation event, and were not expected based on the relatively low flow rates throughout each structure prior to exterior ventilation. At higher measurement elevations, the pressures predicted with "Pressure Zone Leakage" were positive, but also systematically underpredicted prior to the first ventilation event. This trend was evident at all measurement locations in each of the tested structures. The "Localized Leakage" method of defining leaks yielded pressures that remained above atmospheric prior to the first ventilation event, which agreed with experimental observations. This method also predicted pressures that more closely agreed with the experimental data measured throughout each structure.

The disparity in the trends between these two methods is due to the use of the mean zone background pressure in the "Pressure Zone Leakage" method and the local pressure in the "Localized Leakage" method. Within the fire compartment, the mean zone pressure is typically greater than the local pressure at low elevations. In the experiments presented in this work, this disparity in pressure definitions for the flow rate calculation yielded artificially high volumetric flow rates through the modeled leaks, which resulted in artificially low pressure predictions when the "Pressure Zone Leakage" method was used as compared to the "Localized Leakage" method. The difference in computational cost between the "Localized Leakage" method and the "Pressure Zone Leakage"

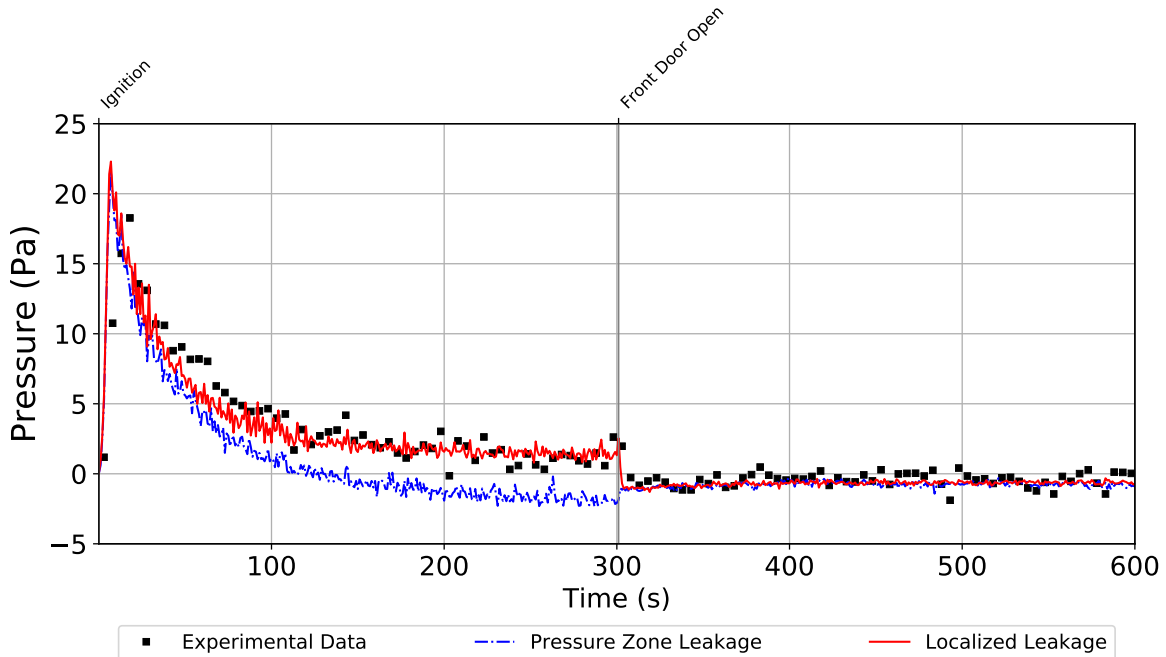


Figure 4.8: Comparison of model pressure predictions with different definitions of zones

method was negligible, so no consideration was given to computational cost when deciding which set of parameters to use. All predictions presented in the following sections were obtained from simulations that used the "Localized Leakage" approach to defining leaks with a single vent defined at the floor level to represent the effective leakage.

4.3 Device Parameter Uncertainty

The instruments described in Sections 3.4 and 3.5 were defined in FDS as devices located in the same positions as the instrumentation in the physical experiments. Because FDS requires that the domain be split into meshes of prismatic cells, a discussion of how the quantities at these defined devices are calculated becomes necessary. FDS determines in which cell the device is located and calculates the requested quantity either at the center of the cell (scalar quantities like temperature and pressure) or at the center of one of the faces of the cell (vector quantities like gas velocity) regardless of the position of the device within the cell [7]. Each quantity is essentially evaluated as the mean over the volume of the cell or the area of the face of the cell. Because of this method of calculating the device quantities, the uncertainty in the position of each device as defined in the model is a maximum of half of the cell length. The uncertainty in the magnitude of a predicted quantity based on the uncertainty of the position of the device in the model is dependent on the predicted quantity, with larger uncertainties in the vicinity of large gradients.

Several quantities are necessary to define a device in the model, but not all were directly measured

during the physical experiments, which increases the uncertainty in the comparisons. Specifically for thermocouples, these properties include the emissivity, density, specific heat, and diameter of the bead. The bead diameter was defined in the model to be 1.3 mm and the emissivity of the bead was defined to be 0.9. The density and specific heat capacity of the thermocouple beads took on the default values in FDS which were values consistent with nickel, 8908 kg/m^3 and 0.44 kJ/kg/K , respectively. Nickel is a major component of Chromel and Alumel, the components in the type-K thermocouples used in these experiments, and these parameter values are likely a good representation of the actual density and specific heat capacity of the thermocouple beads. The bead diameter and emissivity were not directly measured, but preliminary simulations conducted to investigate the sensitivity of the predictions to these parameters found that the emissivity had a negligible effect on the temperature predictions for the maximum temperatures encountered in this work and that the mean deviation of temperature predictions was typically approximately $\pm 5\%$ when the bead diameter was multiplied and divided by a factor of 3, which is a margin that is likely higher than the uncertainty in the physical diameter of the bead.

An additional source of uncertainty was the orientation of each of the defined devices. The thermocouple beads had a small diameter, which would typically favor convective heat transfer over radiative heat transfer, and would limit the sensitivity of the measurements to orientation. There is a possibility that radiative heat exchange between the fire source and the thermocouple beads occurred in the experiments, which could manifest as artificially high temperature measurements that were dependent on the orientation of the thermocouples, the bead diameter, and the location of the thermocouples relative to the fire source and the hot upper gas layer. Because temperature is a scalar quantity, the orientation of the devices in FDS does not affect the calculated value, which neglects this potential effect. Orientation of the bi-directional probes in the experiments may also have a significant effect on the measured gas velocities as any deviation in orientation from orthogonal to the doorway or window would result in a decreased velocity measurement, whereas all velocity devices in the model were aligned perfectly orthogonal to the opening.

5 Single-Story Results

The following sections present the experimental data collected with each distinct ventilation scenario as well as the results of the FDS model simulations that were constructed to simulate each experiment. The sole fuel source for the single-story structure experiments was a relatively low HRR (250 kW) burner. It was expected that neither the structure nor any of the individual rooms would reach a ventilation-limited state during the experiments, effectively ensuring that the HRR remained controlled and constant. By opening external vents, flow paths were created that allowed air to flow into the structure and high temperature gases to flow to different compartments and out of the structure. The effects of these flow paths may be interpreted from temperature, pressure, and velocity data collected throughout the structure. In all of the figures presented in the following sections, discrete data points denote experimental data and solid lines denote model predictions.

5.1 Single-Story: Experiment 1

Experiment 1 conducted in the single-story structure featured the 250 kW gas burner ignited for 900 s as well as venting of the front door (300 s) and window E (600 s).

5.1.1 Experiment 1: Temperature

The temperature data collected by thermocouple arrays throughout the structure as well as model predictions are presented in the following figures. Figure 5.1 displays the temperatures in the living room, where the burner was located, Figure 5.2 displays the temperatures in the hallway that connected all of the bedrooms, Figure 5.3 displays the temperatures in bedroom 1, Figure 5.4 displays the temperatures in bedroom 2, Figure 5.5 displays the temperatures in bedroom 3, Figure 5.6 displays the temperatures in the kitchen, Figure 5.7 displays the temperatures in the breakfast area, and Figure 5.8 displays the temperatures in the dining room. Note that a malfunction occurred which affected the temperature measured 0.02 m below the ceiling in the kitchen, and these data have been excluded from Figure 5.6.

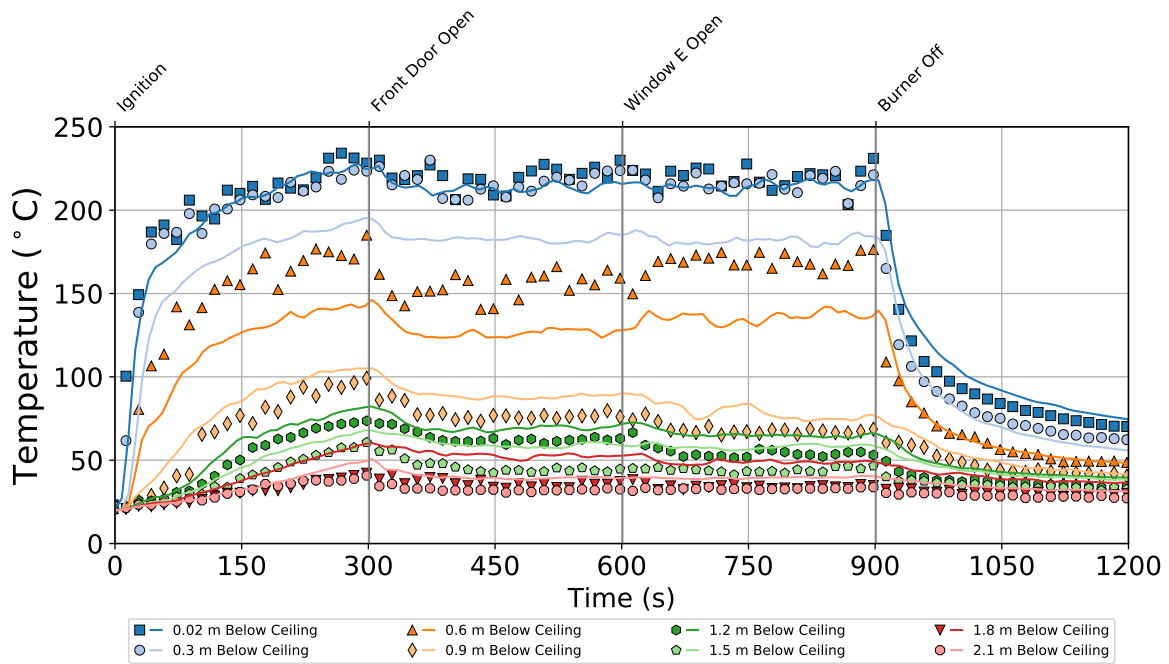


Figure 5.1: Temperatures in the living room of the single-story structure during Experiment 1

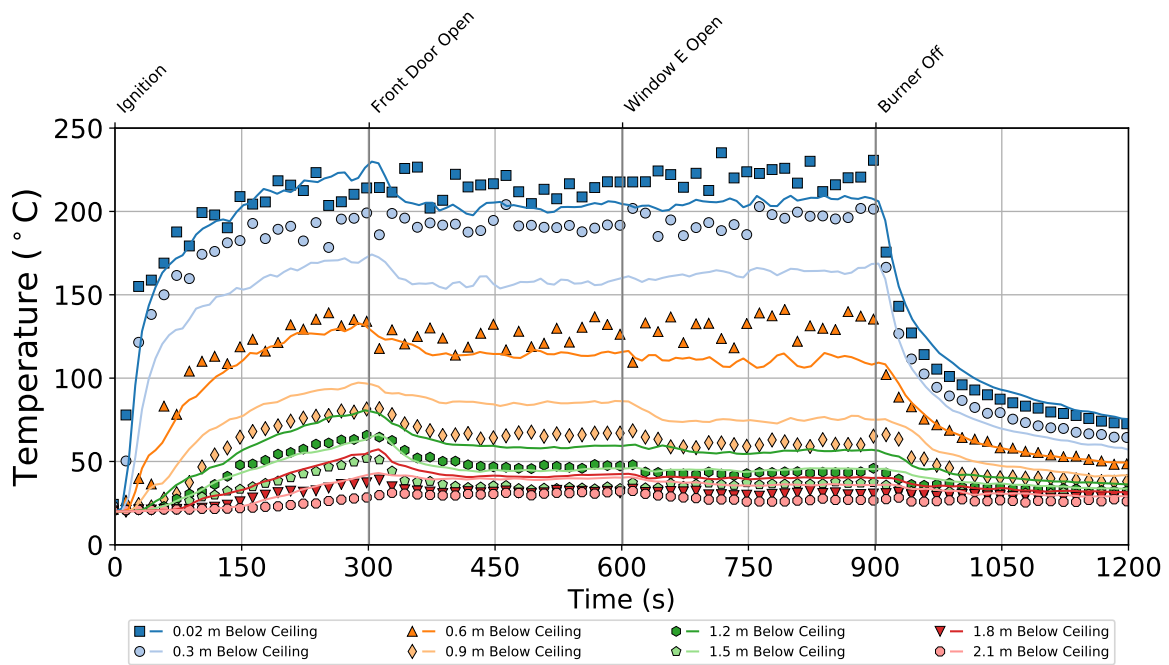


Figure 5.2: Temperatures in the hallway of the single-story structure during Experiment 1

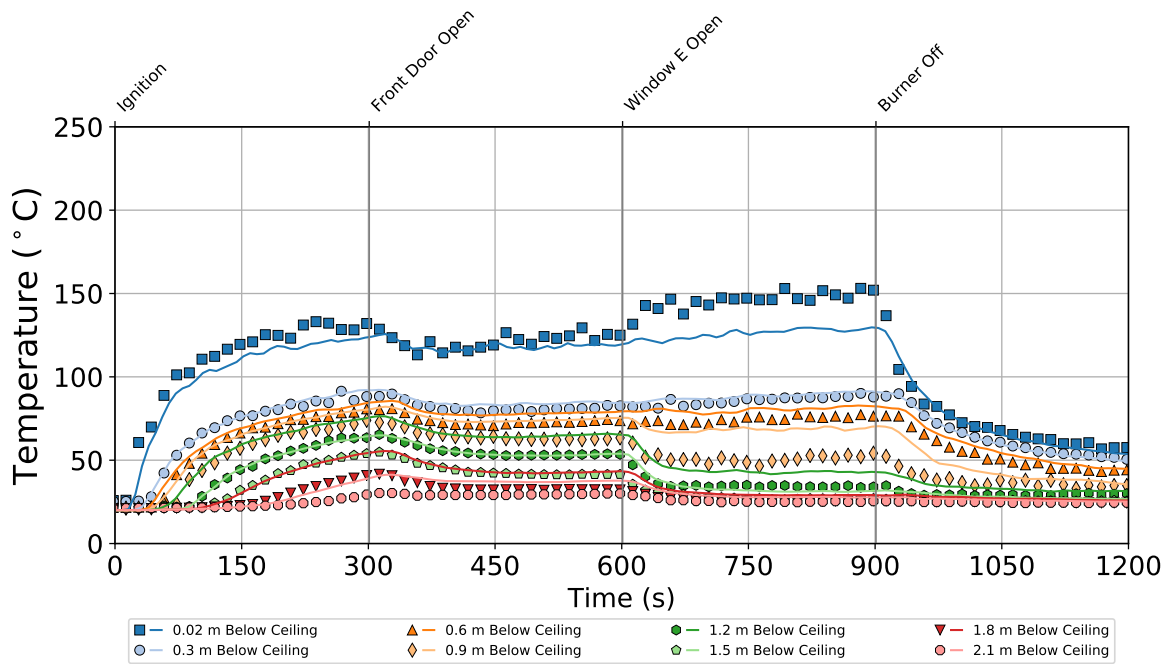


Figure 5.3: Temperatures in bedroom 1 of the single-story structure during Experiment 1

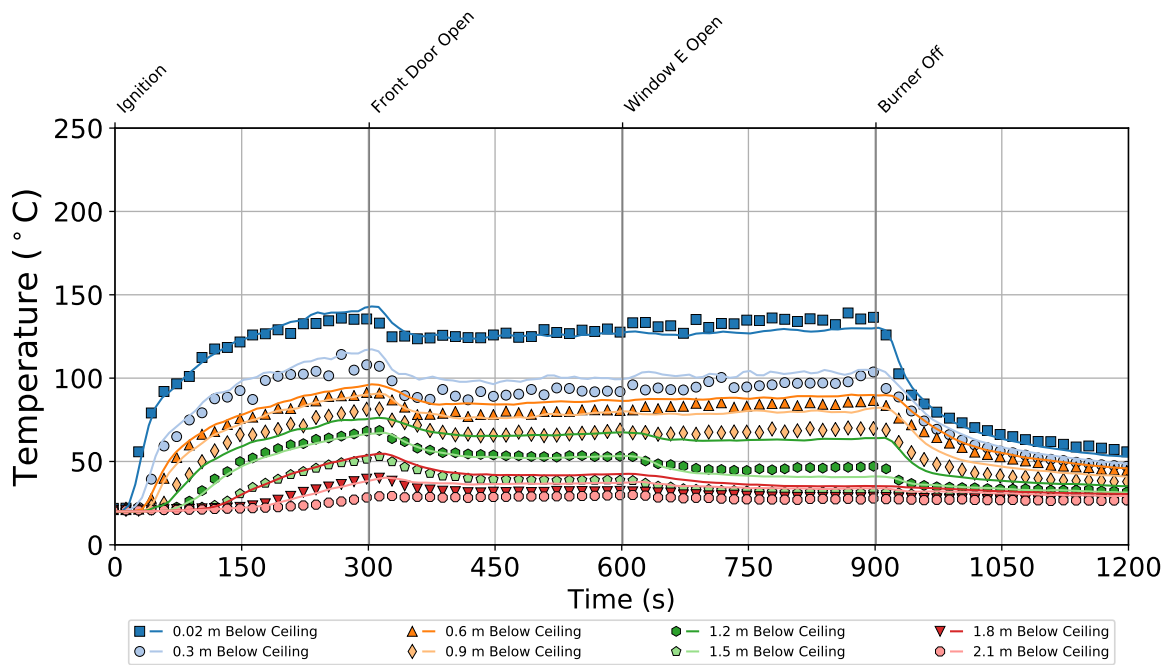


Figure 5.4: Temperatures in bedroom 2 of the single-story structure during Experiment 1

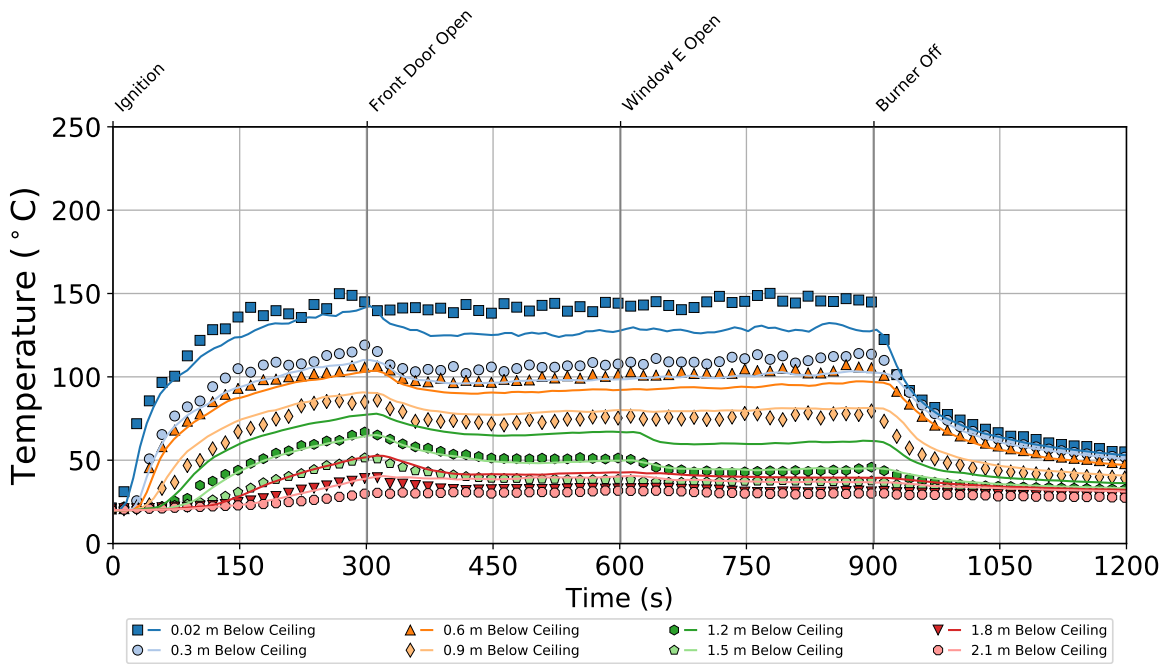


Figure 5.5: Temperatures in bedroom 3 of the single-story structure during Experiment 1

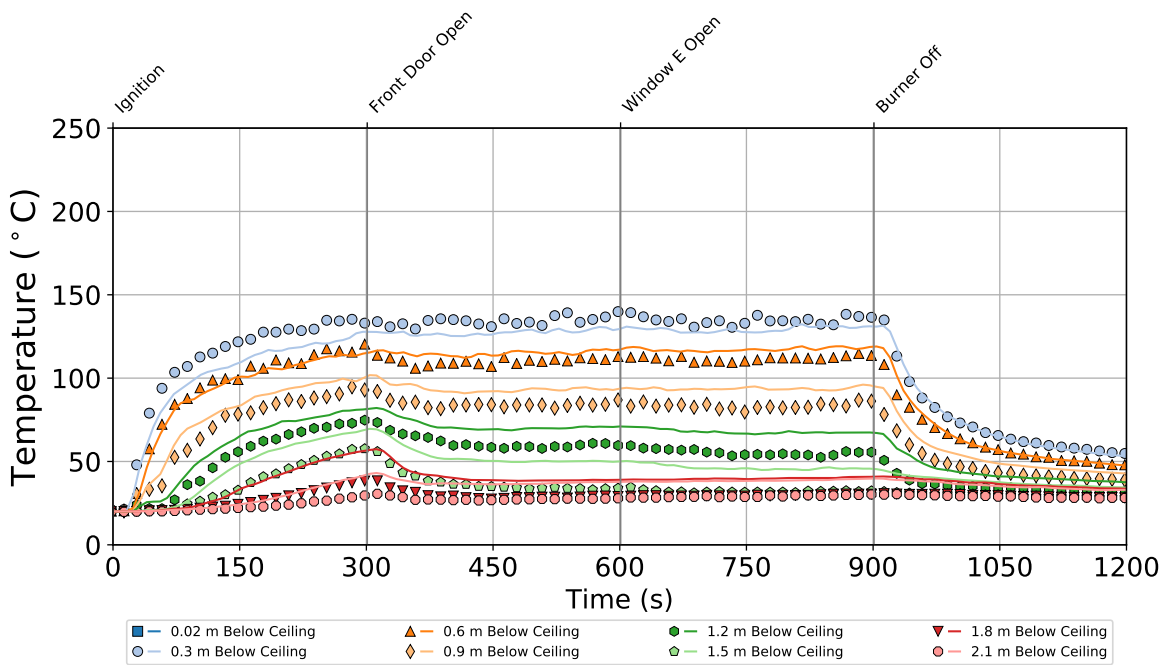


Figure 5.6: Temperatures in the kitchen of the single-story structure during Experiment 1

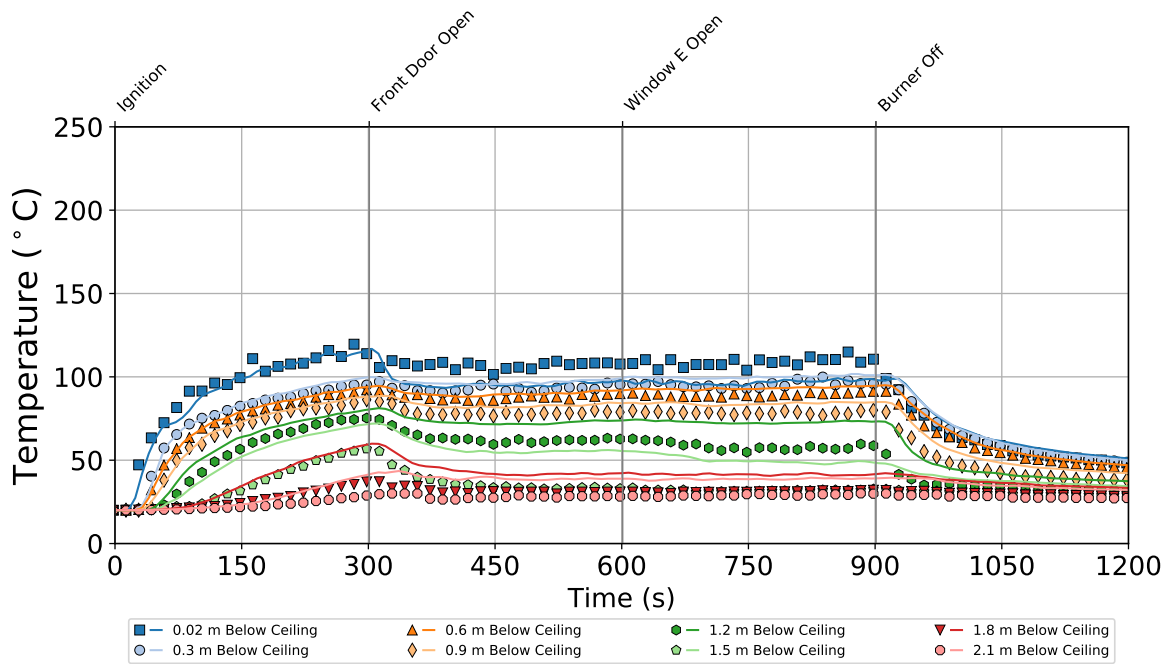


Figure 5.7: Temperatures in the breakfast area of the single-story structure during Experiment 1

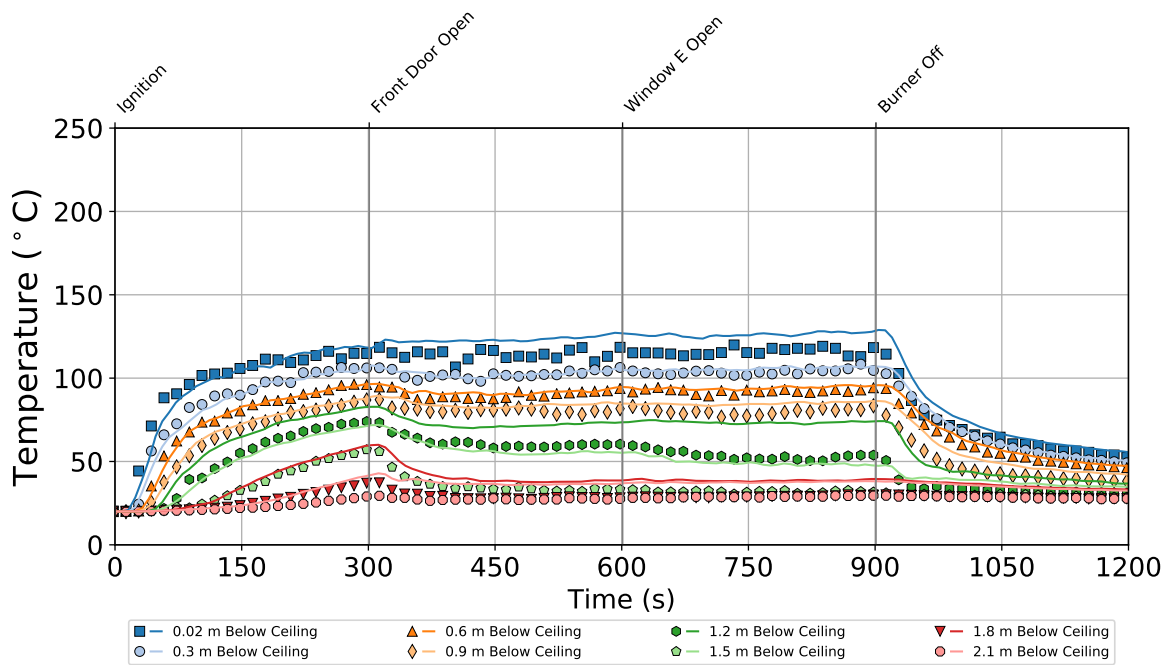


Figure 5.8: Temperatures in the dining room of the single-story structure during Experiment 1

All temperature measurements steadily increased until the front door was opened. At the point the front door was opened, all temperatures decreased or remained steady as bi-directional flow through the front door allowed cool air to enter the structure and hot products of combustion to exit the structure. The gas temperatures were allowed to reach approximately steady values and window E in bedroom 1 was opened. Opening window E created a flow path between the window and the burner that introduced air at low elevation and drove hot gases at high elevation out the window. All temperatures in the other compartments were largely unaffected by opening window E, particularly measurements made 0.9 m below the ceiling and at higher elevations.

The effect of this new flow path on the temperatures in the living room, hallway, and bedroom 1 was generally an increase in temperature for the measurements made 0.6 m below the ceiling and at higher elevations and a decrease in temperature for measurements at lower elevations. These trends indicate that hot gases were carried from the living room to the hallway and bedroom 1 at high elevation, and that additional cool air entered the structure through the open window and flowed toward the burner, cooling the thermocouples along the flow path at elevations closer to the floor.

After the temperatures reached a steady state, the gas supply to the burner was stopped and all temperatures throughout the structure dropped precipitously toward ambient temperature. Throughout the experiment, the temperatures in the bedrooms, dining room, kitchen, and breakfast area were in the range of ambient temperature to 150°C and the temperatures in the hallway and living room ranged from ambient temperature to approximately 230°C.

In general, the model accurately predicted the qualitative features in the data that resulted from the ventilation openings. The model accurately predicted the magnitude of the highest temperatures near the ceiling throughout the structure over the entire course of the experiment. The model underpredicted the experimental temperatures 0.3 m and 0.6 m below the ceiling in the living room and hallway. The model also slightly overpredicted the temperatures at elevations of 0.9 m below the ceiling and lower.

5.1.2 Experiment 1: Pressure

The pressure data collected throughout the structure are presented in the following figures. Figure 5.9 displays the pressures in the living room, where the burner was located, Figure 5.10 displays the pressures in bedroom 1, Figure 5.11 displays the pressures in bedroom 2, Figure 5.12 displays the pressures in bedroom 3, Figure 5.13 displays the pressures in the kitchen, and Figure 5.14 displays the pressures in the dining room. Note that a malfunction occurred which affected the pressure measured 2.1 m below the ceiling in bedroom 1, and these data have been excluded from Figure 5.10.

The pressure increased rapidly at ignition to a global maximum of approximately 17 Pa and quickly decreased to much lower positive pressures at all measurement locations. Venting the front door resulted in a decrease of all measured pressures as high temperature gases were allowed to exhaust through the front door, cool air was introduced, and flow velocities throughout the structure

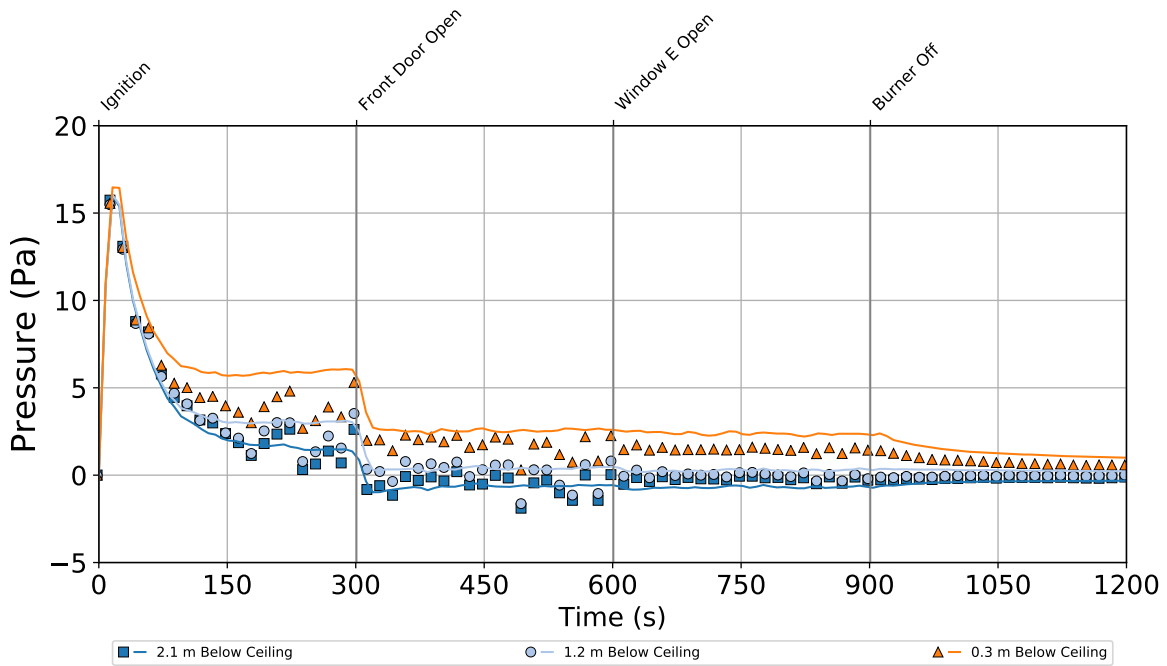


Figure 5.9: Pressures in the living room of the single-story structure during Experiment 1

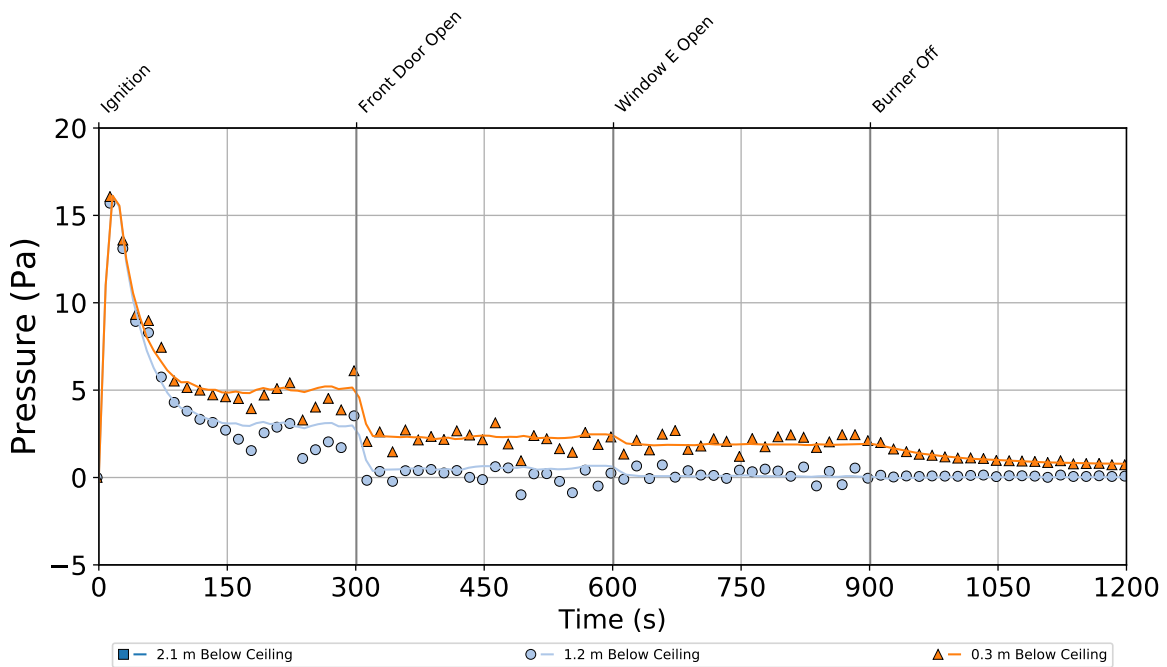


Figure 5.10: Pressures in bedroom 1 of the single-story structure during Experiment 1

increased. The pressures ranged between -5 Pa and 5 Pa from the point that the front door was opened to the end of the experiment. At each ventilation event the pressures throughout the struc-

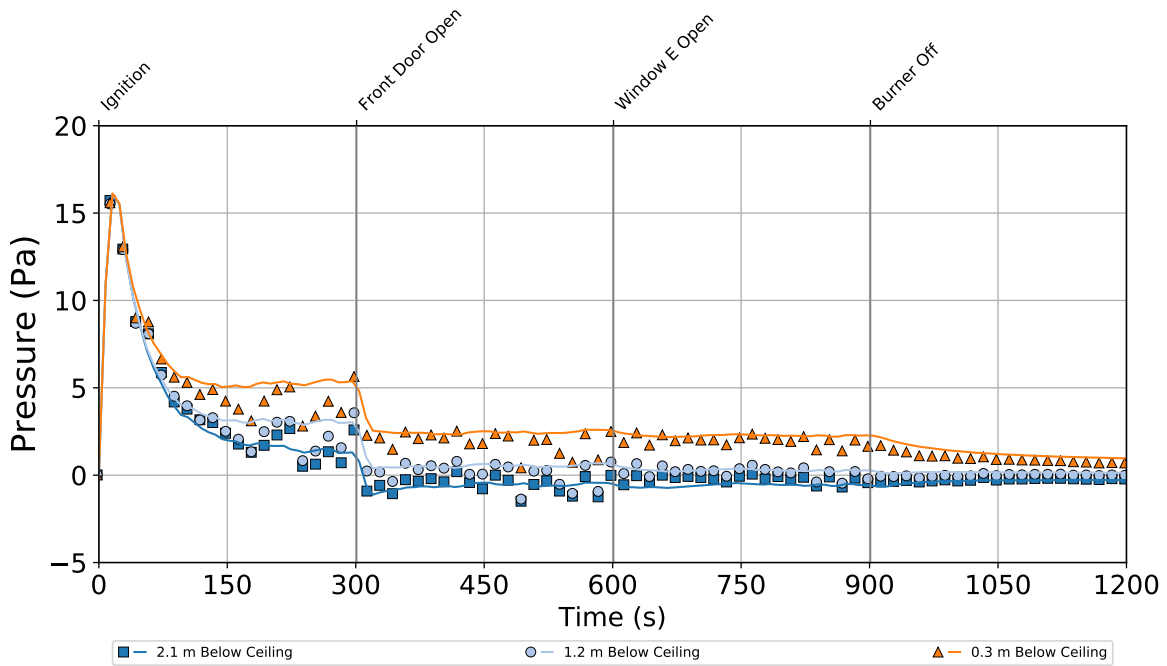


Figure 5.11: Pressures in bedroom 2 of the single-story structure during Experiment 1

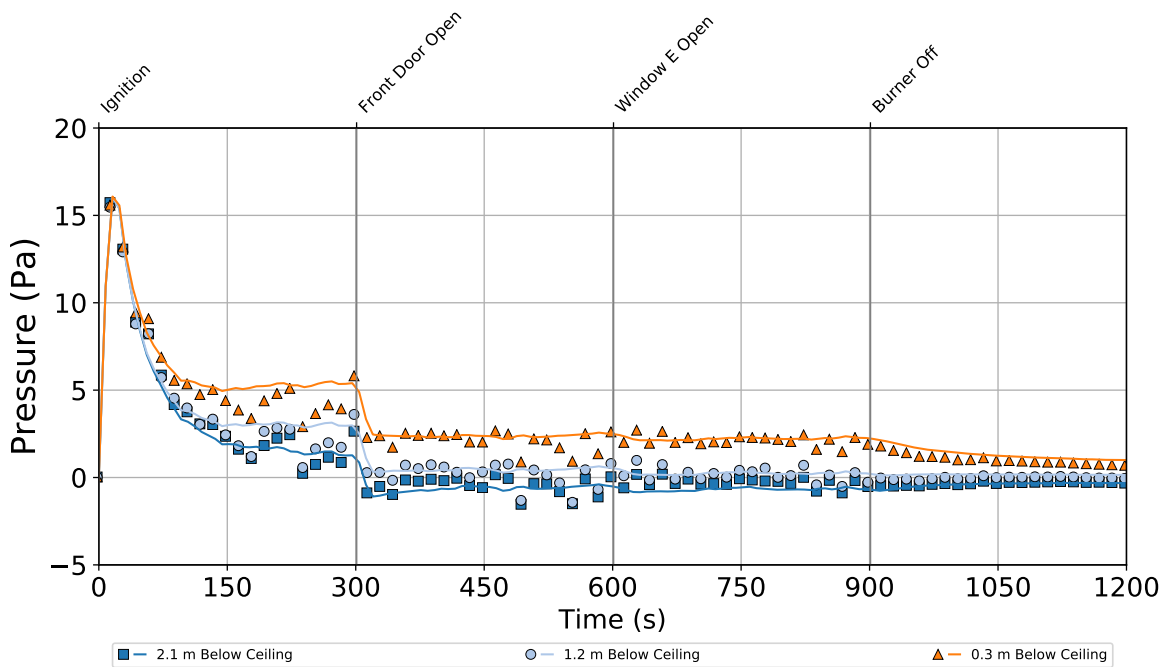


Figure 5.12: Pressures in bedroom 3 of the single-story structure during Experiment 1

ture changed by a relatively small amount to be closer to atmospheric pressure or remained at approximately the same magnitude.

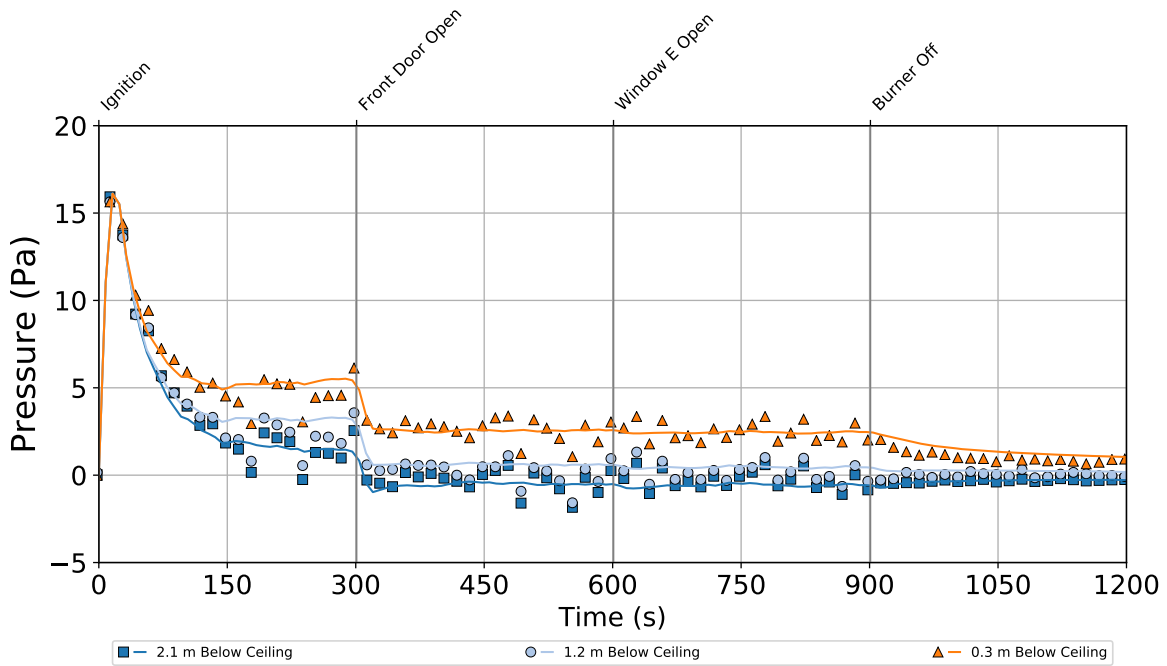


Figure 5.13: Pressures in the kitchen of the single-story structure during Experiment 1

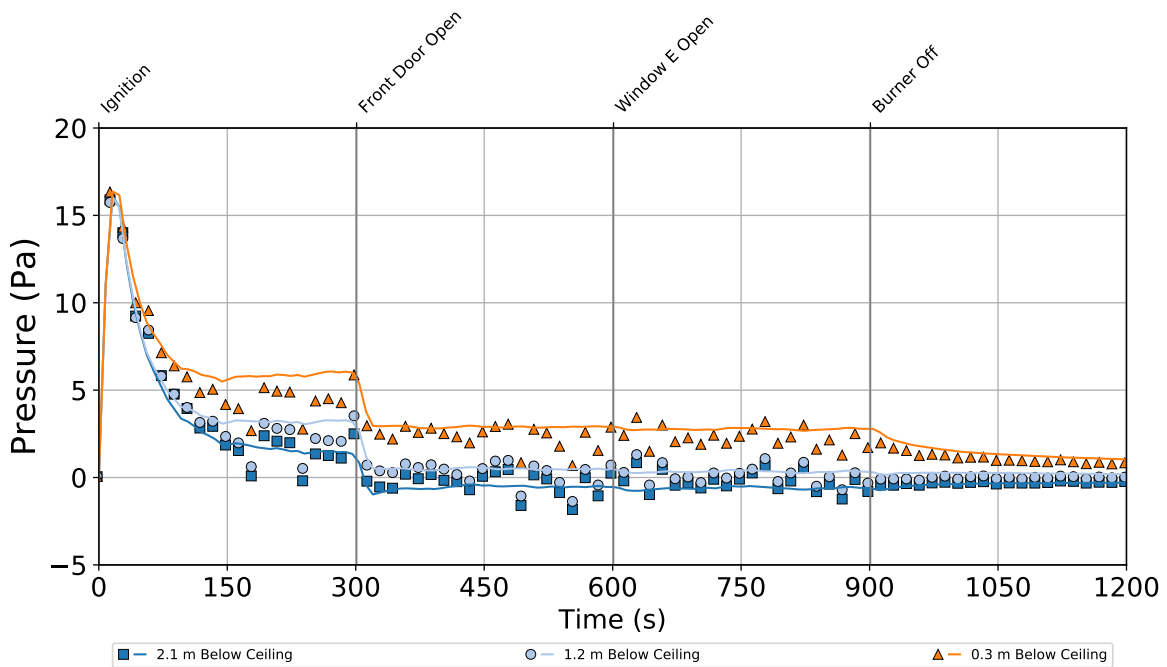


Figure 5.14: Pressures in the dining room of the single-story structure during Experiment 1

The model generally agreed qualitatively with the trends in the experimental data. The model predictions also agreed quantitatively with the peak pressure magnitude. The magnitudes of the

pressures were accurately predicted by the model and the effects of the ventilation events were also captured by the model.

5.1.3 Experiment 1: Velocity

The velocity data collected throughout the structure are presented in the following figures. Figure 5.15 displays the velocities measured in the hallway that connected the living room to the bedrooms, Figure 5.16 displays the velocities at the front door, and Figure 5.17 displays the velocities at window E in bedroom 1. The velocity profiles for the exterior doors and windows are plotted such that positive flows correspond to gases flowing out of the structure. The velocity profile for the hallway is plotted such that positive flows correspond to the positive x-direction (away from the living room) in Figure 3.1.

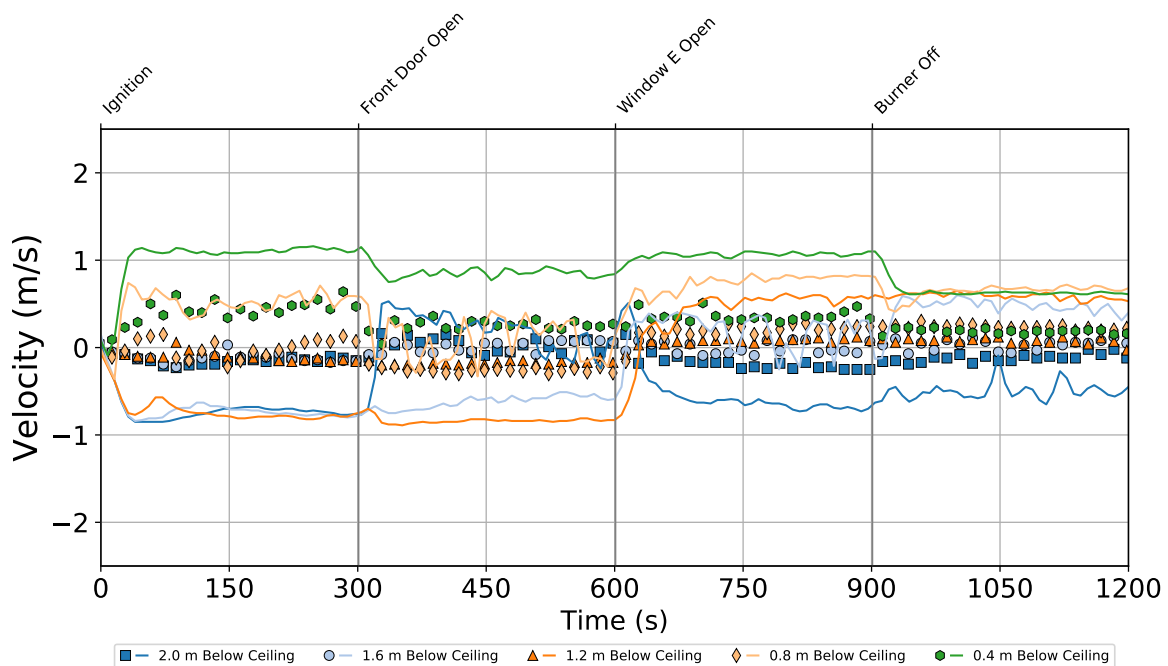


Figure 5.15: Velocities measured in the hallway of the single-story structure during Experiment 1

Conditions in the hallway were quiescent just after ignition with relatively low magnitude flow away from the living room at the uppermost measurement location. The gases in the hallway remained in relatively quiescent conditions after the front door was opened, but there was some apparent recirculation that occurred in the hallway as indicated by relatively low velocity flow in the same direction measured at both 0.4 m and 2.0 m below the ceiling and flow in the opposite direction 0.8 m and 1.2 m below the ceiling. After window E was opened, a new flow path was created where the hot gases at the ceiling flowed away from the living room and the gases at the lowest two measurement elevations flowed toward the living room, with the middle measurement location indicating quiescent conditions as the neutral plane. After the gas flow to the burner was stopped, the flow directions remained unchanged although the magnitudes of flow decreased.

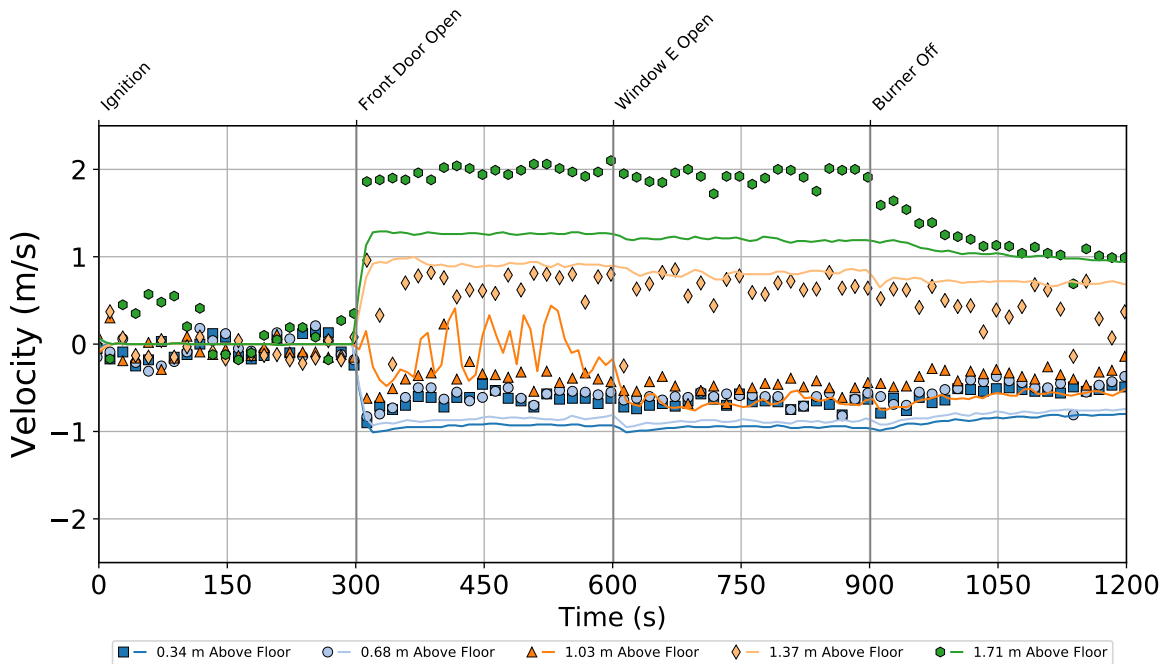


Figure 5.16: Velocities measured in the front door of the single-story structure during Experiment 1

Conditions at the front door were quiescent after ignition but prior to the time when the front door was opened. After the front door was opened, bi-directional flow was immediately evident with relatively high velocity flows out of the structure at the highest two measurement elevations and lower velocity flow 1.03 m above the floor and at lower elevations. This trend remained with little change in magnitude after window E was opened.

Conditions were quiescent at window E in bedroom 1 up to the point when window E was opened. After the window was opened, bi-directional flow was immediately evident with relatively low velocity flows into the structure at the lowest two measurement elevations and higher velocity flow out of the structure 0.72 m above the window sill and at higher elevations. The location of the neutral plane for flow through window E was located at the approximate center of the window from the time that window E was opened to the end of the experiment.

The model accurately predicted the qualitative features of the data and the effect of opening the exterior windows and doors on the directions of flow and relative changes in flow magnitude. The model generally overpredicted the magnitudes of all flow velocities. The one notable exception was an underprediction of the high velocity flow 1.71 m above the floor out of the front door. The predictions of flow velocities in the hallway throughout the experiment indicated relatively strong bi-directional flow immediately following ignition with minor changes in magnitude throughout the remainder of the experiment. The measured velocities indicate lower velocity uni-directional flow between ignition and opening of the front door, which transitioned to circulating flow and weak bi-directional flow after the ventilation events that followed. These predictions are problem-

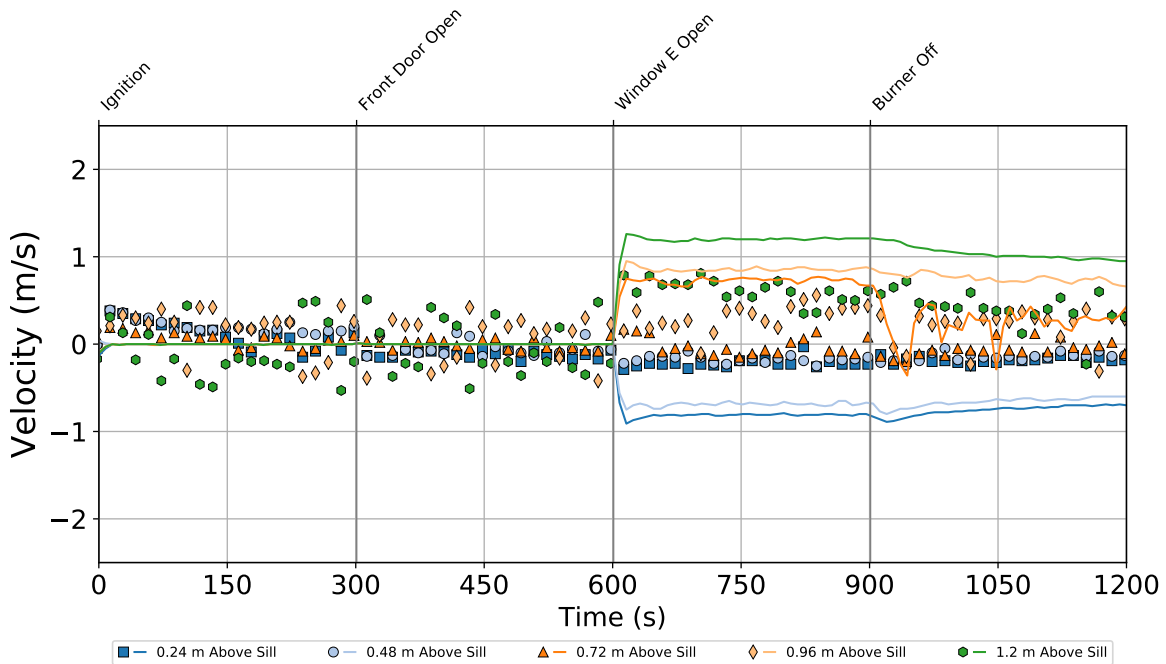


Figure 5.17: Velocities measured in window E of the single-story structure during Experiment 1

atic and indicate an unresolved issue with the bi-directional probes used to measure velocities, the model parameters used in these simulations, or the with the model.

5.2 Single-Story: Experiment 2

Experiment 2 conducted in the single-story structure featured the 250 kW gas burner ignited for 1500 s as well as ventilation of window E (600 s), window C (900 s), and the front door (1200 s).

5.2.1 Experiment 2: Temperature

The temperature data collected by thermocouple arrays throughout the structure are presented in the following figures. Figure 5.18 displays the temperatures in the living room, where the burner was located, Figure 5.19 displays the temperatures in the hallway that connected all of the bedrooms, Figure 5.20 displays the temperatures in bedroom 1, Figure 5.21 displays the temperatures in bedroom 2, Figure 5.22 displays the temperatures in bedroom 3, Figure 5.23 displays the temperatures in the kitchen, Figure 5.24 displays the temperatures in the breakfast area, and Figure 5.25 displays the temperatures in the dining room. Note that a malfunction occurred which affected the temperature measured 0.02 m below the ceiling in the kitchen, and these data have been excluded from Figure 5.23.

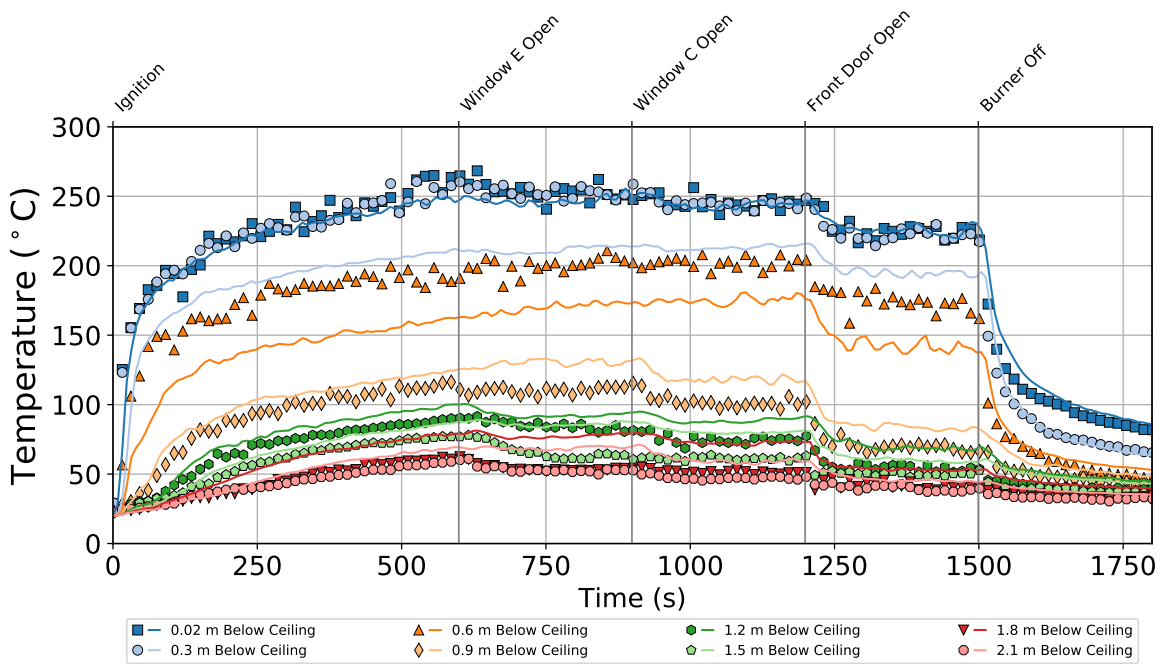


Figure 5.18: Temperatures in the living room of the single-story structure during Experiment 2

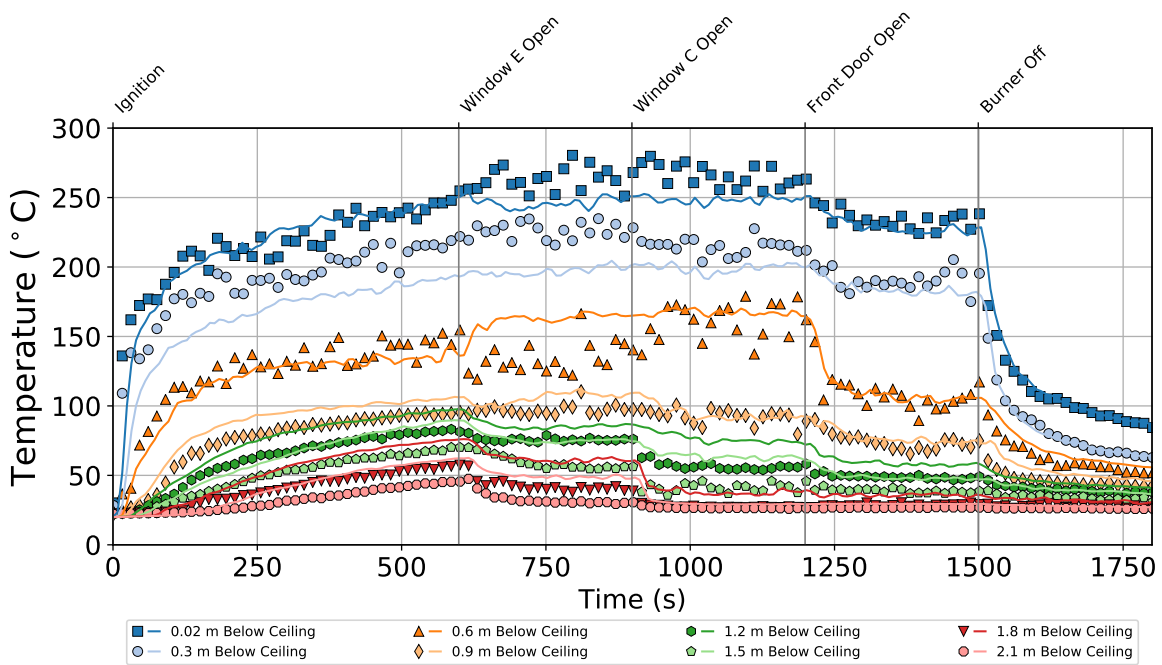


Figure 5.19: Temperatures in the hallway of the single-story structure during Experiment 2

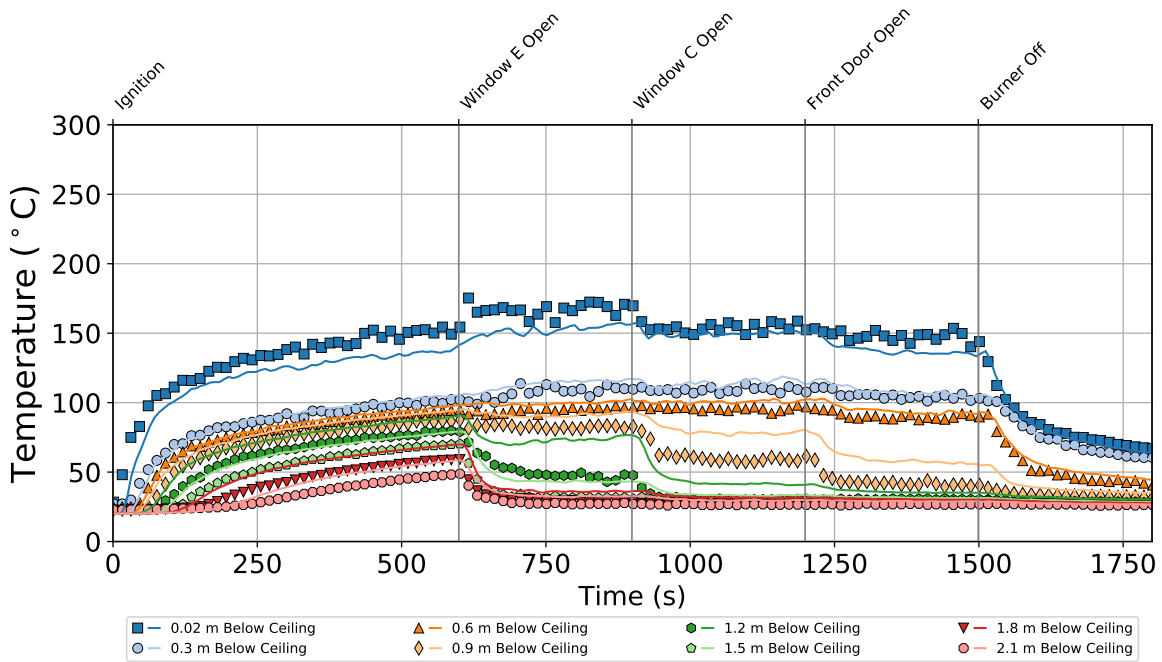


Figure 5.20: Temperatures in bedroom 1 of the single-story structure during Experiment 2

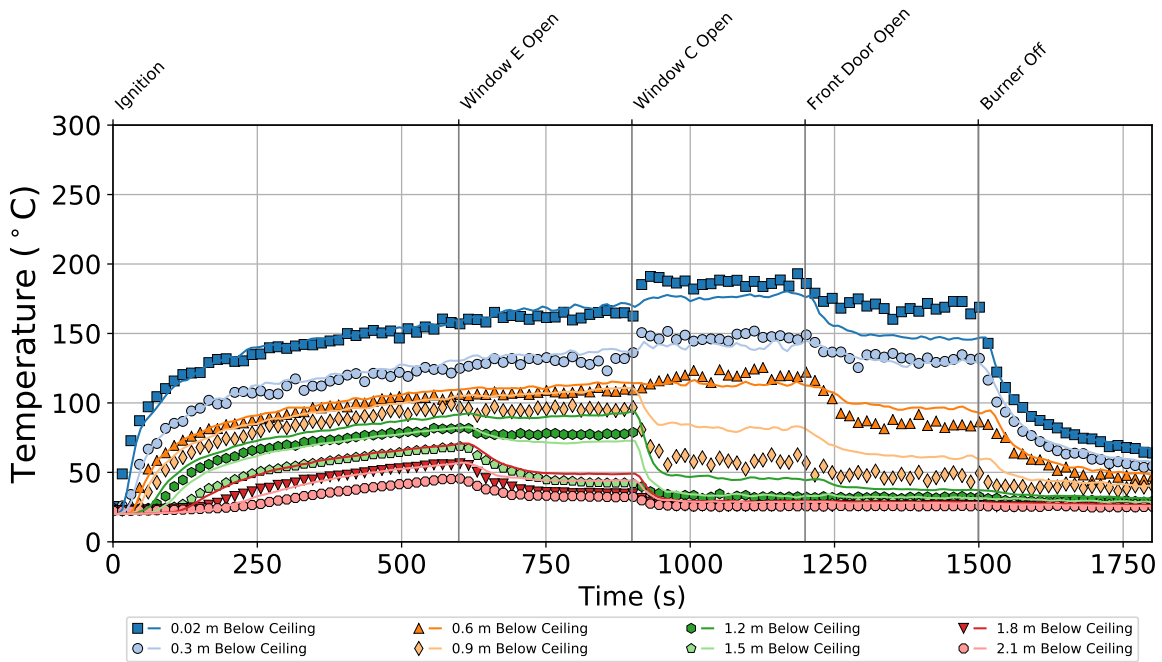


Figure 5.21: Temperatures in bedroom 2 of the single-story structure during Experiment 2

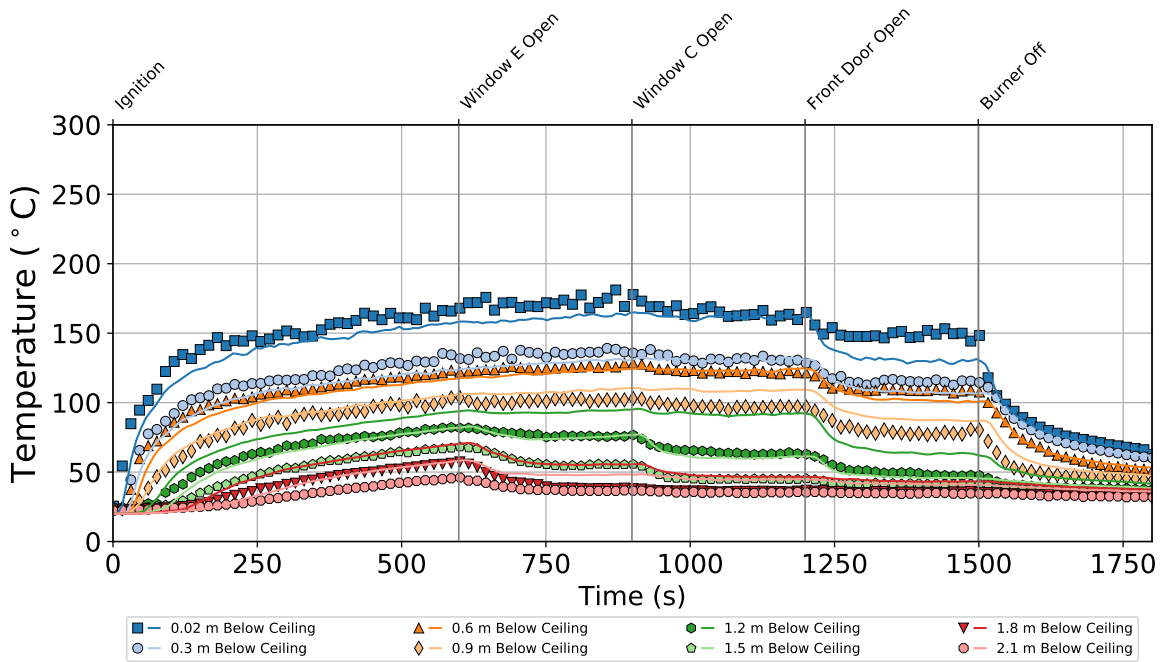


Figure 5.22: Temperatures in bedroom 3 of the single-story structure during Experiment 2

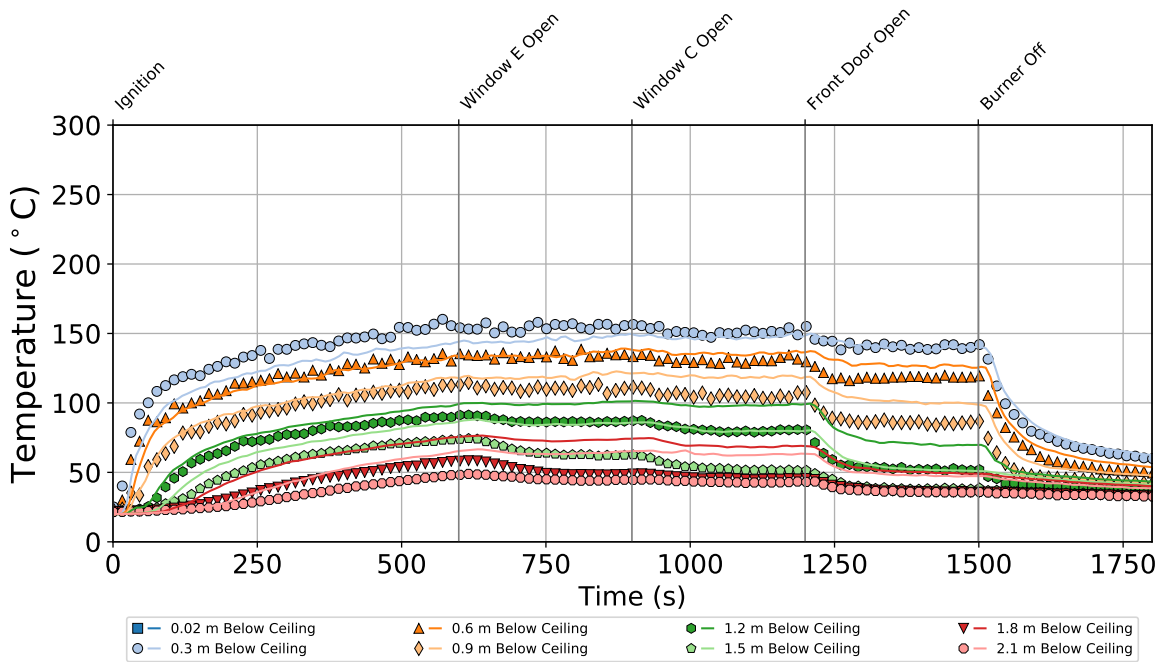


Figure 5.23: Temperatures in the kitchen of the single-story structure during Experiment 2

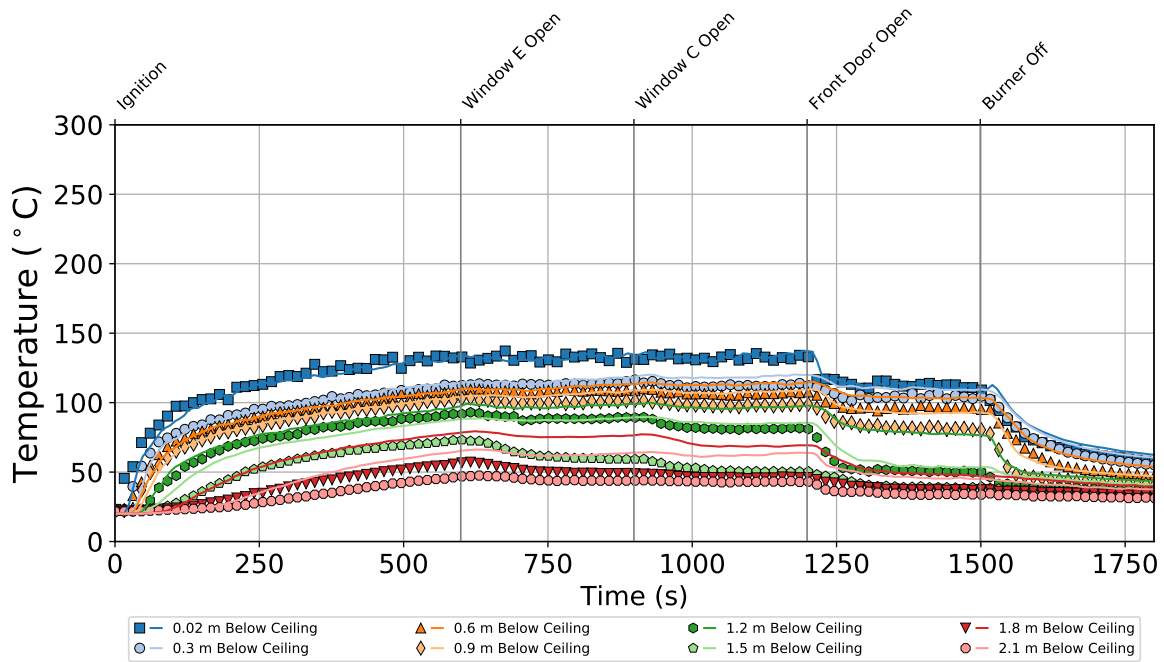


Figure 5.24: Temperatures in the breakfast area of the single-story structure during Experiment 2

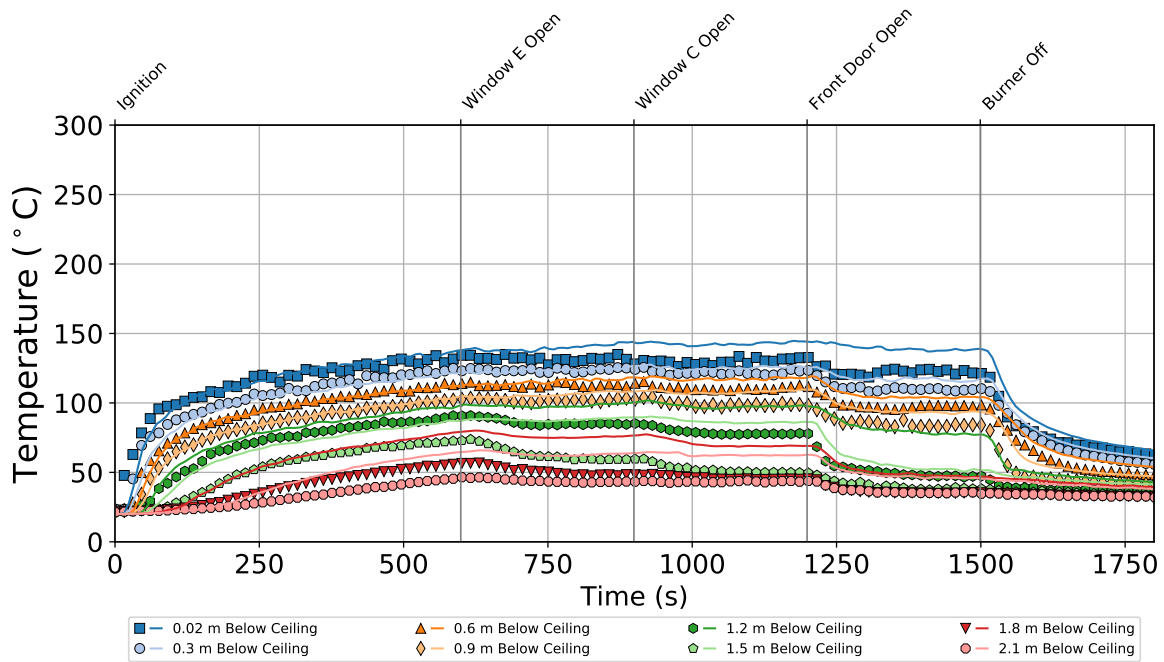


Figure 5.25: Temperatures in the dining room of the single-story structure during Experiment 2

All temperature measurements steadily increased until window E was opened. When window E was opened, all temperatures 0.9 m below the ceiling and at lower elevations throughout the structure decreased or remained steady. The temperatures measured at higher elevations in the hallway and bedrooms increased and the temperatures remained steady at all other measurement positions on the opposite side of the structure from the bedrooms. This indicates bi-directional flow through window E as cool outside air entered the structure through the window and cooled the gases at low elevations while the hot gases exited the structure, which prompted flow throughout the structure that resulted in temperature increases, particularly in bedroom 1. These trends also indicate the development of a two-layer system throughout the structure as the temperatures stratified into a high temperature layer at high elevation and a low temperature layer at low elevation.

After window C in bedroom 2 was opened, the temperatures throughout the structure either remained steady or decreased, with the exception of the temperatures in bedroom 2. The temperatures measured 0.6 m below the ceiling and at higher elevations in bedroom 2 increased, while the temperatures measured at lower elevations decreased. This increase in the gas temperatures near the ceiling was expected because bedroom 2 did not facilitate any flow prior to opening window C. These trends in the temperature data indicate that the new flow path generated between window C and the burner did not dominate the flow in the structure. When the front door was opened, all temperatures measured throughout the structure decreased. This decrease was likely due to the significant increase in ventilation area to exhaust hot gases and introduce cool air into the structure.

Over the course of the experiment, the temperatures in the bedrooms, dining room, kitchen, and breakfast area were in the range of room temperature to 170°C and the temperatures in the hallway and living room ranged from room temperature to approximately 280°C. Ventilation of window E and window C resulted in an increase of approximately 30°C at the highest elevation temperature measurements in bedroom 1 and bedroom 2, respectively.

In general, the model accurately predicted the qualitative features in the data that resulted from the ventilation openings. The model accurately predicted the magnitude of the highest temperatures near the ceiling throughout the structure over the entire course of the experiment. The model underpredicted the experimental temperatures 0.3 m and 0.6 m below the ceiling in the living room. The model also slightly overpredicted the temperatures at elevations of 0.9 m below the ceiling and lower, particularly after window E was opened.

5.2.2 Experiment 2: Pressure

The pressure data collected throughout the structure are presented in the following figures. Figure 5.26 displays the pressures in the living room, where the burner was located, Figure 5.27 displays the pressures in bedroom 1, Figure 5.28 displays the pressures in bedroom 2, Figure 5.29 displays the pressures in bedroom 3, Figure 5.30 displays the pressures in the kitchen, and Figure 5.31 displays the pressures in the dining room. Note that a malfunction occurred which affected the pressure measured 2.1 m below the ceiling in bedroom 1, and these data have been excluded from Figure 5.27.

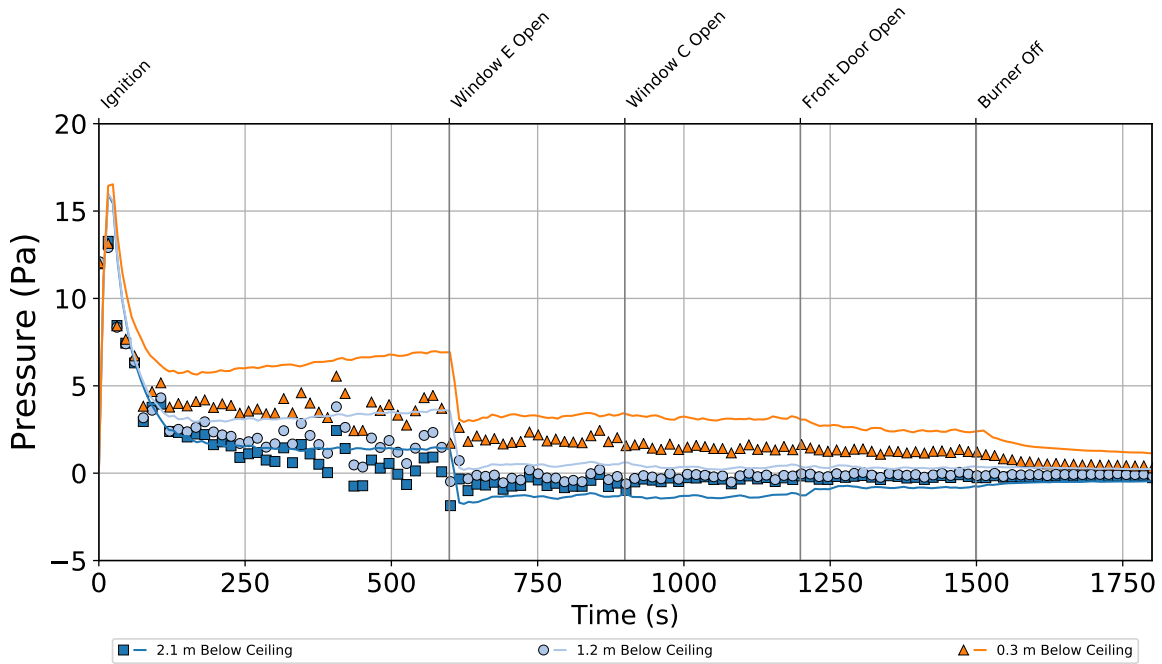


Figure 5.26: Pressures in the living room of the single-story structure during Experiment 2

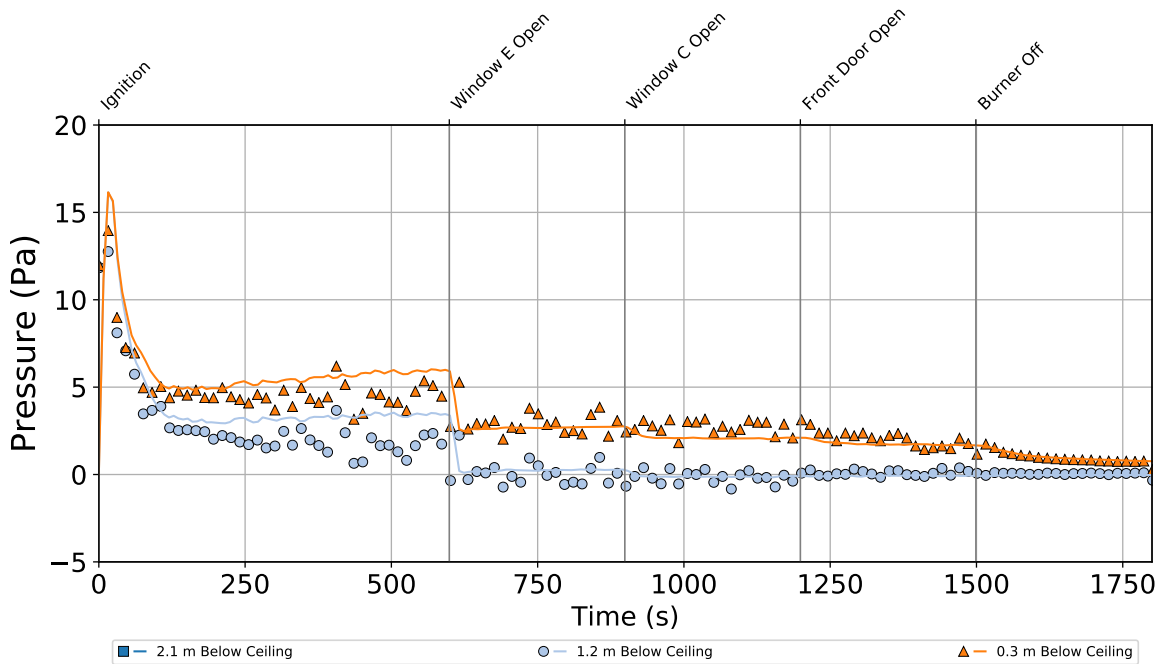


Figure 5.27: Pressures in bedroom 1 of the single-story structure during Experiment 2

The pressures in all measurement locations increased rapidly at ignition to a global maximum in the range of 12 Pa to 15 Pa and very quickly decreased to lower positive pressures. When window E

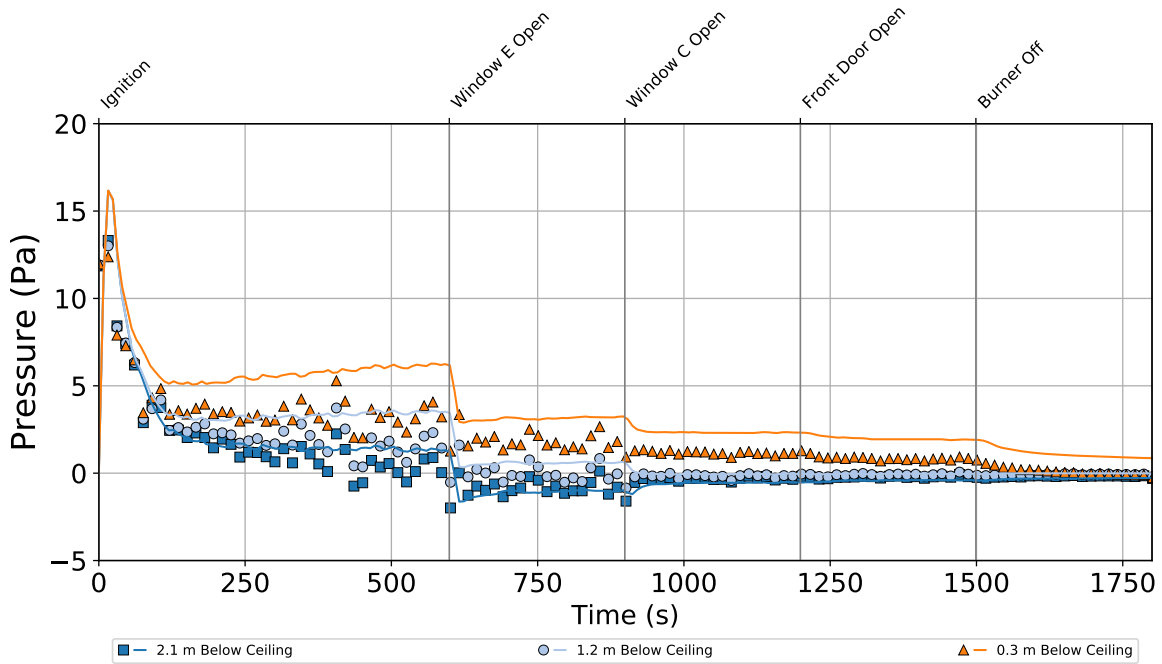


Figure 5.28: Pressures in bedroom 2 of the single-story structure during Experiment 2

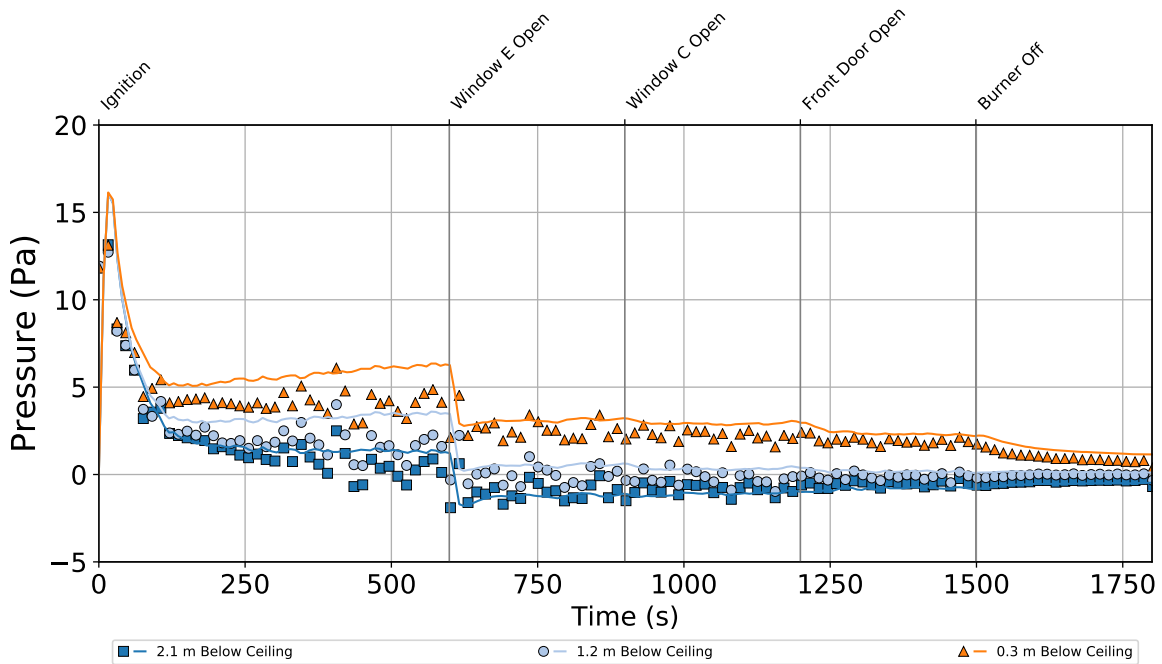


Figure 5.29: Pressures in bedroom 3 of the single-story structure during Experiment 2

was opened, the pressures at all locations decreased such that measurements at the lowest elevation (2.1 m below the ceiling) were below atmospheric and all pressures remained within the range of

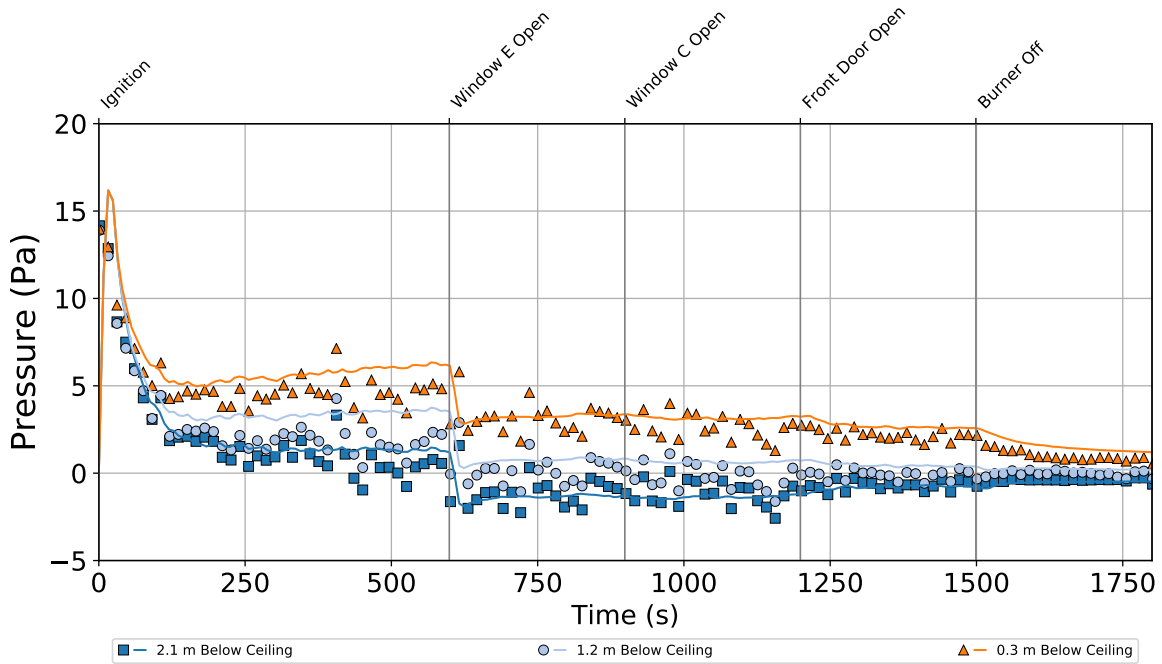


Figure 5.30: Pressures in the kitchen of the single-story structure during Experiment 2

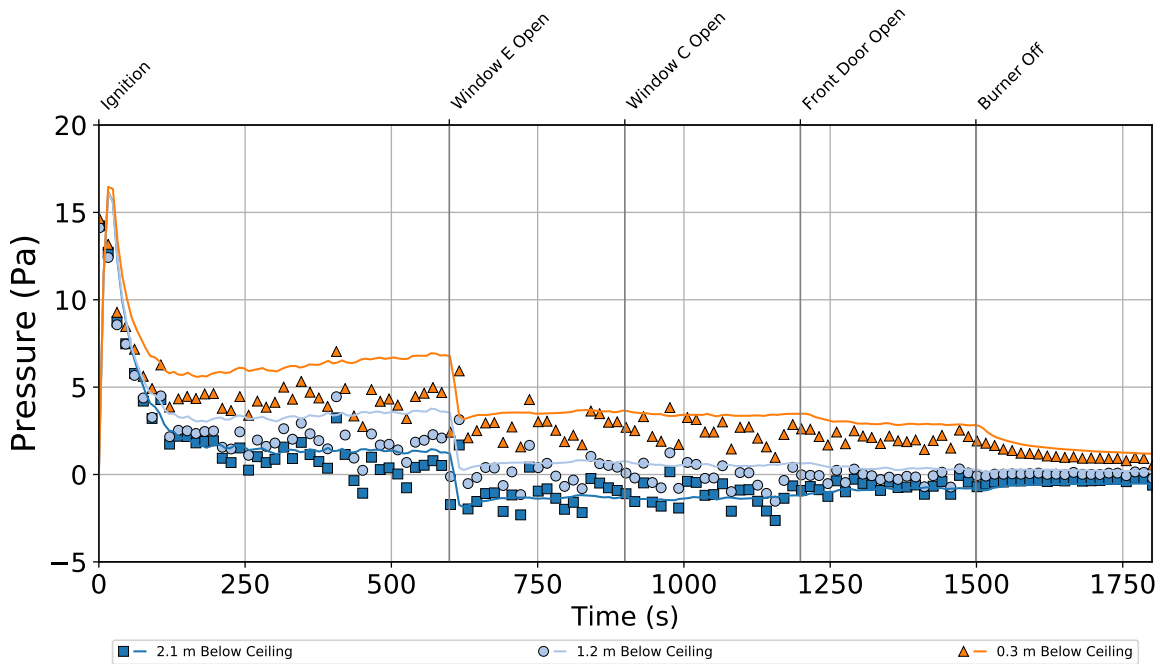


Figure 5.31: Pressures in the dining room of the single-story structure during Experiment 2

-5 Pa to 5 Pa until the end of the experiment.

At each successive ventilation event the pressure magnitudes throughout the structure either changed to be closer to atmospheric pressure by some relatively small amount or remained at the same magnitude. The model generally agreed qualitatively with the trends in the experimental data. The magnitudes of the pressures were generally accurately predicted by the model and the effects of the ventilation events were also generally captured by the model. The pressures predicted 0.3 m below the ceiling steadily increased between ignition and venting window E, whereas this trend was not observed in the experimental data. This pressure increase over time may be an artifact of the method used to define leakage in the single-story structure.

5.2.3 Experiment 2: Velocity

The velocity data collected throughout the structure are presented in the following figures. Figure 5.32 displays the velocities measured in the hallway that connected the living room to the bedrooms, Figure 5.33 displays the velocities at window E in bedroom 1, and Figure 5.34 displays the velocities at the front door. The velocity profiles for the exterior doors and windows are plotted such that positive flows correspond to gases flowing out of the structure. The velocity profile for the hallway is plotted such that positive flows correspond to the positive x-direction in Figure 3.1 (away from the living room).

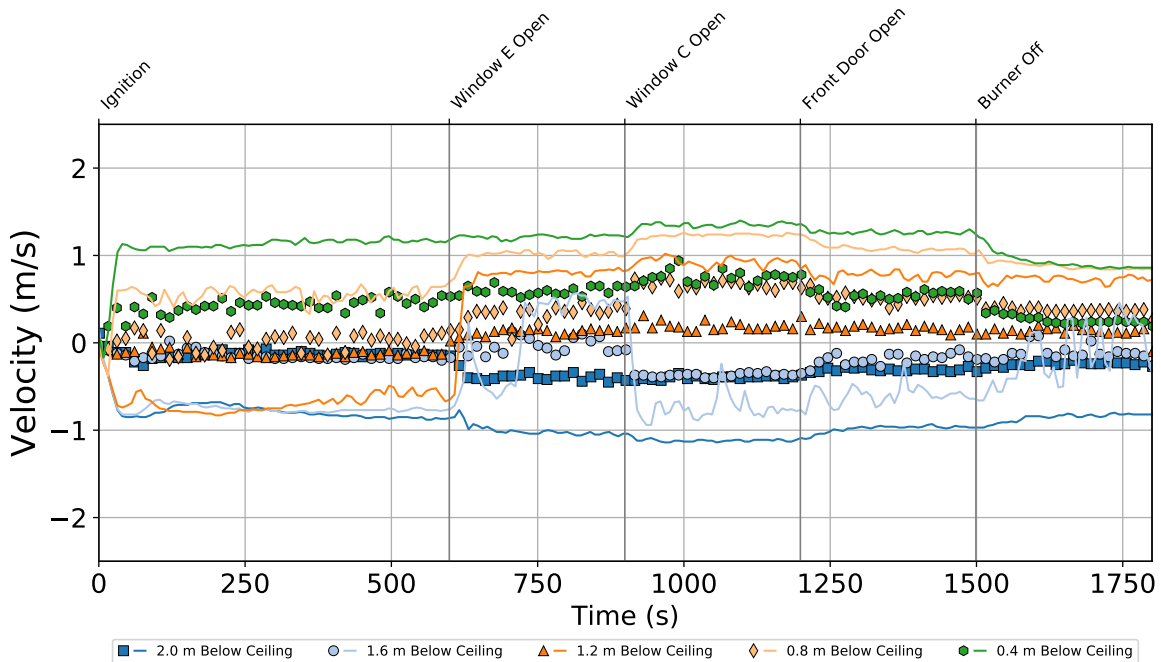


Figure 5.32: Velocities measured in the hallway of the single-story structure during Experiment 2

The gases in the hallway exhibited flow away from the living room 0.4 m below the ceiling just after ignition, all other measurement locations generally indicated quiescent conditions until window E was vented. Bi-directional flow was evident in the hallway after window E was opened with

hot gases at the ceiling flowing away from the living room and cooler air flowing toward the living room and the neutral plane approximately 1.6 m below the ceiling. Just after window C was opened, bi-directional flow in the hallway continued with larger velocity magnitudes in each direction due to the greater total ventilation area. After window C was vented, the neutral plane shifted upward such that it was between 1.2 m and 1.6 m below the ceiling. Venting of the front door resulted in lower magnitude flow through the hallway in each direction without changing the location of the neutral plane, and after the gas flow to the burner was stopped, the flow rates through the hallway decreased further.

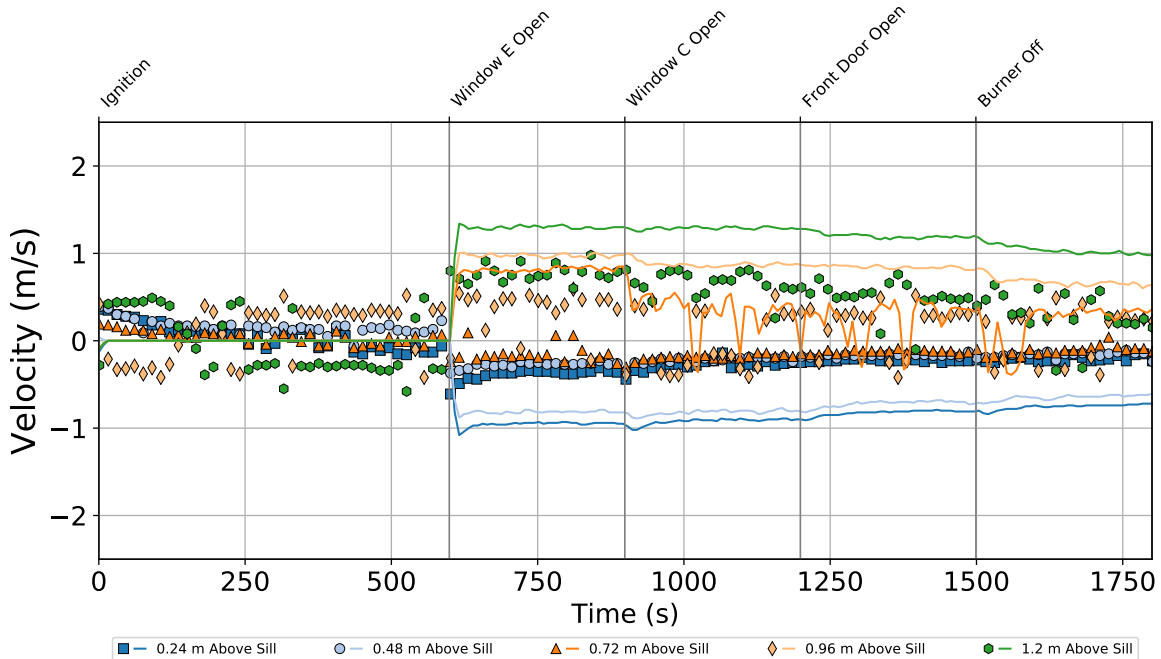


Figure 5.33: Velocities measured in window E of the single-story structure during Experiment 2

Quiescent conditions existed at window E in bedroom 1 until window E was opened. After the window was opened, bi-directional flow was immediately evident with relatively low velocity flows into the structure at the lowest three measurement elevations and higher velocity flow out of the structure at the top two measurement elevations, indicating the location of the neutral plane in the range of 0.72 m and 0.96 m above the window sill. As additional vents were opened, the magnitude of the flow out of window E diminished considerably to the point where flow at the top two measurement elevations oscillated between being directed into and out of the structure.

Flow conditions at the front door were quiescent after ignition and prior to the front door being opened. After the front door was opened, bi-directional flow was immediately evident with relatively high velocity flows out of the structure at the highest two measurement elevations and lower velocity flow into the structure at the lower elevation measurement locations, indicating the location of the neutral plane in the range of 1.03 m to 1.37 m above the floor. This trend remained with little change in magnitude until the gas flow to the burner was stopped.

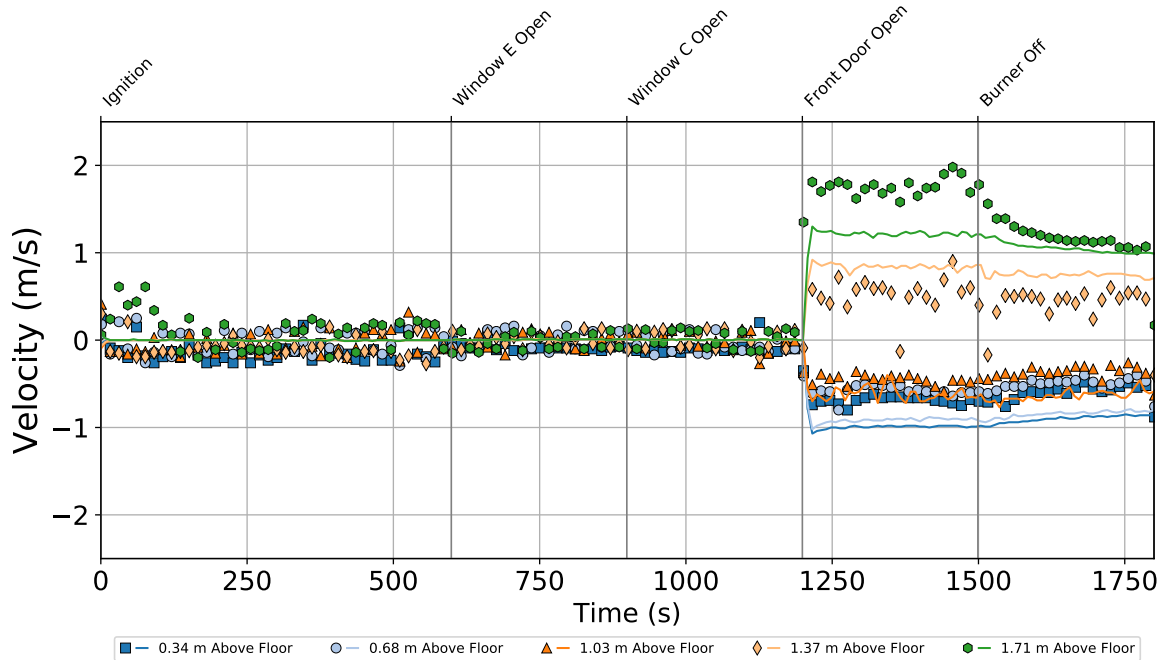


Figure 5.34: Velocities measured in the front door of the single-story structure during Experiment 2

The model generally accurately predicted the qualitative features of the data and the effect of opening the exterior windows and doors on the directions of flow and relative changes in flow velocity magnitude. The model generally overpredicted the magnitudes of all flow velocities. A notable exception was an underprediction of the high velocity flow out the front door at the uppermost measurement elevation after the front door was opened. The model also inaccurately predicted flow out of window E and oscillations between inward and outward flow 0.72 m above the window sill just after window C was opened whereas flow was actually directed into the structure at this elevation.

A similar trend between the experimental data and the model predictions for the flow velocities in the hallway that was described in section 5.1.3 was also evident in Experiment 2. The predictions of flow velocities in the hallway between ignition and ventilation of window E indicated relatively strong bi-directional flow immediately following ignition with minor changes in magnitude throughout the remainder of the experiment. The measured velocities indicate lower velocity uni-directional flow prior to window E opening. Additionally, the flow magnitudes were overpredicted for the remainder of the experiment after window E was opened. These predictions are problematic and indicate an unresolved issue with the bi-directional probes used to measure velocities, the model parameters used in these simulations, or with the model.

5.3 Single-Story: Experiment 3

Experiment 3 conducted in the single-story structure featured the 250 kW gas burner ignited for 900 s as well as ventilation of the back door (300 s) and window E (600 s).

5.3.1 Experiment 3: Temperature

The temperature data collected by thermocouple arrays throughout the structure are presented in the following figures. Figure 5.35 displays the temperatures in the living room, where the burner was located, Figure 5.36 displays the temperatures in the hallway that connected all of the bedrooms, Figure 5.37 displays the temperatures in bedroom 1, Figure 5.38 displays the temperatures in bedroom 2, Figure 5.39 displays the temperatures in bedroom 3, Figure 5.40 displays the temperatures in the kitchen, Figure 5.41 displays the temperatures in the breakfast area, and Figure 5.42 displays the temperatures in the dining room. Note that a malfunction occurred which affected the temperature measured 0.02 m below the ceiling in the kitchen, and these data have been excluded from Figure 5.23.

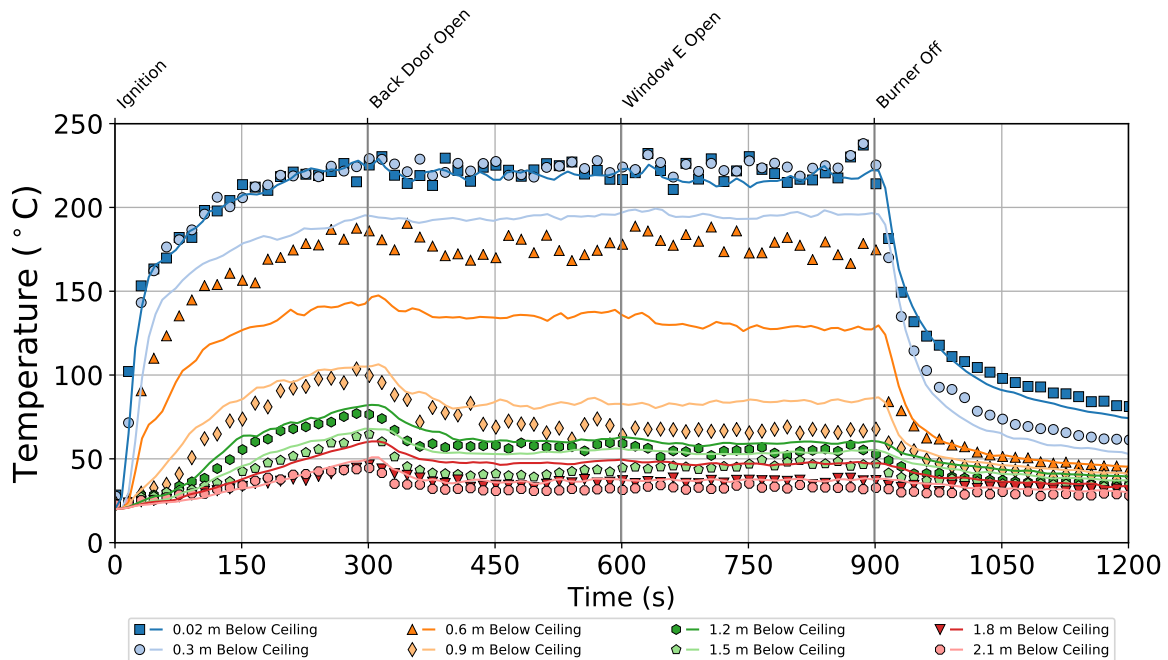


Figure 5.35: Temperatures in the living room of the single-story structure during Experiment 3

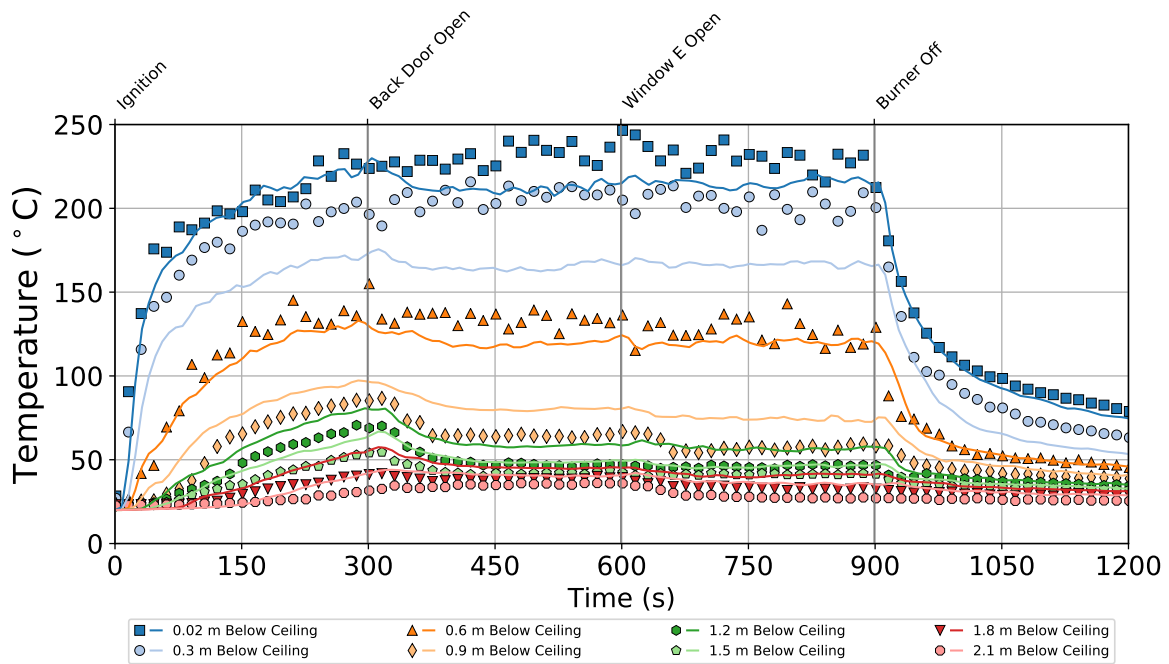


Figure 5.36: Temperatures in the hallway of the single-story structure during Experiment 3

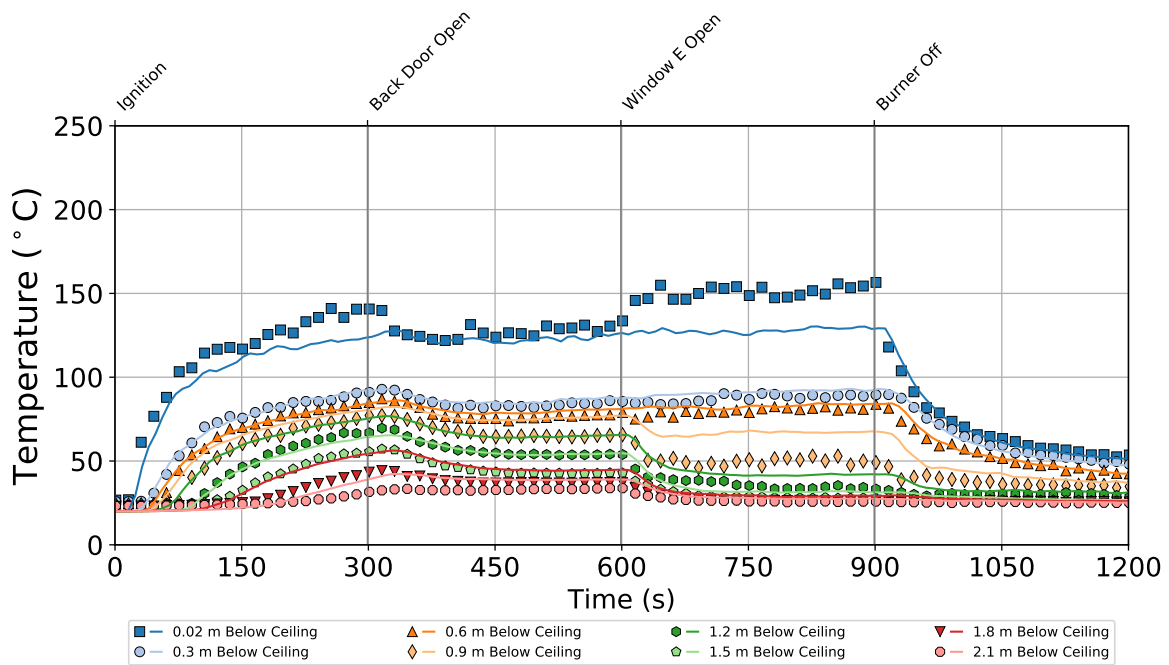


Figure 5.37: Temperatures in bedroom 1 of the single-story structure during Experiment 3

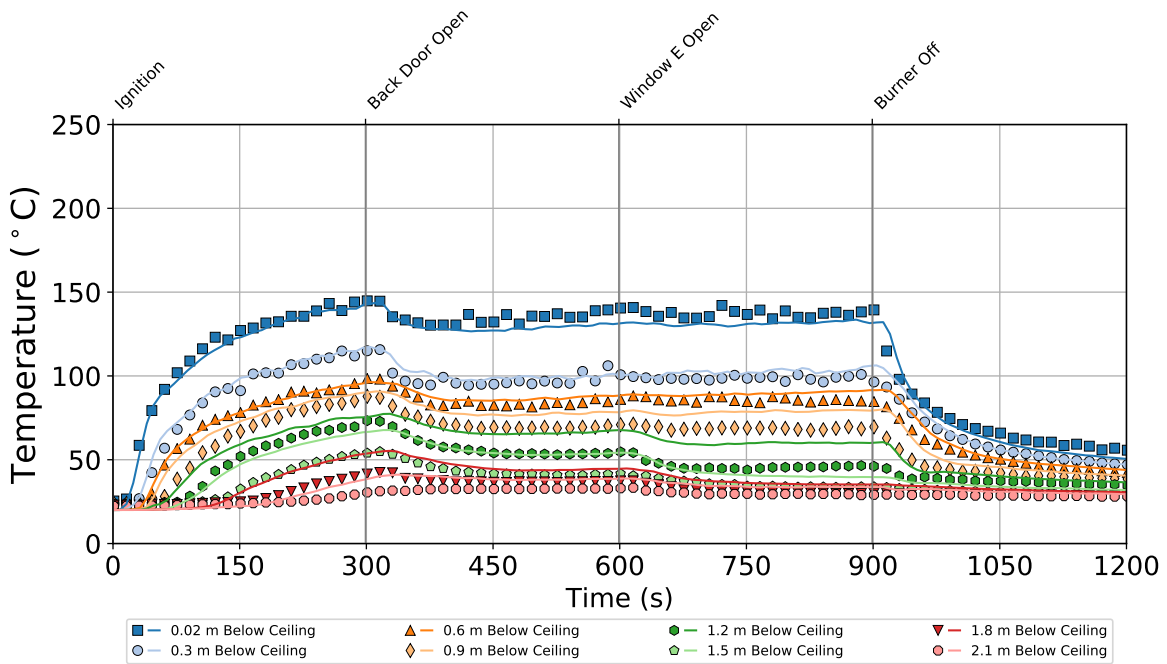


Figure 5.38: Temperatures in bedroom 2 of the single-story structure during Experiment 3

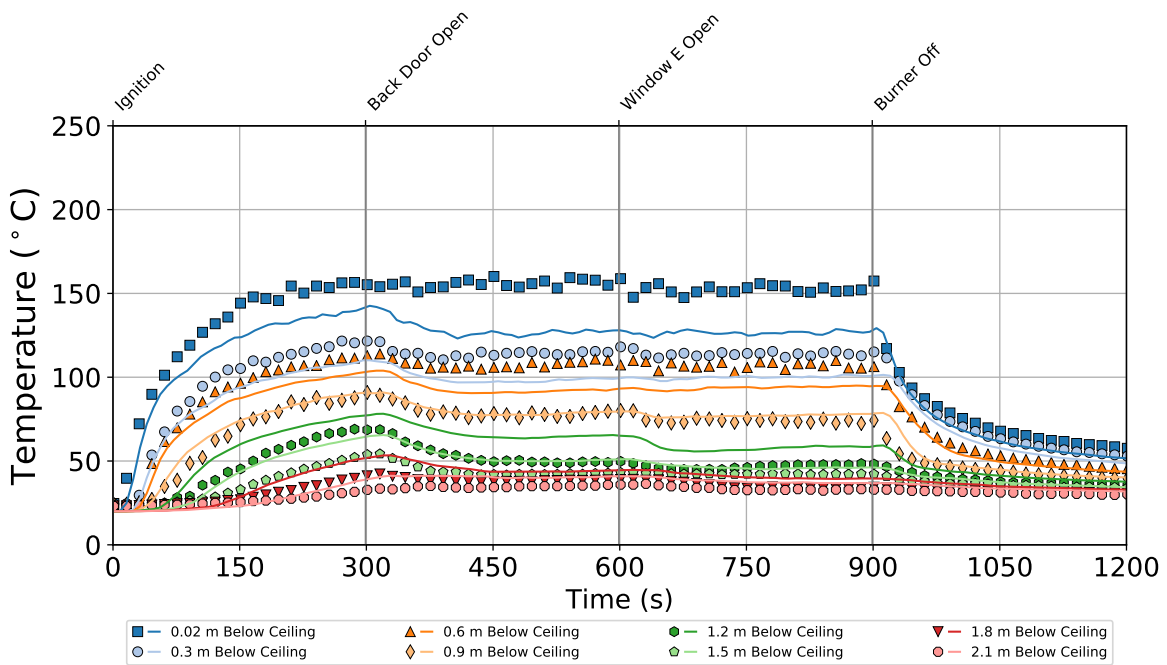


Figure 5.39: Temperatures in bedroom 3 of the single-story structure during Experiment 3

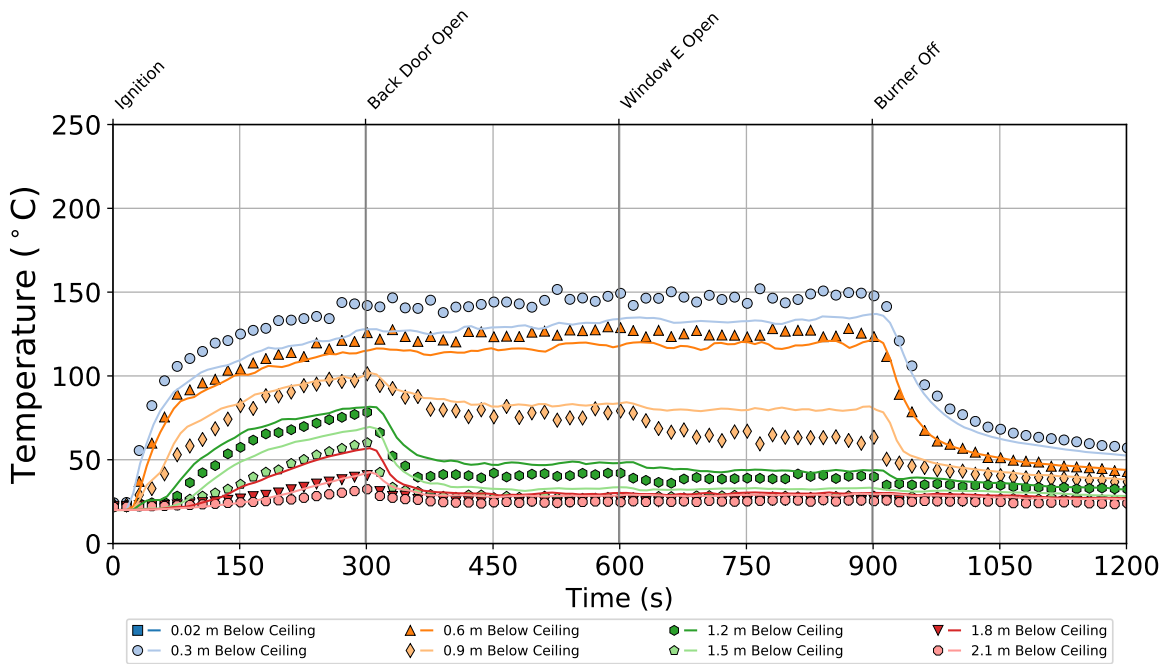


Figure 5.40: Temperatures in the kitchen of the single-story structure during Experiment 3

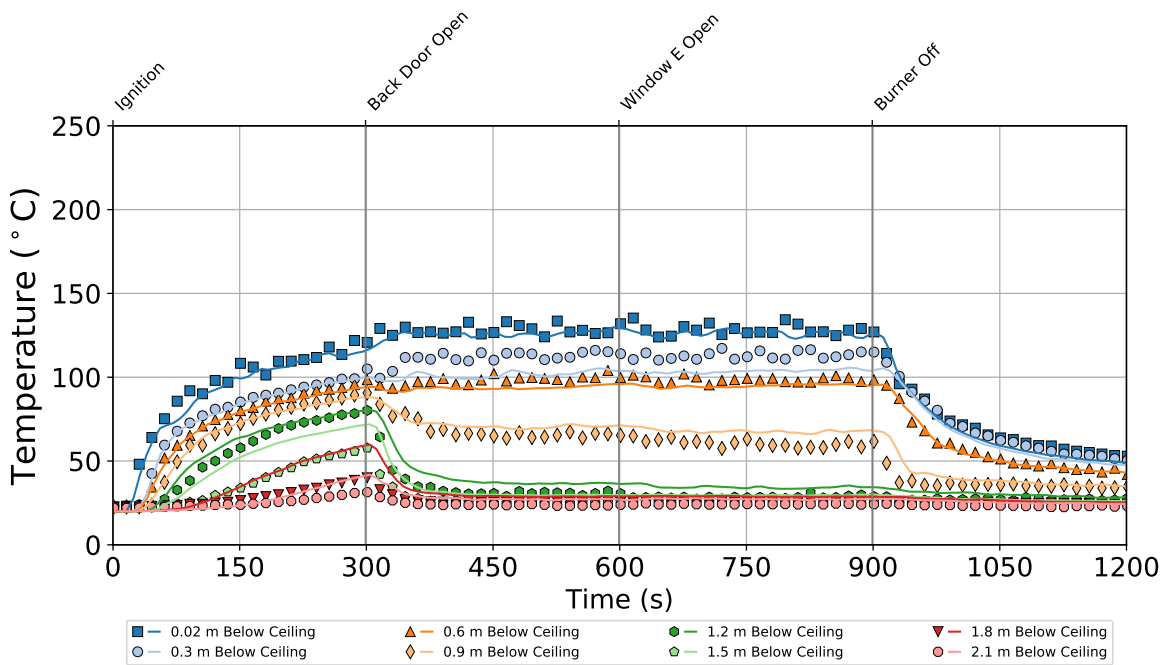


Figure 5.41: Temperatures in the breakfast area of the single-story structure during Experiment 3

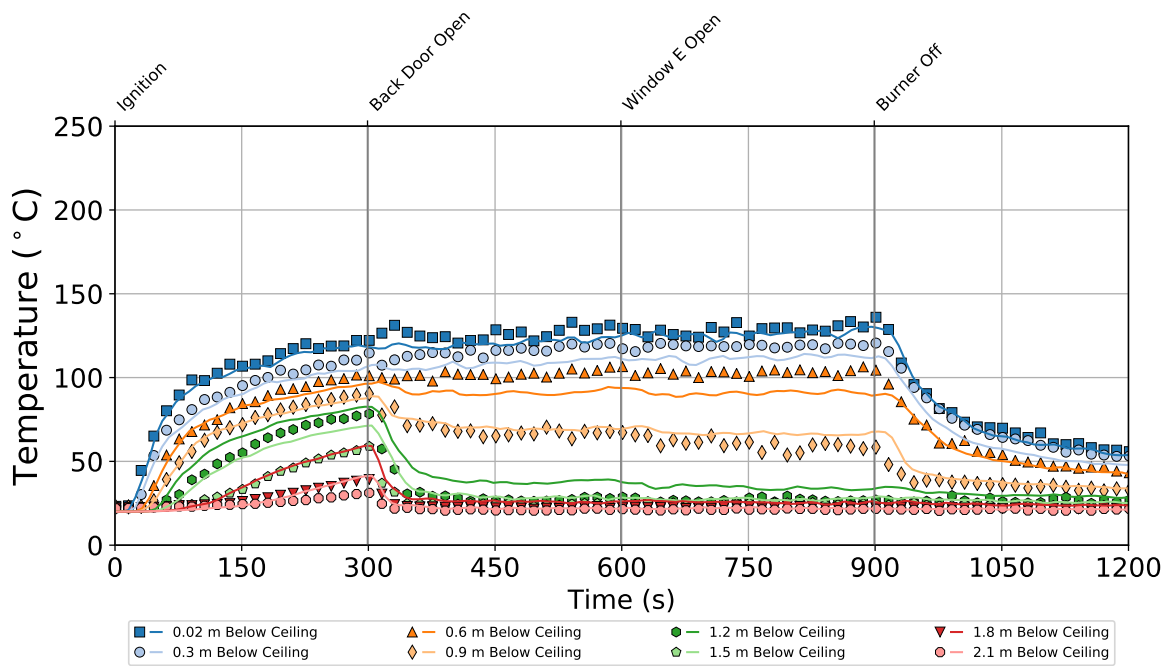


Figure 5.42: Temperatures in the dining room of the single-story structure during Experiment 3

All temperature measurements steadily increased until the back door was opened. After the back door was opened, all temperatures throughout the structure at 0.9 m below the ceiling and lower elevations decreased or remained steady as cool air flowed in through the back door. The temperatures measured at higher elevations increased or remained steady at all measurement locations with the exception of bedroom 1 and bedroom 2, where these temperatures decreased, and bedroom 3, where the highest elevation temperature remained steady while all other temperatures decreased. These trends may be indicative of a reduced rate of flow of hot gases into the hallway and bedrooms and an increased rate of flow of gases out of the bedrooms due to the development of a flow path that connected the gas burner to the back door.

After window E in bedroom 1 was opened, the temperatures throughout the structure generally remained steady. In bedroom 1, the highest elevation temperature increased, temperatures 0.3 m and 0.6 m below the ceiling remained steady, and all lower elevation temperatures decreased as a new flow path was created that brought hot gases into bedroom 1 and cool air in through window E and into the hallway and living room. Over the course of the experiment, temperatures near the ceiling in the living room and hallway were in the range of approximately 130°C to 240°C and the temperatures measured in all other rooms were in the range of ambient to 150°C.

The model generally predicted the qualitative features in the data that resulted from the ventilation openings. The only notable exception is that the model did not predict the changes in temperature at the ceiling of bedroom 1 when the back door and window E were opened. The model predictions also generally agreed quantitatively with the experimental data, particularly at the highest elevation measurement locations. One notable exception to this trend was the underprediction of the ceiling temperature in bedroom 3. The model also underpredicted temperatures measured 0.3 m and 0.6 m below the ceiling at all locations except bedroom 1 and bedroom 2, and slightly overpredicted the temperature measurements at all other elevations.

5.3.2 Experiment 3: Pressure

The pressure data collected throughout the structure are presented in the following figures. Figure 5.43 displays the pressures in the living room, where the burner was located, Figure 5.44 displays the pressures in bedroom 1, Figure 5.45 displays the pressures in bedroom 2, Figure 5.46 displays the pressures in bedroom 3, Figure 5.47 displays the pressures in the kitchen, and Figure 5.48 displays the pressures in the dining room. The pressure measurements 2.1 m below the ceiling in the living room and at 1.2 m and 2.1 m below the ceiling in bedroom 1 did not function properly during Experiment 3 and have been excluded from Figure 5.43 and Figure 5.44.

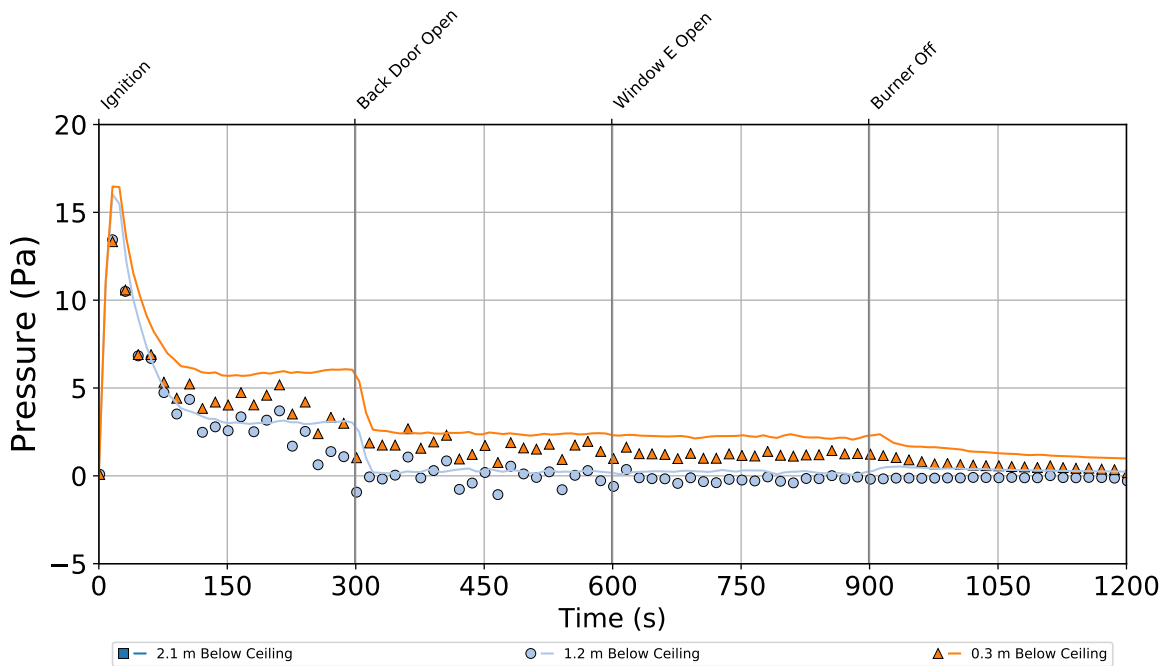


Figure 5.43: Pressures in the living room of the single-story structure during Experiment 3

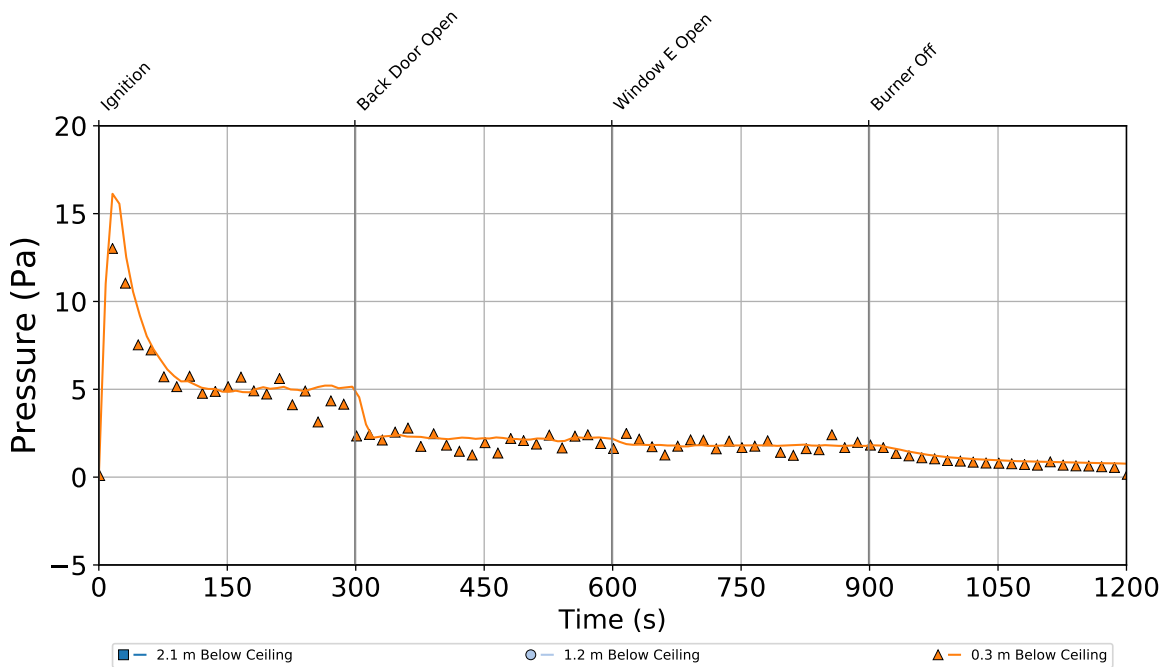


Figure 5.44: Pressures in bedroom 1 of the single-story structure during Experiment 3

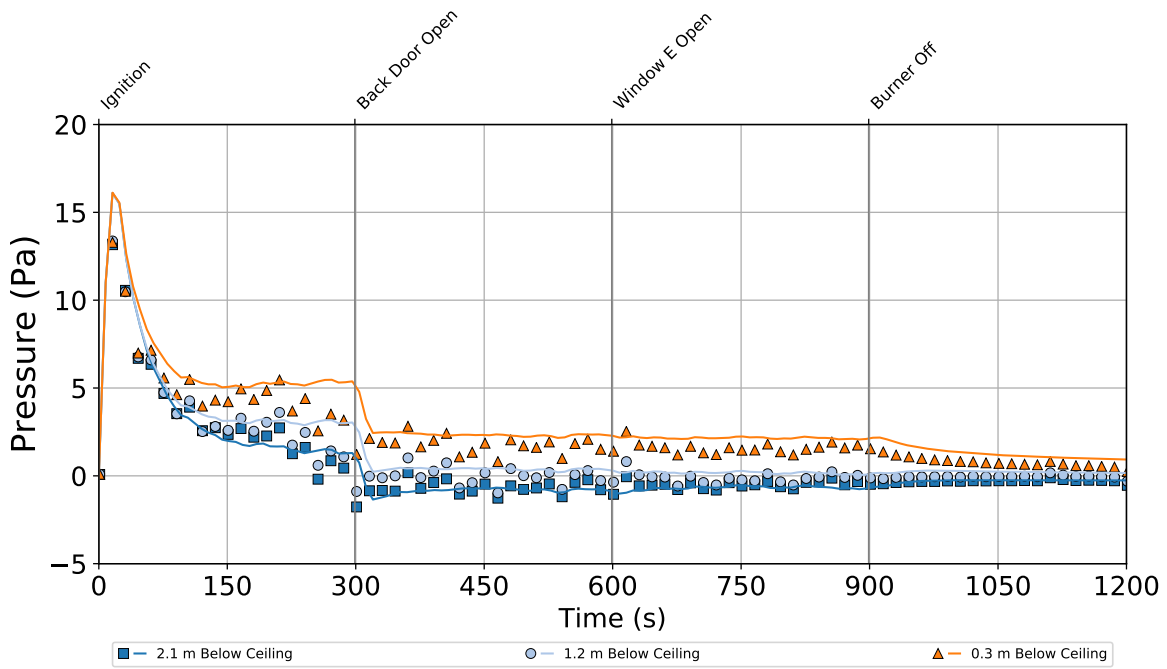


Figure 5.45: Pressures in bedroom 2 of the single-story structure during Experiment 3

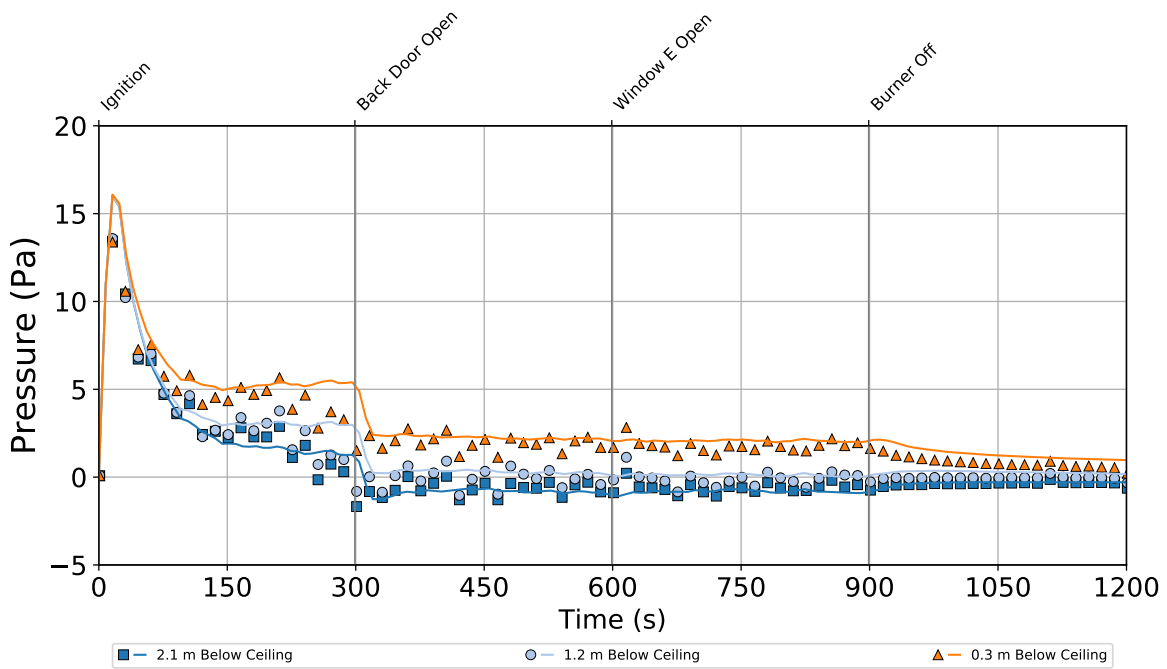


Figure 5.46: Pressures in bedroom 3 of the single-story structure during Experiment 3

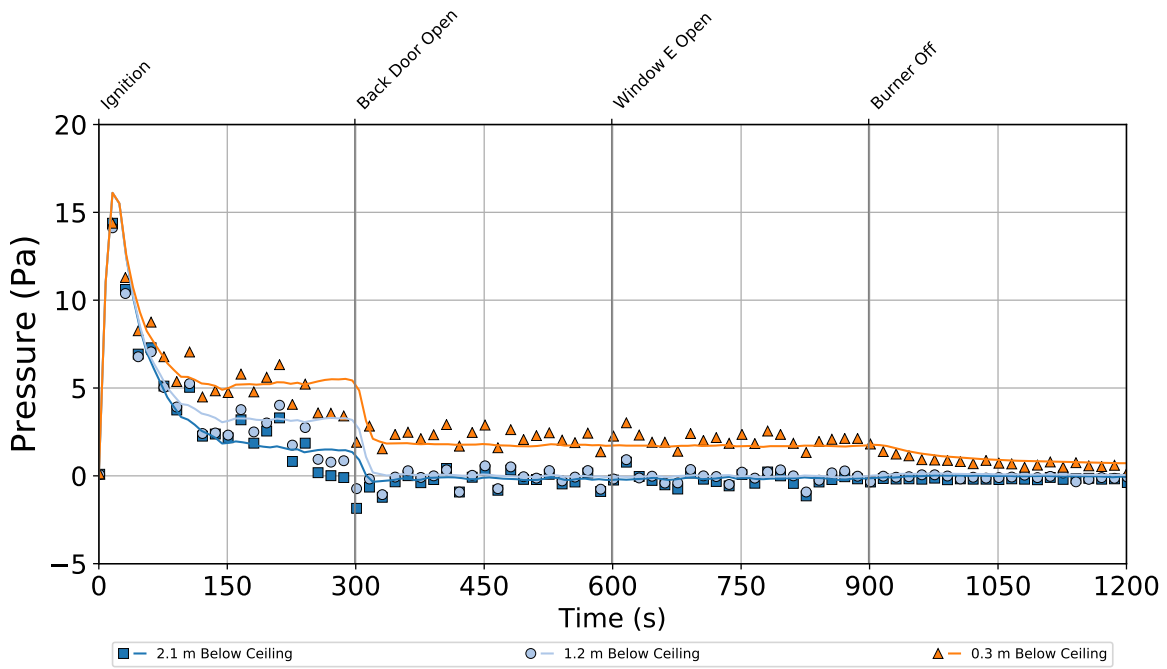


Figure 5.47: Pressures in the kitchen of the single-story structure during Experiment 3

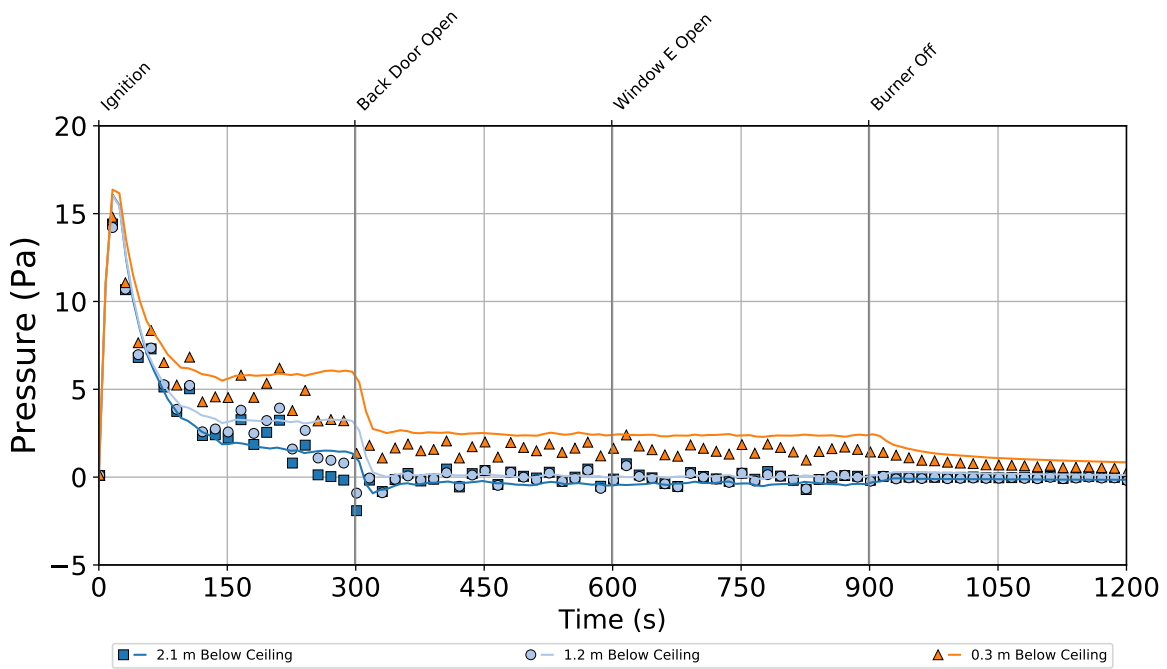


Figure 5.48: Pressures in the dining room of the single-story structure during Experiment 3

The pressure increased rapidly at ignition to a global maximum of approximately 13 Pa and quickly decreased to lower positive pressures at all measurement locations. When the back door was opened, the pressures at all locations decreased such that pressures at the lowest elevations were below atmospheric pressure and the pressures 1.2 m below the ceiling were approximately atmospheric. After the back door was opened, the pressures at all measurement locations were in the range of -5 Pa to 5 Pa. At each successive ventilation event the pressure magnitudes throughout the structure either changed to be closer to atmospheric pressure by some relatively small amount or remained at the same magnitude.

The model generally agreed qualitatively with the trends in the experimental data caused by ventilation events. The magnitudes of the pressures were accurately predicted by the model as well as the magnitudes of the pressure changes due to ventilation events. The pressures measured 0.3 m below the ceiling in the living room and the dining room throughout the experiment were overpredicted by the model. This overprediction may be an artifact of the representation of leakage and the location of the vent that corresponded to leakage in the model.

5.3.3 Experiment 3: Velocity

The velocity data collected throughout the structure are presented in the following figures. Figure 5.49 displays the velocities measured in the hallway and Figure 5.50 displays the velocities at window E in bedroom 1. The velocity profiles for the exterior doors and windows are plotted such that positive flows correspond to gases flowing out of the structure. The velocity profile for the hallway is plotted such that positive flows correspond to the positive x-direction (away from the living room) in Figure 3.1.

A relatively low velocity flow away from the living room was measured 0.4 m below the ceiling in the hallway immediately after ignition without any significant flow at the lower elevations. After the back door was opened, the magnitude of the flow velocity away from the living room 0.4 m below the ceiling decreased, and low velocity flow toward the living room was initiated 0.8 m below the ceiling. Just after window E was opened, weakly bi-directional flow was evident in the hallway with the neutral plane at an indeterminate elevation. When gas flow to the burner stopped, the magnitudes of all flow decreased, although the directions of flow remained unchanged.

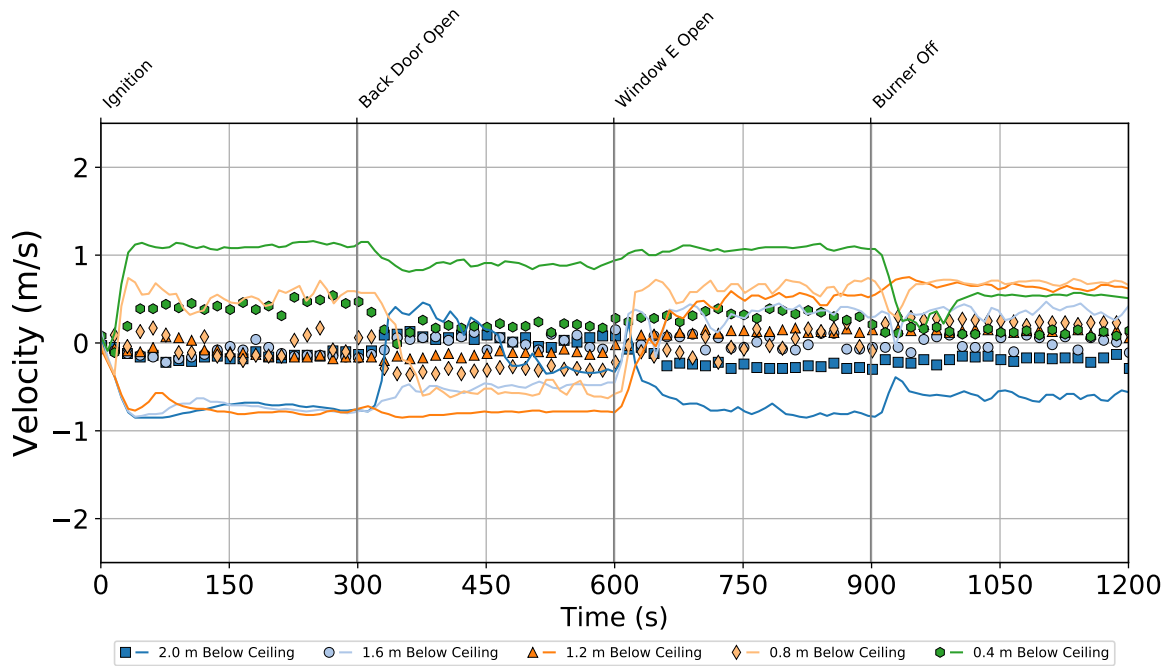


Figure 5.49: Velocities measured in the hallway of the single-story structure during Experiment 3

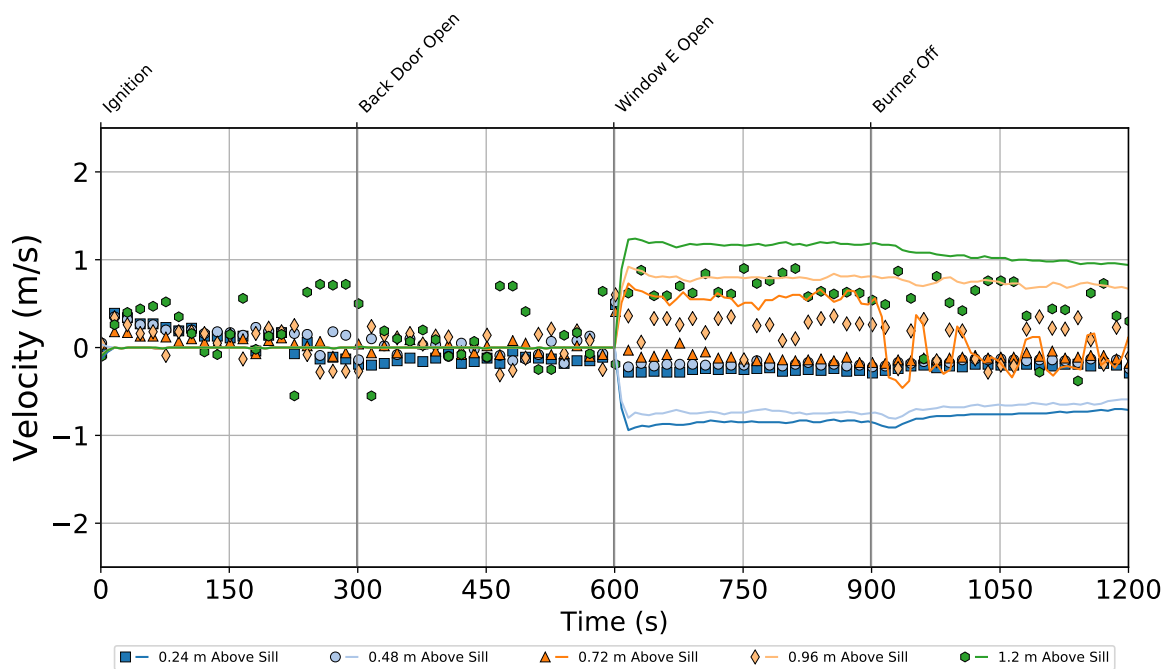


Figure 5.50: Velocities measured in window E of the single-story structure during Experiment 3

Conditions were quiescent at window E in bedroom 1 up to the point where window E was opened. After the window was opened, bi-directional flow was immediately evident with low velocity flows

into the structure at the lowest three measurement elevations and higher velocity flow out of the structure at the top two measurement elevations, locating the neutral plane in the range of 0.72 m to 0.96 m above the window sill. As additional vents were opened and gas flow to the burner was stopped, the magnitudes of the flows into and out of window E gradually decreased.

The model accurately predicted the qualitative features of the data and the effect of opening the exterior windows and doors on the directions of flow and relative changes in flow velocity magnitude. The model erroneously predicted the elevation of the neutral plane in window E at a lower elevation than observed. The model generally overpredicted the magnitudes of all flow velocities.

A similar trend between the experimental data and the model predictions for the flow velocities in the hallway that was described for Experiment 1 and Experiment 2 was also evident in the results of Experiment 3. The predictions of flow velocities in the hallway throughout Experiment 3 indicated relatively strong bi-directional flow immediately following ignition with minor changes in magnitude throughout the remainder of the experiment. The measured velocities indicate lower velocity uni-directional flow prior to the back door opening. The conditions in the hallway between ventilation of the back door and window E may have been stagnant or characterized by circulation. The model prediction indicates some circulation with the measurements 0.4 m below the ceiling and 2.0 m below the ceiling directed toward the living room and measurements between these elevations stagnant or directed away from the living room. These predictions are problematic and indicate an unresolved issue with the bi-directional probes used to measure velocities, the model parameters used in these simulations, or with the model.

6 Two-Story Results

The following sections present the experimental data collected with each distinct ventilation scenario as well as the results of the FDS models that were constructed to simulate each experiment in the two-story structure. The sole fuel source for the two-story structure experiments was a 500 kW burner flame. It was expected that neither the structure nor any of the individual rooms would reach a ventilation-limited state during the experiments, effectively ensuring that the HRR remained controlled and constant. By opening external vents, flow paths were created that allowed high temperature gases to flow to different compartments and out of the structure and cool air to flow into the structure. The effects of these flow paths may be interpreted from temperature, pressure, and velocity data collected throughout the structure. In all of the figures presented in the following sections, discrete data points denote experimental data and solid lines denote model predictions.

6.1 Two-Story: Experiment 4

Experiment 4 conducted on the two-story structure featured the 500 kW gas burner ignited for 1500 s as well as ventilation of the front door (600 s), window K in bedroom 3 (900 s), and window L in bedroom 4 (1200 s).

6.1.1 Experiment 4: Temperature

The temperature data collected by thermocouple arrays throughout the structure are presented in the following figures. Figure 6.1 displays the temperatures at the center of the family room, Figure 6.2 displays the temperatures in the foyer, Figure 6.3 displays the temperatures under the second story hallway, Figure 6.4 displays the temperatures in the kitchen, Figure 6.5 displays the temperatures at the middle of the second story hallway, Figure 6.6 displays the temperatures in the master bedroom, Figure 6.7 displays the temperatures in bedroom 2, Figure 6.8 displays the temperatures in bedroom 3, and Figure 6.9 displays the temperatures in bedroom 4.

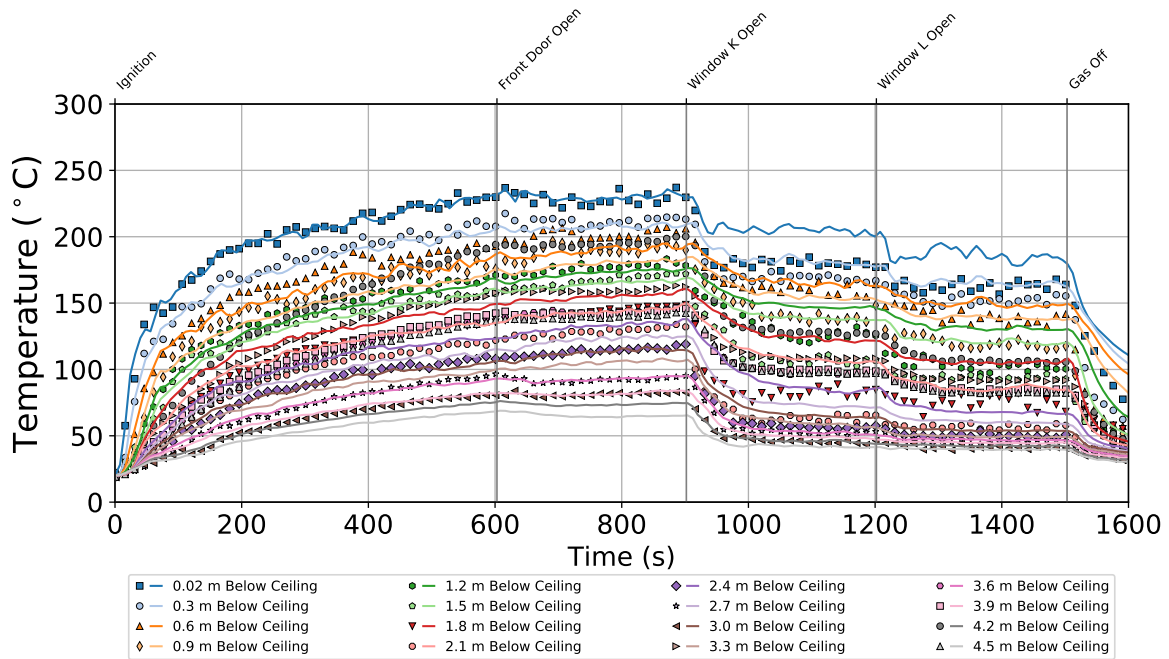


Figure 6.1: Temperatures in the center of the family room of the two-story structure during Experiment 4

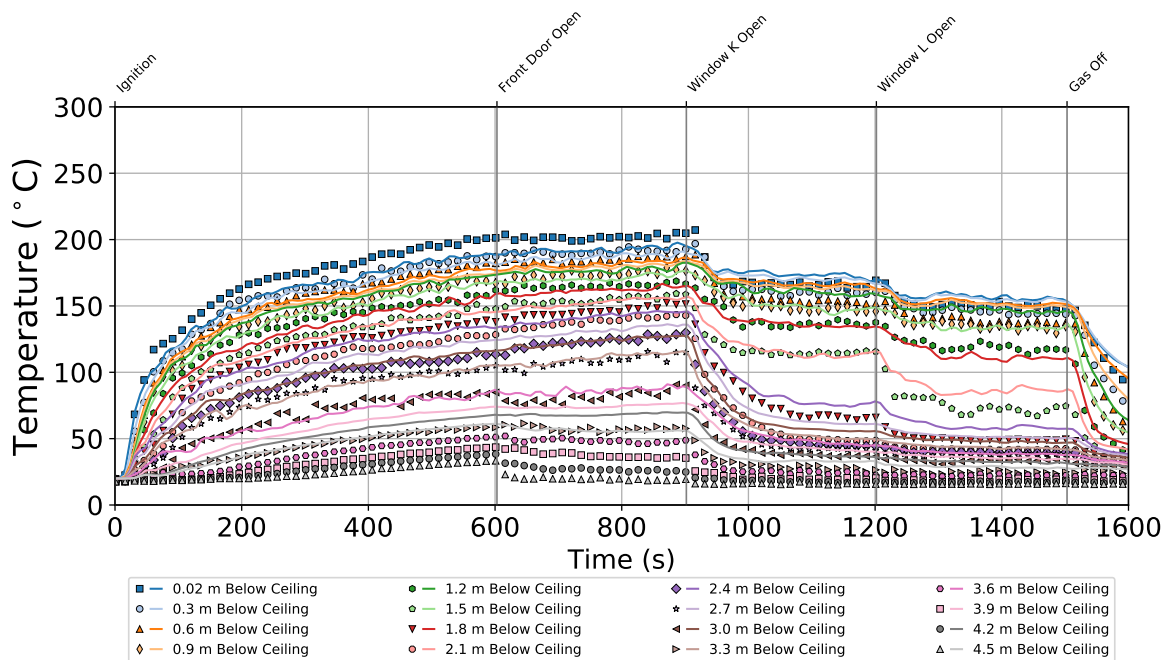


Figure 6.2: Temperatures in the foyer of the two-story structure during Experiment 4

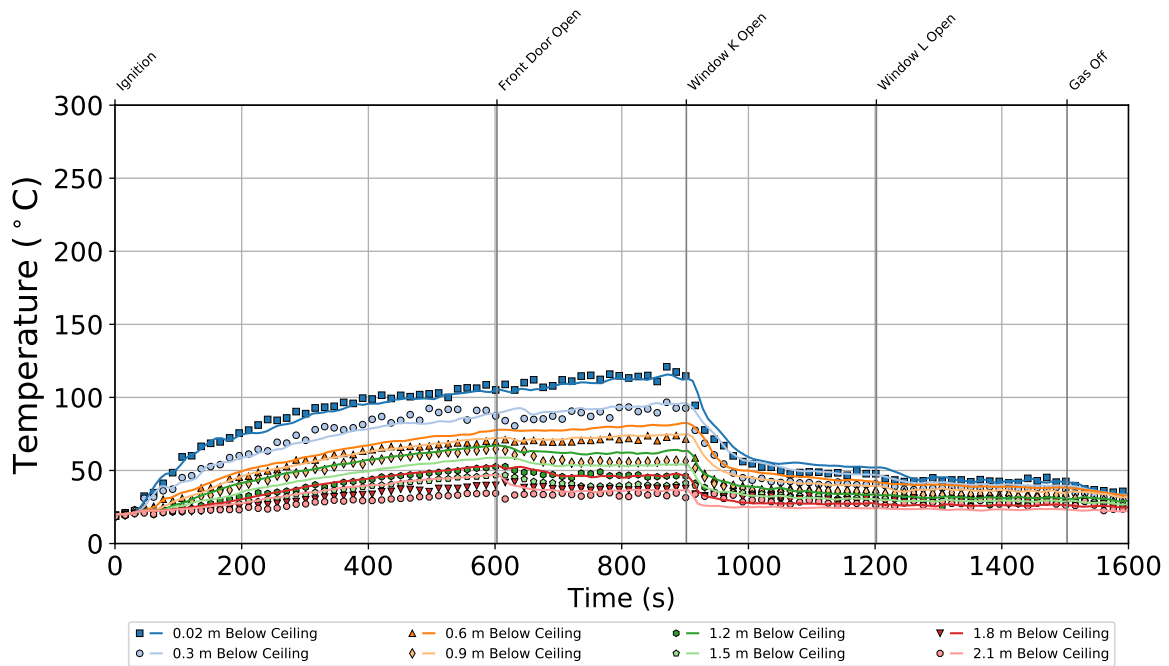


Figure 6.3: Temperatures under the hallway of the two-story structure during Experiment 4

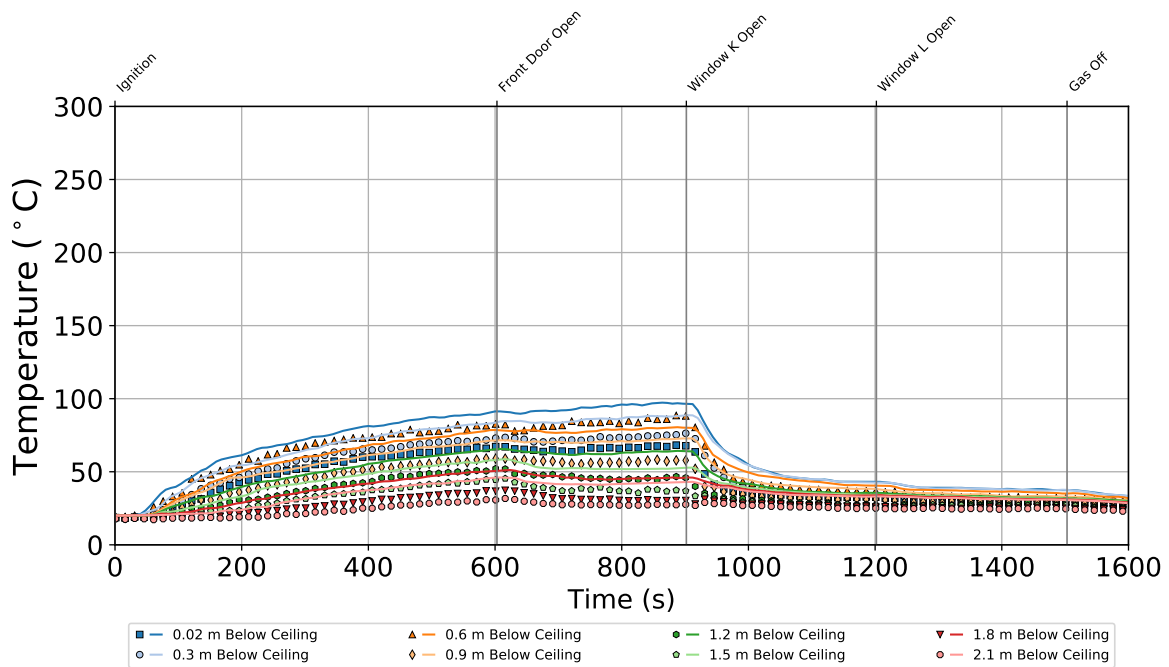


Figure 6.4: Temperatures in the kitchen of the two-story structure during Experiment 4

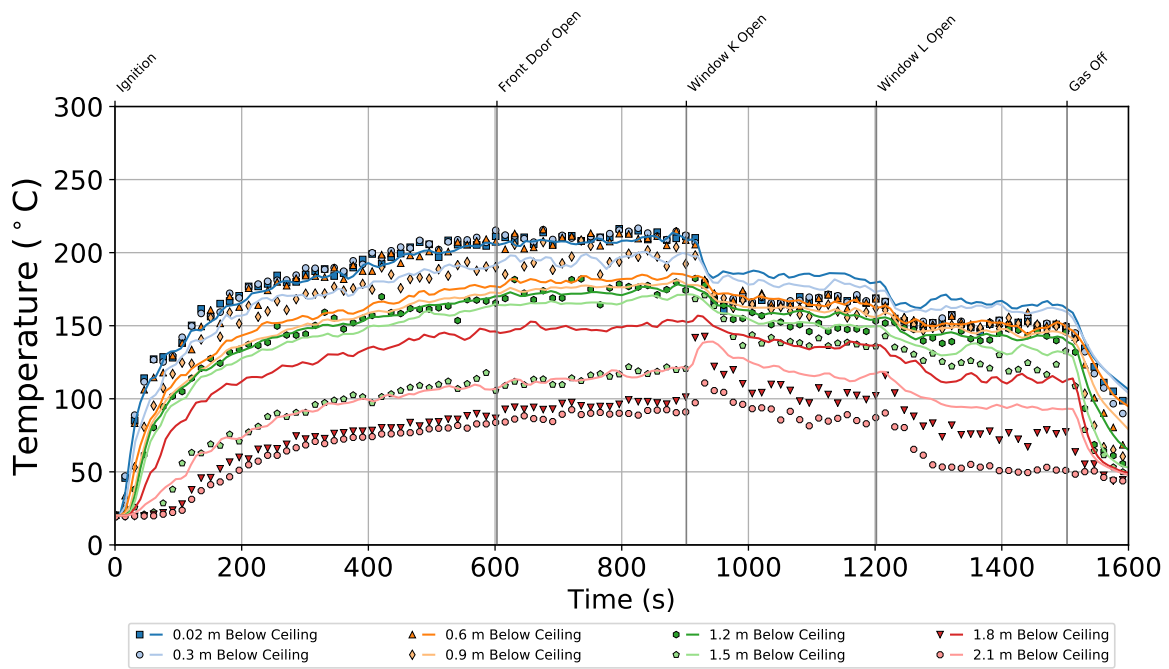


Figure 6.5: Temperatures in the middle of the second story hallway in the two-story structure during Experiment 4

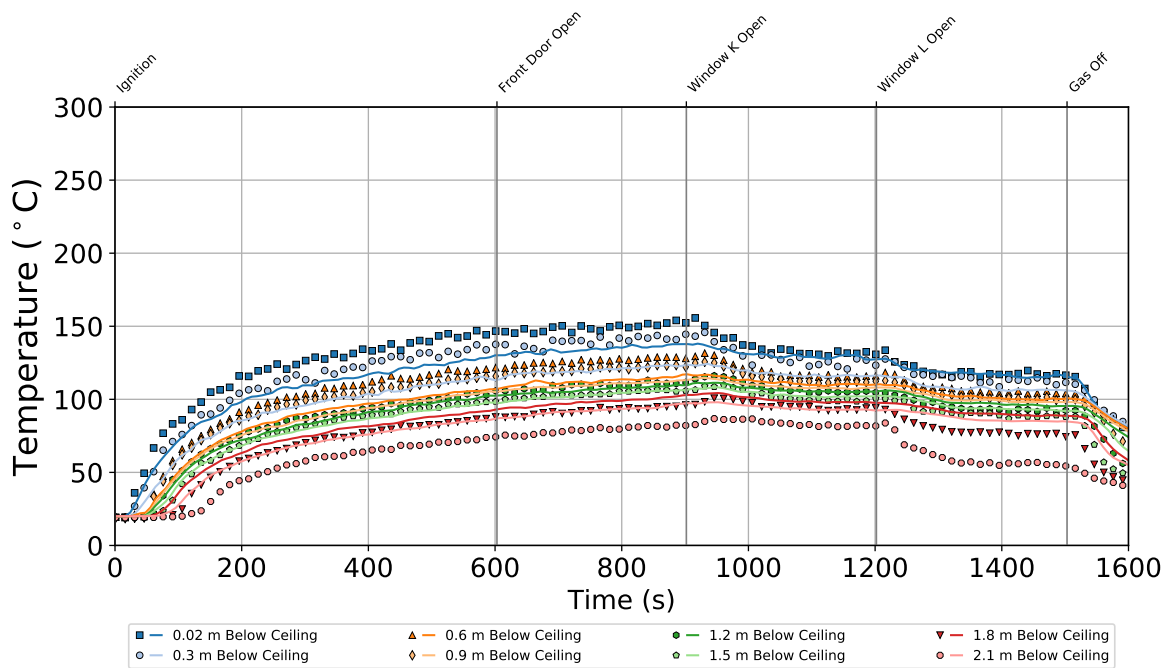


Figure 6.6: Temperatures in the master bedroom of the two-story structure during Experiment 4

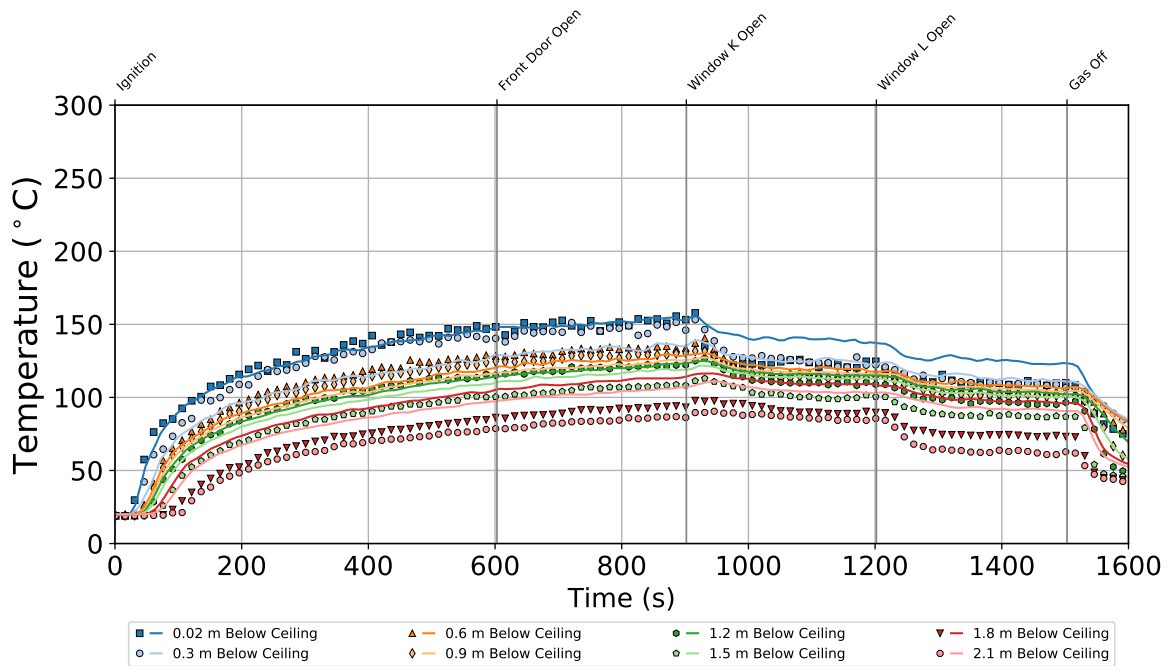


Figure 6.7: Temperatures in bedroom 2 of the two-story structure during Experiment 4

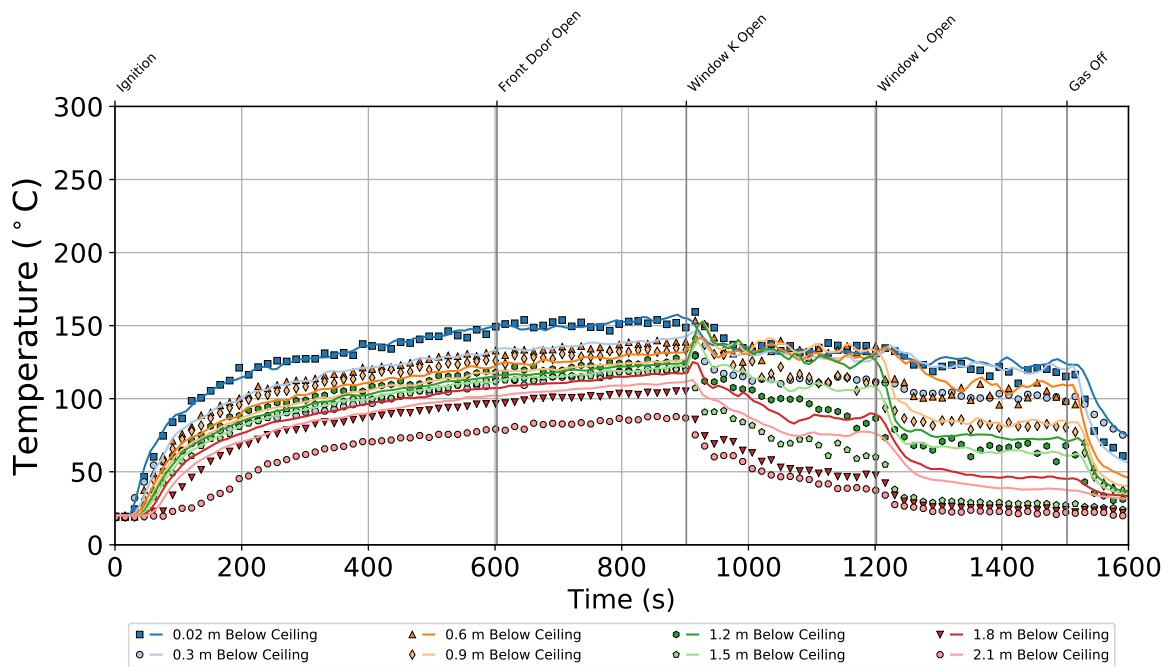


Figure 6.8: Temperatures in bedroom 3 of the two-story structure during Experiment 4

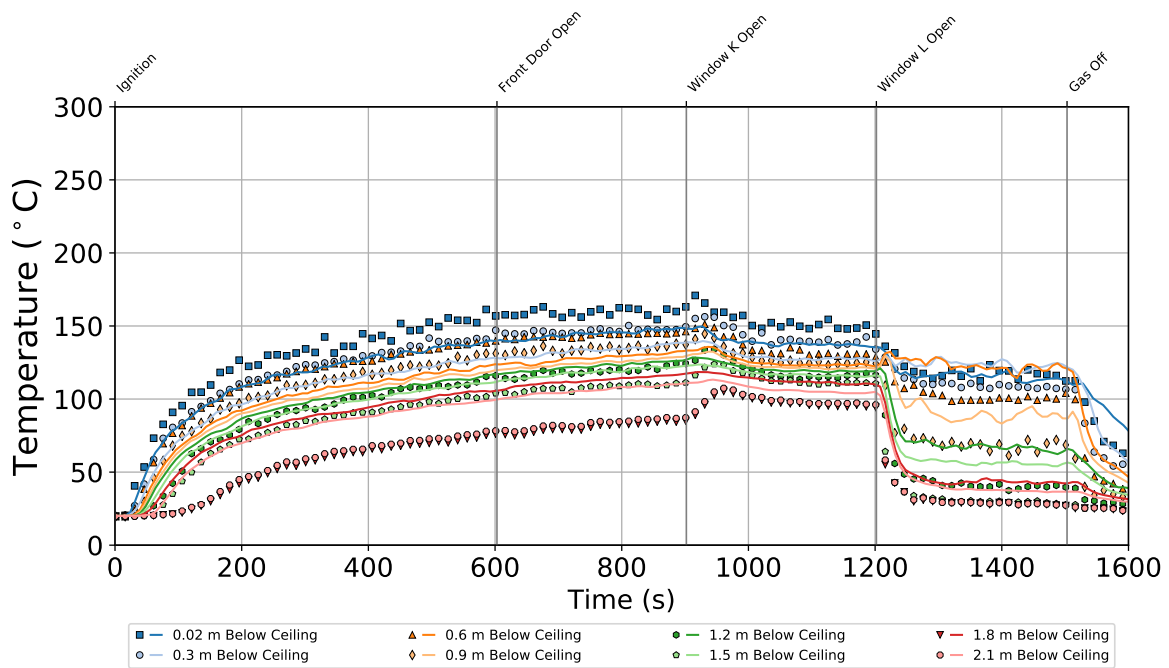


Figure 6.9: Temperatures in bedroom 4 of the two-story structure during Experiment 4

After ignition, all temperatures steadily increased until the front door was opened. When the front door was opened, the temperatures measured 0.9 m below the ceiling and at lower elevations under the second story hallway as well as the temperatures measured 3.9 m below the ceiling and at lower elevations in the foyer decreased slightly, while all other temperature measurements remained steady or slightly increased. Ventilation of the front door decreased temperatures at low elevations on the first story and drove an increase in temperatures on the second story as a flow path was created that introduced cool air into the first floor and increased the flow of hot gases to the second story.

When window K in bedroom 3 was opened, all temperatures measured in the center of the family room, the foyer, under the second story hallway, the kitchen, master bedroom, and bedroom 2 decreased. At the same time, the temperatures measured 1.5 m below the ceiling and at lower elevations in the middle of the second story hallway increased while all other temperatures measured in the hallway decreased. The temperatures in bedroom 3 measured 1.2 m below the ceiling and at higher elevations temporarily increased when window K was opened and immediately decreased for the rest of the experiment. The temperatures at lower elevations in bedroom 3 were characterized by a sharp decrease when window K was vented. All temperatures measured in bedroom 4 temporarily increased when window K was vented and subsequently decreased to temperatures that remained steady until window L was opened. These trends are consistent with the formation of paths where hot gases that had accumulated at high elevation in the second story flowed out of window K and was displaced by cool air flowing into and cooling the second story via bedroom 3.

Ventilation of window L resulted in a decrease of all temperatures throughout the structure. The temperatures measured in bedroom 3 and bedroom 4 indicated bi-directional flow after window L was opened. The elevation of the interface of the two layers in bedroom 3 was between 1.2 m and 1.5 m below the ceiling and the elevation of the interface in bedroom 4 was approximately 0.9 m below the ceiling. The temperatures measured throughout the first story during Experiment 4 ranged from ambient temperature to 100°C, with the maximum temperatures measured under the second story hallway closer to approximately 120°C. The temperatures measured in the regions of the structure that spanned the height of both stories and the temperatures measured in the second story hallway peaked in the range of 200°C to 250°C, and the temperatures in the bedrooms on the second story ranged from ambient temperature to approximately 160°C throughout the experiment.

The temperatures measured 3.3 m below the ceiling and at lower elevations in the center of the family room diverged from the general trend that consisted of stratification of the temperatures with respect to elevation. Particularly notable was the temperature measured 4.2 m below the ceiling that was comparable to the temperature measured 0.9 m below the ceiling throughout the experiment. The unique geometry of the two-story structure included an open hallway in the second story that facilitated flow from the ceiling of the family room down the stairs and into the low elevation areas of the family room. Visual observations indicated that hot gases circulated around the second story hallway, which resulted in a deviation from formation of a classic hot gas layer filling from the ceiling of the family room downward. Additionally, a review of the data collected with the fully furnished two-story structure indicates a similar trend that was particularly noticeable when the initiating fuel package was located outside of the family room [39]. This phenomenon may have attributed to the non-stratification of the temperatures in the family room.

A similar phenomenon was observed in the kitchen, where the highest temperature measurements were made 0.6 m below the ceiling throughout the experiment. The kitchen and family room likely experienced these trends because these rooms were connected in this open-concept design.

In general, the model accurately predicted the qualitative features in the data that resulted from the ventilation openings. The model typically accurately predicted the temperatures near the ceiling and overpredicted temperatures measured at elevations near the floor. The model erroneously predicted stratification of the gas temperatures as a function of elevation in the family room and in the kitchen. The temperatures measured at elevations ranging from 1.8 m to 3.0 m below the ceiling in the center of the family room were overpredicted by the model and, due to prediction of stratification of the temperature profile, the temperatures measured at elevations of 3.3 m below the ceiling and at lower elevations were underpredicted. The model overpredicted all measured temperatures in the kitchen.

The temperatures in the foyer were overpredicted at all elevations lower than 0.6 m below the ceiling, and overpredicted at all elevations after window K was opened. The temperatures under the second story hallway were accurately predicted 0.02 m and 0.3 m below the ceiling, but overpredicted at all lower elevations. The model underpredicted temperatures measured at elevations ranging from 0.3 m to 0.9 m below the ceiling and overpredicted the temperatures 1.5 m below the ceiling and at lower elevations in the middle of the second story hallway. Temperatures measured 0.3 m to 0.9 m below the ceiling were generally underpredicted and temperatures measured 1.8 m and 2.1 m below the ceiling in all bedrooms on the second story of the two-story structure were overpredicted. Some non-stratification of temperatures was predicted but not observed in bedroom 3 between ventilation of window K and window L, with the highest temperatures predicted 0.6 m and 0.9 m below the ceiling. A similar inaccurate prediction was observed in bedroom 4 after ventilation of window L, where the highest temperatures were predicted at elevations 0.3 m and 0.6 m below the ceiling, whereas measured temperatures remained stratified with the highest temperature measured 0.02 m below the ceiling.

6.1.2 Experiment 4: Pressure

The pressure data collected throughout the structure are presented in the following figures. Figure 6.10 displays the pressures in the family room, Figure 6.11 displays the pressures next to the front door, Figure 6.12 displays the pressures in the living room, Figure 6.13 displays the pressures in the den, Figure 6.14 displays the pressures in the master bedroom, Figure 6.15 displays the pressures in bedroom 2, Figure 6.16 displays the pressures in bedroom 3, and Figure 6.17 displays the pressures in bedroom 4.

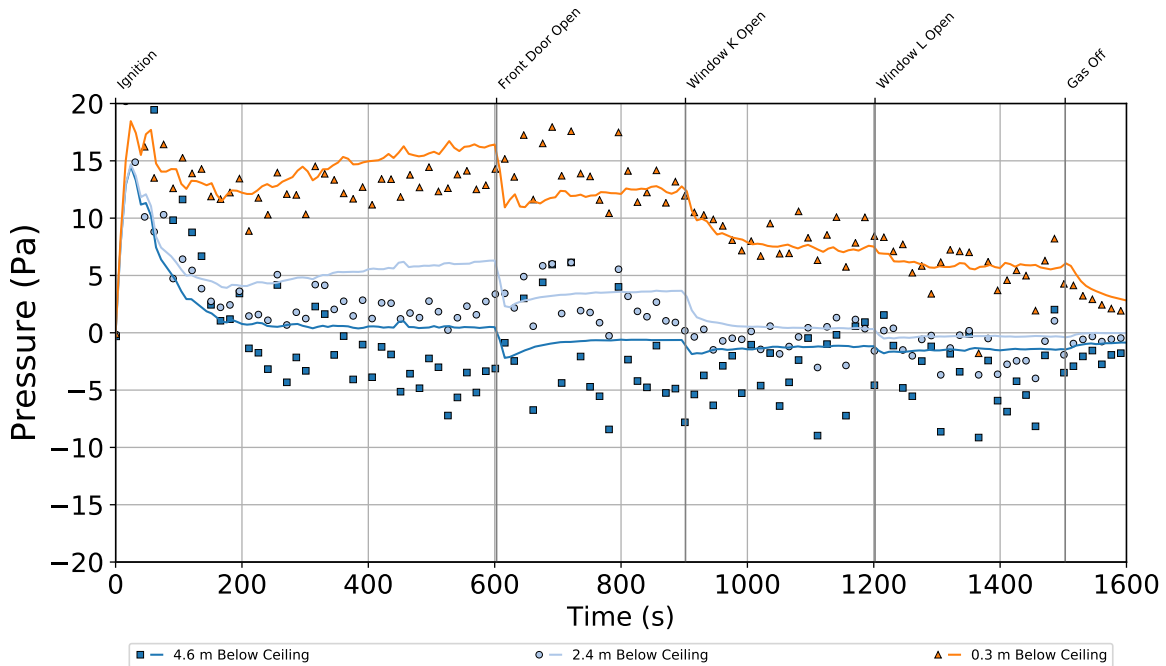


Figure 6.10: Pressures in the family room of the two-story structure during Experiment 4

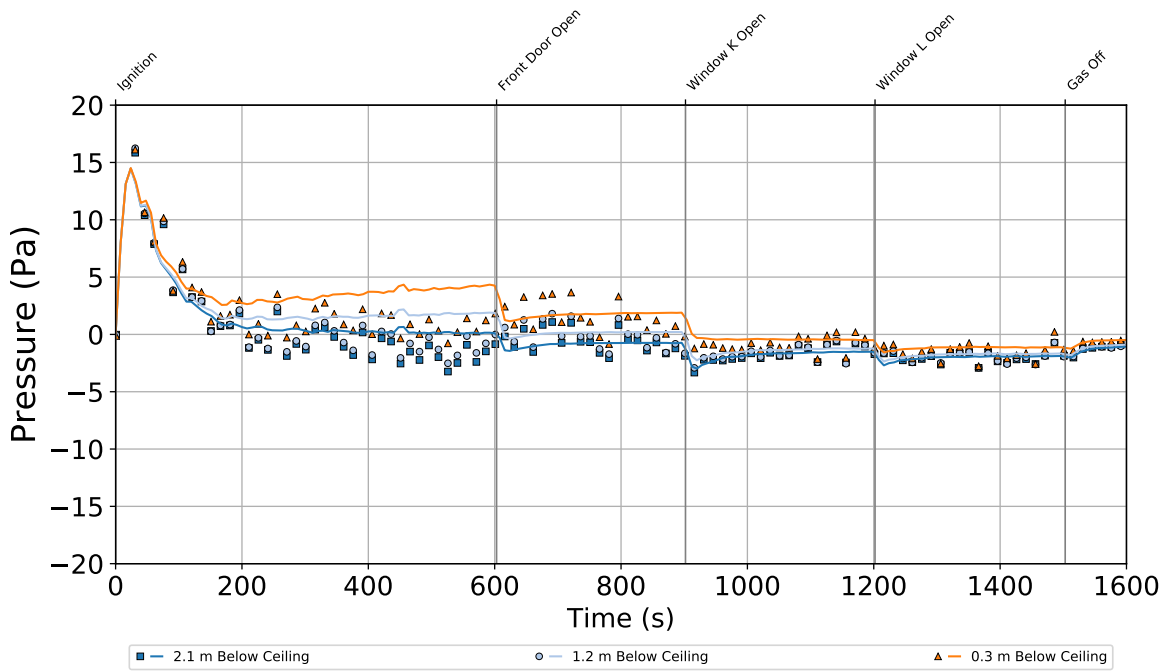


Figure 6.11: Pressures next to the front door of the two-story structure during Experiment 4

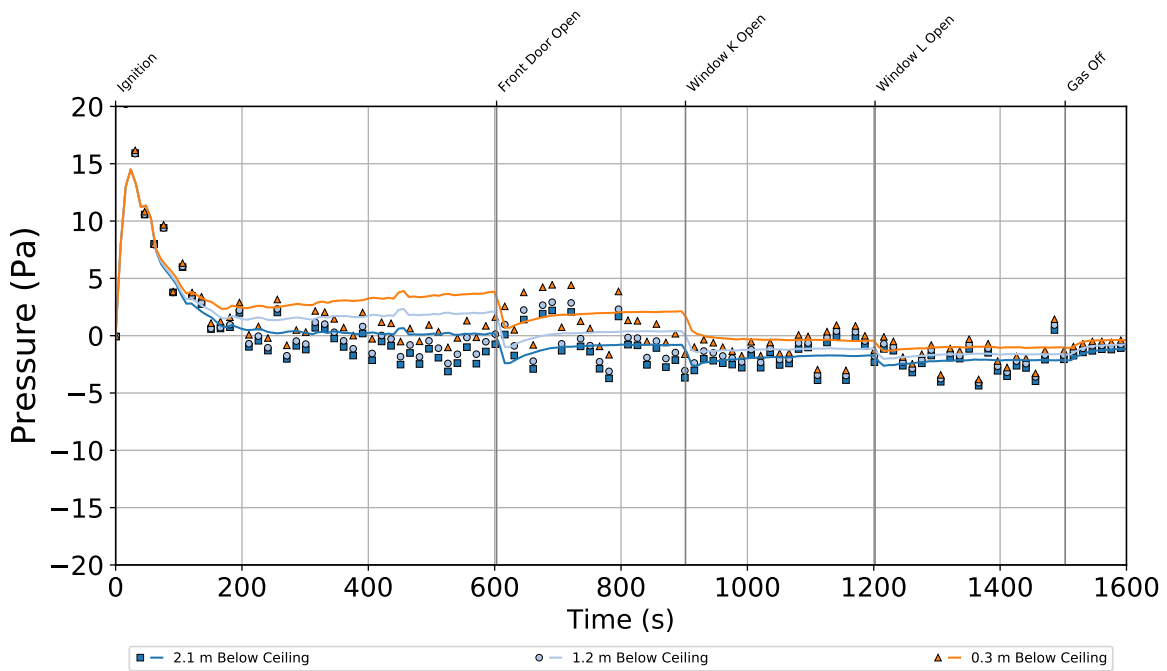


Figure 6.12: Pressures in the living room of the two-story structure during Experiment 4

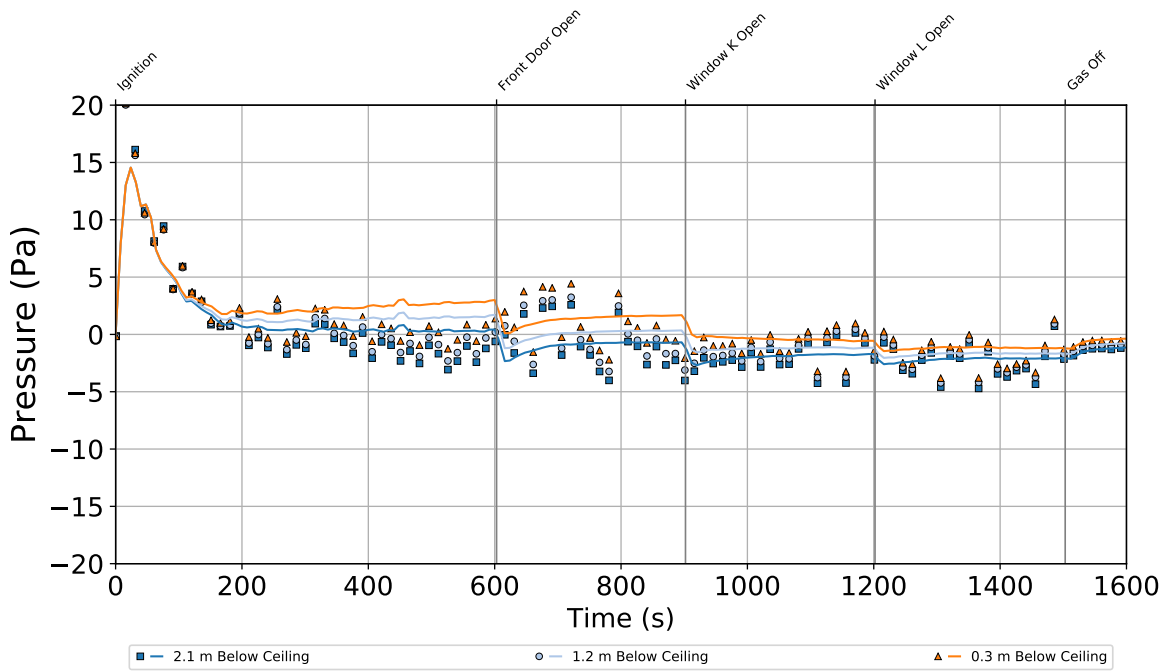


Figure 6.13: Pressures in the den of the two-story structure during Experiment 4

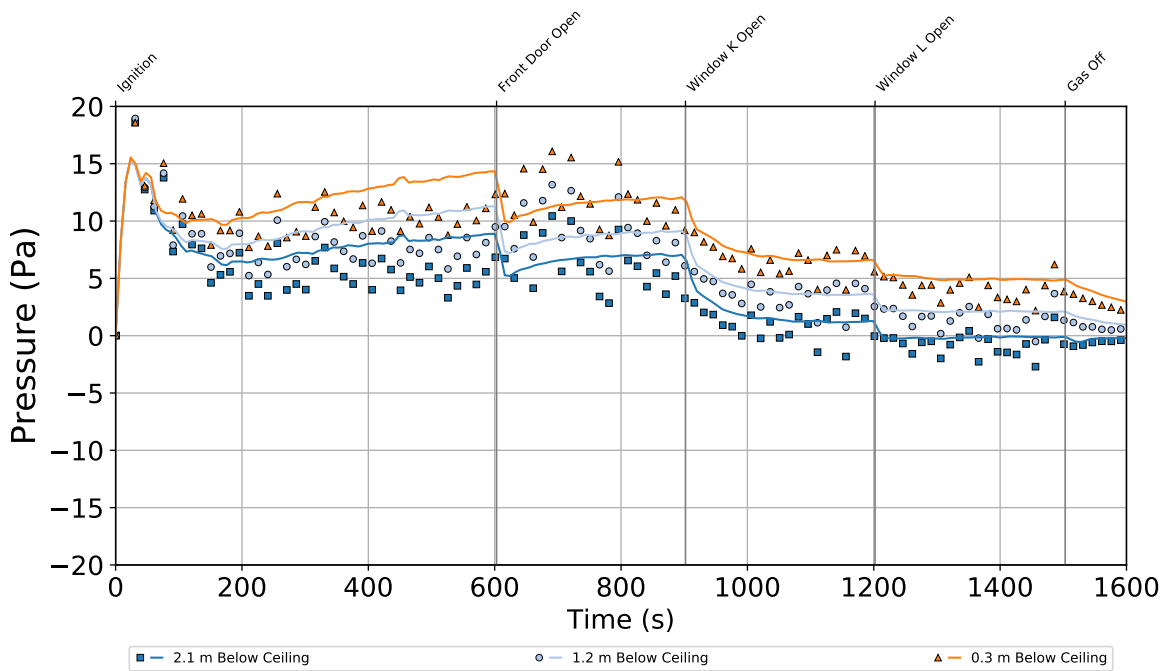


Figure 6.14: Pressures in the master bedroom of the two-story structure during Experiment 4

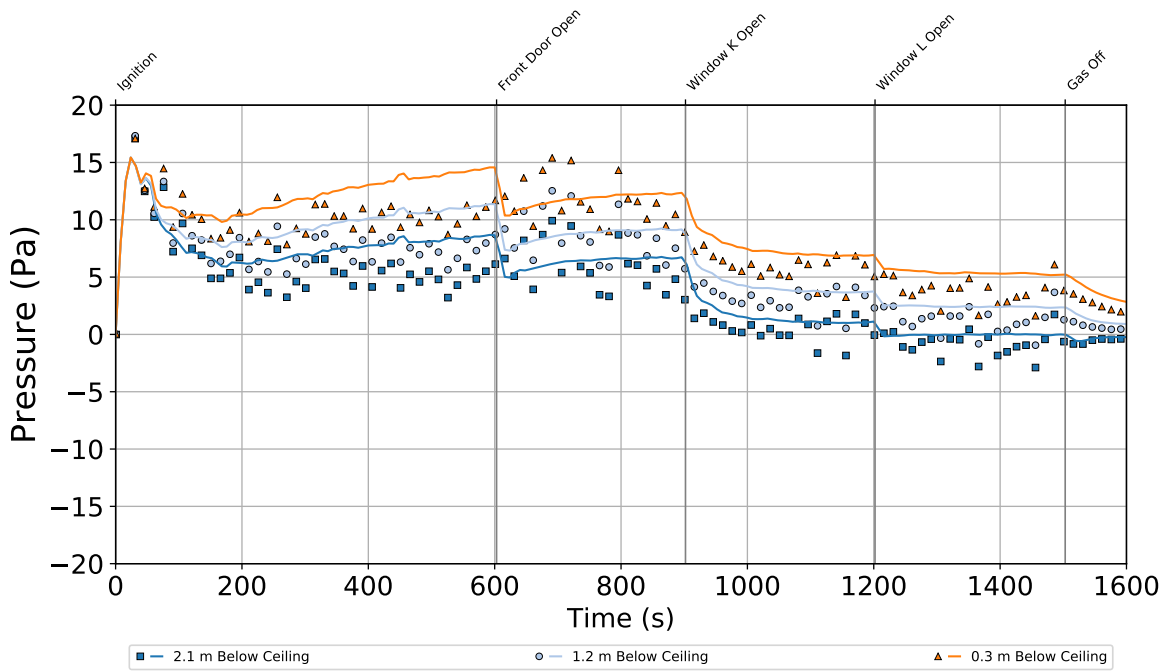


Figure 6.15: Pressures in bedroom 2 of the two-story structure during Experiment 4

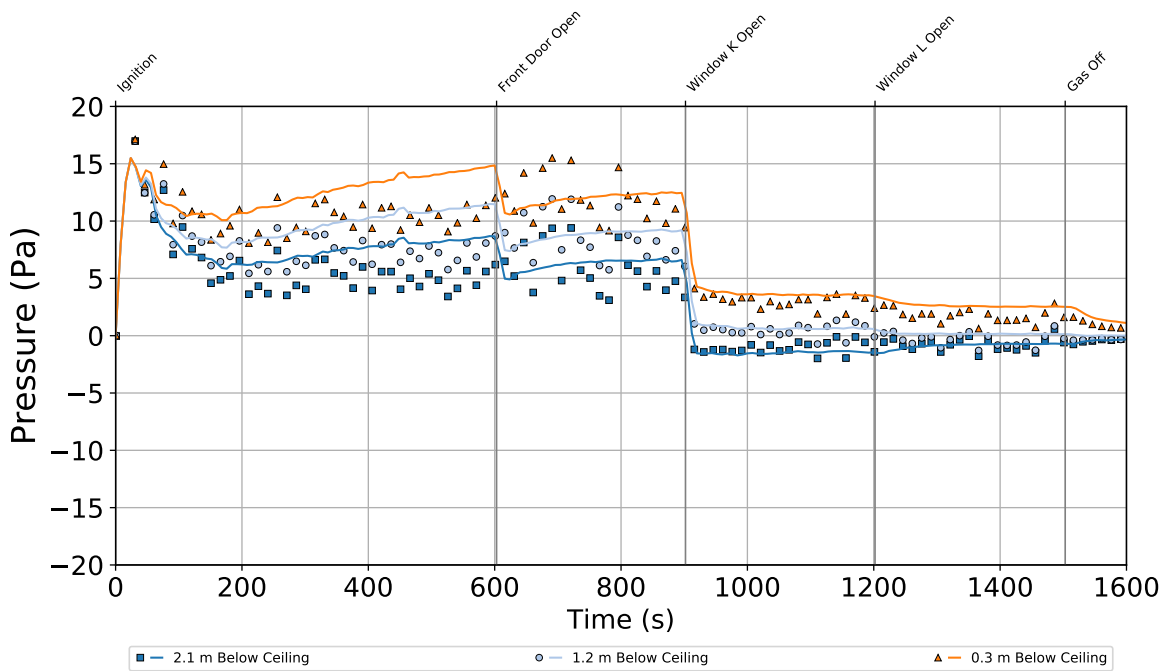


Figure 6.16: Pressures in bedroom 3 of the two-story structure during Experiment 4

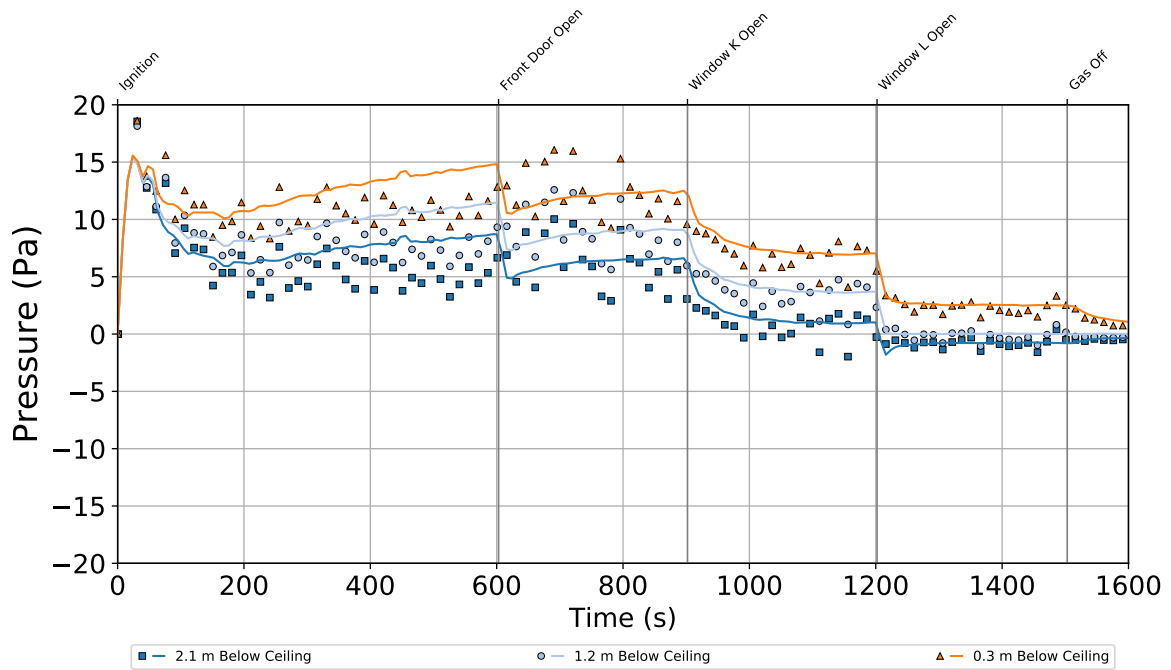


Figure 6.17: Pressures in bedroom 4 of the two-story structure during Experiment 4

The pressures throughout the structure increased immediately after ignition to a global maximum in the range of 13 Pa to 18 Pa at all measurement locations followed by a gradual decay in pressure magnitude toward atmospheric pressure. The pressure measured 4.6 m below the ceiling of the family room reached a peak of approximately 42 Pa for a short duration approximately 15 s into the experiment. All pressure measurements from the first story and those collected 4.6 m below the ceiling in the family room achieved pressures below atmospheric pressure prior to ventilation of the front door. All measurements from the second story and those collected at higher elevations in areas that were open to the second story were above atmospheric pressure prior to ventilation of the front door. The negative pressures are indicative of air flow throughout the first story entrained by the hot plume from the burner. Positive pressures at high elevations and in the second story compartments indicate higher temperatures and may also indicate a positive net mass flow due to the dominance of buoyancy throughout the structure. Upon ventilation of the front door, all measured pressures immediately increased and then gradually decreased until window K was opened.

All measured pressures increased or decreased such that they were closer to atmospheric pressure with each subsequent ventilation event. The lowest elevation pressure in bedroom 3 decreased to below atmospheric pressure when window K was opened and the lowest elevation pressure in bedroom 4 decreased to below atmospheric pressure when window L was opened. These pressure decreases indicate flow into the structure at low elevation, while pressures above ambient at higher elevations in these rooms indicate flow out of the structure. Pressures measured on the first story ranged from -5 Pa to 5 Pa throughout the experiment, while those measured on the second story ranged from approximately -2 Pa to 15 Pa. Pressures measured at high elevations in the family room were in the range of 5 Pa to 15 Pa and the pressures near the floor in the family room were in the range of -5 Pa to atmospheric pressure throughout the experiment.

Pressures were overpredicted at all measurement locations and elevations throughout the structure between ignition and opening the front door, and pressures were predicted to increase over time although the measured pressures remained steady after the initial increase and decrease in pressure caused by ignition of the burner. When the front door was opened, the trend in the measurements was an increase in all measured pressures, whereas a decrease in all pressures was predicted. After ventilation of the front door, the model qualitatively and quantitatively captured the trends in the measured data. The overprediction of pressures between ignition and ventilation of the front door may be an artifact of the representation of leakage and the location of the vent that corresponded to leakage in the model.

6.1.3 Experiment 4: Velocity

The velocity data collected throughout the structure are presented in the following figures. Figure 6.18 displays the velocities measured at the front door, Figure 6.19 displays the velocities measured in window K, Figure 6.20 displays the velocities measured in window L. The velocity profiles for the exterior doors and windows are plotted such that positive flows correspond to gas flow out of the structure.

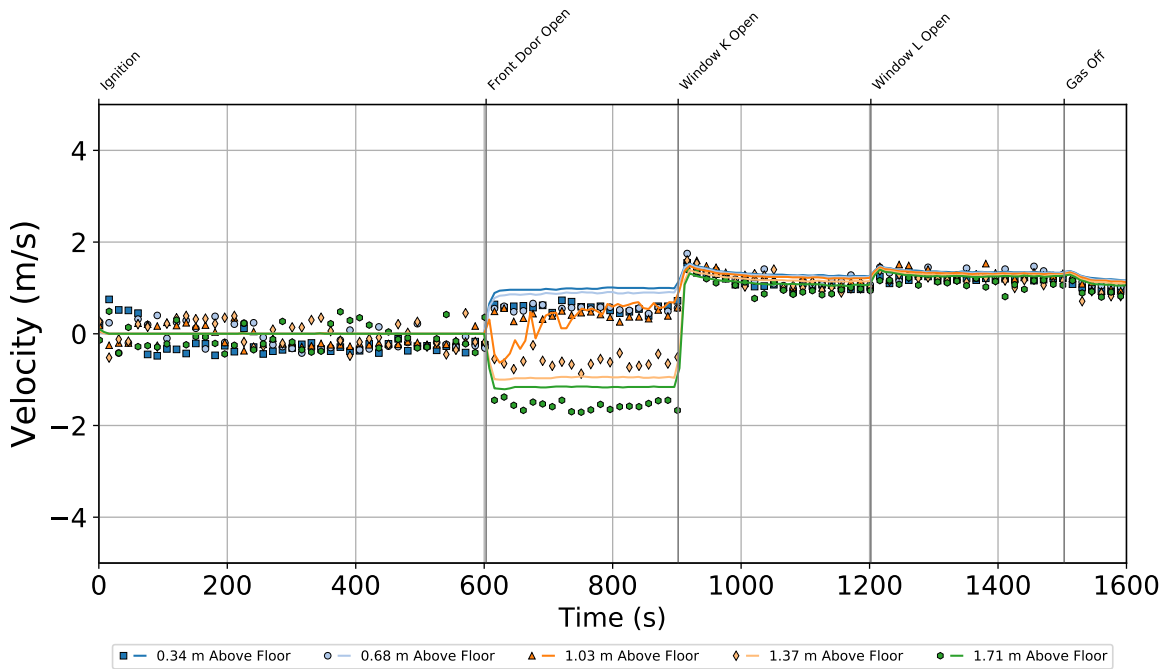


Figure 6.18: Velocities in the front door of the two-story structure during Experiment 4

The gases at the front door remained quiescent until the front door was opened, at which point bi-directional flow was immediately evident with the neutral plane located in the range of 1.03 m to 1.37 m above the floor. When window K was opened, the flow through the front door was directed completely into the structure as flow paths were created that connected the front door to the burner and from the burner to window K. Ventilation of window L did not significantly change the direction of flow or the flow velocity magnitude through the front door.

When window K was opened, much of the flow through the window was directed out of the structure. The neutral plane appeared at an elevation between 0.24 m and 0.48 m above the window sill. Ventilation of window L resulted in migration of the neutral plane upward such that it was located in the range of 0.48 m to 0.72 m above the window sill. Concurrently, the velocity of the flow of gases out of the structure through window K decreased significantly from opening of window K until the end of the experiment. These trends are consistent with exhaust of accumulated hot gases and a decrease in the buoyant force driving flow out of the structure as the volume of accumulated gases decreased and window L was opened, which created an additional high elevation vent in the structure.

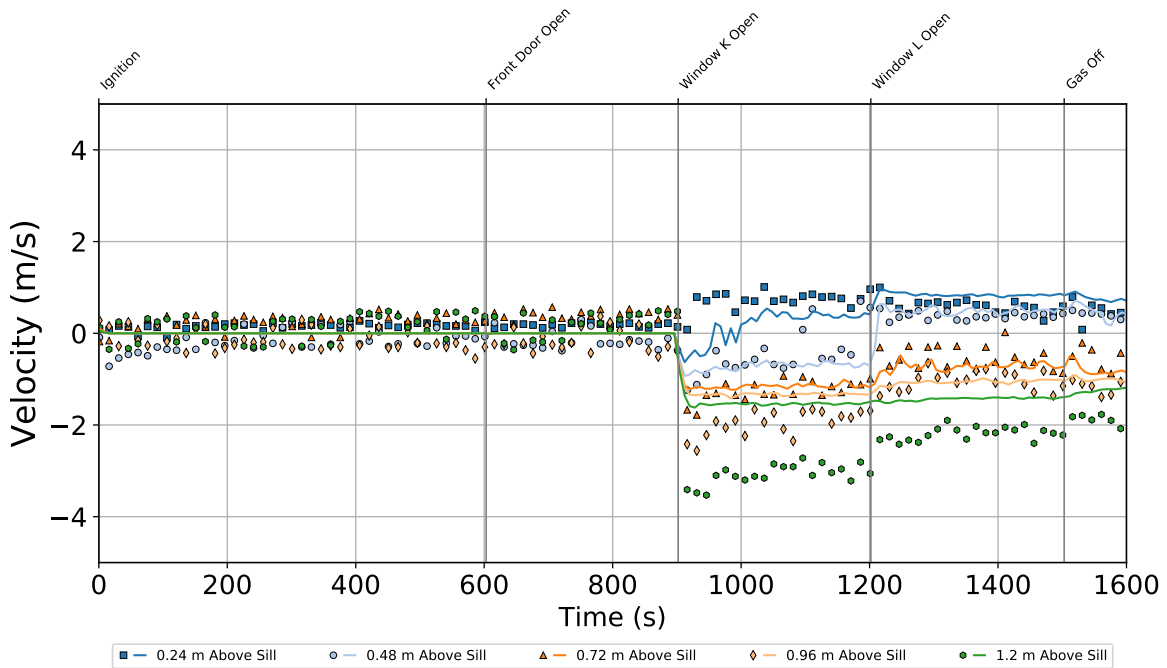


Figure 6.19: Velocities in window K of the two-story structure during Experiment 4

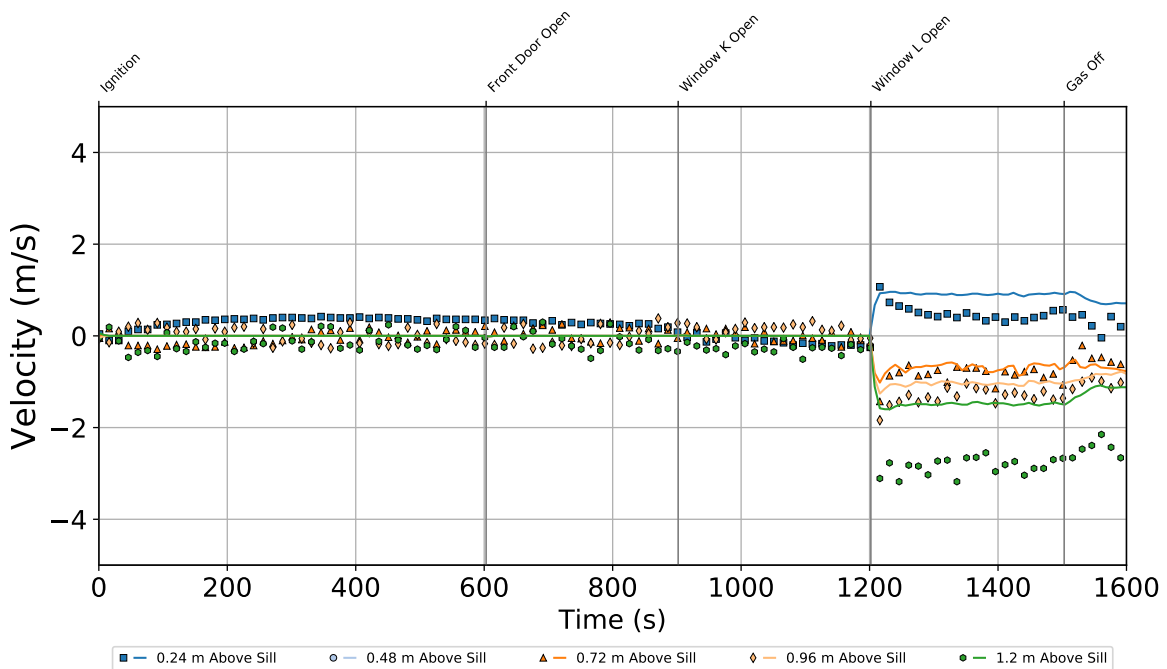


Figure 6.20: Velocities in window L of the two-story structure during Experiment 4

The bi-directional probe located 0.48 m above the window sill in window L malfunctioned and these data have not been included in Figure 6.20. When window L was vented, the neutral plane

appeared in the range of 0.24 m to 0.72 m above the window sill. Bi-directional flow through the window was steady through the remainder of the experiment with velocities in and out of the structure comparable to flow through window K.

The model accurately predicted the qualitative features of the data and the effect of opening the exterior windows and doors on the directions of flow and relative changes in flow velocity magnitude. The model also generally overpredicted flow velocities out of the structure through ventilation openings, but produced accurate predictions of the uni-directional flow velocity magnitude into the front door after ventilation of window K. One notable exception was an underprediction of the flow velocity out of the structure at the highest elevation measurement points for all vents considered in Experiment 4.

6.2 Two-Story: Experiment 5

Experiment 5 conducted on the two-story structure featured the 500 kW gas burner ignited for 1200 s accompanied by ventilation of the front door (600 s) and window B in the family room (900 s).

6.2.1 Experiment 5: Temperature

The temperature data collected by thermocouple arrays throughout the structure are presented in the following figures. Figure 6.21 displays the temperatures at the center of the family room, Figure 6.22 displays the temperatures in the foyer, Figure 6.23 displays the temperatures under the second story hallway, Figure 6.24 displays the temperatures in the kitchen, Figure 6.25 displays the temperatures at the middle of the second story hallway, Figure 6.26 displays the temperatures in the master bedroom, Figure 6.27 displays the temperatures in bedroom 2, Figure 6.28 displays the temperatures in bedroom 3, and Figure 6.29 displays the temperatures in bedroom 4.

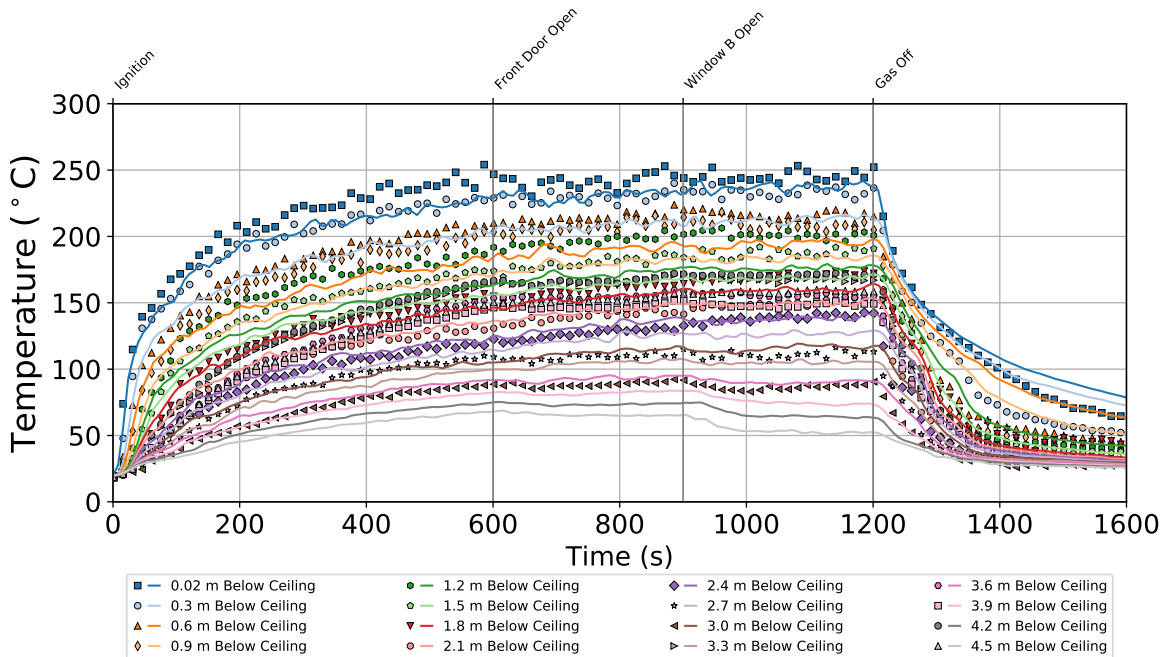


Figure 6.21: Temperatures in the center of the family room of the two-story structure during Experiment 5

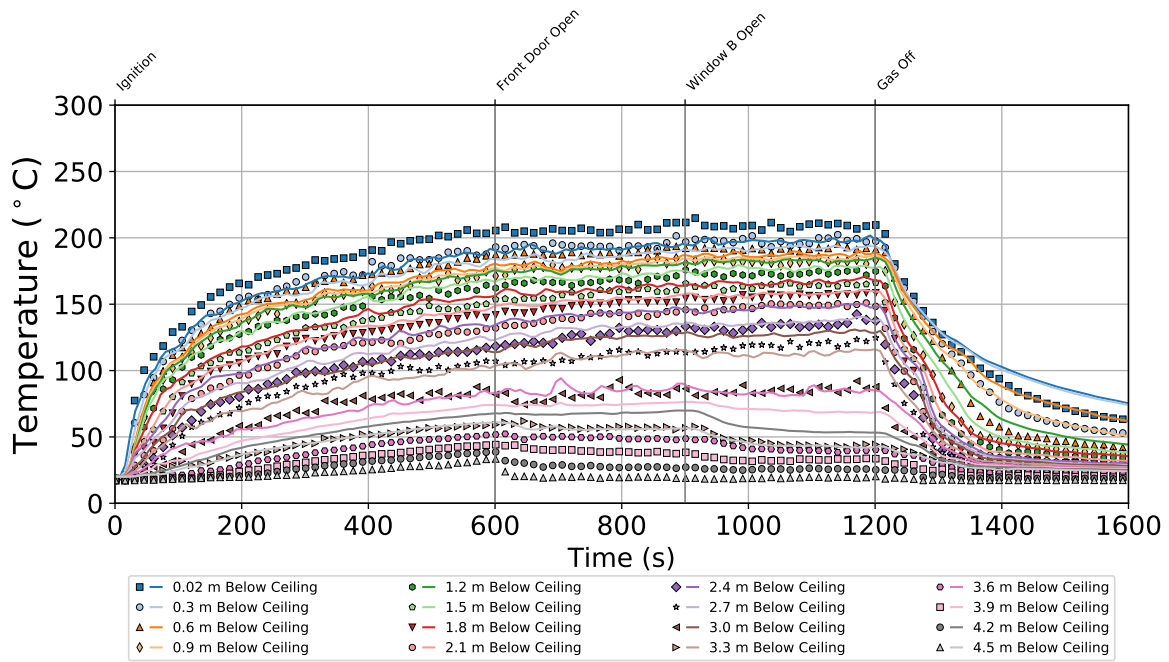


Figure 6.22: Temperatures in the foyer of the two-story structure during Experiment 5

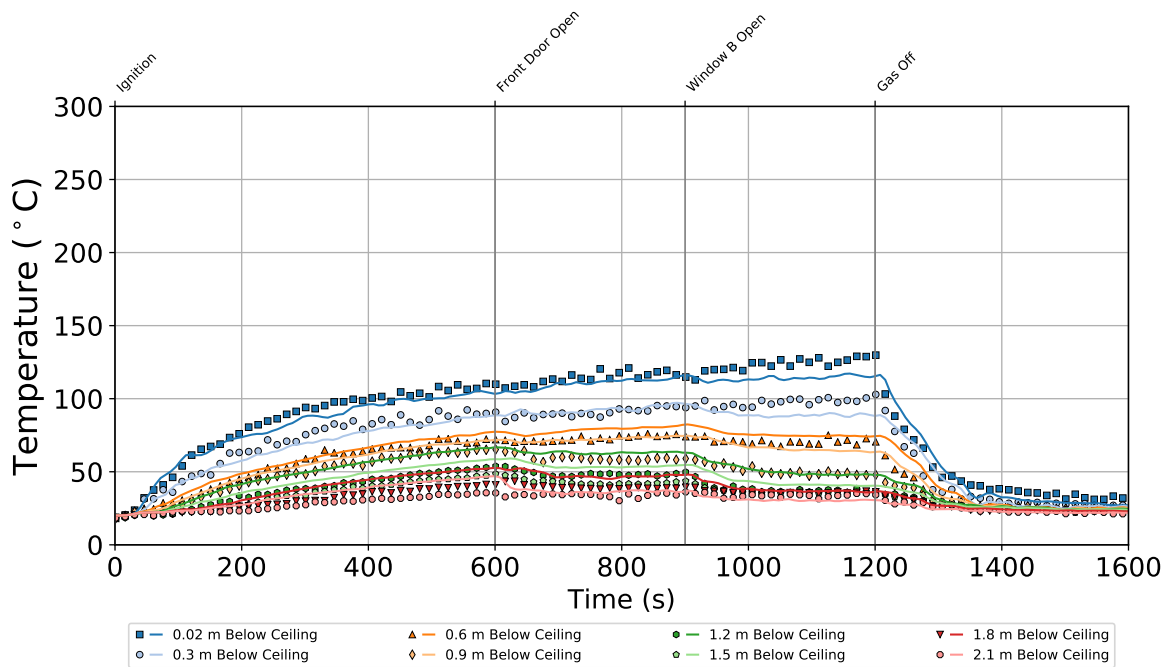


Figure 6.23: Temperatures under hallway of the two-story structure during Experiment 5

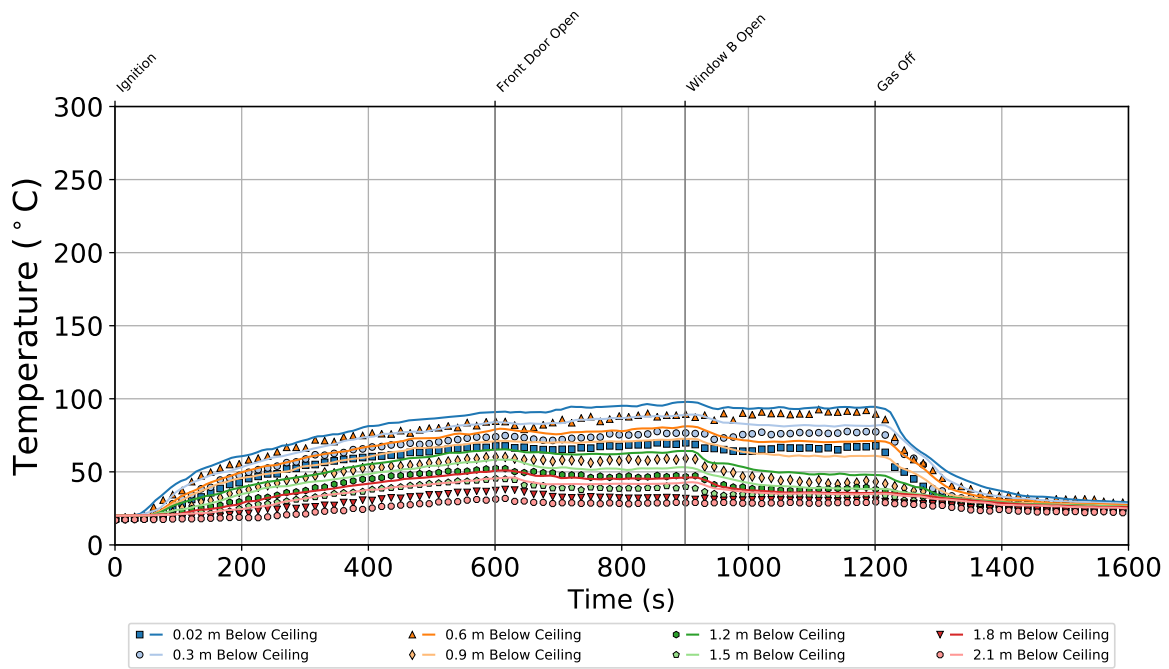


Figure 6.24: Temperatures in kitchen of the two-story structure during Experiment 5

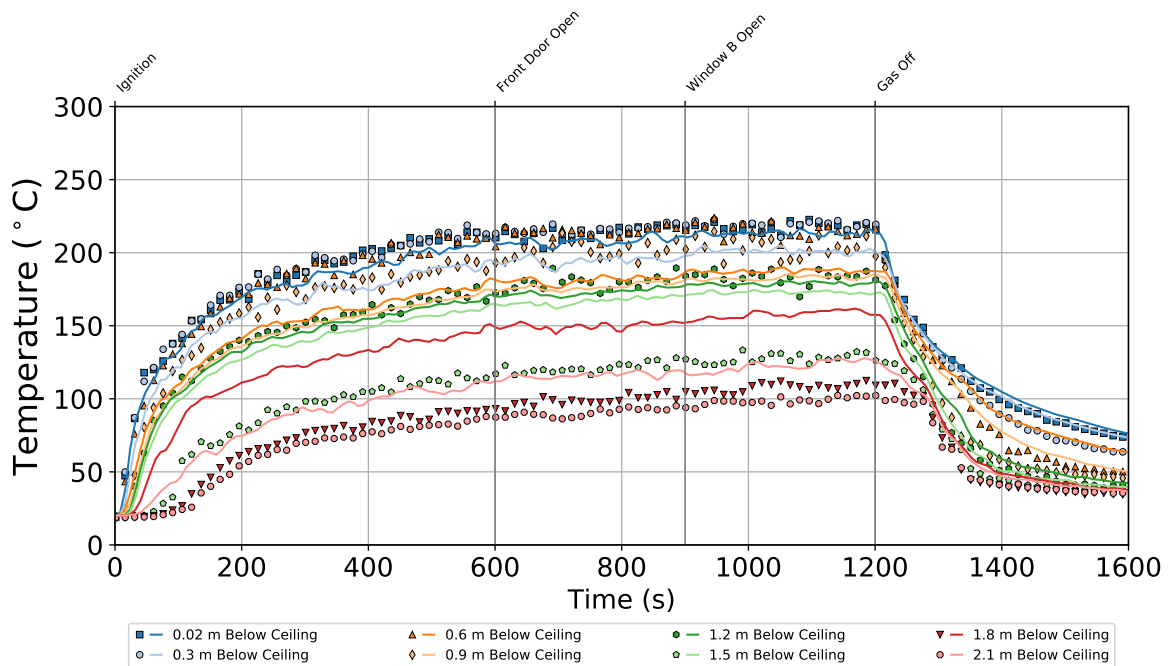


Figure 6.25: Temperatures in middle of second story hallway in the two-story structure during Experiment 5

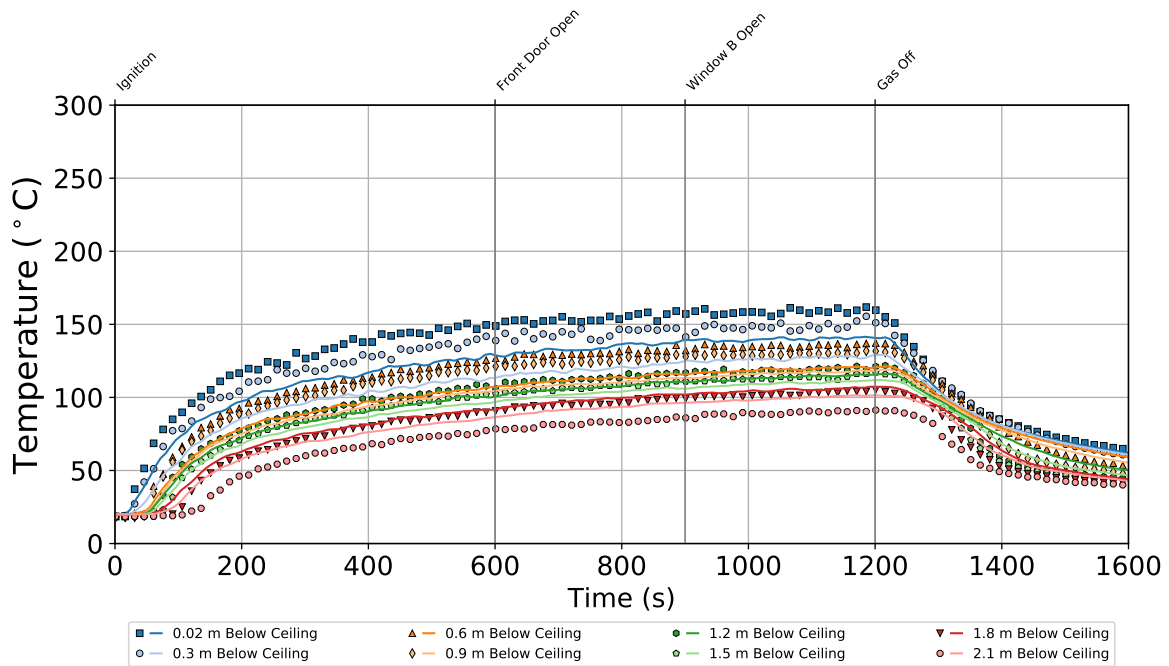


Figure 6.26: Temperatures in the master bedroom of the two-story structure during Experiment 5

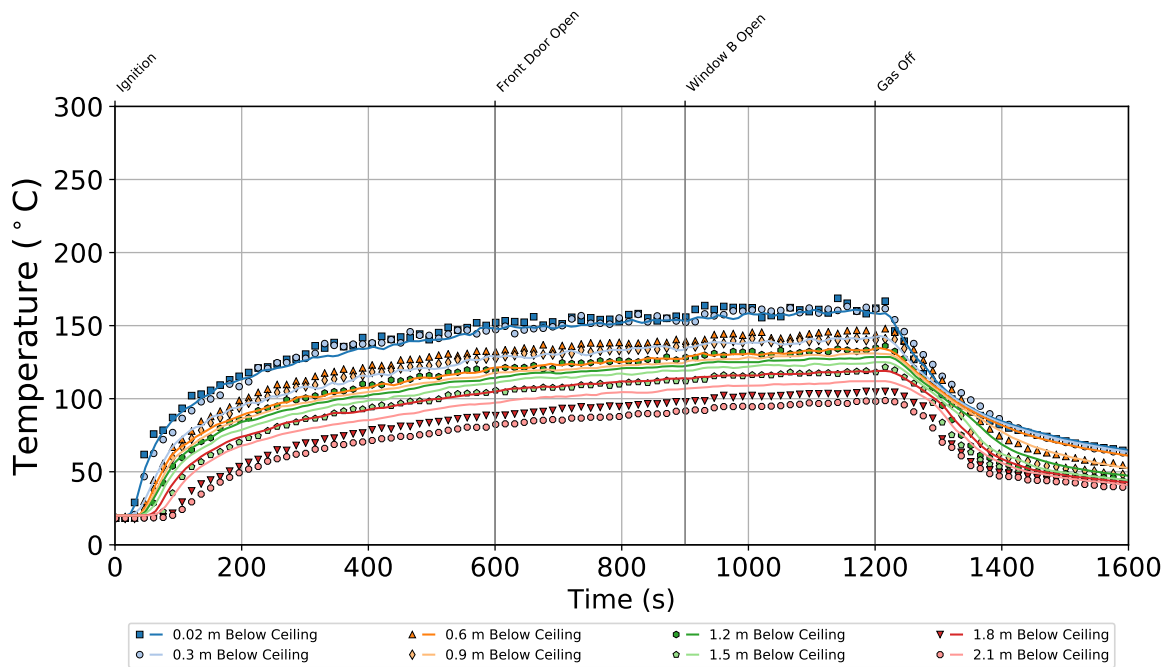


Figure 6.27: Temperatures in the bedroom 2 of the two-story structure during Experiment 5

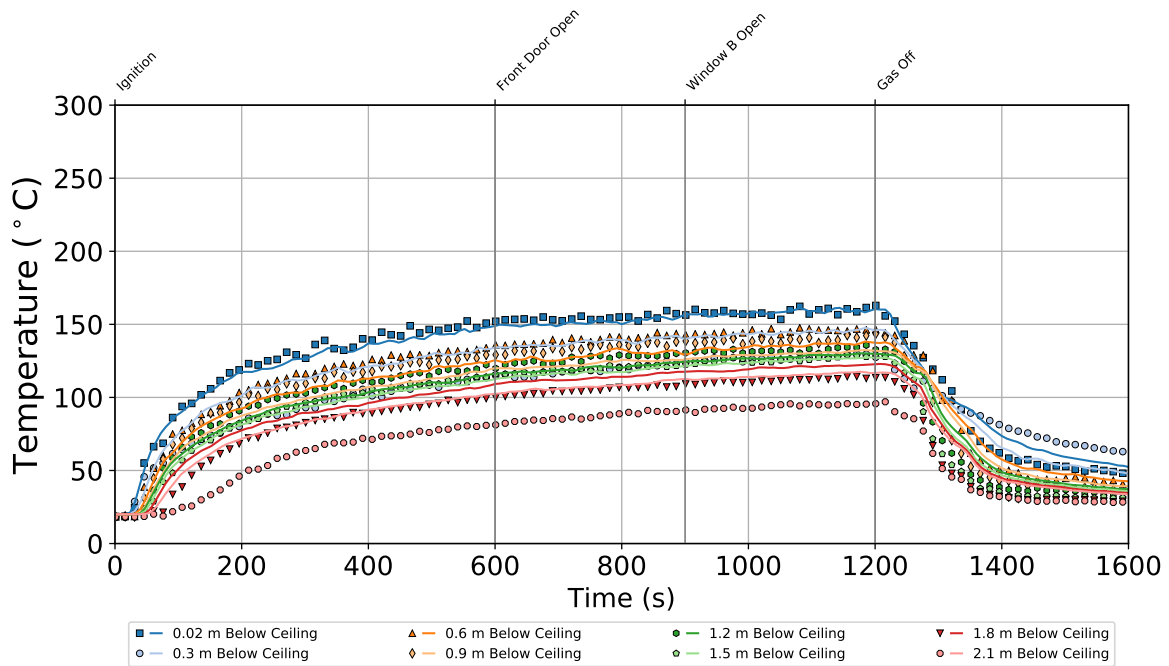


Figure 6.28: Temperatures in the bedroom 3 of the two-story structure during Experiment 5

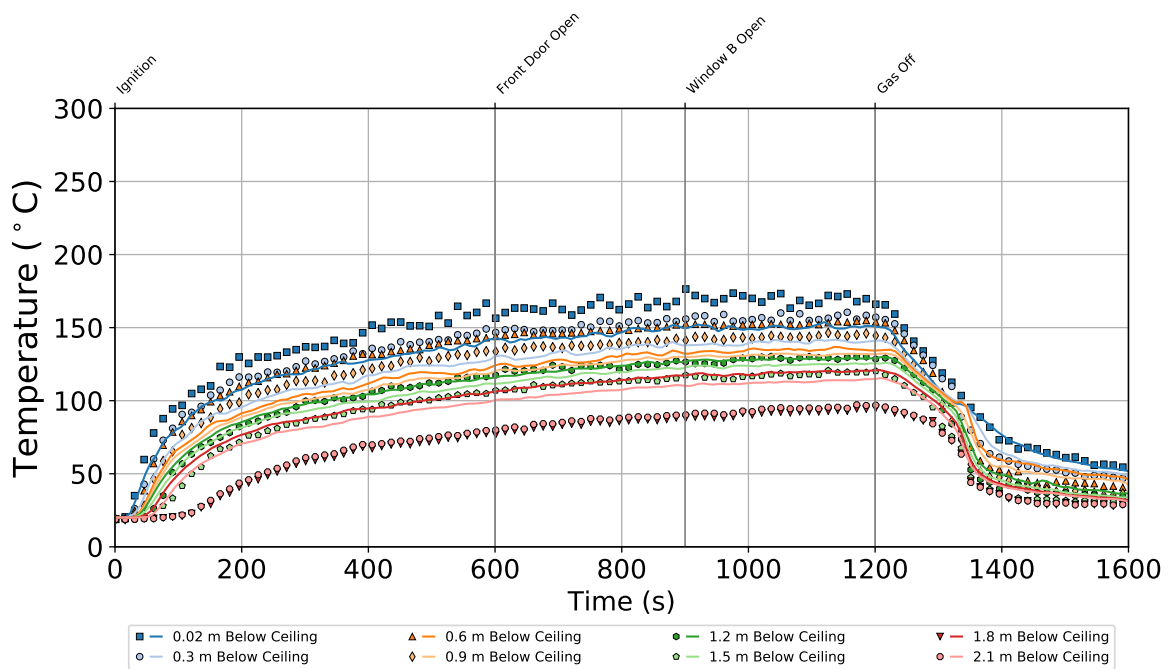


Figure 6.29: Temperatures in the bedroom 4 of the two-story structure during Experiment 5

All temperatures measured throughout the structure steadily increased until the front door was opened. When the front door was opened, the temperatures measured at elevations lower than 0.6 m below the ceiling under the second story hallway and in the kitchen as well as the temperatures measured 3.9 m below the ceiling and at lower elevations in the foyer decreased slightly. At the same time, all other temperatures remained steady or slightly increased. These trends indicated the flow path from the front door to the burner introduced cool air to low elevation areas throughout the structure, effectively lowering the temperatures at low elevations throughout the first story.

When window B was opened, all temperatures measured in the center of the family room and the foyer remained relatively steady, temperatures measured at elevations higher than 0.3 m below the ceiling increased gradually, while those at lower elevations decreased under the second story hallway and in the kitchen, and all temperatures measured on the second story gradually increased. All temperatures throughout the structure quickly decreased when gas flow to the burner was stopped.

The temperatures measured throughout the first story during Experiment 5 ranged from ambient temperature to approximately 100°C, with the maximum temperatures measured under the second story hallway closer to approximately 130°C. Significantly lower temperatures were observed in the living room, laundry room, and the den. The temperatures measured in the regions of the structure that spanned the height of both stories and the temperatures measured in the second story hallway peaked in the range of 200°C to 250°C, and the temperatures in the second story bedrooms ranged from ambient temperature to approximately 170°C throughout the experiment.

The temperatures measured in the center of the family room at elevations 3.3 m below the ceiling and lower diverged from the general trend of stratification of the gas temperatures with respect to elevation. Particularly notable were the temperatures measured 3.3 m and 4.2 m below the ceiling that were comparable to temperatures 1.8 m below the ceiling throughout the experiment. A flow path similar to that described for Experiment 4 was evident in Experiment 5 that resulted in circulation of hot gases and may have contributed to non-stratification of the gas temperatures in the family room. A similar phenomenon was also observed in the kitchen, where the highest temperature measurements were observed 0.6 m below the ceiling throughout the experiment.

In general, the model accurately predicted the qualitative features in the data that resulted from the ventilation openings. The model typically accurately predicted the temperatures near the ceiling and overpredicted temperatures near the floor. The model erroneously predicted stratification of gas temperatures as a function of elevation in the family room and in the kitchen. The temperatures measured at elevations 1.8 m below the ceiling and higher in the center of the family room were underpredicted by the model and temperatures 2.7 m and 3.0 m below the ceiling were overpredicted. Due to the prediction of stratification of the temperature profile that did not occur in the experiments, the temperatures measured 3.3 m below the ceiling and at lower elevations were underpredicted.

The temperatures in the foyer were overpredicted at all elevations lower than 0.9 m below the ceiling throughout the experiment. The temperatures under the second story hallway were accurately predicted 0.02 m and 0.3 m below the ceiling, but overpredicted at all lower elevations. The model underpredicted temperatures measured at elevations ranging from 0.3 m to 0.9 m below the

ceiling and overpredicted the temperatures 1.5 m below the ceiling and at lower elevations in the middle of the second story hallway. There was a distinction between the high temperature gases near the ceiling and cooler air near the floor in the second story hallway that the model did not predict. In general, the model predicted more closely clustered temperature profiles in the bedrooms than were measured in the experiments, effectively underpredicting temperatures near the ceiling and overpredicting temperatures near the floor. The experimental temperatures in the bedrooms steadily spanned over a range of approximately 70°C whereas the predictions spanned over a range of approximately 40°C.

6.2.2 Experiment 5: Pressure

The pressure data collected throughout the structure are presented in the following figures. Figure 6.30 displays the pressures in the family room, Figure 6.31 displays the pressures next to the front door, Figure 6.32 displays the pressures in the living room, Figure 6.33 displays the pressures in the den, Figure 6.34 displays the pressures in the master bedroom, Figure 6.35 displays the pressures in bedroom 2, Figure 6.36 displays the pressures in bedroom 3, and Figure 6.37 displays the pressures in bedroom 4.

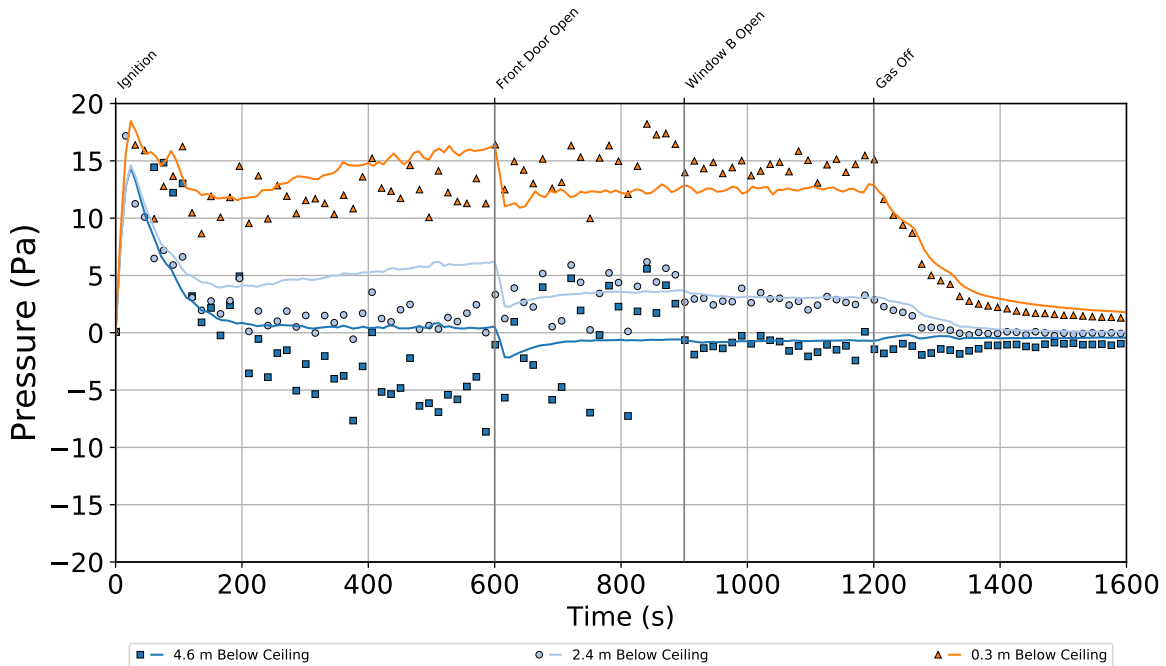


Figure 6.30: Pressures in the family room of the two-story structure during Experiment 5

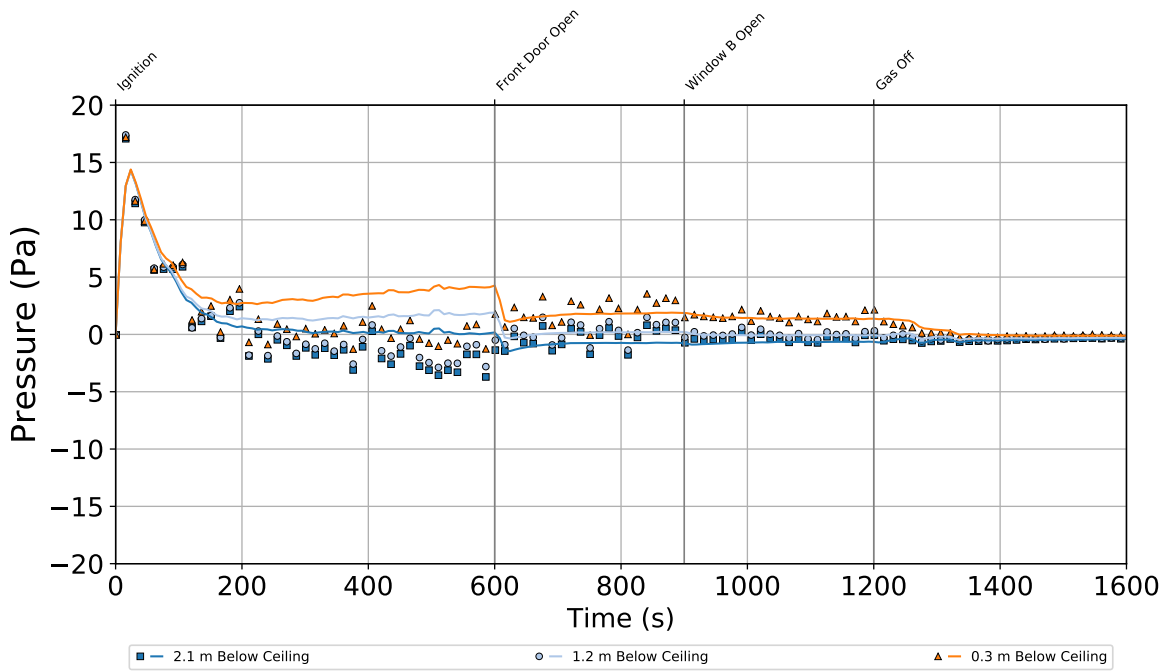


Figure 6.31: Pressures next to the front door of the two-story structure during Experiment 5

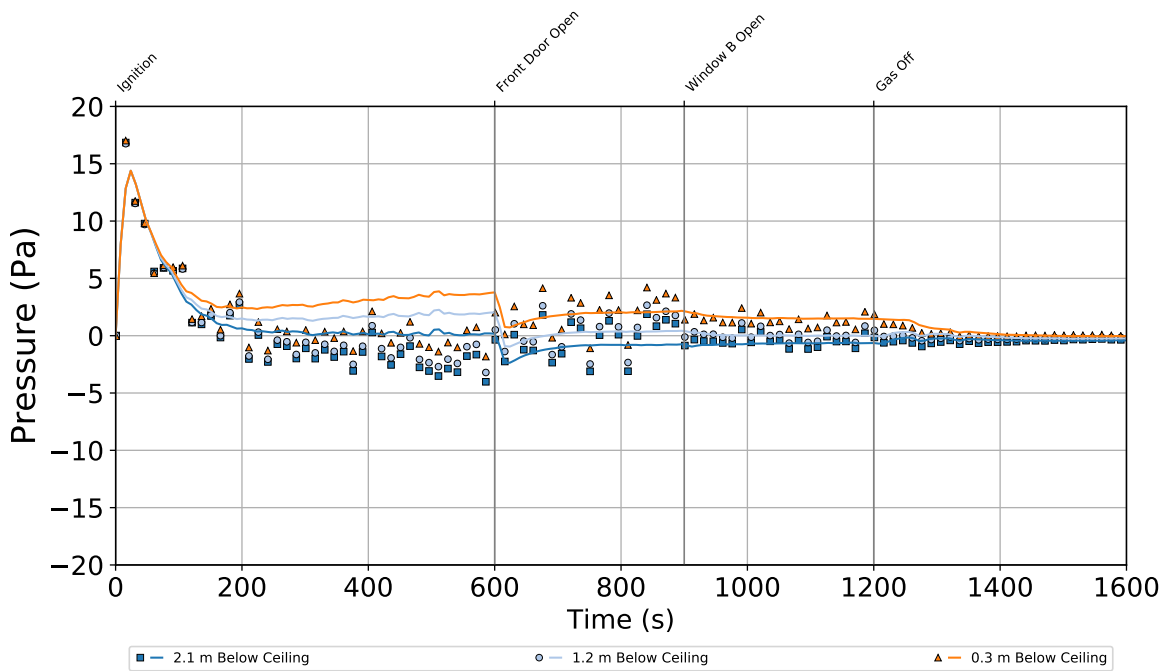


Figure 6.32: Pressures in the living room of the two-story structure during Experiment 5

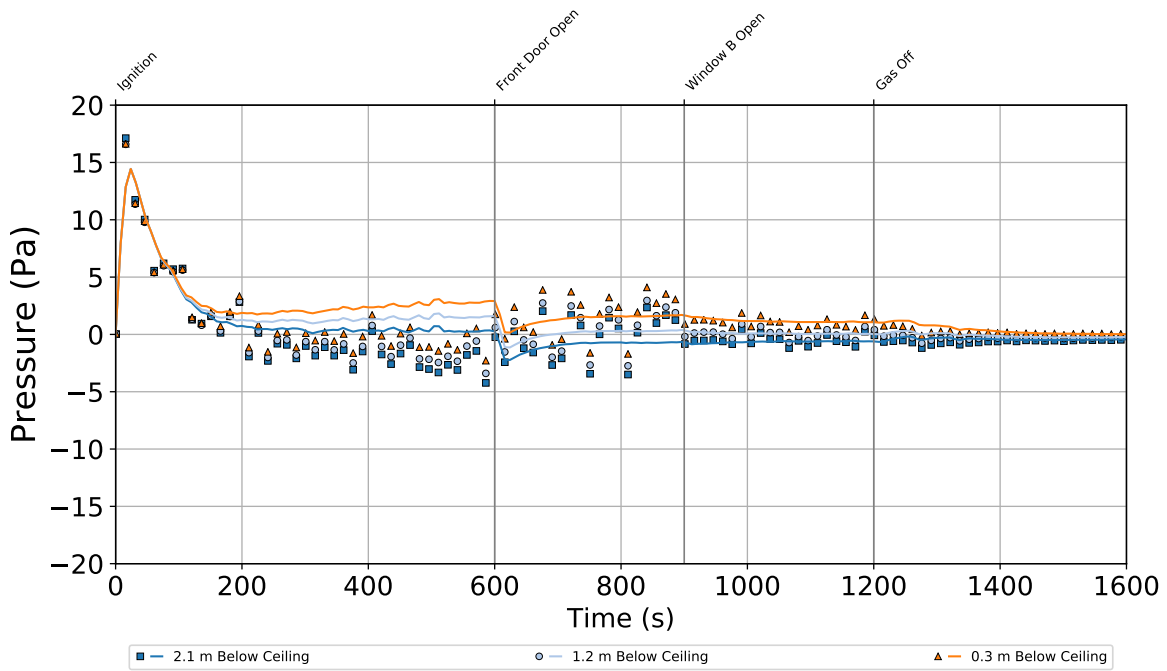


Figure 6.33: Pressures in den of the two-story structure during Experiment 5

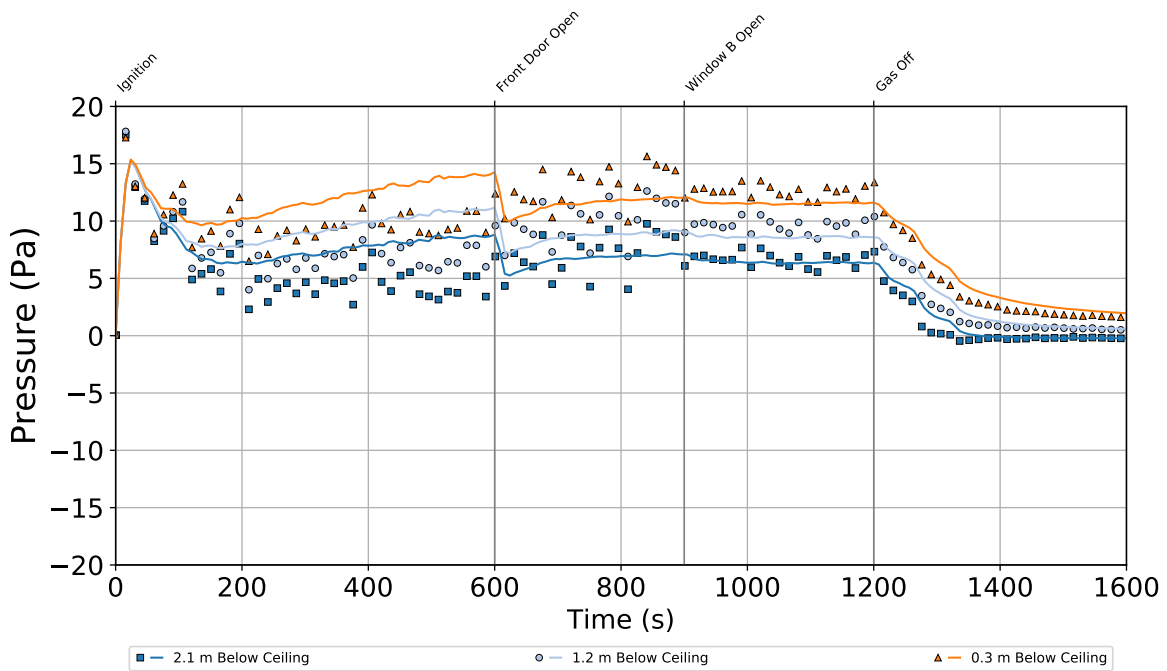


Figure 6.34: Pressures in the master bedroom of the two-story structure during Experiment 5

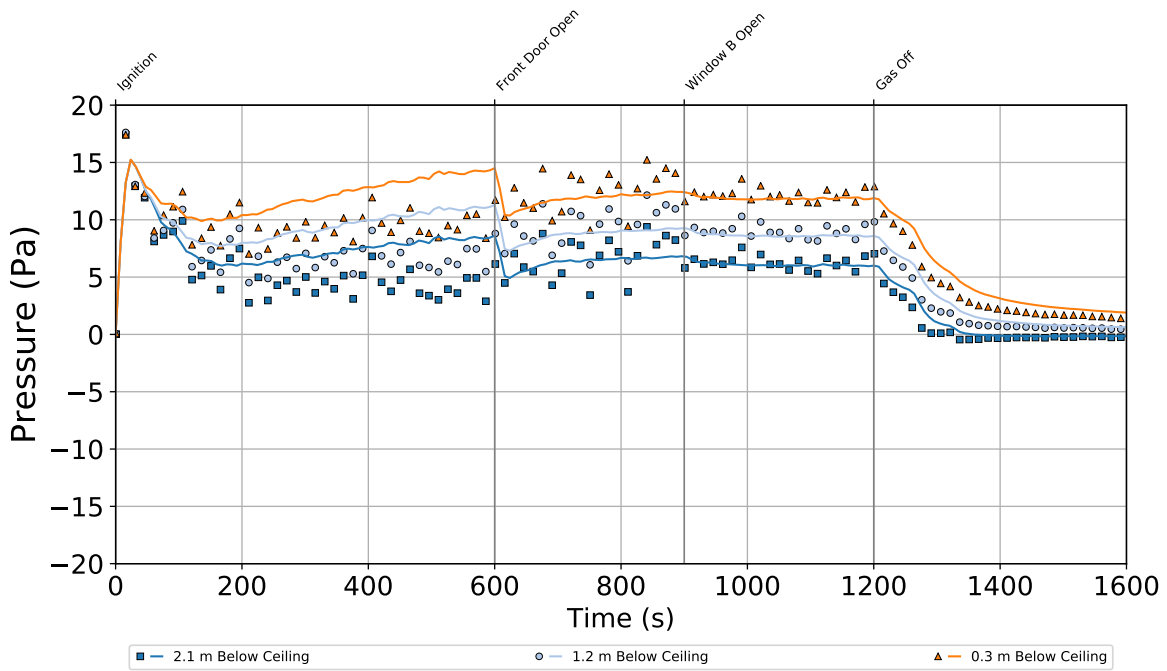


Figure 6.35: Pressures in bedroom 2 of the two-story structure during Experiment 5

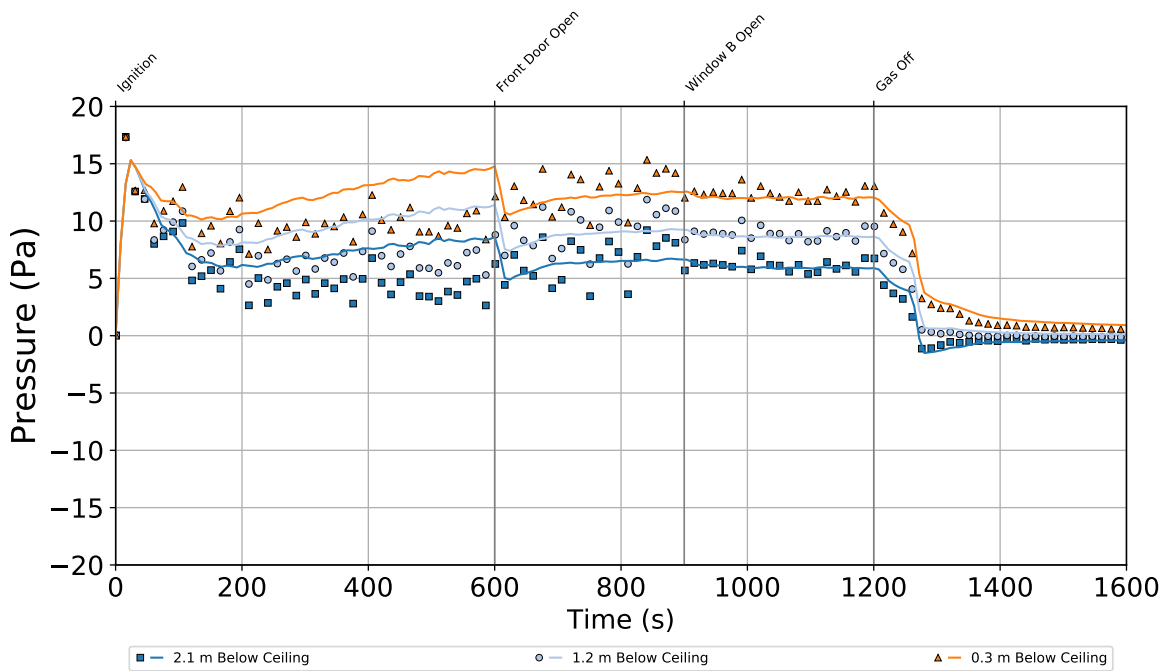


Figure 6.36: Pressures in bedroom 3 of the two-story structure during Experiment 5

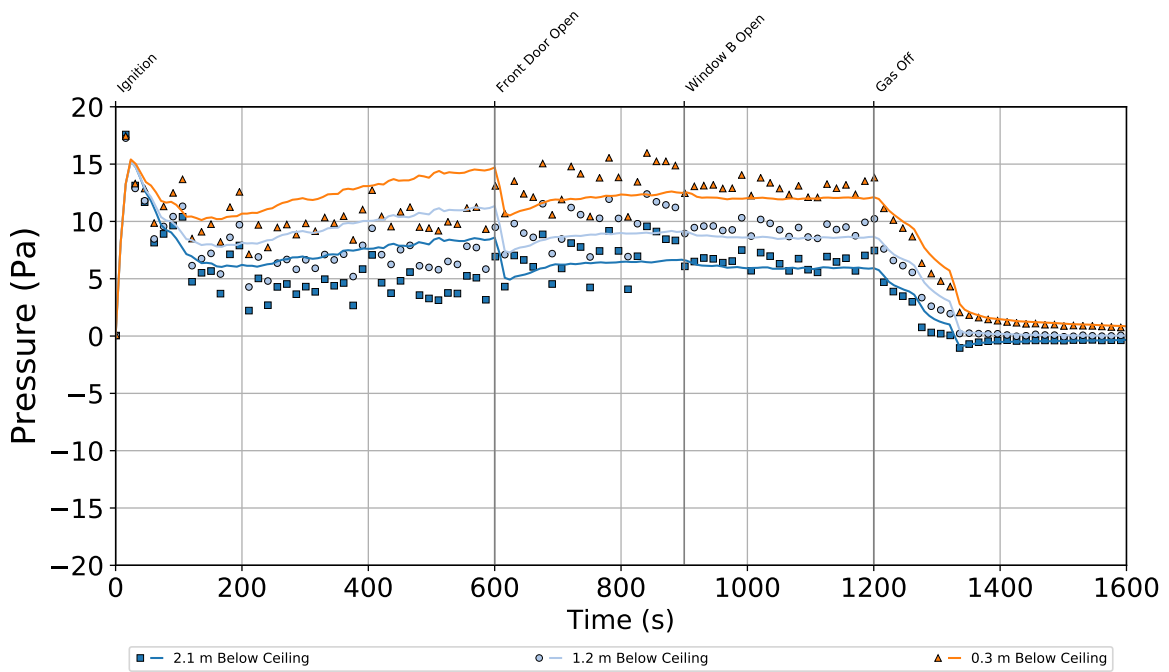


Figure 6.37: Pressures in bedroom 4 of the two-story structure during Experiment 5

The pressures throughout the structure increased immediately after ignition to a global maximum in the range of 12 Pa to 17 Pa at all measurement locations followed by a gradual decay in pressure magnitude. The pressure measured 4.6 m below the ceiling of the family room reached a peak of approximately 36 Pa for a short duration approximately 15 s into the experiment. All pressure measurements from the first story and those collected 4.6 m below the ceiling in the family room achieved pressures below atmospheric pressure prior to ventilation of the front door. All measurements from the second story and those collected at higher elevations in areas that were open to the second story were above atmospheric pressure prior to ventilation of the front door. These negative pressures are indicative of air flow throughout the first story entrained by the burner. Positive pressures at high elevations and in the second story compartments indicate higher temperatures near the ceiling and may indicate a positive net mass flow due to the dominance of buoyancy throughout the structure.

Upon ventilation of the front door, all measured pressures immediately increased and remained steady at low elevations and throughout the first story and gradually increased on the second story until window B was opened. Ventilation of window B resulted in pressures measured on the first story to decrease, but had no significant effect on the pressure measurements from the second story. All measured pressures increased or decreased such that they were closer to atmospheric pressure after gas flow to the burner was stopped. Pressures measured on the first story ranged from -5 Pa to 5 Pa throughout the experiment, while those measured on the second story ranged from approximately -1 Pa to 15 Pa.

The model generally made good qualitative predictions of the data resulting from the ventilation events. The pressure measured 0.3 m below the ceiling in the family room was underpredicted until gas flow to the burner was stopped. This is consistent with the underprediction in gas temperature measured 0.3 m below the ceiling at the center of the family room shown in Figure 6.21. Pressures were overpredicted at all measurement locations and elevations throughout the structure between ignition and opening the front door, and pressures were predicted to increase over time although the measured pressures remained steady after the initial increase and decrease in pressure caused by ignition of the burner. When the front door was opened, the trend in the measurements was an increase in all measured pressures, whereas a decrease in all pressures was predicted. After ventilation of the front door, the model qualitatively and quantitatively captured the trends in the measured data. The overprediction of pressures between ignition and ventilation of the front door may be an artifact of the representation of leakage and the location of the vent that corresponded to leakage in the model.

6.2.3 Experiment 5: Velocity

Figure 6.38 displays the velocities measured at the front door.

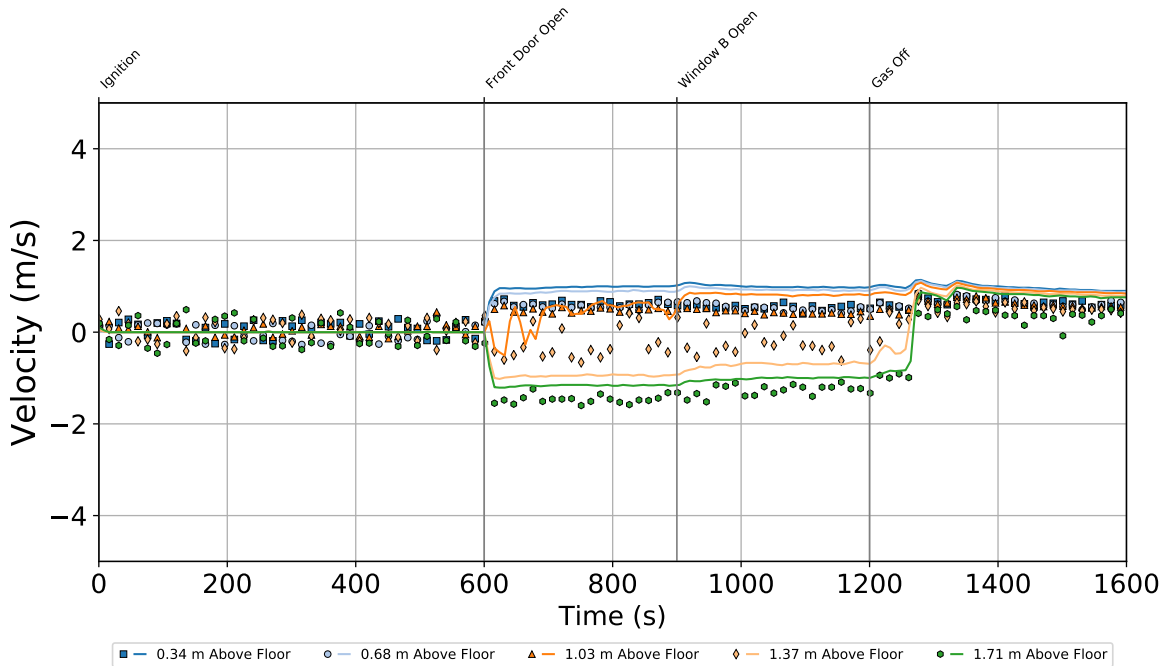


Figure 6.38: Velocities in the front door of the two-story structure during Experiment 5

The gases at the front door remained quiescent until the front door was opened, at which point bi-directional flow was immediately evident with the neutral plane located in the range of 1.03 m to 1.37 m above the floor. A potential instability in the flow through the front door was evident 1.37 m above the floor because the flow alternated between being directed into and out of the structure.

The model accurately predicted the qualitative features of the data and the effect of opening the exterior doors and windows on the directions of flow and relative changes in flow velocity magnitude through the front door. The model also generally overpredicted flow velocities out of the structure and did not predict the apparent instability in flow 1.37 m above the floor throughout the experiment after the front door was opened.

6.3 Two-Story: Experiment 6

Experiment 6 conducted on the two-story structure featured the 500 kW gas burner ignited for 1500 s as well as ventilation of window K in bedroom 3 (600 s), window A in the kitchen (900 s), and the front door (1200 s).

6.3.1 Experiment 6: Temperature

The temperature data collected by thermocouple arrays throughout the structure are presented in the following figures. Figure 6.39 displays the temperatures at the center of the family room, Figure 6.40 displays the temperatures in the foyer, Figure 6.41 displays the temperatures under the second story hallway, Figure 6.42 displays the temperatures in the kitchen, Figure 6.43 displays the temperatures at the middle of the second story hallway, Figure 6.44 displays the temperatures in the master bedroom, Figure 6.45 displays the temperatures in bedroom 2, Figure 6.46 displays the temperatures in bedroom 3, and Figure 6.47 displays the temperatures in bedroom 4.

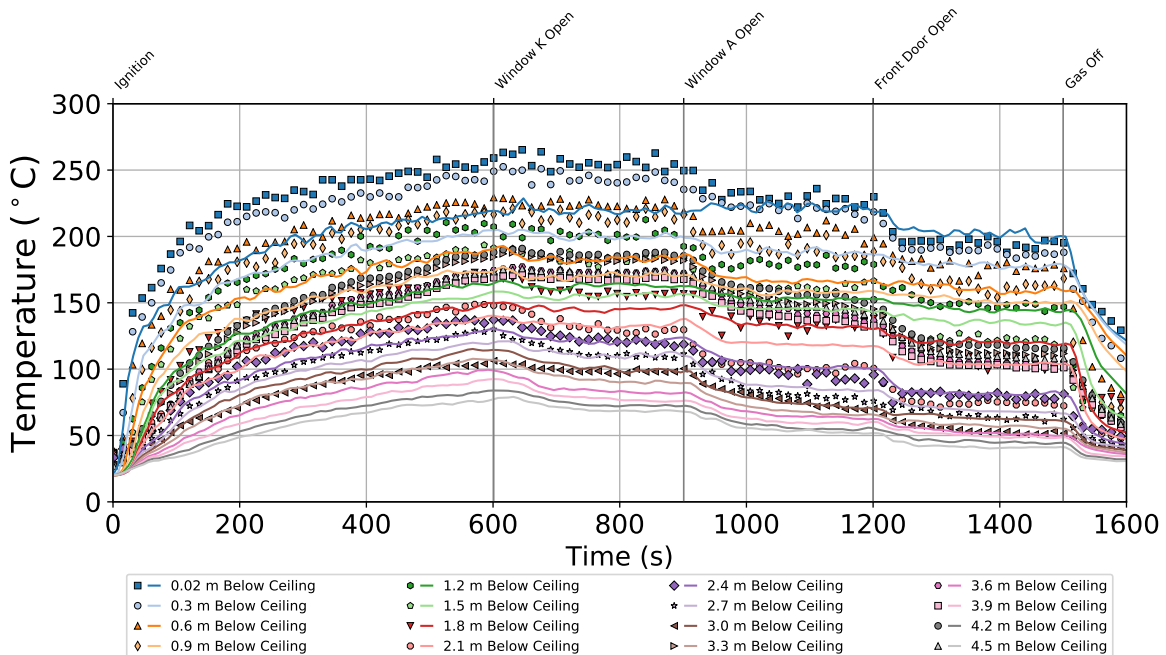


Figure 6.39: Temperatures in the center of the family room of the two-story structure during Experiment 6

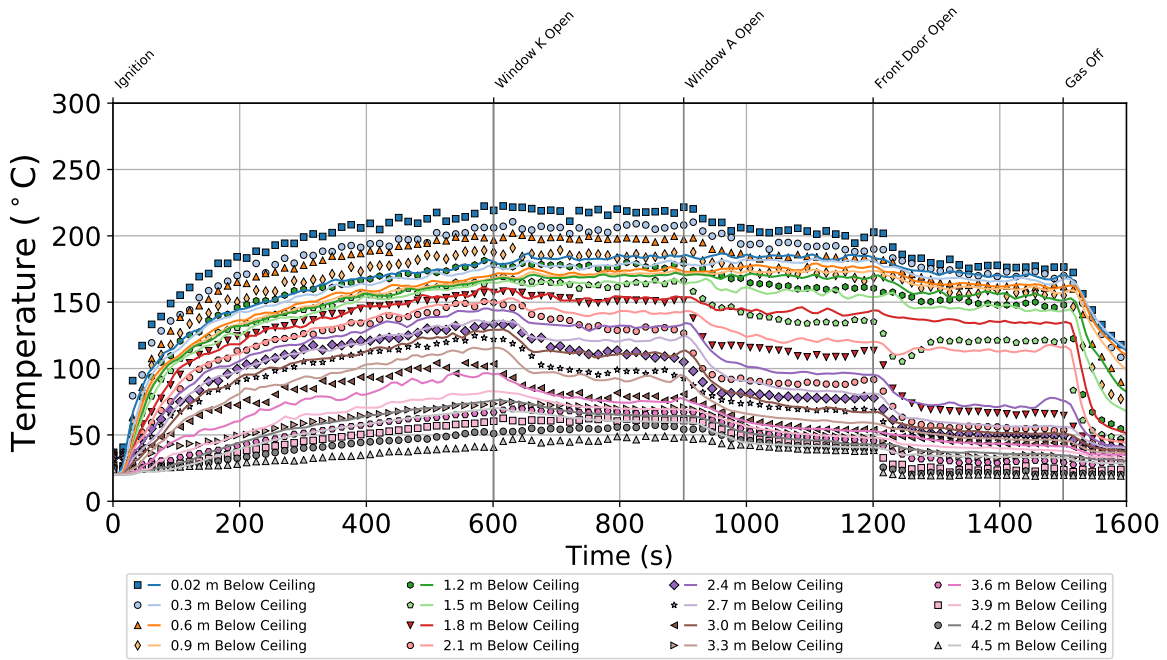


Figure 6.40: Temperatures in the foyer of the two-story structure during Experiment 6

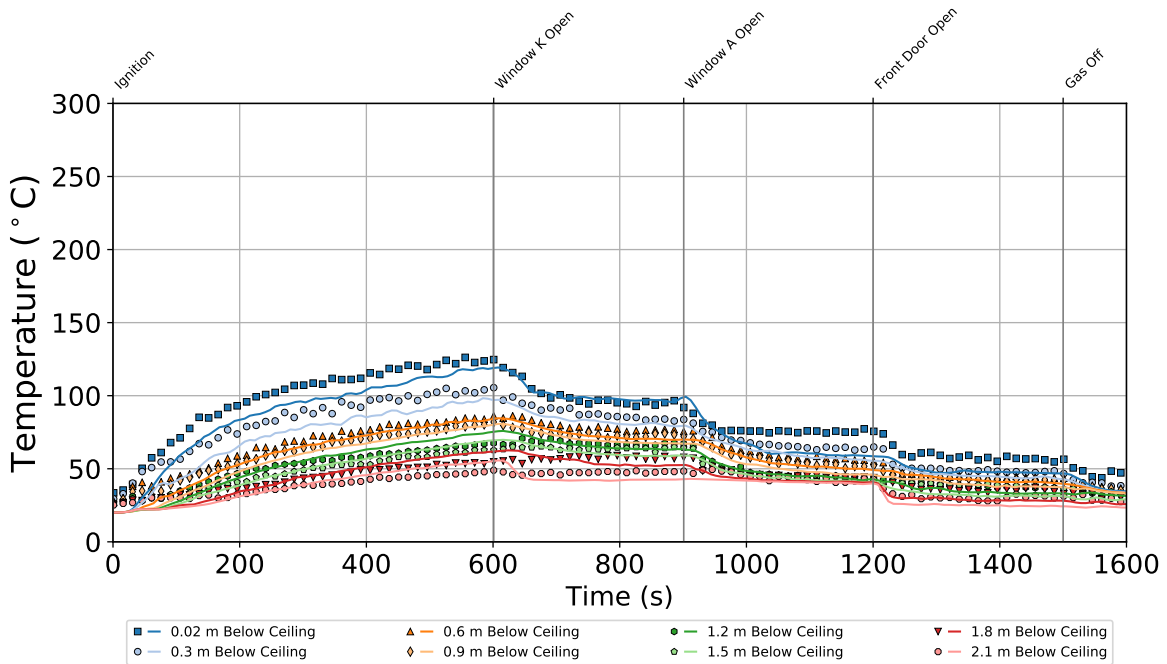


Figure 6.41: Temperatures under hallway of the two-story structure during Experiment 6

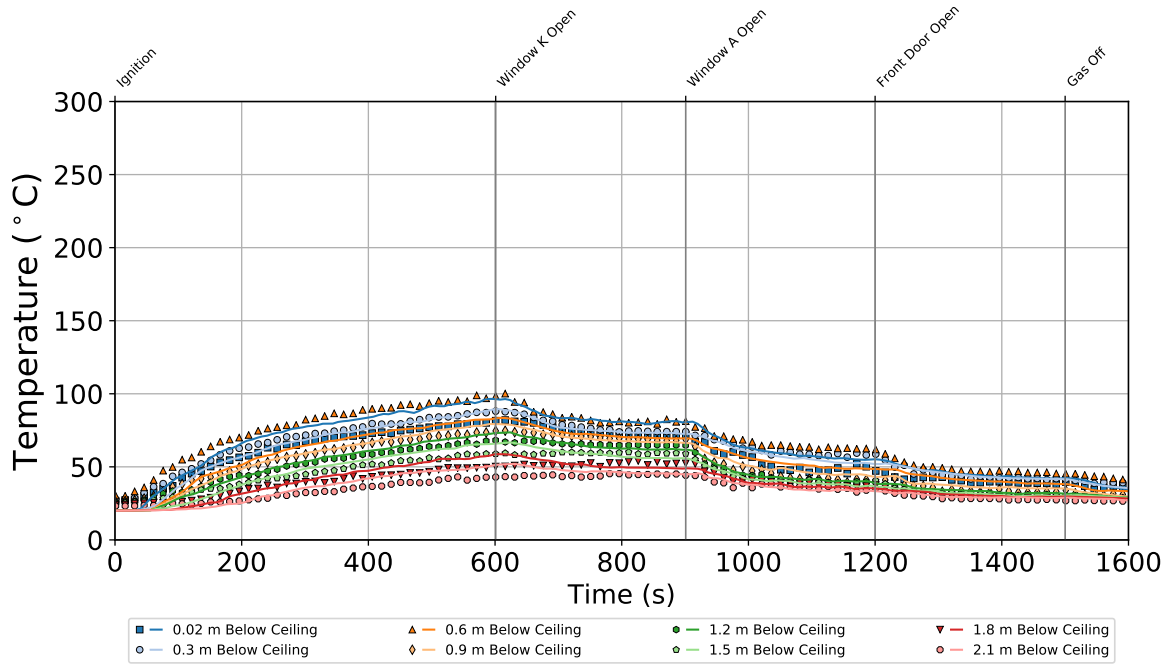


Figure 6.42: Temperatures in the kitchen of the two-story structure during Experiment 6

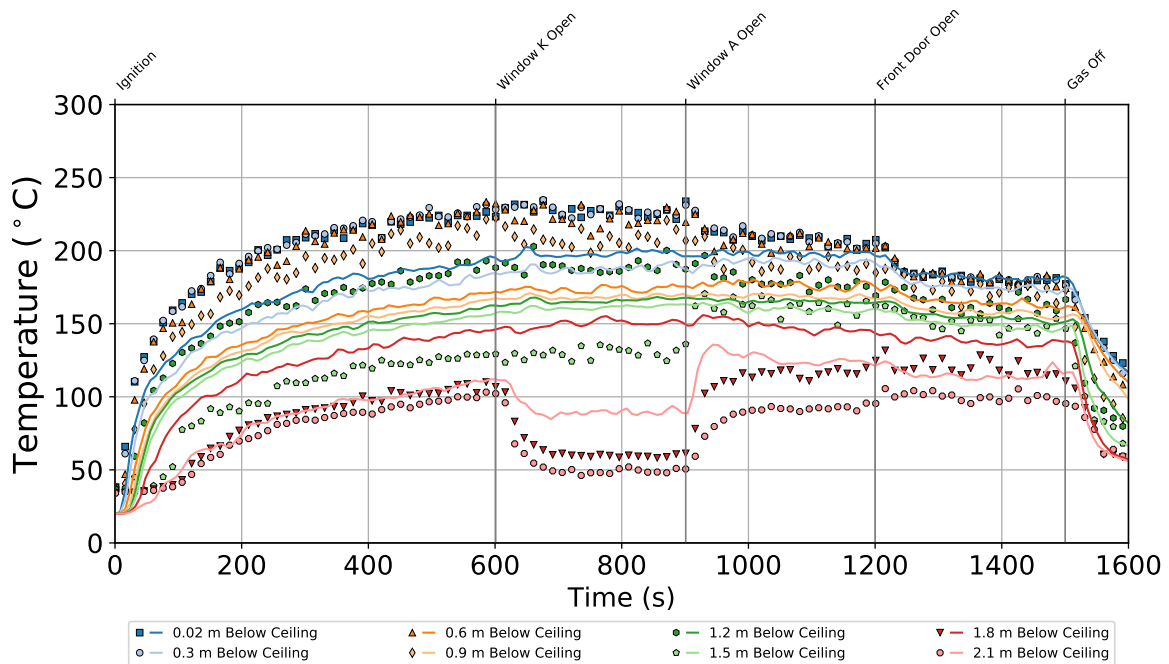


Figure 6.43: Temperatures in the middle of second story hallway in the two-story structure during Experiment 6

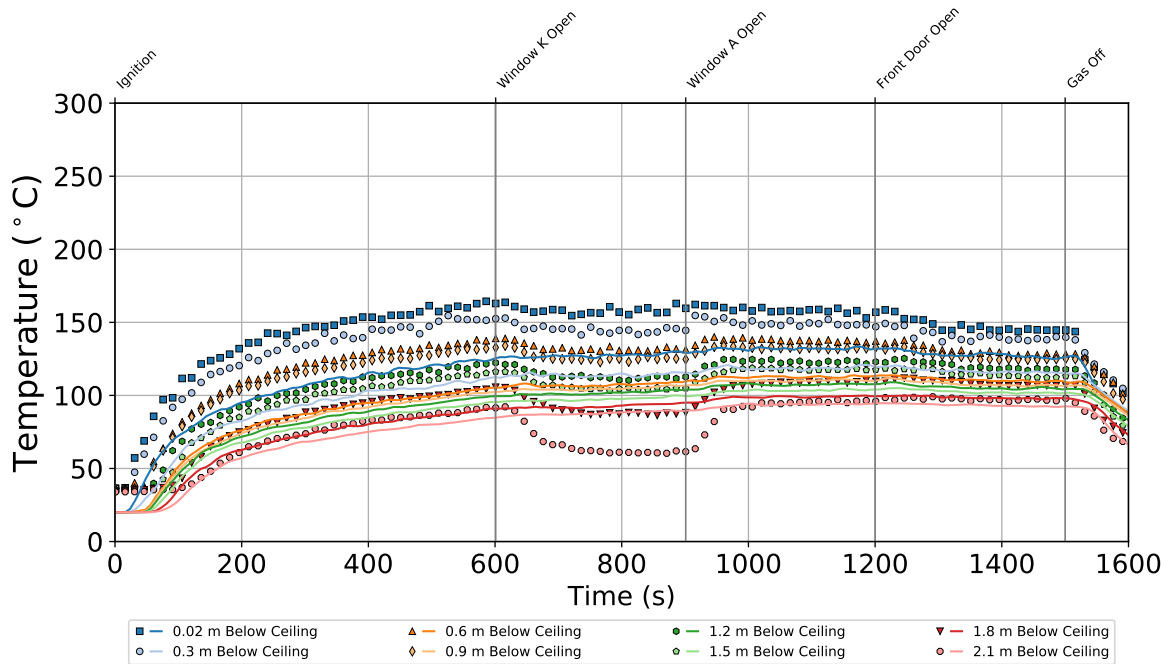


Figure 6.44: Temperatures in the master bedroom of the two-story structure during Experiment 6

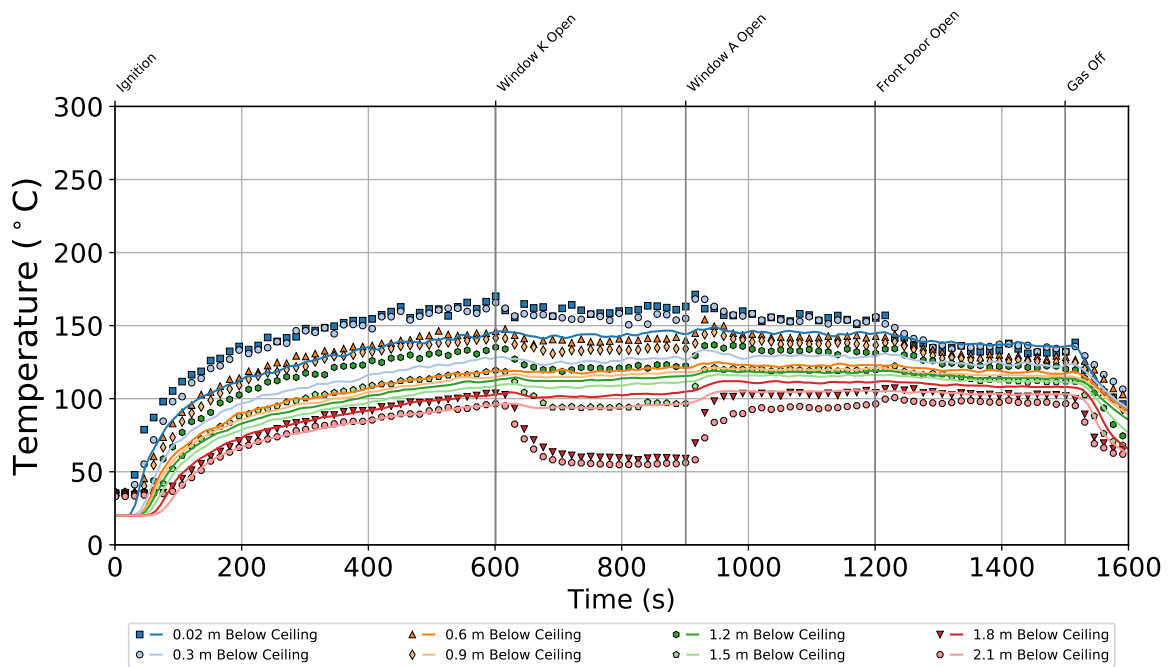


Figure 6.45: Temperatures in bedroom 2 of the two-story structure during Experiment 6

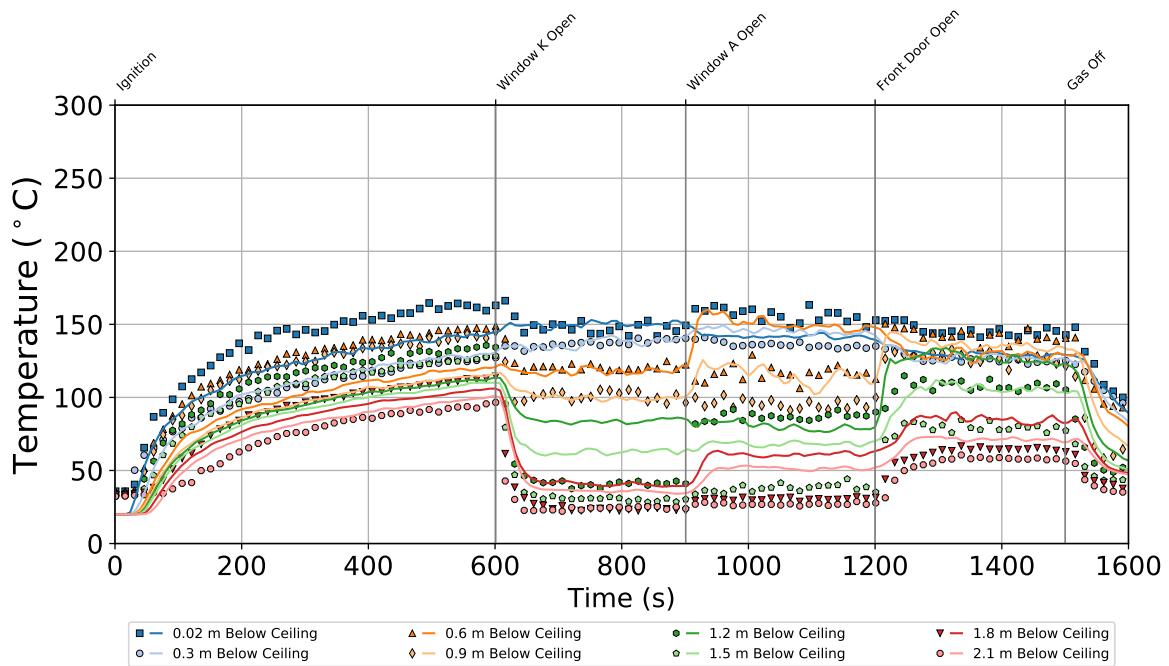


Figure 6.46: Temperatures in bedroom 3 of the two-story structure during Experiment 6

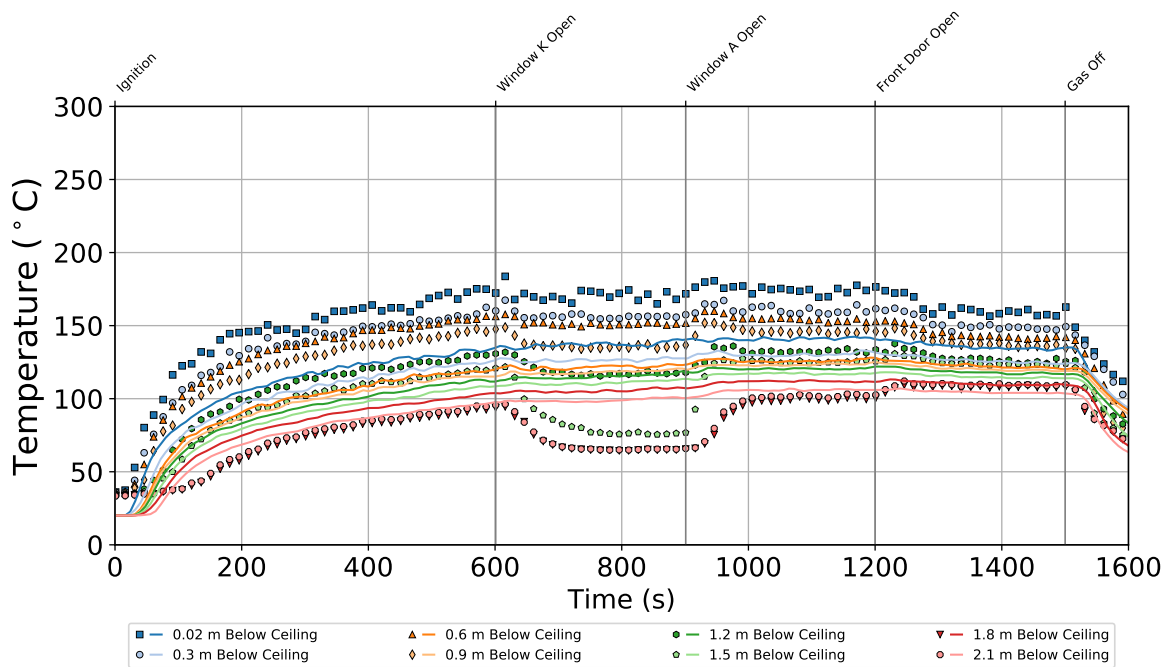


Figure 6.47: Temperatures in bedroom 4 of the two-story structure during Experiment 6

All temperatures steadily increased until window K was vented. When window K was opened, the temperatures measured 0.9 m below the ceiling and at higher elevations under the second story hallway and in the kitchen as well as the temperatures measured 1.8 m below the ceiling and at lower elevations in the foyer and the center of the family room decreased slightly, while all other temperature measurements on the first story remained steady. At the time window K was opened, the temperatures 1.8 m below the ceiling and lower in the middle of the second story hallway decreased significantly while all temperatures in the master bedroom and bedroom 3 decreased, and temperatures measured 0.6 m below the ceiling and lower in bedroom 2 and bedroom 4 decreased. These trends indicate that window K introduced cool air to the second story and allowed accumulated hot gases to flow out of the structure, effectively lowering the temperatures on the second story and in low elevation areas on the first story.

When window A was opened, a flow path from the kitchen to the burner in the family room was created in addition to the flow path from the burner to window K. These two flow paths facilitated movement of hot gases to the second story. All temperatures measured on the first story and in the areas that spanned from the first story to the second story decreased, and temperatures 1.5 m below the ceiling in the middle of the second story hallway increased while those at higher elevations decreased, temperatures measured at elevations up to 0.3 m below the ceiling increased in the master bedroom and bedrooms 2 and 4, and the temperatures 1.2 m and 0.02 m below the ceiling in bedroom 3 increased, while all other temperatures remained steady.

When the front door was opened, an additional flow path from the front door to the burner was created which increased the flow rate of cool air into the structure. This resulted in a decrease in all the temperatures measured on the first story, a decrease in temperatures measured at elevations of 1.5 m below the ceiling and at higher elevations in the middle of the second story hallway, no significant change in the temperatures in the master bedroom and bedrooms 2 and 4, and an increase in temperatures measured up to 0.6 m below the ceiling in bedroom 3. The temperatures measured in the center of the family room at elevations 3.3 m below the ceiling and lower diverged from the general trend of stratification of the gas temperatures with respect to elevation. A flow path similar to that described for Experiment 4 and Experiment 5 was evident in Experiment 6 that resulted in circulation of hot gases and may have contributed to non-stratification of the gas temperatures in the family room. A similar phenomenon was also observed in the kitchen, where the highest temperature measurements were 0.6 m below the ceiling throughout the experiment.

The model accurately predicted the qualitative features in the data measured on the first story that resulted from the ventilation openings, but did not capture the decrease in temperatures in the master bedroom and bedroom 4 after ventilation of window K. The temperature magnitudes near the ceiling on the second story, in the foyer, and in the family room were underpredicted. The temperature magnitudes at low elevations on the second story as well as the temperatures in the kitchen and under the second story hallway were generally accurately predicted.

The model predicted stratification of gas temperatures as a function of elevation in the family room and in the kitchen. The temperatures measured at elevations 1.8 m below the ceiling and higher in the center of the family room were underpredicted by the model and the temperature 3.0 m below the ceiling was overpredicted. Due to the prediction of stratification of the temperature profile

that was not observed in the experiments, the temperatures measured 3.3 m below the ceiling and lower elevations in the family room were underpredicted. All temperature magnitudes from the kitchen were accurately predicted, although the model erroneously predicted stratification of the temperatures. The temperatures in the foyer were underpredicted at all elevations higher than 1.5 m below the ceiling and overpredicted 1.6 m below the ceiling and at lower elevations until ventilation of window A, and all temperatures measured 0.9 m below the ceiling and at higher elevations were overpredicted for the remainder of the experiment.

Temperatures measured at elevations from the ceiling to 1.2 m below the ceiling were underpredicted and temperatures 1.5 m below the ceiling and at lower elevations in the middle of the second story hallway were overpredicted up to the time window A was vented. After ventilation of window A, the model accurately predicted the temperatures 1.5 m below the ceiling and at higher elevations that were in the range of 160°C to 210°C, but overpredicted the temperature magnitudes 1.8 m and 2.1 m below the ceiling. All temperatures above 2.1 m below the ceiling in the master bedroom were underpredicted throughout the experiment. The model underpredicted temperatures measured 1.5 m below the ceiling and at higher elevations in bedrooms 2, 3, and 4 up to the time window K was vented. After ventilation of window K, temperatures 1.5 m below the ceiling and at lower elevations in bedroom 2 and bedroom 4 were overpredicted, and temperatures 1.2 m below the ceiling and at lower elevations in bedroom 3 were overpredicted. The temperatures measured in bedroom 2 were in the range of approximately 90°C to 160°C after ventilation of window A, but the model predicted a temperature range of approximately 100°C to 150°C.

When the front door was vented, the temperatures measured 1.2 m below the ceiling and at lower elevations were overpredicted whereas the temperatures measured at higher elevations were well predicted. The temperatures measured in bedroom 4 were in the range of approximately 100°C to 180°C after ventilation of window A, but the model predicted a temperature range of approximately 110°C to 150°C.

6.3.2 Experiment 6: Pressure

The pressure data collected throughout the structure are presented in the following figures. Figure 6.48 displays the pressures in the family room, Figure 6.49 displays the pressures next to the front door, Figure 6.50 displays the pressures in the living room, Figure 6.51 displays the pressures in the master bedroom, Figure 6.52 displays the pressures in bedroom 2, Figure 6.53 displays the pressures in bedroom 3, and Figure 6.54 displays the pressures in bedroom 4.

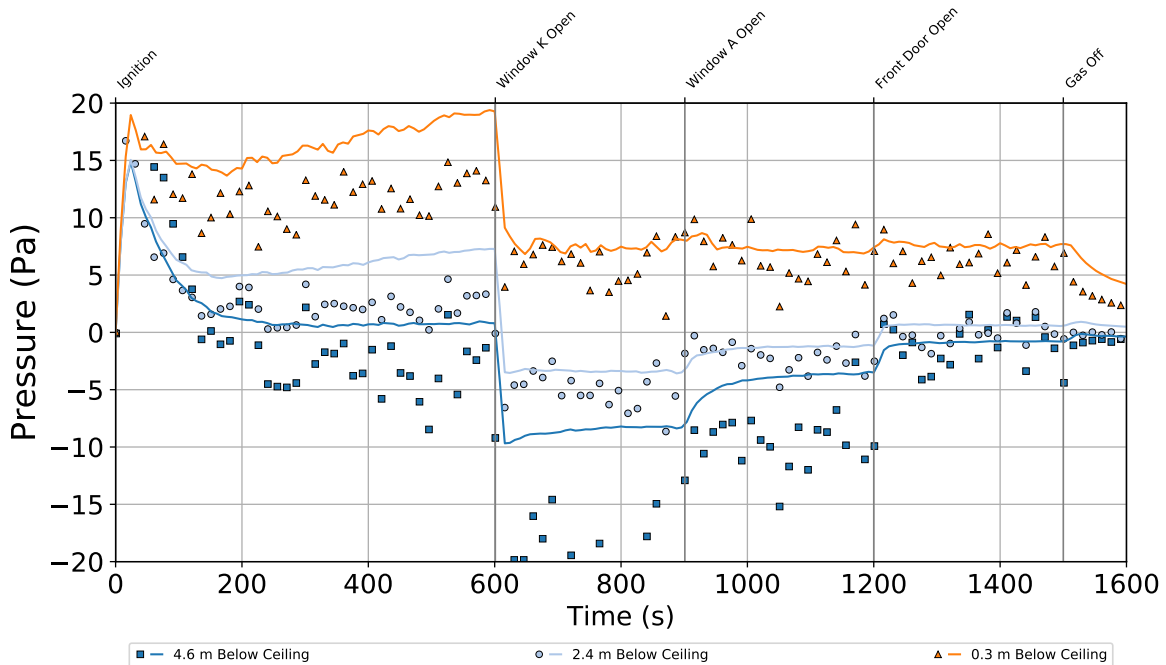


Figure 6.48: Pressures in the family room of the two-story structure during Experiment 6

The pressures throughout the structure increased immediately after ignition to a global maximum in the range of 14 Pa to 20 Pa at all measurement locations followed by a gradual decay in pressure magnitude. The pressure measured 4.6 m below the ceiling of the family room reached a peak of approximately 37 Pa for a short duration approximately 15 s into the experiment. The pressures measured 2.1 m below the ceiling and at lower elevations on the first story and those collected 4.6 m below the ceiling in the family room achieved pressures below atmospheric pressure prior to ventilation of window K. All measurements from the second story and those collected at higher elevations in areas that were open to the second story were above atmospheric pressure prior to ventilation of window K. The negative pressures are indicative of air flow throughout the first story entrained by the burner. Positive pressures at high elevations and in the second story compartments indicate higher temperatures near the ceiling and the dominance of buoyancy throughout the structure.

Upon ventilation of window K, all measured pressures immediately decreased. All pressures measured on the first story as well as the pressure measured 2.4 m below the ceiling in the family room and the lowest elevation measurements on the second story decreased below atmospheric pressure

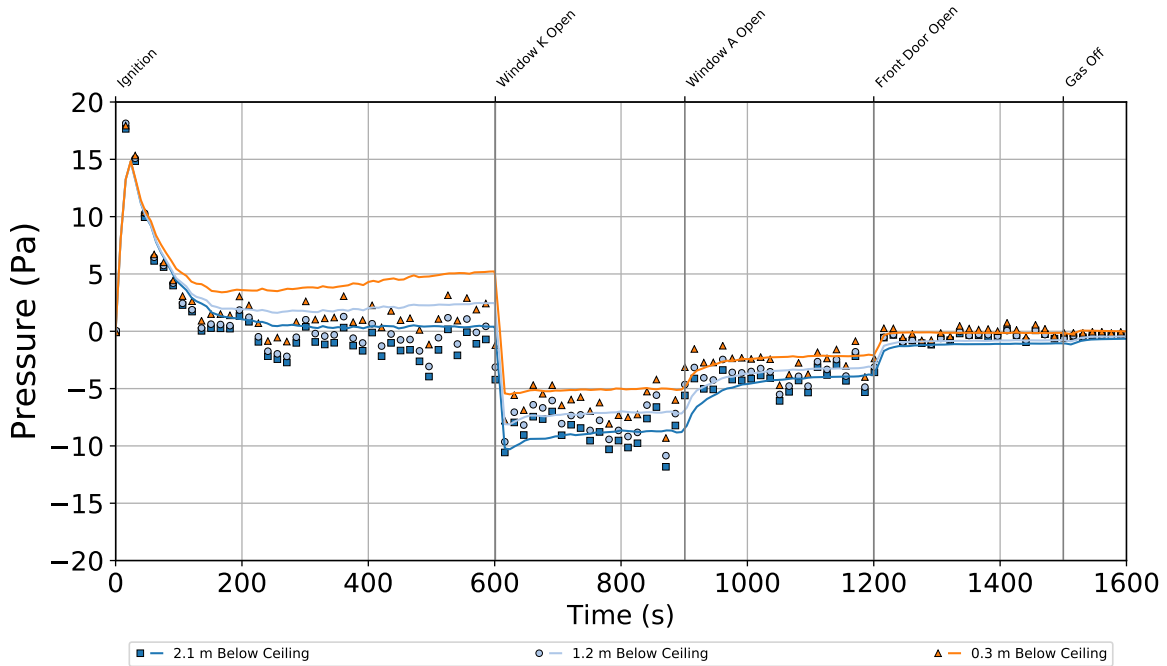


Figure 6.49: Pressures next to the front door of the two-story structure during Experiment 6

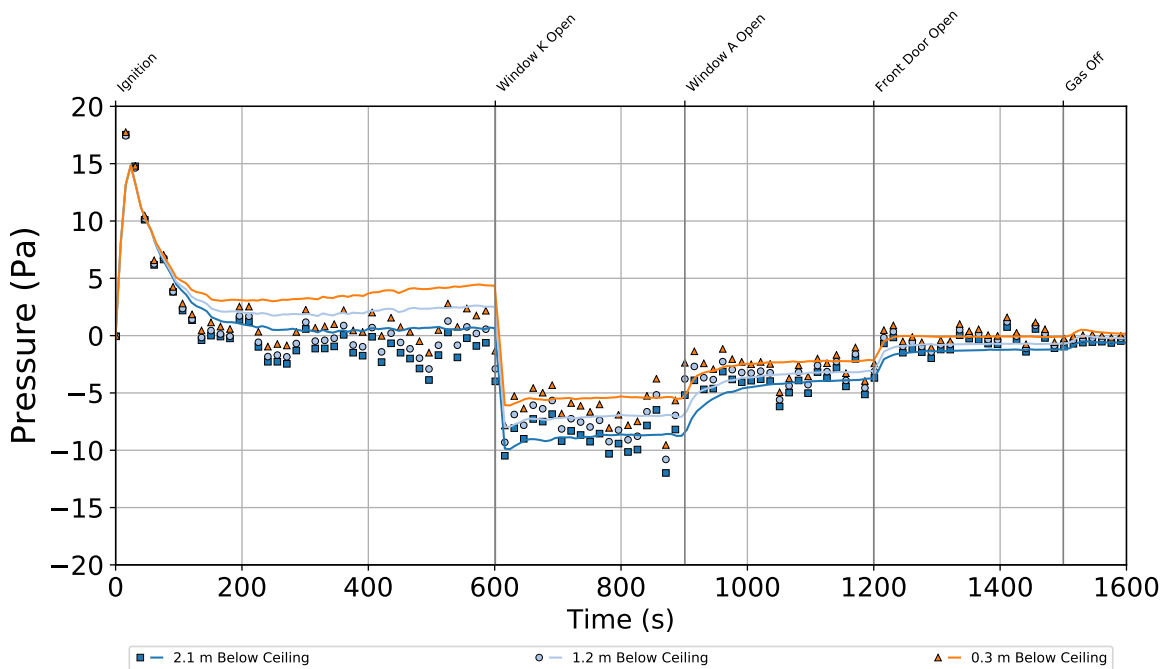


Figure 6.50: Pressures in the living room of the two-story structure during Experiment 6

after venting of window K. These pressure decreases were indicative of increased flow velocities on the first story as cool air was entrained to the burner to displace the accumulated hot gases at

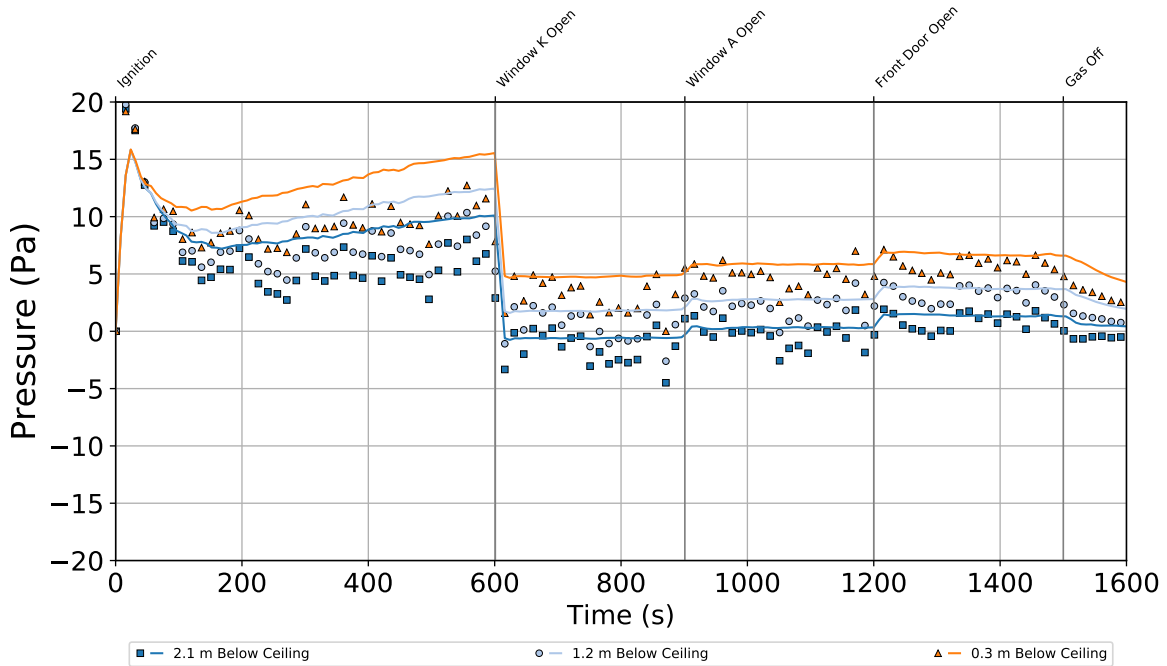


Figure 6.51: Pressures in the master bedroom of the two-story structure during Experiment 6

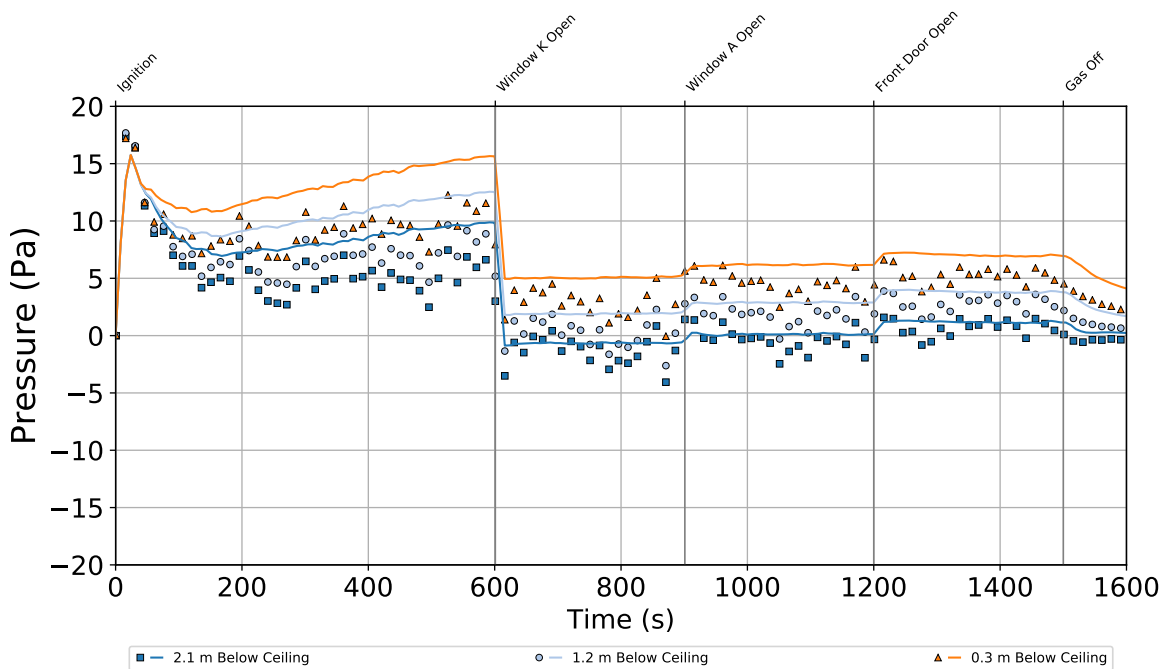


Figure 6.52: Pressures in bedroom 2 of the two-story structure during Experiment 6

the ceiling level and on the second story that were exhausted through window K.

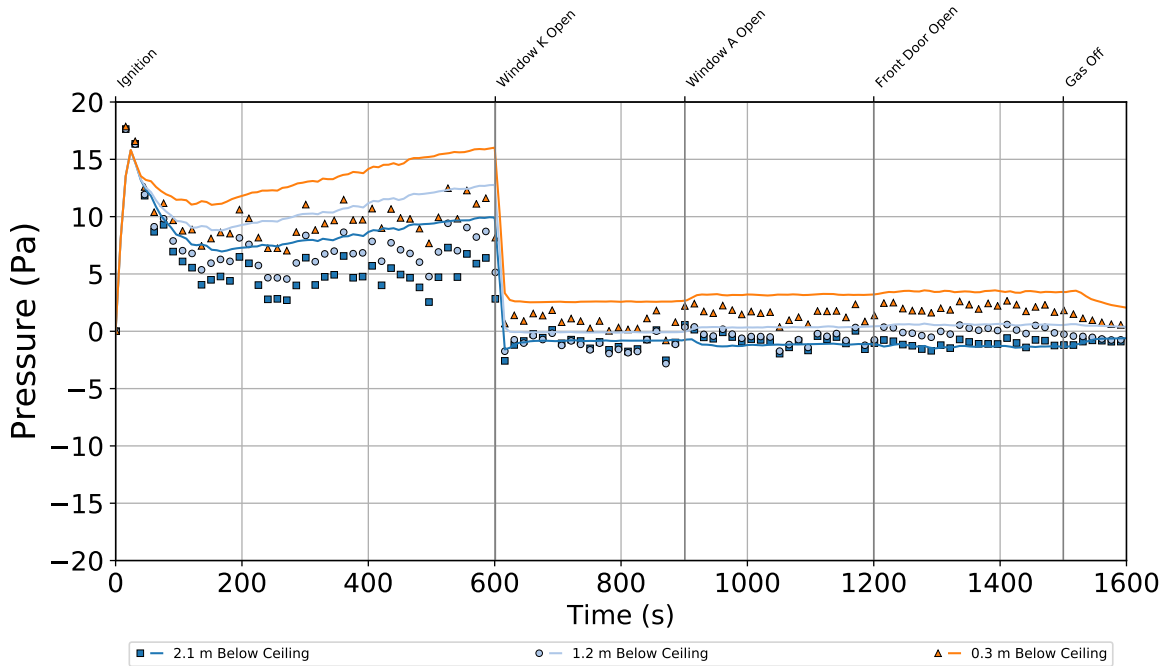


Figure 6.53: Pressures in bedroom 3 of the two-story structure during Experiment 6

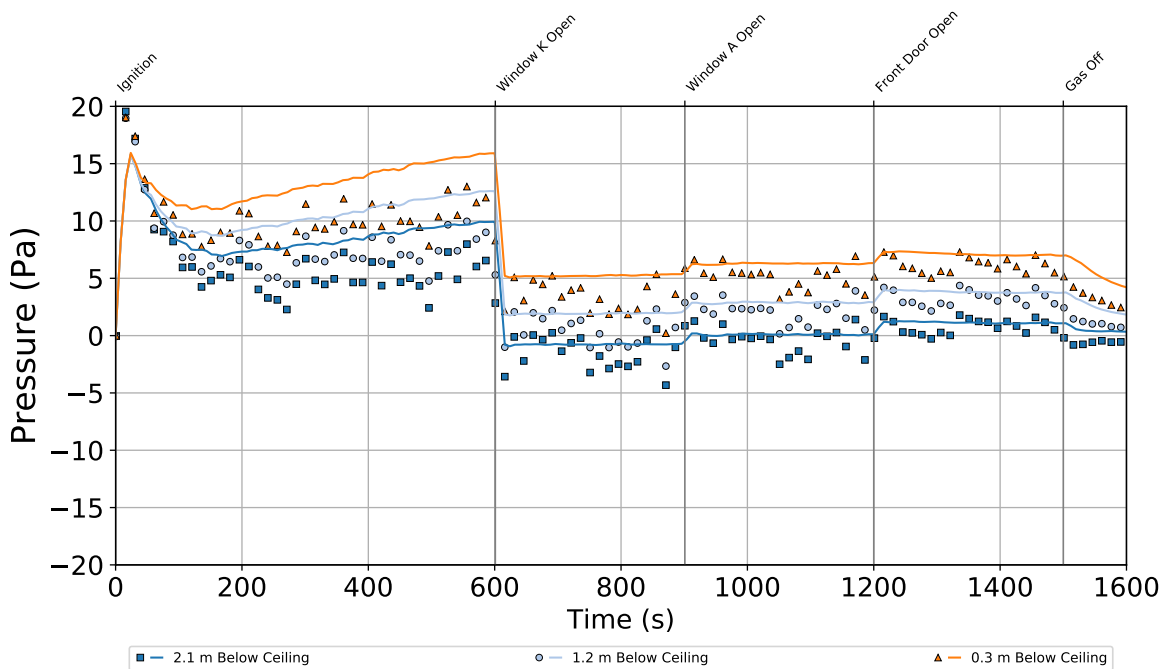


Figure 6.54: Pressures in bedroom 4 of the two-story structure during Experiment 6

Ventilation of window A resulted in an increase of pressures throughout the structure. The first story measurement locations and the lowest elevation measurement location in the family room

experienced a large increase in pressure such that the measurements were closer to atmospheric pressure, and the measurement locations on the second story experienced a relatively small magnitude increase in pressure at all elevations. This increase in pressure was likely caused by the increased ventilation area on the first story that resulted in a larger net mass flow rate into the structure.

When the front door was opened, pressures measured on the first story increased such that they were closer to atmospheric pressure and pressure measurements on the second story and at high elevations in the family room increased to higher positive pressures. Pressures measured on the first story ranged from -10 Pa to 3 Pa throughout the experiment, while those measured on the second story ranged from approximately -3 Pa to 12 Pa. Pressures near the floor in the family room were in the range of approximately -20 Pa to approximately 2 Pa throughout the experiment, with the largest magnitude negative pressure observed immediately after window K was vented.

An effective leakage area between the den and the remainder of the structure was not measured, which led to definition of a single pressure zone that encompassed the internal volume of the structure. Due to this definition, the pressures in the den were not properly predicted and a comparison between the data and the model prediction was not presented in this work. To attempt to predict the pressures in the den would require definition of a distinct pressure zone in the den as well as measurement of an effective leakage area between the den and the remainder of the structure and between the den and the exterior.

Pressures were overpredicted at all measurement locations and elevations throughout the structure between ignition and opening window K, and pressures were predicted to increase over time although the measured pressures remained steady after the initial increase and decrease in pressure caused by ignition of the burner. A decrease in pressure at all measurement locations throughout the structure after ventilation of window K and the increases in pressures with subsequent ventilation events were accurately predicted. The model accurately predicted the magnitudes of the pressure measurements throughout the structure after ventilation of window K. An exception was the pressure measured 4.6 m below the ceiling in the family room, which was overpredicted between ventilation of window K and ventilation of the front door.

6.3.3 Experiment 6: Velocity

The velocity data collected throughout the structure are presented in the following figures. Figure 6.55 displays the velocities measured in window K, Figure 6.56 displays the velocities measured in window A in the kitchen, Figure 6.57 displays the velocities measured at the front door.

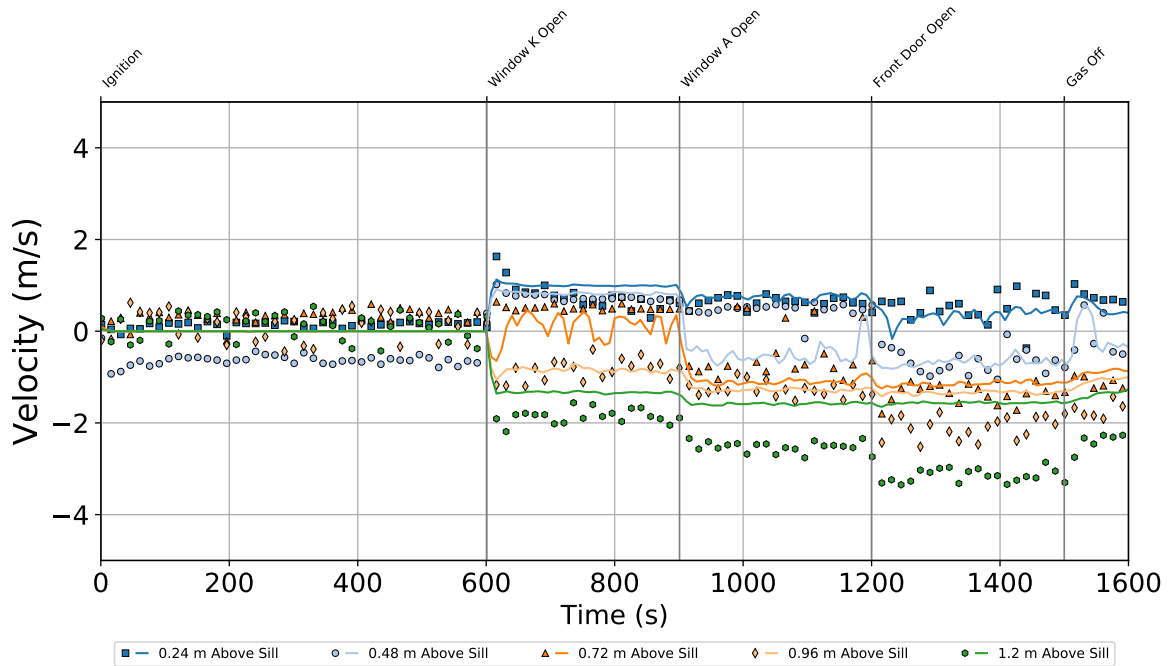


Figure 6.55: Velocities in window K of the two-story structure during Experiment 6

Bi-directional flow was immediately evident after ventilation of window K with the neutral plane located approximately 0.72 m above the window sill. Ventilation of window A resulted in the migration of the neutral plane in window K downward in elevation such that it was in the range of 0.48 m and 0.72 m above the window sill and increased the magnitude of velocity out the window. When the front door was opened, the neutral plane at window K shifted such that it was in the range of 0.24 m to 0.48 m above the window sill and the magnitude of the flow velocity out of the window increased.

When window A was vented, all flow was directed into the structure with a velocity magnitude of approximately 2 m/s. Ventilation of the front door resulted in a decrease of the velocity magnitude flowing into the structure through window A.

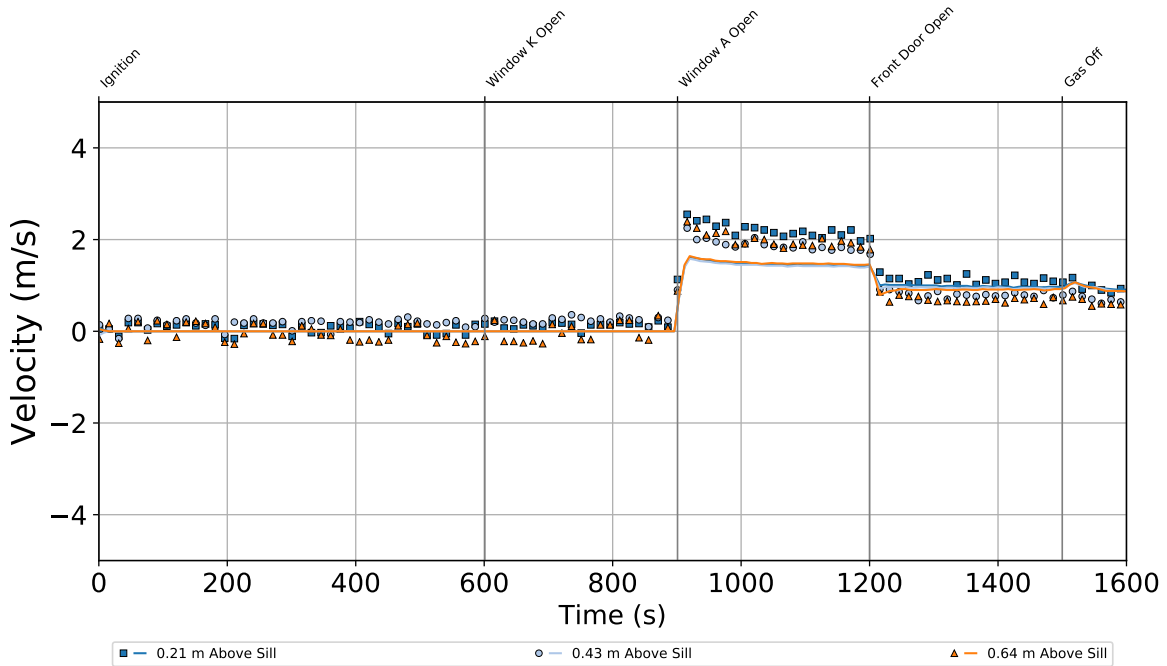


Figure 6.56: Velocities in window A of the two-story structure during Experiment 6

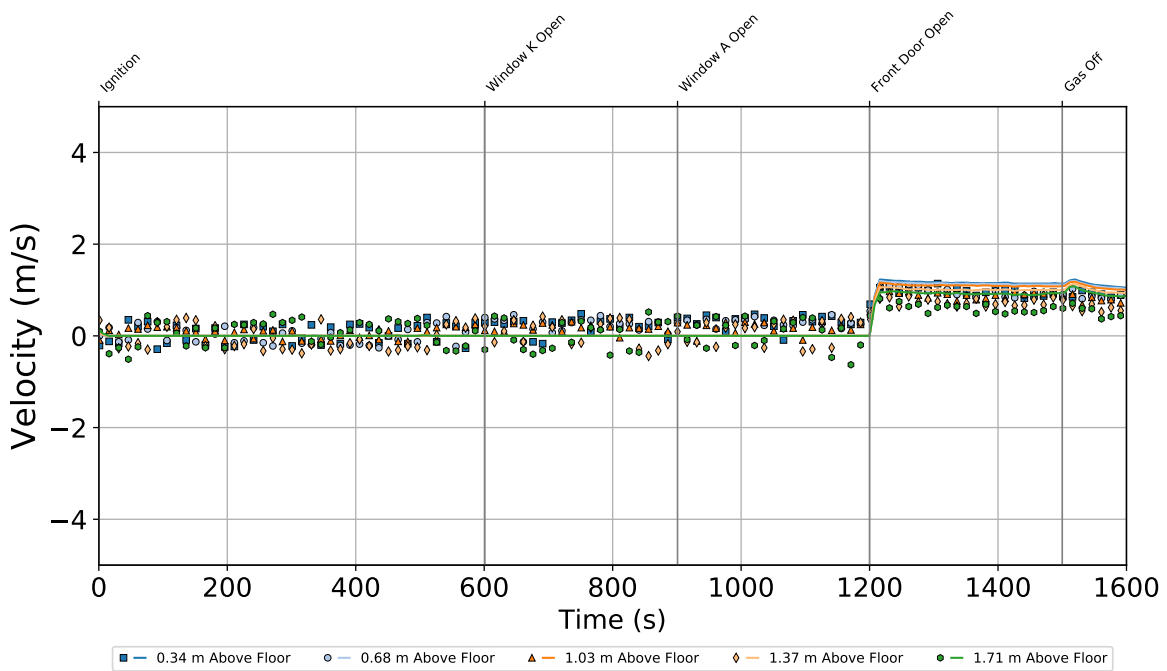


Figure 6.57: Velocities in the front door of the two-story structure during Experiment 6

After the front door was opened, all flow through the front door was directed into the structure with a constant velocity of approximately 1 m/s.

The model accurately predicted the qualitative features of the data and the effect of opening the exterior windows and doors on the directions of flow and relative changes in flow velocity magnitude. The model slightly underpredicted flow velocities out of the structure through window K and the flow velocity magnitudes into the structure through window A, but generally produced accurate predictions of the uni-directional flow velocity magnitude into the front door after ventilation of the front door.

7 Discussion

The discussion of the experimental results is divided into sections that focus on the uncertainty in each measurement and the agreement between experiments and model predictions. In the section on uncertainty, replicate experiments conducted in both the single-story and two-story structure with identical ventilation conditions are examined to identify the mean uncertainty in each measurement. In the section that assesses the accuracy of the model predictions, the ability of the models to predict the key physical phenomena observed in the experiments is evaluated through a discussion of the agreement between the predicted data and the experimental data.

7.1 Experimental Uncertainty

Several of the gas burner experiments were repeated to determine the uncertainty in the measurements. As defined in the *Guide to Expression of Uncertainty in Measurement*, repeatability conditions include the same measurement procedure, conducted by the same observer, using the same instrumentation under the same conditions at the same location over a short period of time [40]. The expanded uncertainty in each experimental measurand was evaluated as the mean instantaneous experimental standard deviation of the replicate experiments. The coverage factor for the expanded uncertainty is 2, which defines an interval estimated to have a level of confidence of 95%, assuming the instantaneous mean approximates the true value with no systematic bias and the measurements are normally distributed about the true value. The mean experimental value of the differential pressure measurements approached 0 Pa as the experiments proceeded, which yielded high relative standard deviations but relatively low absolute standard deviations.

Three replicates of Single-Story Experiment 1 were conducted in this work and these data were analyzed to determine the expanded uncertainty of each measurement for the experiments in the single-story structure. These experiments featured conditions identical to Experiment 1 with the same timing and sequence of events between ignition and extinguishment of the burner. The expanded uncertainty of the temperature measurements over all thermocouples in the single-story structure in the replicates of Experiment 1 was calculated as $\pm 10\%$ ($\pm 4.3^\circ\text{C}$) (calculated with Celsius temperatures). The expanded uncertainty of the velocity measurements in the single-story structure over the replicates of Experiment 1 was approximately $\pm 28\%$ ($\pm 0.1\text{ m/s}$). The expanded uncertainty of the differential pressure measurements for Single-Story Experiment 1 replicates was calculated as $\pm 232\%$ ($\pm 0.9\text{ Pa}$).

Four replicates of Two-Story Experiment 4 were conducted and the data collected in these experiments were analyzed to determine the expanded uncertainty of each measurement for the experiment in the two-story structure. The expanded uncertainty of the temperature measurements in Two-Story Experiment 4 was calculated as $\pm 24\%$ ($\pm 17^\circ\text{C}$) (calculated with Celsius temperatures). The expanded uncertainty of the velocity magnitude measurements through vents open to

the exterior in Two-Story Experiment 4 was calculated as approximately $\pm 44\%$ ($\pm 0.38m/s$). The expanded uncertainty of the static pressure measurements was calculated as $\pm 330\%$ (± 2.8 Pa).

The temperature data was a repeatable measurement with a relatively low estimated uncertainty, particularly at high elevation. Although circulation of hot gases from high elevation areas in the family room and foyer was evident (which may have resulted in non-stratification of temperatures), the temperature data between replicate experiments was highly repeatable. The phenomena that led to this apparent circulation may be important in the context of fire investigations and the fire-induced fluid flows in residential occupancies and further research must be conducted to better understand the physics that drove these gas flows.

7.2 Accuracy of Predictions

The accuracy of the model predictions serves to gauge the suitability of the model, defined with the aforementioned parameters, to represent all of the important physical phenomena that govern the dynamics of fire-driven flow phenomena and the movement of hot gases as a function of ventilation conditions in the two structures. The following descriptions of the model refer to FDS version 6.7.1 as defined with the parameters presented in Section 4. Model predictions may be evaluated against expected values for measured quantities by plotting these quantities against each other [14]. Several of these plots have been replicated in this section to facilitate discussion of the accuracy of the model predictions relative to the measured data. The peak value above ambient conditions for each measured and predicted quantity are plotted in the following figures. To produce these plots, it is assumed that the measured data are normally distributed about the true value, and the expectation is that the model predictions are identical to the experimental data, within experimental uncertainty. In the following figures, the solid black line that runs from the bottom left to the upper right corner of the plot indicates the expected perfect agreement between the experimentally measured data and the model prediction. The dashed black lines offset from the solid black line represent the total estimated expanded experimental uncertainty and correspond to two standard deviations of the mean of the specific measurand.

It is assumed that deviations from perfect agreement between the predictions and the experimental data are the result of simplifying assumptions, model implementation, and uncertainty in defined parameters which manifests as a systematic bias in the predictions. In the analysis presented in the following figures, this systematic bias is assumed to scale the expectation line by a bias factor. The solid red line in the following figures passes through the mean of the distribution and indicates the expectation line multiplied by the bias factor for the distribution. The dashed red lines offset from the solid red line indicate the scatter in the agreement between the model predictions and experimental data (which incorporates model uncertainty as well as uncertainty in defined parameters) and corresponds to two standard deviations of the distribution. For construction of these plots, the stipulation is enforced that the prediction uncertainty may not be smaller than the experimental uncertainty.

Figure 7.1 shows the comparison between the predicted and measured peak temperature rise at all

thermocouples for all thermocouple arrays in the six experiments. The estimated expanded relative uncertainty in the temperature measurements was 0.24, the expanded relative uncertainty for the predicted data was 0.52, and the bias factor for the model was 1.18.

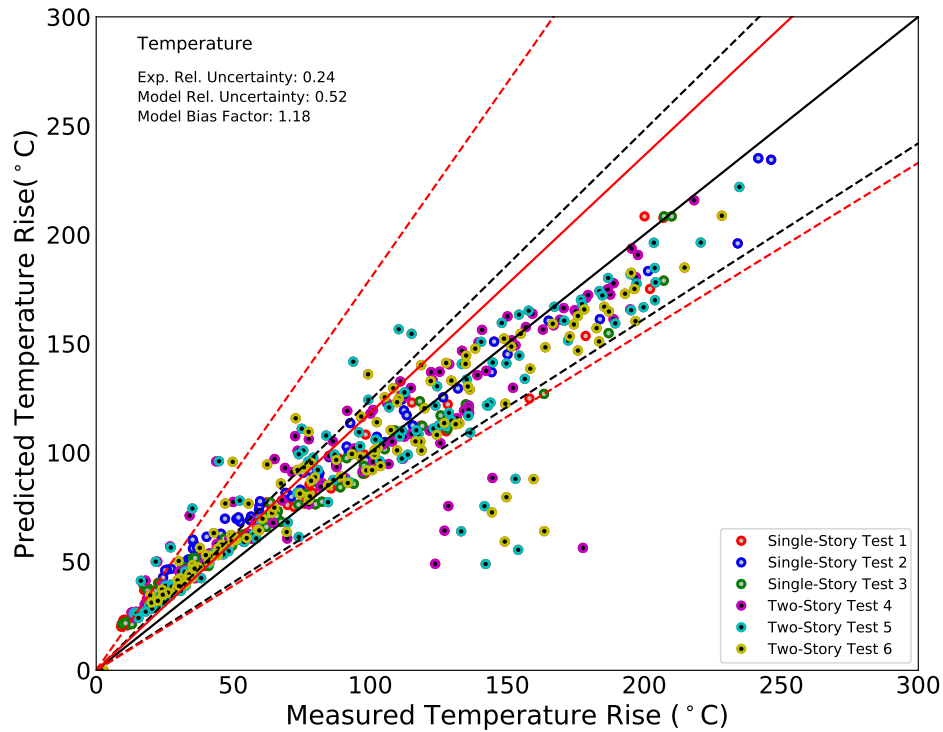


Figure 7.1: Comparison between Temperature Measurements and Predictions. Solid black line indicates perfect agreement between predictions and measurements, dashed black lines indicate experimental expanded uncertainty. Solid red line indicates bias-adjusted perfect agreement line and passes through the mean of the distribution, dashed red lines indicate scatter in agreement between model predictions and experimental data.

A trend in the comparison data presented in Figure 7.1 indicates that the model predictions of temperature rises above approximately 100°C were generally within the experimental experimental uncertainty of perfect agreement for all experiments. The trend for measured temperature rise data below 100°C indicates an overprediction of the measured data that increased in relative magnitude as the measured temperature rise decreased. A similar trend has been noted in prediction of ceiling jet temperatures in other FDS validation studies [14]. These trends are consistent with the model accurately predicting temperatures at high elevations and overpredicting temperatures at low elevations. The data points that appear as potential outliers at the bottom center of the plot correspond to the peak temperatures measured at low elevation in the center of the family room. These data points illustrate the dramatic effect of non-stratification of the temperature that may be attributed to the apparent circulation of hot gases around the second story hallway. These data also indicate the apparent inability of the model to capture the physical phenomena that drove this

apparent circulation. The ultimate cause of the high disparity between the temperature predictions and measurements at low elevation in the family room is unknown and requires further research.

The bias factor and the standard deviation of the comparison between the model and the experimental data on ceiling jet temperature have been compiled for a wide range of FDS validation studies [14]. The model bias factor for prediction of the ceiling jet temperature is 1.04 and the model relative standard deviation ($k = 1$) is 0.13. Although these metrics indicate better accuracy and less scatter when considering the entire corpus of validation studies, it must be noted that the metrics for the current study are calculated based on the prediction of temperature at all elevations and the accuracy of the ceiling jet temperatures in the current study is high.

Figure 7.2 presents the comparison between the predicted and measured pressure rises within each compartment in each of the experiments. The estimated expanded uncertainty of the pressure measurement determined from the literature was 0.23, the expanded relative uncertainty for the predicted data was 0.44, and the bias factor for the model was 0.91. The model predicted consistent peak pressure rise magnitudes regardless of the peak measured pressure rise. The time-averaged model prediction data was not sensitive to the size of the source fire or the geometry of the structure and the resulting peak predicted pressure rises were repeatably in the range of approximately 13 Pa to 18 Pa although the peak measured values ranged from 10 Pa to 42 Pa.

The majority of the data points from Single-Story Experiment 1 and Two-Story Experiments 4 and 6 plotted in Figure 7.2 were clustered within two experimental standard deviations of perfect agreement. A small cluster of data points from the two-story experiments that corresponded to the lowest elevation pressure measurement in the family room were significantly underpredicted. These measurements were made in close proximity to the gas burner, which resulted in higher than expected predicted pressure peaks. The FDS validation guide provides a collection of validation studies in which pressures have been predicted [14]. The model bias factor for prediction of pressure for the collected studies is 0.89, the model relative standard deviation ($k = 1$) is 0.21, and the experimental relative standard deviation ($k = 1$) is 0.21. The bias factor and the experimental standard deviation for this work indicate more accurate agreement and less experimental scatter than for the corpus of validation studies. The model relative standard deviation for the collection of studies that appear in the validation guide is 0.21, which indicates the pressure predictions from the previous validation studies and the pressure predictions from this work are equally scattered about the bias-adjusted expectation line. The larger relative standard deviation of the agreement between the predictions and experiments in this work is likely because of the outliers that correspond to the lowest elevation pressure measurements in the family room of the two-story structure.

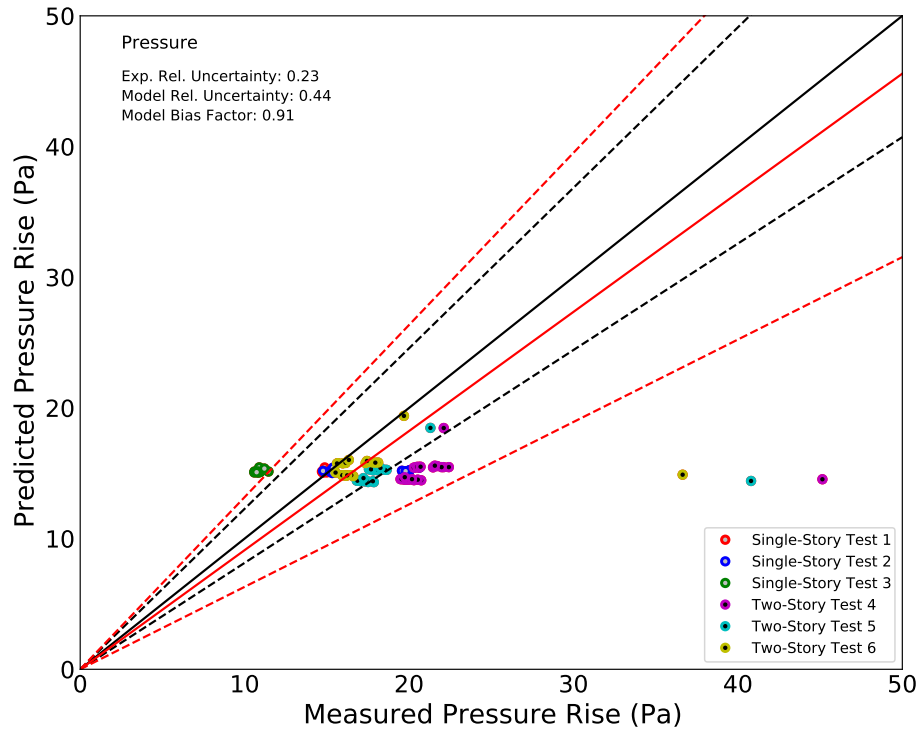


Figure 7.2: Comparison between Pressure Measurements and Predictions. Solid black line indicates perfect agreement between predictions and measurements, dashed black lines indicate experimental expanded uncertainty. Solid red line indicates bias-adjusted perfect agreement line and passes through the mean of the distribution, dashed red lines indicate scatter in agreement between model predictions and experimental data.

Figure 7.3 presents the comparison between the predicted and measured velocity magnitudes at the ventilation openings in each of the experiments as well as through the hallway in the single-story structure. The expanded uncertainty for the velocity measurements was 0.44, the expanded relative uncertainty for the predicted data was 1.24, and the bias factor for the model was 1.61. The model typically underpredicted the velocities measured for the two-story experiments and overpredicted the velocities measured in the single-story structure.

The data points plotted in Figure 7.3 show significant scatter. A trend is evident in the data in which the maximum velocity magnitudes were generally overpredicted at low measured velocity magnitude (below approximately 0.75 m/s) and underpredicted at higher magnitudes. Particularly evident is the underprediction of the maximum velocities in Two-Story Experiment 4 and Experiment 6. These specific experiment configurations featured vent openings on both the first and second story of the structure prior to extinguishment of the burner, which facilitated high ventilation velocities driven by stack effect. The studies that appear in the FDS validation guide that include predictions of gas velocity exhibit a model bias factor of 1.01, which indicates significantly better prediction accuracy than the models compiled in this work [14]. relative standard deviation

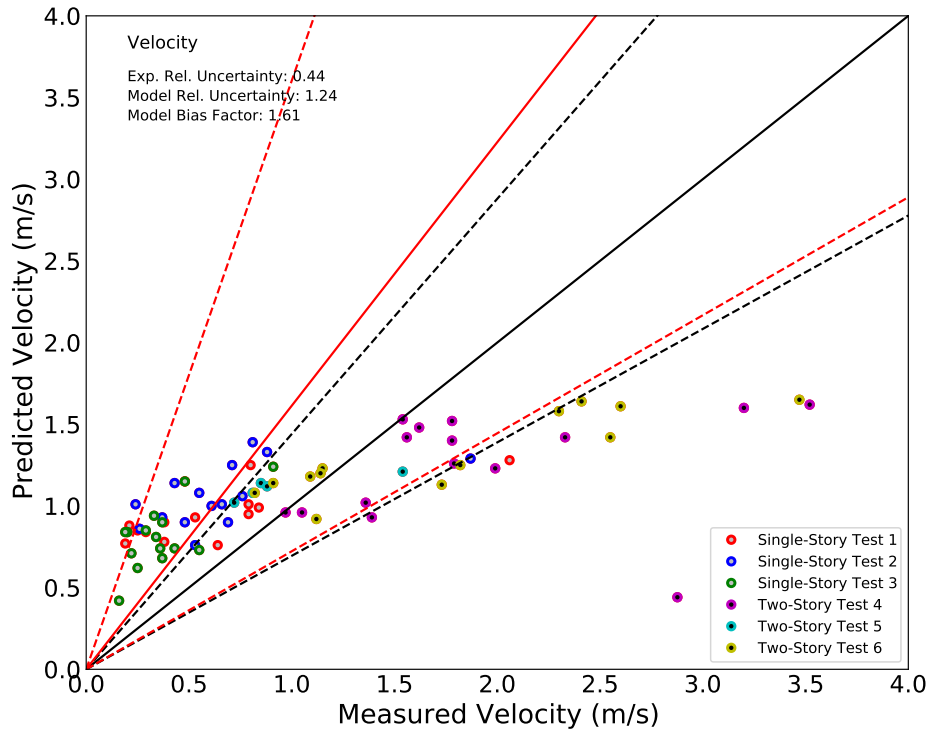


Figure 7.3: Comparison between Velocity Measurements and Predictions. Solid black line indicates perfect agreement between predictions and measurements, dashed black lines indicate experimental expanded uncertainty. Solid red line indicates bias-adjusted perfect agreement line and passes through the mean of the distribution, dashed red lines indicate scatter in agreement between model predictions and experimental data.

of the agreement between the predictions and experiments for velocity predictions in past validation studies is 0.10, while it is significantly higher in the current study. The causes of the disparity between the experimental data and the model predictions in this work is undetermined and additional research and validation exercises to measure velocities in multi-story structures subjected to well-defined ventilation events on multiple stories is recommended.

The figures presented in this section provide point comparisons between measured data and model predictions. These comparisons provide an assessment of the ability of the models to represent the extremes in a given scenario, which is a valid use of fire modeling in the context of fire protection design, fire scene reconstruction, and hypothesis testing in investigations and fire research. These comparisons are better suited for steady-state conditions and, in the form presented here, do not provide an assessment of the ability of the model to predict the evolution of the fire-induced flow dynamics as ventilation conditions change over time. Metrics that are calculated using functional analysis that provide a quantitative assessment of the ability of a fire model to predict experimental data have been described in the literature [41]. These metrics include the norm of the relative difference between the experimental data and model prediction vectors and the cosine similarity

between these vectors. These metrics have been calculated for all data presented in this work and are provided in Appendix A.

The agreement between the model predictions and experimental data for temperatures throughout both structures for all of the experiments described in this work was adequate to provide additional validation for and confidence in the use of the model defined with the aforementioned parameters by fire investigators and fire protection engineers to predict temperatures given a well-defined fire source and ventilation conditions. Practitioners of FDS often seek the peak temperature or conservative estimates of the evolution of temperature in a compartment and it was evident in analyses of the presented data that the models predicted peak temperature rises above approximately 100°C and generally also predicted temperatures at almost all elevations to within experimental uncertainty.

Notable were relative differences higher than experimental uncertainty in areas of each structure that were expected to experience low velocity flows due to lack of proximity of measurement locations to vents and flow paths. These areas were typically at low elevations in rooms remote from the fire and vents. Also notable were the high relative differences at elevations lower than 3.0 m below the ceiling in the family room and foyer of the two-story structure which may have been affected by the apparent circulation of hot gases from the ceiling of the family room. The defined thermocouple bead diameters, the orientation, and the exact position of the thermocouples were potential sources of discrepancy between the data and model predictions. Although the model bias factor for the data presented here was slightly higher than the bias factor calculated for the ceiling jet temperature in past validation studies, the data here can contribute to the corpus of FDS validation data.

The temperature profile measured in the center of the family room in all of the two-story experiments exhibited non-stratification of temperatures 3.3 m below the ceiling and at lower elevations. Temperature profiles in experiments conducted in the same structure with furniture-fueled fires initiated in approximately the same location as the gas burner showed a similar trend of non-stratification of temperatures in the center of the family room, but only after the temperatures and the HRR had reached a peak and were decreasing in magnitude [39]. In contrast, non-stratification of temperatures was immediately evident upon ignition in the gas burner experiments. It is possible that radiant heat flux from the flame incident to the low elevation thermocouple beads in the center of the family room resulted in artificially high temperature readings throughout the experiments.

The HRR of the gas burner increased almost immediately to the full steady state value whereas the furniture-fueled fires required approximately 200 s to 300 s to reach peak HRR. Because of this, radiant heat transfer from the gas burner flame would have a more pronounced effect on the temperature measurements at early times than the furniture-fueled fire. The furniture produced much more soot than the natural gas burner, which resulted in a higher radiative fraction, and would indicate the temperature measurements in the experiments with the furniture-fueled fires would be more affected by radiant heat transfer than the thermocouples in the gas burner experiments. Due to the fact that the temperatures measured in the foyer and beneath the second story hallway in the two-structure were as much as 100°C lower than those measured in the center of the family room at comparable elevations, and because of the immediate effect on the temperatures at low elevation

in the line of sight of the burner flame after ignition, it is likely that radiative heat transfer from the burner flame partially contributed to the non-stratification of measured temperatures in the center of the family room, although gas circulation also appears to have also influenced non-stratification.

The ambient temperature in the laboratory ranged from 9°C to 16°C for the gas burner experiments. The ambient temperature was assumed to be 20°C for all of the simulations. Because the experiments conducted in this work involved an investigation of the influence of ventilation conditions on the fire-induced flow dynamics and temperatures throughout the structures, it is possible that the discrepancy between the actual and assumed ambient temperatures influenced the agreement between the simulation results and experimental measurements. The error introduced by this discrepancy would be most evident at low elevation in areas within close proximity to vents through which cool air flowed into the structure and would manifest as predicted temperatures that were higher than the measured temperatures. The magnitude of the potential error is expected to be a few degrees, which is within the expanded uncertainty of the measurement.

Agreement between the measured and predicted pressures throughout both structures for all experiments described in this work was adequate to serve as a validation case and to increase the confidence of model practitioners in pressure predictions for comparable scenarios in single-story and two-story modern residential structures. With the models and model parameters used in this work, peak pressure increase predictions were generally found to be insensitive to the geometry of the structure and the size of the fire source. The absolute difference between the pressure measurements and predictions were generally within the experimental uncertainty of the measurement. The pressure predictions had notable differences at low elevations throughout the two-story structure and at all elevations in the family room of the two-story structure. The model with the parameters defined as presented in this work predicted pressures with less bias than the corpus of validation studies that have been compiled for FDS version 6.7.1. The cosine similarity between the measured and predicted data curves were below the acceptance criteria at several locations in each structure, which indicates that the predictions did not agree qualitatively with the experimental data trends, although the relative differences were within the acceptance criteria. A potential source of discrepancy was the method used to define leakage in each of the models.

The agreement between the measured and predicted velocities throughout both structures was inadequate to validate the ability of the model defined with the aforementioned parameters to predict velocity magnitudes for the considered scenarios. The model predictions presented in this work were much less accurate than the collection of FDS validation studies indicates. A trend was evident in which measurement magnitudes were overpredicted by more than the expanded uncertainty below approximately 0.75 m/s and above approximately 2.0 m/s, and overall relative differences were significantly higher than the experimental uncertainty in the measurement. An indication of predictions of the elevation of the neutral plane that are generally accurate is a positive cosine similarity value for all elevations at all velocity measurement locations. With the exception of window E in the experiments conducted in the single-story structure, all cosine similarity values were positive.

The model generally captured the qualitative changes in data due to ventilation events as well as the elevation of the neutral plane. The model accurately predicted velocity magnitude and

direction when flow into the structure was uni-directional, particularly on the first story of the two-story structure. Potential sources of discrepancy in the experimental data are the relatively low flow velocities and potential misalignment of the probe relative to the flow direction. The bi-directional probe measurements have been researched, calibrated, and validated extensively against flows with Reynolds numbers greater than 1000, which corresponds to a velocity measurement of 1.2 m/s for the probes used in the experiments described here. Lower velocity flow measurements, which comprise many of the velocities measured in this work, have error that may be higher than 35% [32, 33]. Preliminary simulations showed no significant change in velocity predictions with higher resolution or higher computational cost simulation modes, but more detailed analyses may find these or other model parameters can improve agreement between measured and predicted velocities. Additional research is required before the experimental velocity data presented here may be used to validate deterministic fire models.

8 Conclusions

The gas burner experiments conducted in a single-story structure and a two-story structure resulted in several new sets of validation data for the fire modeling community. The temperatures measured in the experiments were repeatable across replicate experiments with an expanded uncertainty of $\pm 24\%$. The expanded uncertainty of velocity magnitudes was approximately $\pm 44\%$ and the expanded uncertainty of compartment pressure rises was approximately ± 2.8 Pa.

Preliminary simulations were conducted to investigate the sensitivity of model predictions to several model parameters. All final simulations presented in this work were conducted with a uniform grid with a cubic cell size of 0.1 m. The Simplified Very Large Eddy Simulation mode was utilized based on its low computational cost relative to the other simulation modes without a noticeable difference in model agreement. The "Localized Leakage" approach to defining leaks was used in all models to avoid pressures below atmospheric prior to the first ventilation event. A single pressure zone was defined that encompassed the internal volume of each structure to differentiate between the structure and the exterior prior to the first ventilation event. Defining additional pressure zones did not have a significant effect on pressure or temperature predictions.

The model predicted temperatures well at all measurement locations with particularly good agreement for high elevation measurements with temperature rises larger than 100°C above ambient temperature. The model was generally capable of representing the flow paths created by venting exterior doors and windows in both structures. The model represented the pressure magnitudes to a degree of accuracy that was slightly outside the expanded uncertainty throughout the structures. The model was capable of predicting the directions of gas flow as well as the elevation of the neutral plane through exterior vents in each structure, but the flow velocity magnitudes were generally overpredicted at low velocities and underpredicted at high velocities.

The model was unable to predict the peak magnitude of pressure transients that occurred shortly after ignition, specifically in close proximity to the burner. An apparent circulation of hot gases from the ceiling of the family room of the two-story structure over the second story hallway, and down the stairs to low elevation areas of the family room repeatedly occurred and may have contributed to a non-stratified temperature profile in the family room and kitchen. The non-stratification of temperatures in the family room may also have been affected by radiant heat transfer from the burner to the low elevation thermocouples. All simulations of the two-story structure were unable to predict this non-stratification. The apparent circulation of hot gases was attributed to the open-concept design of the structure.

The model represented measured temperatures and pressures adequately to validate the ability of the model defined with the aforementioned parameters to predict the peak measured quantities as well as the evolution of each of these measurements over time. Aspects of gas flow through ventilation openings and key areas of the structures, including gas flow direction and elevation of the neutral plane, were adequate to validate the ability of the model defined with the aforementioned parameters to predict these qualitative features. The errors between the predicted and

measured flow velocity magnitudes were significant and did not validate the ability of the model defined with the aforementioned parameters to predict flow velocities for the scenarios studied in this work. Changes in the simulation mode and resolution of the model did not significantly affect the model predictions, although model practitioners should always conduct resolution convergence studies and sensitivity analyses to ensure that predictions are consistent.

Additional research that more rigorously characterizes the flow field throughout the structures is required to fully understand the cause of the apparent circulation identified in the family room of the two-story structure as well as the cause of the large disparity between the predicted and measured velocity magnitudes shown in this work. An opportunity to expand on this research and aid in the validation and/or the improvement of fire modeling involves gas burner experiments with well-defined growing HRRs as well as HRRs that are expected to produce ventilation-limited conditions. Future research may also investigate the effect of wind, ambient temperature, and weather conditions on the data collected as well as the model predictions presented in this work.

9 Summary

UL Firefighter Safety Research Institute (UL FSRI) conducted a study to examine how ventilation impacts fire damage patterns in single family homes. The structures included a traditional 111 m² single-story ranch style structure and a 297 m² two-story colonial style structure. The two-story colonial had a contemporary open floor plan design with a two-story family room and open foyer. The experiments were planned with the assistance of a technical panel that included members of ATF, IAAI, NAFI, NASFM, NIST, NIST OSAC, and NFPA 921.

The scenarios consisted of gas burner fires in the structures with exterior ventilation that created flow paths which connected the source fires with remote intake and exhaust vents. In the single-story structure, the gas burner was located against an interior wall in the living room for all experiments. In the two-story structure, the gas burner was located against a wall in the family room for all experiments. In each of the single-story and two-story structures, three distinct ventilation scenarios were tested.

Instrumentation was installed to measure gas temperature, gas pressure, and gas velocity within the structures. The single-story structure had 140 instruments installed, and the two-story structure had 195 instruments installed. During the experiments, each channel was scanned every second and recorded on a computerized data acquisition system. In total, 5 experiments were conducted in the single-story structure and 8 experiments were conducted in the two-story structure. All of the experiments were conducted at UL's Large Fire Laboratory in Northbrook, IL.

Computational models were constructed using the Fire Dynamics Simulator (Version 6.7.1) to simulate the experiments conducted in this work. The model predicted temperatures well at all measurement locations with particularly good agreement for temperature rises larger than 100°C. The model represented the pressure magnitudes to a degree of accuracy that was slightly outside the expanded uncertainty throughout the structures. The agreement between predicted and measured temperatures and pressures was adequate to validate the ability of the model to predict the peak measured quantities as well as the temporal evolution of each of these measurements for similar scenarios. The model was capable of predicting the elevation of the neutral plane through exterior vents in each structure, but the flow velocity magnitudes were generally overpredicted at low velocities and underpredicted at high velocities. The errors between the predicted and measured flow velocity magnitudes were significant and did not validate the ability of the model to predict flow velocities for the scenarios studied in this work. Sensitivity analyses showed that changes in the model parameters did not significantly affect the model predictions.

References

- [1] United States Fire Administration (USFA). Fire in the United States 2008-2017. Technical report, 2019.
- [2] N Brushlinsky, M Ahrens, S Sokolov, and P Wagner. World Fire Statistics, 2019.
- [3] Residential Building Fire Trends (2008-2017). www.usfa.fema.gov/data/statistics, 2019.
- [4] National Fire Protection Association. *NFPA 921, Guide for Fire and Explosion Investigations*, 2017.
- [5] NIJ Forensic Science Technology Working Group. NIJ Forensic Science Technology Working Group Operational Requirements, 2016. <https://www.nij.gov/topics/forensics/documents/2016-forensic-twg-table.pdf>, December 2016.
- [6] ASTM E 1355-12(2018). Standard Guide for Evaluating the Predictive Capability of Deterministic Fire Models. Standard, West Conshohocken, PA, 2018.
- [7] K. McGrattan, S. Hostikka, J. Floyd, R. McDermott, and M. Vanella. *Fire Dynamics Simulator, User's Guide*. National Institute of Standards and Technology, Gaithersburg, Maryland, USA, and VTT Technical Research Centre of Finland, Espoo, Finland, Sixth edition, September 2019.
- [8] K. McGrattan, S. Hostikka, J. Floyd, R. McDermott, and M. Vanella. *Fire Dynamics Simulator, Technical Reference Guide Volume 1: Mathematical Model*. National Institute of Standards and Technology, Gaithersburg, Maryland, USA, and VTT Technical Research Centre of Finland, Espoo, Finland, sixth edition, September 2019.
- [9] R. McDermott, K. McGrattan, and J. Floyd. A Simple Reaction Time Scale for Under-Resolved Fire Dynamics. In *Fire Safety Science – Proceedings of the 10th International Symposium*, pages 809–820, University of Maryland, College Park, Maryland, USA, 2011.
- [10] McDermott R. Vaari J., Floyd J. CFD Simulations of Co-Flow Diffusion Flames. In *Proceedings of the International Symposium of Fire Safety Science*, volume 10, pages 781–794, College Park, MD, June 2011. International Association for Fire Safety Science.
- [11] G.P. Forney. Smokeview, A Tool for Visualizing Fire Dynamics Simulation Data, Volume I: User's Guide. NIST Special Publication 1017-1, National Institute of Standards and Technology, Gaithersburg, Maryland, January 2017.
- [12] G.P. Forney. Smokeview, A Tool for Visualizing Fire Dynamics Simulation Data, Volume II: Technical Reference Guide. NIST Special Publication 1017-2, National Institute of Standards and Technology, Gaithersburg, Maryland, January 2017.

- [13] K. McGrattan, S. Hostikka, J. Floyd, R. McDermott, and M. Vanella. *Fire Dynamics Simulator, Technical Reference Guide, Volume 2: Verification*. National Institute of Standards and Technology, Gaithersburg, Maryland, USA, and VTT Technical Research Centre of Finland, Espoo, Finland, sixth edition, January 2017.
- [14] K. McGrattan, S. Hostikka, J. Floyd, R. McDermott, and M. Vanella. *Fire Dynamics Simulator, Technical Reference Guide Volume 3: Validation*. National Institute of Standards and Technology, Gaithersburg, Maryland, USA, and VTT Technical Research Centre of Finland, Espoo, Finland, sixth edition, September 2019.
- [15] M.H. Salley. Verification and Validation of Selected Fire Models for Nuclear Power Plant Applications - Supplement 1. NUREG 1824, U.S. Nuclear Regulatory Commission, November 2016.
- [16] G. Hadjisophocleous and Q. Jia. Comparison of FDS Prediction of Smoke Movement in a 10-Storey Building with Experimental Data. *Fire Technology*, 45:163–177, 2009.
- [17] Y. Wang, E. Zalok, and G. Hadjisophocleous. An Experimental Study of Smoke Movement in Multi-Storey Buildings. *Fire Technology*, 47:1141–1169, 2011.
- [18] L. Audouin, L. Rigollet, H. Prétrel, W. Le Saux, and M. Röwekamp. OECD PRISME project: Fires in Confined and Ventilated Nuclear-Type Multi-Compartments - Overview and Main Experimental Results. *Fire Safety Journal*, 62:80 – 101, 2013. Special Issue on PRISME – Fire Safety in Nuclear Facilities.
- [19] J. Wahlqvist and P. van Hees. Validation of FDS for Large-Scale Well-Confined Mechanically Ventilated Fire Scenarios with Emphasis on Predicting Ventilation System Behavior. *Fire Safety Journal*, 62:102 – 114, 2013. Special Issue on PRISME – Fire Safety in Nuclear Facilities.
- [20] G. Rein, C. Abecassis Empis, and R. Carvel, editors. *The Dalmarnock Fire Tests: Experiments and Modelling*. School of Engineering and Electronics, University of Edinburgh, 2007.
- [21] R.W. Bukowski, R.D. Peacock, J.D. Averill, T.G. Cleary, N.P. Bryner, W.D. Walton, P.A. Reneke, and E.D. Kuligowski. Performance of Home Smoke Alarms. NIST Technical Note 1455-1, NIST, Gaithersburg, Maryland, February 2008.
- [22] R.K. Janardhan and S. Hostikka. Experiments and Numerical Simulations of Pressure Effects in Apartment Fires. *Fire Technology*, 53:1353 – 1377, 2017.
- [23] S. Kerber. Impact of Ventilation on Fire Behavior in Legacy and Contemporary Residential Construction. Report, Underwriters Laboratories, 2012.
- [24] S. Kerber. Study of Effectiveness of Fire Service Vertical Ventilation and Suppression Tactics in Single Family Homes. Report, Underwriters Laboratories, 2013.
- [25] J.L. Mattern. It's Official: Americans Are Obsessed with Ranch Homes. <https://www.countryliving.com/real-estate/a44039/ranch-home-united-states/>, July 2017. Accessed: 2019-02-17.

- [26] New Single-family Homes in 2017. <https://www.census.gov/construction/charts/interactive/>, 2017. Accessed: 2019-02-17.
- [27] ASTM International. *ASTM E779-10(2018), Standard Test Method for Determining Air Leakage Rate by Fan Pressurization*, 2018.
- [28] A.K. Persilly and K. Saito. Airtightness of Commercial and Institutional Buildings: Blowing Holes in the Myth of Tight Buildings. In *Thermal Envelopes VII Conference*, 1998.
- [29] L.G. Blevins. Behavior of Bare and Aspirated Thermocouples in Compartment Fires. In *National Heat Transfer Conference, 33rd Proceedings*, pages 15–17, 1999.
- [30] W.M. Pitts, E. Braun, R. Peacock, H. Mitler, E. Johnson, P. Reneke, and L.G. Blevins. Temperature Uncertainties for Bare-Bead and Aspirated Thermocouple Measurements in Fire Environments. *ASTM Special Technical Publication*, 1427:3–15, 2003.
- [31] A. Hamins, A. Maranghides, R. Johnsson, M. Donnelly, G. Yang, G. Mulholland, and R.L. Anleitner. Report of Experimental Results for the International Fire Model Benchmarking and Validation Exercise 3. NIST Special Publication 1013-1, National Institute of Standards and Technology, Gaithersburg, Maryland, May 2006. Joint Publication of NIST and the US Nuclear Regulatory Commission (NUREG/CR-6905).
- [32] B.J. McCaffrey and G. Heskestad. A Robust Bidirectional Low-Velocity Probe for Flame and Fire Application. *Combustion and Flame*, 26:125 – 127, 1976.
- [33] L.A. Kent and M.E. Schneider. The Design and Application of Bi-Directional Velocity Probes for Measurements in Large Pool Fires. *ISA Transactions*, 26:25 – 32, 1987.
- [34] R.A. Bryant. A Comparison of Gas Velocity Measurements in a Full-Scale Enclosure Fire. *Fire Safety Journal*, 44:793–800, 2009.
- [35] N. Benichou, M.A. Sultan, C. MacCallum, and J.D. Hum. Thermal Properties of Wood, Gypsum, and Insulation at Elevated Temperatures. IRC Internal Report, National Research Council of Canada, October 2001.
- [36] USG Sheetrock Brand Ultralight Panels. <https://www.usg.com/content/usgcom/en/products/walls/drywall/drywall-panels/lightweight-panels/sheetrock-ultralight-panels.141134.html>, 2019. Accessed: 2020-02-14.
- [37] K. McGrattan and S. Miles. *SFPE Handbook of Fire Protection Engineering*, chapter Modeling Fires Using Computational Fluid Dynamics (CFD). Springer, Fifth edition, 2016.
- [38] R.G. Rehm and H.R. Baum. The Equations of Motion for Thermally Driven, Buoyant Flows. *Journal of Research of the National Bureau of Standards*, 83, 1978.
- [39] D. Madrzykowski and C. Weinschenk. Impact of Fixed Ventilation on Fire Damage Patterns in Full-Scale Structures. Technical report, Underwriters Laboratories, 2019.

- [40] Joint Committee for Guides in Metrology. Evaluation of measurement data – Guide to the expression of uncertainty in measurement. Guidance Document JCGM 100:2008, 2008.
- [41] R.D. Peacock, P.A. Reneke, W.D. Davis, and W.W. Jones. Quantifying Fire Model Evaluation Using Functional Analysis. *Fire Safety Journal*, 33:167–184, 1999.
- [42] ISO 16730:2008(E). Fire safety engineering - Assessment, verification and validation of calculation methods. Standard, International Organization for Standardization, 2008.

Appendix A Metrics to Assess Agreement Between Measured Data and Predictions

Functional analysis using vector mathematics on the predicted and measured data provide quantitative measures of the agreement between the data. The norm is a vector operation that yields the length of a vector, and the inner product between two vectors is an operation that yields the product of the length of the two vectors and the cosine of the angle between the vectors [41]. By treating the experimental data and model predictions as many-dimensional vectors and using these operations, the relative difference between the two curves as well as the relative shapes of the curves may be calculated. In this work, the Euclidian norm of the difference between the experimental and prediction vectors was used to calculate the relative difference, and a weighted average of the Euclidian inner product and the Secant inner product was used to calculate the cosine similarity between the vectors, as described in ASTM and ISO standards on assessment of the predictive capabilities of deterministic fire models [6,42].

The relative difference and the cosine similarity between the experimental and predicted data sets have been calculated and are presented in the following tables. These metrics provide an evaluation of the ability of the model with the defined model parameters to represent the key flow dynamics and physical phenomena in the two structures in response to the ventilation events. These tabulated metrics also serve as a benchmark against which to compare as newer versions of FDS are released.

Lower relative difference is correlated with better agreement, such that a relative difference of zero indicates the predicted and experimental data curves are identical. The cosine similarity between the predicted and experimental curves is in the range of -1 and 1. A cosine similarity of 1 indicates the curves have the same functional form, a cosine similarity of -1 indicates the curves have the same functional form but are directed opposite each other, and a cosine of 0 indicates that there is no correlation between the two data curves.

The relative difference is the best measure of agreement between the model predictions and the experimental data curves, but because the metric is calculated over the entire length of the two vectors, the relative shapes of the curves must also be considered to assess the predictive capabilities of the model. ASTM E 1355 *Standard Guide for Evaluating the Predictive Capability of Deterministic Fire Models* provides the guidance that curves are in agreement when the hybrid norm is less than 0.3 and the cosine similarity calculated as a hybrid of the Euclidian inner product and the Secant inner product is greater than 0.9. No basis is provided for this guidance, and it was not followed strictly in the assessment provided in this work. A major conclusion that may be drawn from the ASTM standard is that both metrics must be considered together to assess the capabilities of the model.

Acceptable agreement between the prediction and the experimental data depends on the measur-

and, the scenario, and the application for which the model was used. In this work, predictions were considered to agree with the experimental data if the calculated relative difference was within the expanded uncertainty of the mean of each measurement. For temperature measurements, the model agreed with the experimental data when the relative difference was 0.24 or less. Velocity predictions agreed with the experimental measurements when the relative difference was 0.47 or lower. Pressure measurements converged on atmospheric pressure which resulted in increasingly large magnitudes of relative difference as the experiments progressed. The relative difference metric was excessively high for the pressure predictions. To provide a metric for the pressure that was insensitive to the small magnitude values, the norm of the absolute differences of pressure are presented in the following tables. The pressure prediction is considered to agree with the experimental data if the absolute difference is below 0.9 Pa for the single-story experiments and below 2.8 Pa for the two-story experiments.

Analysis of these data indicate that when the relative or absolute difference was within acceptable agreement as defined in the previous paragraph, experimental data curves were qualitatively well represented when the cosine similarity between the prediction and experimental data was above 0.5.

Table A.1: Model Agreement Metrics for Single-Story Experiment 1 Temperatures

Distance below Ceiling	0.02 m		0.3 m		0.6 m		0.9 m		1.2 m		1.5 m		1.8 m		2.1 m	
	Rel. Diff.	Cosine	Rel. Diff.	Cosine	Rel. Diff.	Cosine	Rel. Diff.	Cosine	Rel. Diff.	Cosine	Rel. Diff.	Cosine	Rel. Diff.	Cosine	Rel. Diff.	Cosine
Living Room	0.04	0.77	0.15	0.82	0.19	0.68	0.16	0.56	0.16	0.63	0.26	0.58	0.38	0.56	0.18	0.61
Bedroom 1	0.10	0.68	0.05	0.72	0.08	0.78	0.22	0.68	0.22	0.78	0.22	0.82	0.26	0.81	0.19	0.71
Bedroom 2	0.04	0.78	0.09	0.59	0.06	0.78	0.16	0.78	0.24	0.80	0.30	0.81	0.28	0.81	0.22	0.64
Bedroom 3	0.10	0.72	0.07	0.84	0.07	0.87	0.08	0.80	0.27	0.78	0.23	0.83	0.25	0.76	0.21	0.66
Hallway	0.06	0.70	0.16	0.68	0.12	0.58	0.24	0.65	0.24	0.66	0.24	0.66	0.24	0.72	0.26	0.55
Dining Room	0.07	0.71	0.03	0.73	0.03	0.81	0.07	0.83	0.26	0.79	0.46	0.68	0.37	0.74	0.27	0.62
Kitchen	-	-	0.06	0.76	0.04	0.77	0.12	0.72	0.18	0.81	0.34	0.77	0.33	0.77	0.28	0.66
Breakfast Area	0.09	0.70	0.04	0.84	0.04	0.87	0.07	0.84	0.19	0.80	0.45	0.77	0.36	0.63	0.30	0.56

Table A.2: Model Agreement Metrics for Single-Story Experiment 1 Pressures

Distance below Ceiling	0.3 m		1.2 m		2.1 m	
	Abs. Diff. [Pa]	Cosine	Abs. Diff. [Pa]	Cosine	Abs. Diff. [Pa]	Cosine
Living Room	1.34	0.68	1.03	0.65	1.00	0.65
Bedroom 1	0.98	0.66	1.00	0.65	-	-
Bedroom 2	1.07	0.66	1.02	0.64	0.96	0.66
Bedroom 3	1.02	0.66	1.03	0.64	0.98	0.65
Dining Room	1.05	0.65	1.07	0.63	1.03	0.62
Kitchen	1.16	0.64	1.06	0.63	1.04	0.63

Table A.3: Model Agreement Metrics for Single-Story Experiment 1 Velocities

Location of Probe	Lowest		Low-Mid		Middle		High-Mid		Highest	
	Rel. Diff.	Cosine	Rel. Diff.	Cosine	Rel. Diff.	Cosine	Rel. Diff.	Cosine	Rel. Diff.	Cosine
Hallway	1.30	0.48	2.56	0.26	2.20	0.46	1.15	0.33	1.24	0.47
Front Door	1.97	0.69	1.90	0.55	1.58	0.34	1.77	0.45	1.60	0.62
Window E	1.35	0.54	1.35	0.42	3.07	-0.02	1.02	0.37	0.93	0.49

Table A.4: Model Agreement Metrics for Single-Story Experiment 2 Temperatures

Distance below Ceiling	0.02 m		0.3 m		0.6 m		0.9 m		1.2 m		1.5 m		1.8 m		2.1 m	
	Rel. Diff.	Cosine	Rel. Diff.	Cosine	Rel. Diff.	Cosine	Rel. Diff.	Cosine	Rel. Diff.	Cosine	Rel. Diff.	Cosine	Rel. Diff.	Cosine	Rel. Diff.	Cosine
Living Room	0.04	0.68	0.15	0.70	0.17	0.59	0.16	0.58	0.16	0.59	0.24	0.53	0.36	0.56	0.23	0.57
Bedroom 1	0.08	0.57	0.05	0.54	0.05	0.60	0.19	0.62	0.28	0.69	0.19	0.86	0.21	0.88	0.18	0.78
Bedroom 2	0.07	0.61	0.05	0.49	0.07	0.56	0.19	0.59	0.18	0.82	0.34	0.72	0.28	0.79	0.25	0.72
Bedroom 3	0.07	0.64	0.05	0.72	0.04	0.82	0.09	0.63	0.26	0.70	0.27	0.77	0.29	0.79	0.25	0.71
Hallway	0.06	0.60	0.10	0.59	0.12	0.50	0.12	0.58	0.21	0.56	0.33	0.55	0.40	0.57	0.35	0.58
Dining Room	0.08	0.65	0.04	0.64	0.05	0.68	0.07	0.73	0.24	0.67	0.42	0.66	0.48	0.71	0.41	0.61
Kitchen	-	-	0.06	0.70	0.04	0.67	0.11	0.67	0.18	0.77	0.32	0.77	0.42	0.80	0.39	0.70
Breakfast Area	0.03	0.60	0.04	0.80	0.05	0.77	0.08	0.77	0.19	0.74	0.41	0.70	0.46	0.74	0.40	0.68

Table A.5: Model Agreement Metrics for Single-Story Experiment 2 Pressures

Distance below Ceiling	0.3 m		1.2 m		2.1 m	
	Abs. Diff. [Pa]	Cosine	Abs. Diff. [Pa]	Cosine	Abs. Diff. [Pa]	Cosine
Living Room	2.17	0.69	1.39	0.66	1.24	0.66
Bedroom 1	1.29	0.68	1.33	0.66	-	-
Bedroom 2	2.00	0.68	1.37	0.66	1.10	0.67
Bedroom 3	1.49	0.68	1.41	0.65	1.12	0.66
Dining Room	1.65	0.64	1.80	0.61	1.58	0.61
Kitchen	2.06	0.65	1.77	0.60	1.59	0.61

Table A.6: Model Agreement Metrics for Single-Story Experiment 2 Velocities

Location of Probe	Lowest		Low-Mid		Middle		High-Mid		Highest	
	Rel. Diff.	Cosine	Rel. Diff.	Cosine	Rel. Diff.	Cosine	Rel. Diff.	Cosine	Rel. Diff.	Cosine
Hallway	1.40	0.50	1.26	0.37	2.32	0.44	0.93	0.48	1.06	0.52
Front Door	2.08	0.49	2.09	0.46	1.68	0.52	1.94	0.47	1.63	0.51
Window E	1.05	0.43	1.15	0.33	2.68	-0.29	1.30	0.32	0.89	0.57

Table A.7: Model Agreement Metrics for Single-Story Experiment 3 Temperatures

Distance below Ceiling	0.02 m		0.3 m		0.6 m		0.9 m		1.2 m		1.5 m		1.8 m		2.1 m	
	Rel. Diff.	Cosine	Rel. Diff.	Cosine	Rel. Diff.	Cosine	Rel. Diff.	Cosine	Rel. Diff.	Cosine	Rel. Diff.	Cosine	Rel. Diff.	Cosine	Rel. Diff.	Cosine
Living Room	0.04	0.68	0.14	0.83	0.24	0.69	0.18	0.55	0.10	0.64	0.18	0.64	0.26	0.51	0.12	0.62
Bedroom 1	0.11	0.64	0.04	0.73	0.05	0.72	0.20	0.65	0.19	0.74	0.19	0.81	0.20	0.80	0.14	0.71
Bedroom 2	0.05	0.77	0.06	0.68	0.05	0.78	0.13	0.75	0.20	0.78	0.24	0.79	0.22	0.77	0.16	0.56
Bedroom 3	0.15	0.71	0.12	0.80	0.12	0.84	0.06	0.76	0.21	0.79	0.17	0.80	0.18	0.76	0.15	0.64
Hallway	0.07	0.65	0.18	0.70	0.10	0.56	0.23	0.59	0.19	0.68	0.15	0.71	0.22	0.59	0.21	0.55
Dining Room	0.05	0.63	0.08	0.74	0.05	0.75	0.09	0.68	0.14	0.83	0.26	0.90	0.25	0.81	0.14	0.63
Kitchen	-	-	0.10	0.71	0.06	0.71	0.14	0.65	0.14	0.73	0.20	0.85	0.23	0.82	0.15	0.62
Breakfast Area	0.04	0.61	0.07	0.67	0.10	0.68	0.08	0.68	0.21	0.76	0.27	0.76	0.27	0.77	0.11	0.68

Table A.8: Model Agreement Metrics for Single-Story Experiment 3 Pressures

Distance below Ceiling	0.3 m		1.2 m		2.1 m	
	Abs. Diff. [Pa]	Cosine	Abs. Diff. [Pa]	Cosine	Abs. Diff. [Pa]	Cosine
Living Room	1.72	0.51	1.40	0.47	-	-
Bedroom 1	1.35	0.49	-	-	-	-
Bedroom 2	1.48	0.50	1.40	0.47	1.34	0.47
Bedroom 3	1.42	0.50	1.40	0.47	1.34	0.47
Dining Room	1.39	0.49	1.40	0.47	1.35	0.46
Kitchen	1.55	0.51	1.38	0.47	1.36	0.46

Table A.9: Model Agreement Metrics for Single-Story Experiment 3 Velocities

Location of Probe	Lowest		Low-Mid		Middle		High-Mid		Highest	
	Rel. Diff.	Cosine	Rel. Diff.	Cosine	Rel. Diff.	Cosine	Rel. Diff.	Cosine	Rel. Diff.	Cosine
Window E	1.16	0.41	1.26	0.45	2.23	-0.14	1.38	0.36	0.78	0.44

Table A.10: Model Agreement Metrics for Two-Story Experiment 4 Temperatures

Distance below Ceiling	0.02 m		0.3 m		0.6 m		0.9 m		1.2 m		1.5 m		1.8 m		2.1 m	
	Rel. Diff.	Cosine	Rel. Diff.	Cosine	Rel. Diff.	Cosine	Rel. Diff.	Cosine	Rel. Diff.	Cosine	Rel. Diff.	Cosine	Rel. Diff.	Cosine	Rel. Diff.	Cosine
Living Room	0.21	0.50	0.20	0.78	0.23	0.78	0.25	0.82	0.33	0.76	0.40	0.67	0.36	0.66	0.35	0.63
Under Hallway	0.04	0.70	0.08	0.64	0.13	0.69	0.19	0.65	0.28	0.62	0.24	0.55	0.23	0.65	0.22	0.50
Foyer	0.05	0.71	0.04	0.70	0.05	0.80	0.07	0.77	0.13	0.71	0.28	0.64	0.39	0.65	0.37	0.70
Dining Room	0.09	0.73	0.09	0.71	0.13	0.76	0.25	0.72	0.33	0.74	0.37	0.71	0.40	0.72	0.39	0.64
Laundry Room	0.19	0.72	0.23	0.68	0.23	0.78	0.24	0.82	0.28	0.79	0.31	0.78	0.42	0.62	0.46	0.58
Kitchen	0.41	0.75	0.19	0.83	0.08	0.71	0.23	0.82	0.31	0.76	0.33	0.66	0.38	0.61	0.42	0.59
Master Bedroom	0.09	0.65	0.13	0.59	0.10	0.76	0.08	0.82	0.04	0.74	0.03	0.77	0.10	0.71	0.24	0.64
Bedroom 2	0.08	0.65	0.09	0.61	0.06	0.74	0.15	0.84	0.04	0.77	0.12	0.75	0.25	0.70	0.29	0.69
Bedroom 3	0.04	0.56	0.19	0.61	0.08	0.55	0.09	0.65	0.16	0.61	0.27	0.67	0.30	0.66	0.42	0.64
Bedroom 4	0.09	0.61	0.10	0.64	0.13	0.58	0.11	0.60	0.13	0.77	0.16	0.86	0.38	0.83	0.26	0.84
End Hallway	0.06	0.66	0.07	0.68	0.05	0.68	0.05	0.67	0.12	0.59	0.35	0.56	0.42	0.48	0.43	0.54
Mid Hallway	0.06	0.69	0.08	0.67	0.11	0.61	0.09	0.60	0.04	0.59	0.34	0.54	0.54	0.52	0.39	0.56
Family Room	0.08	0.63	0.05	0.66	0.06	0.61	0.09	0.61	0.11	0.65	0.14	0.61	0.24	0.62	0.30	0.61
Den	0.14	0.67	0.16	0.71	0.17	0.76	0.20	0.81	0.25	0.79	0.27	0.74	0.31	0.73	0.37	0.59

Table A.11: Model Agreement Metrics for Two-Story Experiment 4 Temperatures

Distance below Ceiling	2.4 m		2.7 m		3.0 m		3.3 m		3.6 m		3.9 m		4.2 m		4.5 m	
	Rel. Diff.	Cosine	Rel. Diff.	Cosine	Rel. Diff.	Cosine	Rel. Diff.	Cosine	Rel. Diff.	Cosine	Rel. Diff.	Cosine	Rel. Diff.	Cosine	Rel. Diff.	Cosine
Foyer	0.27	0.73	0.26	0.73	0.46	0.66	0.89	0.58	0.80	0.59	0.93	0.54	1.11	0.50	1.15	0.54
Family Room	0.25	0.63	0.32	0.63	0.38	0.62	0.38	0.75	0.37	0.77	0.44	0.74	0.61	0.71	0.52	0.72

Table A.12: Model Agreement Metrics for Two-Story Experiment 4 Pressures

Distance below Ceiling	0.3 m		1.2 m		2.1 m	
	Abs. Diff. [Pa]	Cosine	Abs. Diff. [Pa]	Cosine	Abs. Diff. [Pa]	Cosine
Master Bedroom	2.24	0.56	2.22	0.55	2.27	0.54
Bedroom 2	2.37	0.57	2.26	0.56	2.16	0.56
Bedroom 3	2.19	0.58	2.17	0.57	2.11	0.56
Bedroom 4	2.15	0.57	2.19	0.56	2.19	0.55
Front Door	1.98	0.51	1.77	0.52	1.51	0.55
Living Room	2.08	0.49	1.98	0.49	1.76	0.52
Den	2.00	0.49	1.93	0.49	1.88	0.50

Table A.13: Model Agreement Metrics for Two-Story Experiment 4 Pressures

Distance below Ceiling	0.3 m		2.4 m		4.6 m	
	Abs. Diff. [Pa]	Cosine	Abs. Diff. [Pa]	Cosine	Abs. Diff. [Pa]	Cosine
Family Room	2.71	0.53	2.50	0.49	5.50	0.49

Table A.14: Model Agreement Metrics for Two-Story Experiment 4 Velocities

Location of Probe	Lowest		Low-Mid		Middle		High-Mid		Highest	
	Rel. Diff.	Cosine	Rel. Diff.	Cosine	Rel. Diff.	Cosine	Rel. Diff.	Cosine	Rel. Diff.	Cosine
Front Door	2.18	0.59	2.04	0.57	1.97	0.51	2.00	0.56	1.83	0.61
Window K	1.49	0.37	1.49	0.32	1.78	0.49	1.70	0.53	1.62	0.51
Window L	2.16	0.55	-	-	1.47	0.46	1.61	0.60	1.59	0.69

Table A.15: Model Agreement Metrics for Two-Story Experiment 5 Temperatures

Distance below Ceiling	0.02 m		0.3 m		0.6 m		0.9 m		1.2 m		1.5 m		1.8 m		2.1 m	
	Rel. Diff.	Cosine	Rel. Diff.	Cosine	Rel. Diff.	Cosine	Rel. Diff.	Cosine	Rel. Diff.	Cosine	Rel. Diff.	Cosine	Rel. Diff.	Cosine	Rel. Diff.	Cosine
Living Room	0.16	0.55	0.16	0.85	0.19	0.76	0.29	0.64	0.34	0.72	0.35	0.72	0.33	0.71	0.32	0.65
Under Hallway	0.06	0.65	0.07	0.60	0.09	0.67	0.21	0.65	0.29	0.65	0.22	0.65	0.20	0.59	0.17	0.53
Foyer	0.07	0.76	0.06	0.71	0.07	0.81	0.08	0.79	0.10	0.82	0.12	0.76	0.11	0.78	0.12	0.82
Dining Room	0.06	0.68	0.05	0.74	0.07	0.76	0.27	0.69	0.30	0.72	0.34	0.68	0.38	0.73	0.38	0.68
Laundry Room	0.16	0.65	0.22	0.61	0.22	0.79	0.23	0.81	0.27	0.77	0.30	0.72	0.39	0.65	0.44	0.63
Kitchen	0.40	0.69	0.13	0.78	0.14	0.68	0.25	0.70	0.28	0.72	0.28	0.69	0.32	0.60	0.37	0.63
Master Bedroom	0.13	0.69	0.16	0.64	0.13	0.79	0.12	0.84	0.06	0.80	0.05	0.82	0.06	0.81	0.14	0.72
Bedroom 2	0.03	0.69	0.13	0.67	0.09	0.77	0.09	0.86	0.06	0.84	0.08	0.81	0.09	0.76	0.19	0.75
Bedroom 3	0.04	0.62	0.17	0.68	0.08	0.74	0.09	0.80	0.06	0.82	0.06	0.80	0.11	0.82	0.28	0.77
Bedroom 4	0.12	0.66	0.12	0.71	0.13	0.80	0.10	0.80	0.04	0.75	0.09	0.80	0.37	0.75	0.26	0.77
End Hallway	0.04	0.62	0.09	0.67	0.07	0.68	0.08	0.73	0.10	0.62	0.39	0.58	0.29	0.57	0.26	0.59
Mid Hallway	0.04	0.70	0.10	0.66	0.15	0.62	0.12	0.64	0.05	0.65	0.40	0.59	0.54	0.57	0.28	0.61
Family Room	0.06	0.72	0.11	0.74	0.13	0.70	0.15	0.69	0.13	0.71	0.10	0.76	0.06	0.70	0.07	0.67
Den	0.10	0.61	0.14	0.68	0.16	0.76	0.19	0.80	0.24	0.77	0.24	0.77	0.27	0.75	0.32	0.66

Table A.16: Model Agreement Metrics for Two-Story Experiment 5 Temperatures

Distance below Ceiling	2.4 m		2.7 m		3.0 m		3.3 m		3.6 m		3.9 m		4.2 m		4.5 m	
	Rel. Diff.	Cosine	Rel. Diff.	Cosine	Rel. Diff.	Cosine	Rel. Diff.	Cosine	Rel. Diff.	Cosine	Rel. Diff.	Cosine	Rel. Diff.	Cosine	Rel. Diff.	Cosine
Foyer	0.16	0.78	0.19	0.74	0.48	0.64	1.00	0.53	0.79	0.60	0.88	0.61	1.05	0.53	1.19	0.54
Family Room	0.07	0.71	0.14	0.62	0.30	0.67	0.37	0.78	0.39	0.78	0.45	0.78	0.58	0.78	0.59	0.71

Table A.17: Model Agreement Metrics for Two-Story Experiment 5 Pressures

Distance below Ceiling	0.3 m		1.2 m		2.1 m	
	Abs. Diff. [Pa]	Cosine	Abs. Diff. [Pa]	Cosine	Abs. Diff. [Pa]	Cosine
Master Bedroom	2.10	0.59	2.06	0.59	2.13	0.58
Bedroom 2	2.18	0.59	2.11	0.59	2.07	0.58
Bedroom 3	2.12	0.58	2.16	0.60	2.08	0.58
Bedroom 4	2.06	0.59	2.10	0.59	2.07	0.58
Front Door	1.93	0.54	1.69	0.54	1.39	0.57
Living Room	1.98	0.51	1.87	0.49	1.58	0.52
Den	1.85	0.49	1.78	0.49	1.66	0.51

Table A.18: Model Agreement Metrics for Two-Story Experiment 5 Pressures

Distance below Ceiling	0.3 m		2.4 m		4.6 m	
	Abs. Diff. [Pa]	Cosine	Abs. Diff. [Pa]	Cosine	Abs. Diff. [Pa]	Cosine
Family Room	2.61	0.56	2.40	0.53	4.49	0.51

Table A.19: Model Agreement Metrics for Two-Story Experiment 5 Velocities

Location of Probe	Lowest		Low-Mid		Middle		High-Mid		Highest	
	Rel. Diff.	Cosine	Rel. Diff.	Cosine	Rel. Diff.	Cosine	Rel. Diff.	Cosine	Rel. Diff.	Cosine
Front Door	2.21	0.63	2.08	0.59	1.91	0.51	2.12	0.47	1.67	0.68

Table A.20: Model Agreement Metrics for Two-Story Experiment 6 Temperatures

	0.02 m		0.3 m		0.6 m		0.9 m		1.2 m		1.5 m		1.8 m		2.1 m	
	Rel. Diff.	Cosine	Rel. Diff.	Cosine	Rel. Diff.	Cosine	Rel. Diff.	Cosine	Rel. Diff.	Cosine	Rel. Diff.	Cosine	Rel. Diff.	Cosine	Rel. Diff.	Cosine
Distance below Ceiling	0.06	0.59	0.05	0.78	0.05	0.75	0.07	0.75	0.07	0.71	0.09	0.71	0.11	0.73	0.11	0.65
Living Room	0.11	0.65	0.10	0.60	0.08	0.65	0.08	0.65	0.08	0.63	0.09	0.64	0.12	0.58	0.12	0.65
Under Hallway	0.15	0.71	0.12	0.66	0.12	0.76	0.08	0.74	0.06	0.75	0.11	0.64	0.26	0.65	0.27	0.65
Foyer	0.06	0.60	0.06	0.64	0.07	0.75	0.06	0.70	0.08	0.73	0.08	0.72	0.17	0.63	0.16	0.60
Dining Room	0.05	0.70	0.06	0.69	0.06	0.78	0.05	0.82	0.05	0.82	0.06	0.79	0.13	0.66	0.14	0.69
Laundry Room	0.15	0.60	0.05	0.63	0.18	0.66	0.06	0.70	0.06	0.68	0.08	0.64	0.09	0.56	0.11	0.55
Kitchen	0.20	0.64	0.24	0.61	0.21	0.74	0.20	0.80	0.15	0.70	0.14	0.73	0.11	0.72	0.15	0.63
Master Bedroom	0.11	0.65	0.20	0.62	0.17	0.71	0.16	0.82	0.13	0.76	0.08	0.70	0.21	0.65	0.22	0.68
Bedroom 2	0.11	0.59	0.05	0.58	0.19	0.53	0.18	0.59	0.26	0.51	0.32	0.70	0.28	0.78	0.27	0.82
Bedroom 3	0.21	0.60	0.20	0.66	0.21	0.73	0.18	0.74	0.10	0.71	0.15	0.63	0.25	0.58	0.18	0.61
Bedroom 4	0.11	0.57	0.16	0.65	0.13	0.66	0.13	0.62	0.05	0.55	0.17	0.48	0.40	0.49	0.48	0.48
End Hallway	0.12	0.70	0.17	0.66	0.21	0.62	0.19	0.56	0.12	0.62	0.17	0.48	0.50	0.51	0.32	0.55
Mid Hallway	0.13	0.66	0.16	0.69	0.17	0.65	0.19	0.65	0.18	0.66	0.16	0.63	0.11	0.58	0.14	0.62
Family Room																

Table A.21: Model Agreement Metrics for Two-Story Experiment 6 Temperatures

	2.4 m		2.7 m		3.0 m		3.3 m		3.6 m		3.9 m		4.2 m		4.5 m	
	Rel. Diff.	Cosine	Rel. Diff.	Cosine	Rel. Diff.	Cosine	Rel. Diff.	Cosine	Rel. Diff.	Cosine	Rel. Diff.	Cosine	Rel. Diff.	Cosine	Rel. Diff.	Cosine
Distance below Ceiling	0.18	0.70	0.17	0.67	0.28	0.66	0.44	0.55	0.32	0.54	0.31	0.56	0.35	0.57	0.44	0.58
Foyer	0.06	0.61	0.05	0.63	0.08	0.67	0.48	0.73	0.49	0.75	0.51	0.74	0.56	0.73	0.59	0.71
Family Room																

Table A.22: Model Agreement Metrics for Two-Story Experiment 6 Pressures

Distance below Ceiling	0.3 m		1.2 m		2.1 m	
	Abs. Diff. [Pa]	Cosine	Abs. Diff. [Pa]	Cosine	Abs. Diff. [Pa]	Cosine
Master Bedroom	2.94	0.60	2.67	0.59	2.63	0.57
Bedroom 2	3.28	0.62	2.92	0.60	2.60	0.58
Bedroom 3	3.09	0.65	2.81	0.63	2.53	0.62
Bedroom 4	2.93	0.61	2.79	0.60	2.59	0.57
Front Door	2.35	0.56	2.00	0.60	1.68	0.62
Living Room	2.21	0.56	2.07	0.58	1.77	0.60

Table A.23: Model Agreement Metrics for Two-Story Experiment 6 Pressures

Distance below Ceiling	0.3 m		2.4 m		4.6 m	
	Abs. Diff. [Pa]	Cosine	Abs. Diff. [Pa]	Cosine	Abs. Diff. [Pa]	Cosine
Family Room	3.82	0.57	2.86	0.51	7.42	0.61

Table A.24: Model Agreement Metrics for Two-Story Experiment 6 Velocities

Location of Probe	Lowest		Low-Mid		Middle		High-Mid		Highest	
	Rel. Diff.	Cosine	Rel. Diff.	Cosine	Rel. Diff.	Cosine	Rel. Diff.	Cosine	Rel. Diff.	Cosine
Front Door	2.02	0.84	2.00	0.90	1.99	0.89	2.02	0.80	2.02	0.70
Window K	1.68	0.49	1.48	0.25	1.80	0.43	1.72	0.48	1.65	0.58
Window A	1.71	0.92	-	-	1.83	0.91	-	-	1.84	0.91

Appendix B FDS Input Files

The input file for the simulation of Single-Story Experiment 1 is provided below.

```
&HEAD CHID='Single_Story_Gas_1' /

&TIME T_END=1800. /

&MISC SIMULATION_MODE='SVLES' /

&MESH IJK=36,32,30, XB=-0.2,3.4,-0.6,2.6,0.0,3.0, MULT_ID='mesh' /
&MULT ID='mesh', DX=3.6, DY=3.2, L_UPPER=3, J_UPPER=2 /

&REAC FUEL='METHANE', SOOT_YIELD=0.001 /

&SURF ID='BURNER', HRRPUA=694., COLOR='ORANGE', RAMP_Q='burner' /
&RAMP ID='burner', T= 0., F=0. /
&RAMP ID='burner', T= 5., F=1. /
&RAMP ID='burner', T= 900., F=1. /
&RAMP ID='burner', T= 905., F=0. /
&OBST XB= 8.7, 9.3,1.6,2.2,0.4,0.6, SURF_IDS='BURNER','WALL','WALL' /

&MATL ID='GYPSUM BOARD'
FY1='Sheetrock UltraLight Panels',
SPECIFIC_HEAT=1.0
CONDUCTIVITY=0.16
DENSITY=480.0 /

&SURF ID='WALL',
RGB=200,200,200
DEFAULT=.TRUE.
MATL_ID='GYPSUM BOARD'
BACKING='VOID'
THICKNESS=0.025 /

&SURF ID='DOOR',
COLOR='GRAY'
MATL_ID='GYPSUM BOARD'
THICKNESS=0.05 /

&SURF ID='WINDOW',
MATL_ID='GYPSUM BOARD',
THICKNESS=0.05
COLOR='BLUE'
TRANSPARENCY=0.1/

&OBST XB= 0.0,14.0,0.0,0.1,0.0,2.4 / Front Facade
&OBST XB= 0.0,14.0,7.8,7.9,0.0,2.4 / Rear Facade
&OBST XB= 0.0, 0.1,0.1,7.8,0.0,2.4 / Left Facade
&OBST XB=13.9,14.0,0.1,7.8,0.0,2.4 / Right Facade

&OBST XB=0.0,14.0,0.0,7.9,2.4,2.5, COLOR='INVISIBLE' / Ceiling

&DEVC ID='FRONT DOOR TIMER', QUANTITY='TIME', XYZ=-0.1,-0.4,0.1, SETPOINT= 300.0, INITIAL_STATE=.TRUE. /
&DEVC ID='KITCH DOOR TIMER', QUANTITY='TIME', XYZ=-0.1,-0.4,0.1, SETPOINT=1320.0, INITIAL_STATE=.TRUE. /
&DEVC ID='BR1 WINDOW TIMER', QUANTITY='TIME', XYZ=-0.1,-0.4,0.1, SETPOINT= 600.0, INITIAL_STATE=.TRUE. /
&DEVC ID='BR1 WIND 2 TIMER', QUANTITY='TIME', XYZ=-0.1,-0.4,0.1, SETPOINT=1220.0, INITIAL_STATE=.TRUE. /
&DEVC ID='BR2 WINDOW TIMER', QUANTITY='TIME', XYZ=-0.1,-0.4,0.1, SETPOINT=1230.0, INITIAL_STATE=.TRUE. /
&DEVC ID='BR3 WINDOW TIMER', QUANTITY='TIME', XYZ=-0.1,-0.4,0.1, SETPOINT=1250.0, INITIAL_STATE=.TRUE. /
&DEVC ID='KIT WINDOW TIMER', QUANTITY='TIME', XYZ=-0.1,-0.4,0.1, SETPOINT=1260.0, INITIAL_STATE=.TRUE. /
&DEVC ID='DR WINDOW TIMER', QUANTITY='TIME', XYZ=-0.1,-0.4,0.1, SETPOINT=1275.0, INITIAL_STATE=.TRUE. /
&DEVC ID='LR WINDOW TIMER', QUANTITY='TIME', XYZ=-0.1,-0.4,0.1, SETPOINT=1200.0, INITIAL_STATE=.TRUE. /

&OBST XB= 3.8, 4.7,0.0,0.1,0.0,2.0, SURF_ID='DOOR', PERMIT_HOLE=.FALSE., DEVC_ID='FRONT DOOR TIMER' /
&OBST XB= 0.5, 2.3,7.8,7.9,0.0,2.0, SURF_ID='DOOR', PERMIT_HOLE=.FALSE., DEVC_ID='KITCH DOOR TIMER' /
&OBST XB= 4.5, 5.4,7.8,7.9,1.0,2.0, SURF_ID='WINDOW', PERMIT_HOLE=.FALSE., DEVC_ID='KIT WINDOW TIMER' /
&OBST XB= 0.6, 2.4,0.0,0.1,0.6,2.0, SURF_ID='WINDOW', PERMIT_HOLE=.FALSE., DEVC_ID='DR WINDOW TIMER' /
&OBST XB= 5.8, 8.5,0.0,0.1,0.6,2.0, SURF_ID='WINDOW', PERMIT_HOLE=.FALSE., DEVC_ID='LR WINDOW TIMER' /
&OBST XB=11.6,12.5,0.0,0.1,0.6,2.0, SURF_ID='WINDOW', PERMIT_HOLE=.FALSE., DEVC_ID='BR1 WINDOW TIMER' /
&OBST XB=13.9,14.0,1.5,2.4,0.6,2.0, SURF_ID='WINDOW', PERMIT_HOLE=.FALSE., DEVC_ID='BR1 WIND 2 TIMER' /
&OBST XB=12.1,13.0,7.8,7.9,0.6,2.0, SURF_ID='WINDOW', PERMIT_HOLE=.FALSE., DEVC_ID='BR2 WINDOW TIMER' /
&OBST XB= 7.6, 8.5,7.8,7.9,0.6,2.0, SURF_ID='WINDOW', PERMIT_HOLE=.FALSE., DEVC_ID='BR3 WINDOW TIMER' /

&HOLE XB= 3.8, 4.7,0.0,0.1,0.0,2.0 / FRONT DOOR
&HOLE XB= 0.5, 2.3,7.8,7.9,0.0,2.0 / KITCHEN DOOR
&HOLE XB= 4.5, 5.4,7.8,7.9,1.0,2.0 / KITCHEN WINDOW
&HOLE XB= 0.6, 2.4,0.0,0.1,0.6,2.0 / DINING ROOM WINDOW
&HOLE XB= 5.8, 8.5,0.0,0.1,0.6,2.0 / LIVING ROOM WINDOW
&HOLE XB=11.6,12.5,0.0,0.1,0.6,2.0 / BEDROOM 1 FRONT WINDOW
&HOLE XB=13.9,14.0,1.5,2.4,0.6,2.0 / BEDROOM 1 SIDE WINDOW
&HOLE XB=12.1,13.0,7.8,7.9,0.6,2.0 / BEDROOM 2 BACK WINDOW
&HOLE XB= 7.6, 8.5,7.8,7.9,0.6,2.0 / BEDROOM 3 BACK WINDOW

&OBST XB= 2.8, 2.9,0.1,3.0,0.0,2.4, SURF_ID='WALL' / Instruments, Front
&OBST XB= 3.6, 3.7,0.1,3.0,0.0,2.4, SURF_ID='WALL' / Instruments, Front
```

```

&OBST XB= 2.9, 3.6,2.9,3.0,0.0,2.4, SURF_ID='WALL' / Instruments, Front
&OBST XB= 9.3, 9.4,0.1,3.9,0.0,2.4, SURF_ID='WALL' / Instruments, Front
&OBST XB=10.0,10.1,0.1,3.8,0.0,2.4, SURF_ID='WALL' / Instruments, Front

&OBST XB= 0.1, 1.4,4.0,4.1,0.0,2.4, SURF_ID='WALL' / Breakfast Wall
&OBST XB= 1.3, 1.4,4.1,4.8,0.0,2.4, SURF_ID='WALL' / Breakfast Wall

&OBST XB= 2.6, 4.9,4.0,4.1,0.0,2.4, SURF_ID='WALL' / Kitchen Wall
&OBST XB= 4.9, 5.7,4.0,4.1,2.0,2.4, SURF_ID='WALL' / Kitchen Door Soffit
&OBST XB= 2.6, 2.7,4.1,4.8,0.0,2.4, SURF_ID='WALL' / Kitchen Wall

&OBST XB= 5.7, 8.0,4.0,4.1,0.0,2.4, SURF_ID='WALL' / Bedroom 3 Wall
&OBST XB= 7.9, 8.0,4.1,4.8,0.0,2.4, SURF_ID='WALL' / Bedroom 3 Wall
&OBST XB= 6.5, 6.6,4.1,7.8,0.0,2.4, SURF_ID='WALL' / Bedroom 3 - Kitchen Wall
&OBST XB= 7.9,11.1,4.8,4.9,0.0,2.4, SURF_ID='WALL' / Bedroom 3 Wall
&HOLE XB= 8.5, 9.2,4.8,4.9,0.0,2.1 / Bedroom 3 Door
&OBST XB= 9.3, 9.4,4.9,7.8,0.0,2.4, SURF_ID='WALL' / Bedroom 3 - Instruments Wall
&OBST XB=11.1,11.2,3.9,7.8,0.0,2.4, SURF_ID='WALL' / Bedroom 2 - Instruments Wall

&OBST XB= 9.4,13.9,3.8,3.9,0.0,2.4, SURF_ID='WALL' / Bedroom 2 - Bedroom 1 Wall
&OBST XB=12.3,12.4,3.9,4.6,0.0,2.4, SURF_ID='WALL' / Bedroom 2 Closet
&HOLE XB=11.1,11.2,4.0,4.7,0.0,2.1 / Bedroom 2 Door
&HOLE XB=10.2,11.0,3.8,3.9,0.0,2.1 / Bedroom 1 Door

&VENT XB = 3.8,8.8,0.4,3.4,0.0,0.0, ID='FLOOR LEAK', SURF_ID='WALL' /
&HVAC ID = 'FLOOR LEAK', TYPE_ID='LEAK', VENT_ID='FLOOR LEAK', VENT2_ID='AMBIENT', AREA=0.08 /
&VENT SURF_ID='OPEN', MB='ZMAX' /
&VENT SURF_ID='OPEN', MB='XMIN' /
&VENT SURF_ID='OPEN', MB='XMAX' /
&VENT SURF_ID='OPEN', MB='YMIN' /
&VENT SURF_ID='OPEN', MB='YMAX' /

&ZONE XB = 0.1,13.9,0.1,7.8,0.1,2.4 /

&DUMP DT_HRR=15., DT_DEVC=15., SIG_FIGS=4, SIG_FIGS_EXP=2 /

&DEVC XB=12.05,12.05,0.05,0.05,0.74,1.86 ID='1BDPT', QUANTITY='THERMOCOUPLE', POINTS=5, TIME_HISTORY=.TRUE. /
&DEVC XB=12.05,12.05,0.05,0.05,0.74,1.86 ID='1BDPV', QUANTITY='V-VELOCITY', POINTS=5, TIME_HISTORY=.TRUE., CONVERSION_FACTOR=-1.0 /
&DEVC XB=10.25,10.25,0.4,0.4,0.3,2.1 ID='1PT', QUANTITY='PRESSURE', POINTS=3, TIME_HISTORY=.TRUE. /
&DEVC XB=10.9,10.9,1.9,1.9,2.39,0.255 ID='1TC', QUANTITY='THERMOCOUPLE', POINTS=8, TIME_HISTORY=.TRUE. /
&DEVC XB=13.95,13.95,1.95,1.95,0.74,1.86 ID='2BDPT', QUANTITY='THERMOCOUPLE', POINTS=5, TIME_HISTORY=.TRUE. /
&DEVC XB=13.95,13.95,1.95,1.95,0.74,1.86 ID='2BDPV', QUANTITY='U-VELOCITY', POINTS=5, TIME_HISTORY=.TRUE. /
&DEVC XB=11.35,11.35,7.5,7.5,0.3,2.1 ID='2PT', QUANTITY='PRESSURE', POINTS=3, TIME_HISTORY=.TRUE. /
&DEVC XB=12.4,12.4,5.2,5.2,2.39,0.255 ID='2TC', QUANTITY='THERMOCOUPLE', POINTS=8, TIME_HISTORY=.TRUE. /
&DEVC XB=8.05,8.05,7.85,7.85,0.74,1.86 ID='3BDPT', QUANTITY='THERMOCOUPLE', POINTS=5, TIME_HISTORY=.TRUE. /
&DEVC XB=8.05,8.05,7.85,7.85,0.74,1.86 ID='3BDPV', QUANTITY='V-VELOCITY', POINTS=5, TIME_HISTORY=.TRUE. /
&DEVC XB=9.15,9.15,7.5,7.5,0.3,2.1 ID='3PT', QUANTITY='PRESSURE', POINTS=3, TIME_HISTORY=.TRUE. /
&DEVC XB=7.8,7.8,5.3,5.3,2.39,0.255 ID='3TC', QUANTITY='THERMOCOUPLE', POINTS=8, TIME_HISTORY=.TRUE. /
&DEVC XB=9.75,9.75,4.35,4.35,0.4,2.0 ID='4BDPT', QUANTITY='THERMOCOUPLE', POINTS=5, TIME_HISTORY=.TRUE. /
&DEVC XB=9.75,9.75,4.35,4.35,0.4,2.0 ID='4BDPV', QUANTITY='U-VELOCITY', POINTS=5, TIME_HISTORY=.TRUE. /
&DEVC XB=9.15,9.15,0.4,0.4,0.3,2.1 ID='4PT', QUANTITY='PRESSURE', POINTS=3, TIME_HISTORY=.TRUE. /
&DEVC XB=9.5,9.5,4.3,4.3,2.39,0.255 ID='4TC', QUANTITY='THERMOCOUPLE', POINTS=8, TIME_HISTORY=.TRUE. /
&DEVC XB=7.15,7.15,0.05,0.05,0.74,1.86 ID='5BDPT', QUANTITY='THERMOCOUPLE', POINTS=5, TIME_HISTORY=.TRUE. /
&DEVC XB=7.15,7.15,0.05,0.05,0.74,1.86 ID='5BDPV', QUANTITY='V-VELOCITY', POINTS=5, TIME_HISTORY=.TRUE., CONVERSION_FACTOR=-1.0 /
&DEVC XB=0.25,0.25,4.85,4.85,0.3,2.1 ID='5PT', QUANTITY='PRESSURE', POINTS=3, TIME_HISTORY=.TRUE. /
&DEVC XB=6.5,6.5,2.0,2.0,2.39,0.255 ID='5TC', QUANTITY='THERMOCOUPLE', POINTS=8, TIME_HISTORY=.TRUE. /
&DEVC XB=4.25,4.25,0.05,0.05,0.20,1.80 ID='6BDPT', QUANTITY='THERMOCOUPLE', POINTS=5, TIME_HISTORY=.TRUE. /
&DEVC XB=4.25,4.25,0.05,0.05,0.20,1.80 ID='6BDPV', QUANTITY='V-VELOCITY', POINTS=5, TIME_HISTORY=.TRUE., CONVERSION_FACTOR=-1.0 /
&DEVC XB=0.4,0.4,3.85,3.85,0.3,2.1 ID='6PT', QUANTITY='PRESSURE', POINTS=3, TIME_HISTORY=.TRUE. /
&DEVC XB=1.4,1.4,2.0,2.0,2.39,0.255 ID='6TC', QUANTITY='THERMOCOUPLE', POINTS=8, TIME_HISTORY=.TRUE. /
&DEVC XB=4.95,4.95,7.85,7.85,1.10,1.90 ID='7BDPT', QUANTITY='THERMOCOUPLE', POINTS=5, TIME_HISTORY=.TRUE. /
&DEVC XB=4.95,4.95,7.85,7.85,1.10,1.90 ID='7BDPV', QUANTITY='V-VELOCITY', POINTS=5, TIME_HISTORY=.TRUE. /
&DEVC XB=4.4,4.4,6.0,6.0,2.39,0.255 ID='7TC', QUANTITY='THERMOCOUPLE', POINTS=8, TIME_HISTORY=.TRUE. /
&DEVC XB=2.2,2.2,6.0,6.0,2.39,0.255 ID='8TC', QUANTITY='THERMOCOUPLE', POINTS=8, TIME_HISTORY=.TRUE. /

&SLCF PBZ=2.2, QUANTITY='TEMPERATURE', CELL_CENTERED=.TRUE. /
&SLCF PBZ=2.2, QUANTITY='PRESSURE_ZONE', CELL_CENTERED=.TRUE. /
&SLCF PBZ=2.2, QUANTITY='PRESSURE', CELL_CENTERED=.TRUE. /

&TAIL /

The input file for the simulation of Two-Story Experiment 4 is provided below.

&HEAD CHID='Two_Story_Gas_4' /

&TIME T_END=1800.0 /

&MISC SIMULATION_MODE='SVLES', SHARED_FILE_SYSTEM=.FALSE. /

&MESH IJK=27,31,30, XB=-0.5,2.2,-1.0,2.1,0.1,3.1, MULT_ID='mesh' /
&MULT ID='mesh', DX=2.7, DY=3.1, DZ=3.0, I_UPPER=5, J_UPPER=3, K_UPPER=1 /

&DEVC ID='FRONT DOOR TIMER', QUANTITY='TIME', XYZ=0.5,1.0,0.5, SETPOINT= 600.0, INITIAL_STATE=.TRUE. /
&DEVC ID='BR3 WINDOW TIMER', QUANTITY='TIME', XYZ=0.5,1.0,0.5, SETPOINT= 900.0, INITIAL_STATE=.TRUE. /
&DEVC ID='BR4 WINDOW TIMER', QUANTITY='TIME', XYZ=0.5,1.0,0.5, SETPOINT=1200.0, INITIAL_STATE=.TRUE. /

&REAC FUEL='METHANE', SOOT_YIELD=0.001 /

&SURF ID='BURNER', HRRPUA=1388., COLOR='ORANGE', RAMP_Q='burner' /

```

```

&RAMP ID='burner', T= 0., F=0. /
&RAMP ID='burner', T= 5., F=1. /
&RAMP ID='burner', T= 1500., F=1. /
&RAMP ID='burner', T= 1505., F=0. /

&OBST XB=11.4,12.0,8.4,9.0,0.4,0.6, SURF_IDS='BURNER','WALL','WALL' /

&MATL ID='GYPSUM BOARD'
FYI='Sheetrock UltraLight Panels',
SPECIFIC_HEAT=1.0
CONDUCTIVITY=0.16
DENSITY=480.0 /

&SURF ID='WALL',
COLOR='GRAY 80'
DEFAULT=.TRUE.
MATL_ID='GYPSUM BOARD'
BACKING='VOID'
THICKNESS=0.013 /

&SURF ID = 'WINDOW'
COLOR = 'LIGHT BLUE'
MATL_ID = 'GYPSUM BOARD'
THICKNESS = 0.05/

&SURF ID = 'DOOR'
COLOR = 'BLUE'
MATL_ID = 'GYPSUM BOARD'
THICKNESS = 0.05/

&SURF ID = 'CARPET'
COLOR = 'BROWN'
MATL_ID = 'GYPSUM BOARD'
THICKNESS = 0.004/

&VENT XB=3.3,8.7,1.5,3.4,0.1,0.1, ID='FLOOR LEAK', SURF_ID='WALL', COLOR='FOREST GREEN' /
&HVAC ID = 'FLOOR LEAK', TYPE_ID='LEAK', VENT_ID='FLOOR LEAK', VENT2_ID='AMBIENT', AREA=0.18 /
&VENT SURF_ID='OPEN', MB='ZMAX' /
&VENT SURF_ID='OPEN', MB='XMIN' /
&VENT SURF_ID='OPEN', MB='XMAX' /
&VENT SURF_ID='OPEN', MB='YMIN' /
&VENT SURF_ID='OPEN', MB='YMAX' /

&OBST XB=7.4,8.3, 0.0,0.1, 0.1,2.2, TRANSPARENCY=0.4, SURF_ID='DOOR', DEVC_ID='FRONT DOOR TIMER' / 01-Front Door-S
&OBST XB=13.2,14.1, 10.3,10.4, 0.7,2.2, TRANSPARENCY=0.4, SURF_ID='WINDOW' / 01-Den Window
&OBST XB=9.6,11.4, 10.3,10.4, 0.7,2.2, TRANSPARENCY=0.4, SURF_ID='WINDOW' / 01-Family Room Window-E
&OBST XB=6.9,8.7, 10.3,10.4, 0.7,2.2, TRANSPARENCY=0.4, SURF_ID='WINDOW' / 01-Family Room Window-W
&OBST XB=4.3,6.1, 10.3,10.4, 0.1,2.2, TRANSPARENCY=0.4, SURF_ID='DOOR' / 01-Kitchen Door
&OBST XB=0.3,1.2, 10.3,10.4, 1.3,2.1, TRANSPARENCY=0.4, SURF_ID='WINDOW' / 01-Kitchen Window-N
&OBST XB=1.1,2.0, 0.0,0.1, 0.7,2.2, TRANSPARENCY=0.4, SURF_ID='WINDOW' / 01-Laundry Window-S
&OBST XB=3.7,5.6, 0.0,0.1, 0.7,2.2, TRANSPARENCY=0.4, SURF_ID='WINDOW' / 01-DR Window-S
&OBST XB=15.2,15.3, 1.8,3.6, 0.7,2.2, TRANSPARENCY=0.4, SURF_ID='WINDOW' / 01-LR Window-E
&OBST XB=0.0,0.1, 9.1,10.1, 1.3,2.2, TRANSPARENCY=0.4, SURF_ID='WINDOW' / 01-Kitchen Window-W
&OBST XB=12.1,14.0, 0.0,0.1, 0.7,2.2, TRANSPARENCY=0.4, SURF_ID='WINDOW' / 01-LR Window-S
&OBST XB=13.2,14.1, 10.3,10.4, 3.8,5.4, TRANSPARENCY=0.4, SURF_ID='WINDOW' / 02-B2 Window-N
&OBST XB=3.3,5.1, 10.3,10.4, 3.8,5.4, TRANSPARENCY=0.4, SURF_ID='WINDOW' / 02-Master BR Window-N
&OBST XB=1.1,2.0, 0.0,0.1, 3.8,5.3, TRANSPARENCY=0.4, SURF_ID='WINDOW' / 02-Master Bath Window-S
&OBST XB=12.2,14.0, 0.0,0.1, 3.8,5.3, TRANSPARENCY=0.4, SURF_ID='WINDOW', DEVC_ID='BR3 WINDOW TIMER' / 02-B3 Window-S
&OBST XB=3.7,5.6, 0.0,0.1, 3.8,5.3, TRANSPARENCY=0.4, SURF_ID='WINDOW', DEVC_ID='BR4 WINDOW TIMER' / 02-B4 Window-S

&OBST XB=10.1,11.2, 3.5,3.5, 0.1,2.1 / 01-Stairs Door
&OBST XB=1.0,1.1, 3.7,4.4, 0.1,2.1 / 01-Kitchen Pantry Door

&OBST XB=9.0,10.1, 3.2,3.4, 0.1,0.3, / 01-Lower Stairs
&OBST XB=9.0,10.1, 3.1,3.2, 0.1,0.5, / 01-Lower Stairs
&OBST XB=9.0,10.1, 3.0,3.1, 0.1,0.5, / 01-Lower Stairs
&OBST XB=9.0,10.1, 2.9,3.0, 0.1,0.5, / 01-Lower Stairs
&OBST XB=9.0,10.1, 2.8,2.9, 0.1,0.7, / 01-Lower Stairs
&OBST XB=9.0,10.1, 2.7,2.8, 0.1,0.7, / 01-Lower Stairs
&OBST XB=9.0,10.1, 2.6,2.7, 0.1,0.8, / 01-Lower Stairs
&OBST XB=9.0,10.1, 2.9,3.0, 0.1,0.7, / 01-Lower Stairs
&OBST XB=9.0,10.1, 2.4,2.6, 0.1,0.8, / 01-Lower Stairs
&OBST XB=9.0,10.1, 2.3,2.4, 0.1,1.0, / 01-Lower Stairs
&OBST XB=9.0,10.1, 2.2,2.3, 0.1,1.0, / 01-Lower Stairs
&OBST XB=9.0,10.1, 2.1,2.2, 0.1,1.2, / 01-Lower Stairs
&OBST XB=9.0,10.1, 2.0,2.1, 0.1,1.2, / 01-Lower Stairs
&OBST XB=9.0,10.1, 1.9,2.0, 0.1,1.2, / 01-Lower Stairs
&OBST XB=9.0,10.1, 1.7,1.9, 0.1,1.4, / 01-Lower Stairs
&OBST XB=9.0,10.1, 1.6,1.7, 0.1,1.4, / 01-Lower Stairs
&OBST XB=9.0,10.1, 3.4,3.5, 0.1,0.3, / 01-Lower Stairs
&OBST XB=9.0,10.1, 2.4,2.5, 0.1,1.0, / 01-Lower Stairs

&OBST XB=10.1,11.2, 1.7,1.9, 0.1,1.8, / 02-Upper Stairs
&OBST XB=10.1,11.2, 1.9,2.0, 0.1,2.0, / 02-Upper Stairs
&OBST XB=10.1,11.2, 2.0,2.2, 0.1,2.0, / 02-Upper Stairs
&OBST XB=10.1,11.2, 2.2,2.3, 0.1,2.1, / 02-Upper Stairs
&OBST XB=10.1,11.2, 2.3,2.4, 0.1,2.1, / 02-Upper Stairs
&OBST XB=10.1,11.2, 2.4,2.5, 0.1,2.1, / 02-Upper Stairs
&OBST XB=10.1,11.2, 2.5,2.6, 0.1,2.3, / 02-Upper Stairs
&OBST XB=10.1,11.2, 2.6,2.7, 0.1,2.3, / 02-Upper Stairs
&OBST XB=10.1,11.2, 2.7,2.9, 0.1,2.5, / 02-Upper Stairs
&OBST XB=10.1,11.2, 2.9,3.0, 0.1,2.5, / 02-Upper Stairs

```

&OBST XB=10.1,11.2, 3.0,3.1, 0.1,2.7, / 02-Upper Stairs
 &OBST XB=10.1,11.2, 3.1,3.2, 0.1,2.7, / 02-Upper Stairs
 &OBST XB=10.1,11.2, 3.2,3.5, 0.1,2.8, / 02-Upper Stairs
 &OBST XB=10.1,11.2, 1.6,1.7, 0.1,1.8, / 02-Upper Stairs
 &OBST XB=10.1,11.2, 2.4,2.5, 0.1,2.3, / 02-Upper Stairs
 &OBST XB=10.1,11.2, 2.9,3.0, 0.1,2.7, / 02-Upper Stairs
 &OBST XB=10.1,11.2, 3.2,3.5, 0.1,2.9, / 02-Upper Stairs
 &OBST XB=9.0,11.2, 0.1,1.7, 0.1,1.6, / Stairs Sub Landing

 &OBST XB=10.1,10.1, 3.4,3.5, 0.1,2.6 / 01-Int-Wall-Between Stairs
 &OBST XB=10.1,10.1, 1.6,3.4, 0.1,2.9 / 01-Int-Wall-Between Stairs
 &OBST XB=6.2,6.3, 0.1,1.3, 0.1,2.6 / 01-Int-Wall Downstairs
 &OBST XB=6.2,7.0, 1.3,1.4, 0.1,2.6 / 01-Int-Wall Downstairs
 &OBST XB=6.9,7.0, 0.1,0.5, 0.1,2.6 / 01-Int-Wall Downstairs
 &OBST XB=6.9,7.0, 1.0,1.3, 0.1,2.6 / 01-Int-Wall Downstairs
 &OBST XB=8.9,9.0, 3.4,3.6, 0.1,2.6 / 01-Int-Wall Downstairs
 &OBST XB=8.9,9.0, 0.1,3.4, 0.1,2.8 / 01-Int-Wall Downstairs
 &OBST XB=11.2,11.3, 0.1,3.5, 0.1,2.6 / 01-Int-Wall Downstairs
 &OBST XB=13.8,15.2, 5.3,5.3, 0.1,2.6 / 01-Int-Wall Downstairs
 &OBST XB=1.0,1.1, 2.6,3.7, 0.1,2.6 / 01-Int-Wall Downstairs
 &OBST XB=1.0,1.1, 4.4,5.3, 0.1,2.6 / 01-Int-Wall Downstairs
 &OBST XB=1.0,1.1, 3.7,4.4, 2.1,2.6 / 01-Int-Wall Downstairs
 &OBST XB=2.3,2.4, 2.6,3.1, 0.1,2.6 / 01-Int-Wall Downstairs
 &OBST XB=2.3,2.4, 4.2,5.4, 0.1,2.6 / 01-Int-Wall Downstairs
 &OBST XB=3.0,3.1, 0.1,4.5, 0.1,2.6 / 01-Int-Wall Downstairs
 &OBST XB=5.0,5.1, 4.6,5.4, 0.1,2.6 / 01-Int-Wall Downstairs
 &OBST XB=0.1,1.3, 2.5,2.6, 0.1,2.6 / 01-Int-Wall Downstairs
 &OBST XB=0.1,1.0, 5.3,5.3, 0.1,2.6 / 01-Int-Wall Downstairs
 &OBST XB=1.3,2.1, 2.5,2.6, 2.1,2.6 / 01-Int-Wall Downstairs
 &OBST XB=2.0,3.0, 0.1,0.1, 0.1,2.6 / 01-Int-Wall Downstairs
 &OBST XB=2.1,3.0, 2.5,2.6, 0.1,2.6 / 01-Int-Wall Downstairs
 &OBST XB=2.4,5.1, 4.5,4.6, 0.1,2.6 / 01-Int-Wall Downstairs
 &OBST XB=6.2,6.2, 0.1,1.4, 0.1,2.6 / 01-Int-Wall Downstairs
 &OBST XB=12.0,12.1, 7.1,10.3, 0.1,2.6 / 01-Int-Wall Downstairs
 &OBST XB=12.0,12.2, 6.9,7.0, 0.1,2.6 / 01-Int-Wall Downstairs
 &OBST XB=12.1,12.3, 6.8,6.9, 0.1,2.6 / 01-Int-Wall Downstairs
 &OBST XB=12.2,12.4, 6.7,6.8, 2.1,2.6 / 01-Int-Wall Downstairs
 &OBST XB=12.3,12.5, 6.6,6.7, 2.1,2.6 / 01-Int-Wall Downstairs
 &OBST XB=12.4,12.6, 6.5,6.6, 2.1,2.6 / 01-Int-Wall Downstairs
 &OBST XB=12.5,12.7, 6.4,6.5, 2.1,2.6 / 01-Int-Wall Downstairs
 &OBST XB=12.6,12.8, 6.3,6.4, 2.1,2.6 / 01-Int-Wall Downstairs
 &OBST XB=12.7,12.9, 6.2,6.3, 2.1,2.6 / 01-Int-Wall Downstairs
 &OBST XB=12.8,12.9, 6.1,6.2, 2.1,2.6 / 01-Int-Wall Downstairs
 &OBST XB=12.9,13.0, 6.1,6.2, 0.1,2.6 / 01-Int-Wall Downstairs
 &OBST XB=12.9,13.1, 6.0,6.1, 0.1,2.6 / 01-Int-Wall Downstairs
 &OBST XB=13.0,13.2, 5.9,6.0, 0.1,2.6 / 01-Int-Wall Downstairs
 &OBST XB=13.1,13.3, 5.8,5.9, 0.1,2.6 / 01-Int-Wall Downstairs
 &OBST XB=13.2,13.4, 5.7,5.8, 0.1,2.6 / 01-Int-Wall Downstairs
 &OBST XB=13.3,13.5, 5.6,5.7, 0.1,2.6 / 01-Int-Wall Downstairs
 &OBST XB=13.4,13.5, 5.8,5.9, 0.1,2.6 / 01-Int-Wall Downstairs
 &OBST XB=13.4,13.6, 5.5,5.6, 0.1,2.6 / 01-Int-Wall Downstairs
 &OBST XB=13.5,13.6, 5.9,6.0, 0.1,2.6 / 01-Int-Wall Downstairs
 &OBST XB=13.5,13.7, 5.4,5.5, 0.1,2.6 / 01-Int-Wall Downstairs
 &OBST XB=13.6,13.7, 5.3,5.4, 0.1,2.6 / 01-Int-Wall Downstairs
 &OBST XB=13.6,14.0, 6.0,6.1, 0.1,2.6 / 01-Int-Wall Downstairs
 &OBST XB=13.8,15.2, 5.3,5.4, 0.1,2.6 / 01-Int-Wall Downstairs
 &OBST XB=14.8,15.2, 6.0,6.1, 0.1,2.6 / 01-Int-Wall Downstairs
 &OBST XB=8.9,9.0, 0.1,3.4, 2.8,2.9 / 01-Int-Wall Downstairs
 &OBST XB=0.1,1.1, 5.3,5.4, 0.1,2.6 / 01-Int-Wall Downstairs
 &OBST XB=6.1,6.7, 7.8,10.3, 1.0,1.1, RGB=245,206,158, SURF_ID='WALL'/ K-Counter Top
 &OBST XB=6.2,6.7, 7.8,10.3, 0.1,1.0, RGB=245,206,158, SURF_ID='WALL'/ K-Counter
 &OBST XB=15.2,15.3, 1.8,3.6, 0.1,0.7 / 01-E-Ext-Wall
 &OBST XB=15.2,15.3, 0.0,1.8, 0.1,2.6 / 01-E-Ext-Wall
 &OBST XB=15.2,15.3, 3.6,5.3, 0.1,2.6 / 01-E-Ext-Wall
 &OBST XB=15.2,15.3, 1.8,3.6, 2.2,2.6 / 01-E-Ext-Wall
 &OBST XB=15.2,15.3, 5.3,10.4, 0.1,2.6 / 01-E-Ext-Wall
 &OBST XB=6.1,6.9, 10.3,10.4, 0.1,2.6 / 01-N-Ext-Wall
 &OBST XB=6.9,8.7, 10.3,10.4, 2.2,2.6 / 01-N-Ext-Wall
 &OBST XB=6.9,8.7, 10.3,10.4, 0.1,0.7 / 01-N-Ext-Wall
 &OBST XB=8.7,9.6, 10.3,10.4, 0.1,2.6 / 01-N-Ext-Wall
 &OBST XB=9.6,11.4, 10.3,10.4, 0.1,0.7 / 01-N-Ext-Wall
 &OBST XB=9.6,11.4, 10.3,10.4, 2.2,2.6 / 01-N-Ext-Wall
 &OBST XB=11.4,13.2, 10.3,10.4, 0.1,2.6 / 01-N-Ext-Wall
 &OBST XB=13.2,14.1, 10.3,10.4, 0.1,0.7 / 01-N-Ext-Wall
 &OBST XB=13.2,14.1, 10.3,10.4, 2.2,2.6 / 01-N-Ext-Wall
 &OBST XB=14.1,15.2, 10.3,10.4, 0.1,2.6 / 01-N-Ext-Wall
 &OBST XB=0.0,0.3, 10.3,10.4, 0.1,2.6 / 01-N-Ext-Wall
 &OBST XB=0.3,1.2, 10.3,10.4, 0.1,1.3 / 01-N-Ext-Wall
 &OBST XB=0.3,1.2, 10.3,10.4, 2.1,2.6 / 01-N-Ext-Wall
 &OBST XB=1.2,4.3, 10.3,10.4, 0.1,2.6 / 01-N-Ext-Wall
 &OBST XB=4.3,6.1, 10.3,10.4, 2.2,2.6 / 01-N-Ext-Wall
 &OBST XB=0.0,0.1, 0.1,5.3, 0.1,2.6 / 01-W-Ext-Wall
 &OBST XB=0.0,0.1, 9.1,10.1, 0.1,1.3 / 01-W-Ext-Wall
 &OBST XB=0.0,0.1, 5.3,9.1, 0.1,2.6 / 01-W-Ext-Wall
 &OBST XB=0.0,0.1, 10.1,10.3, 0.1,2.6 / 01-W-Ext-Wall
 &OBST XB=0.0,0.1, 9.1,10.1, 2.2,2.6 / 01-W-Ext-Wall
 &OBST XB=6.2,7.0, 4.5,5.4, 0.1,2.6 / 01-Int-Wall Center Col. Picture
 &OBST XB=10.1,10.2, 3.5,3.6, 0.1,2.6 / 01-Int-Wall of Stairs Door
 &OBST XB=10.2,11.2, 3.5,3.6, 2.1,2.6 / 01-Int-Wall of Stairs Door
 &OBST XB=11.2,11.2, 3.5,3.6, 0.1,2.1 / 01-Int-Wall of Stairs Door
 &OBST XB=11.2,11.3, 3.5,3.6, 0.1,2.6 / 01-col
 &OBST XB=12.0,12.1, 7.0,7.1, 0.1,2.6 / 01-col

&OBST XB=5.1,5.2,4.8,5.3,2.9,5.7 / 02-Int-Wall Upstairs West Half
&OBST XB=5.1,5.2,4.0,4.8,4.9,5.7 / 02-Int-Wall Upstairs West Half
&OBST XB=5.3,6.1,3.5,3.6,4.9,5.7 / 02-Int-Wall Upstairs West Half
&OBST XB=6.1,6.2,3.5,3.6,2.9,5.7 / 02-Int-Wall Upstairs West Half
&OBST XB=0.1,1.3,5.1,5.1,2.9,5.7 / 02-Int-Wall Upstairs West Half
&OBST XB=1.3,2.0,5.1,5.1,4.9,5.7 / 02-Int-Wall Upstairs West Half
&OBST XB=2.0,2.1,5.1,5.1,2.9,5.7 / 02-Int-Wall Upstairs West Half
&OBST XB=5.2,6.2,5.3,5.3,2.9,5.7 / 02-Int-Wall Upstairs West Half
&OBST XB=6.2,6.2,0.1,0.5,2.9,5.7 / 02-Int-Wall Upstairs West Half
&OBST XB=6.2,6.2,2.3,3.5,2.9,5.7 / 02-Int-Wall Upstairs West Half
&OBST XB=6.2,6.2,0.5,2.3,5.1,5.7 / 02-Int-Wall Upstairs West Half
&OBST XB=0.1,2.2,6.1,6.2,2.9,5.7 / 02-Int-Wall Upstairs West Half
&OBST XB=2.1,2.2,5.3,6.1,2.9,5.7 / 02-Int-Wall Upstairs West Half
&OBST XB=2.1,2.2,6.2,6.3,2.9,5.7 / 02-Int-Wall Upstairs West Half
&OBST XB=2.1,2.2,7.1,10.3,2.9,5.7 / 02-Int-Wall Upstairs West Half
&OBST XB=2.1,2.2,6.3,7.1,4.9,5.7 / 02-Int-Wall Upstairs West Half
&OBST XB=5.1,6.2,5.3,5.4,2.9,5.7 / 02-Int-Wall Upstairs West Half
&OBST XB=6.2,6.2,5.4,10.3,2.9,5.7 / 02-Int-Wall Upstairs West Half
&OBST XB=15.2,15.3,0.0,5.3,2.6,2.8 / 02-E-Ext-Wall
&OBST XB=15.2,15.3,5.3,10.4,2.8,5.7 / 02-E-Ext-Wall
&OBST XB=15.2,15.3,5.3,10.4,2.6,2.8 / 02-E-Ext-Wall
&OBST XB=15.2,15.3,0.0,5.3,2.8,5.7 / 02-E-Ext-Wall
&OBST XB=11.5,11.6,6.4,6.5,2.9,5.7 / 02-Int-Wall-B2 S-Bath 2-B3
&OBST XB=11.6,11.7,6.3,6.4,4.9,5.7 / 02-Int-Wall-B2 S-Bath 2-B3
&OBST XB=11.7,11.8,6.2,6.3,4.9,5.7 / 02-Int-Wall-B2 S-Bath 2-B3
&OBST XB=11.8,11.9,6.1,6.2,4.9,5.7 / 02-Int-Wall-B2 S-Bath 2-B3
&OBST XB=11.9,12.0,6.0,6.1,4.9,5.7 / 02-Int-Wall-B2 S-Bath 2-B3
&OBST XB=12.0,12.1,5.9,6.0,4.9,5.7 / 02-Int-Wall-B2 S-Bath 2-B3
&OBST XB=12.1,12.2,5.8,5.9,4.9,5.7 / 02-Int-Wall-B2 S-Bath 2-B3
&OBST XB=12.2,12.5,5.7,5.8,2.9,5.7 / 02-Int-Wall-B2 S-Bath 2-B3
&OBST XB=12.3,12.4,5.3,5.5,2.9,5.7 / 02-Int-Wall-B2 S-Bath 2-B3
&OBST XB=12.3,12.4,5.6,5.7,2.9,5.7 / 02-Int-Wall-B2 S-Bath 2-B3
&OBST XB=12.3,15.2,5.5,5.6,2.9,5.7 / 02-Int-Wall-B2 S-Bath 2-B3
&OBST XB=12.4,12.6,5.8,5.9,2.9,5.7 / 02-Int-Wall-B2 S-Bath 2-B3
&OBST XB=12.5,12.7,5.9,6.0,2.9,5.7 / 02-Int-Wall-B2 S-Bath 2-B3
&OBST XB=12.6,12.8,6.0,6.1,2.9,5.7 / 02-Int-Wall-B2 S-Bath 2-B3
&OBST XB=12.7,13.0,6.1,6.2,2.9,5.7 / 02-Int-Wall-B2 S-Bath 2-B3
&OBST XB=12.9,13.0,5.6,6.1,2.9,5.7 / 02-Int-Wall-B2 S-Bath 2-B3
&OBST XB=11.5,11.5,6.5,6.6,2.9,5.7 / 02-Int-Wall-B2 S-Bath 2-B3
&OBST XB=11.2,11.3,0.1,3.5,2.9,5.7 / 02-Int-Wall-B2 S-Bath 2-B3
&OBST XB=11.2,11.4,3.5,3.6,2.9,5.7 / 02-Int-Wall-B2 S-Bath 2-B3
&OBST XB=11.4,12.2,3.5,3.6,4.9,5.7 / 02-Int-Wall-B2 S-Bath 2-B3
&OBST XB=12.2,12.4,3.5,3.6,2.9,5.7 / 02-Int-Wall-B2 S-Bath 2-B3
&OBST XB=12.3,12.4,3.3,3.5,2.9,5.7 / 02-Int-Wall-B2 S-Bath 2-B3
&OBST XB=12.3,12.4,3.6,4.1,2.9,5.7 / 02-Int-Wall-B2 S-Bath 2-B3
&OBST XB=12.3,12.4,4.8,5.3,2.9,5.7 / 02-Int-Wall-B2 S-Bath 2-B3
&OBST XB=12.3,12.4,4.1,4.8,4.9,5.7 / 02-Int-Wall-B2 S-Bath 2-B3
&OBST XB=12.3,15.2,3.2,3.3,2.9,5.7 / 02-Int-Wall-B2 S-Bath 2-B3
&OBST XB=13.2,13.3,3.3,3.9,2.9,5.7 / 02-Int-Wall-B2 S-Bath 2-B3
&OBST XB=13.2,15.2,3.9,4.0,2.9,5.7 / 02-Int-Wall-B2 S-Bath 2-B3
&OBST XB=10.1,10.1,1.8,2.0,2.9,3.0 / 02-Int-Wall-Between Stairs
&OBST XB=10.1,10.1,2.0,2.2,2.9,3.1 / 02-Int-Wall-Between Stairs
&OBST XB=10.1,10.1,2.2,2.4,2.9,3.2 / 02-Int-Wall-Between Stairs
&OBST XB=10.1,10.1,2.4,2.6,2.9,3.3 / 02-Int-Wall-Between Stairs
&OBST XB=10.1,10.1,2.6,2.8,2.9,3.4 / 02-Int-Wall-Between Stairs
&OBST XB=10.1,10.1,2.8,3.0,2.9,3.5 / 02-Int-Wall-Between Stairs
&OBST XB=10.1,10.1,3.0,3.2,2.9,3.6 / 02-Int-Wall-Between Stairs
&OBST XB=10.1,10.1,3.2,3.4,2.9,3.7 / 02-Int-Wall-Between Stairs
&OBST XB=6.2,7.0,0.1,3.4,2.6,2.8, SURF_ID='CARPET' / 02-Floor
&OBST XB=6.2,10.1,3.4,3.5,2.6,2.8, SURF_ID='CARPET' / 02-Floor
&OBST XB=6.2,15.2,3.5,5.3,2.6,2.8, SURF_ID='CARPET' / 02-Floor
&OBST XB=11.2,15.2,0.1,3.5,2.6,2.8, SURF_ID='CARPET' / 02-Floor
&OBST XB=0.1,6.2,0.1,5.3,2.6,2.8, SURF_ID='CARPET' / 02-Floor
&OBST XB=6.2,6.3,5.4,10.3,2.8,2.9, SURF_ID='CARPET' / 02-Floor
&OBST XB=6.2,15.2,5.3,5.4,2.8,2.9, SURF_ID='CARPET' / 02-Floor
&OBST XB=10.3,15.2,5.4,5.5,2.8,2.9, SURF_ID='CARPET' / 02-Floor
&OBST XB=10.4,15.2,5.5,5.6,2.8,2.9, SURF_ID='CARPET' / 02-Floor
&OBST XB=10.5,15.2,5.6,5.7,2.8,2.9, SURF_ID='CARPET' / 02-Floor
&OBST XB=10.6,15.2,5.7,5.8,2.8,2.9, SURF_ID='CARPET' / 02-Floor
&OBST XB=10.7,15.2,5.8,5.9,2.8,2.9, SURF_ID='CARPET' / 02-Floor
&OBST XB=10.8,15.2,5.9,6.0,2.8,2.9, SURF_ID='CARPET' / 02-Floor
&OBST XB=10.9,15.2,6.0,6.1,2.8,2.9, SURF_ID='CARPET' / 02-Floor
&OBST XB=11.0,15.2,6.1,6.2,2.8,2.9, SURF_ID='CARPET' / 02-Floor
&OBST XB=11.1,15.2,6.2,6.3,2.8,2.9, SURF_ID='CARPET' / 02-Floor
&OBST XB=11.2,15.2,6.3,6.4,2.8,2.9, SURF_ID='CARPET' / 02-Floor
&OBST XB=11.3,15.2,6.4,6.5,2.8,2.9, SURF_ID='CARPET' / 02-Floor
&OBST XB=11.4,15.2,6.5,6.6,2.8,2.9, SURF_ID='CARPET' / 02-Floor
&OBST XB=11.5,15.2,6.6,6.7,2.8,2.9, SURF_ID='CARPET' / 02-Floor
&OBST XB=11.6,15.2,6.7,6.8,2.8,2.9, SURF_ID='CARPET' / 02-Floor
&OBST XB=11.7,15.2,6.8,6.9,2.8,2.9, SURF_ID='CARPET' / 02-Floor
&OBST XB=11.8,15.2,6.9,7.0,2.8,2.9, SURF_ID='CARPET' / 02-Floor
&OBST XB=11.9,15.2,7.0,7.1,2.8,2.9, SURF_ID='CARPET' / 02-Floor
&OBST XB=12.0,15.2,7.1,10.3,2.8,2.9, SURF_ID='CARPET' / 02-Floor
&OBST XB=6.2,6.3,5.4,10.3,2.6,2.8, SURF_ID='CARPET' / 02-Floor
&OBST XB=6.2,15.2,5.3,5.4,2.6,2.8, SURF_ID='CARPET' / 02-Floor
&OBST XB=10.3,15.2,5.4,5.5,2.6,2.8, SURF_ID='CARPET' / 02-Floor
&OBST XB=10.4,15.2,5.5,5.6,2.6,2.8, SURF_ID='CARPET' / 02-Floor
&OBST XB=10.5,15.2,5.6,5.7,2.6,2.8, SURF_ID='CARPET' / 02-Floor
&OBST XB=10.6,15.2,5.7,5.8,2.6,2.8, SURF_ID='CARPET' / 02-Floor
&OBST XB=10.7,15.2,5.8,5.9,2.6,2.8, SURF_ID='CARPET' / 02-Floor
&OBST XB=10.8,15.2,5.9,6.0,2.6,2.8, SURF_ID='CARPET' / 02-Floor
&OBST XB=10.9,15.2,6.0,6.1,2.6,2.8, SURF_ID='CARPET' / 02-Floor

```

&OBST XB=11.0,15.2, 6.1,6.2, 2.6,2.8, SURF_ID='CARPET' / 02-Floor
&OBST XB=11.1,15.2, 6.2,6.3, 2.6,2.8, SURF_ID='CARPET' / 02-Floor
&OBST XB=11.2,15.2, 6.3,6.4, 2.6,2.8, SURF_ID='CARPET' / 02-Floor
&OBST XB=11.3,15.2, 6.4,6.5, 2.6,2.8, SURF_ID='CARPET' / 02-Floor
&OBST XB=11.4,15.2, 6.5,6.6, 2.6,2.8, SURF_ID='CARPET' / 02-Floor
&OBST XB=11.5,15.2, 6.6,6.7, 2.6,2.8, SURF_ID='CARPET' / 02-Floor
&OBST XB=11.6,15.2, 6.7,6.8, 2.6,2.8, SURF_ID='CARPET' / 02-Floor
&OBST XB=11.7,15.2, 6.8,6.9, 2.6,2.8, SURF_ID='CARPET' / 02-Floor
&OBST XB=11.8,15.2, 6.9,7.0, 2.6,2.8, SURF_ID='CARPET' / 02-Floor
&OBST XB=11.9,15.2, 7.0,7.1, 2.6,2.8, SURF_ID='CARPET' / 02-Floor
&OBST XB=12.0,15.2, 7.1,10.3, 2.6,2.8, SURF_ID='CARPET' / 02-Floor
&OBST XB=6.2,7.0, 0.1,3.4, 2.8,2.9, SURF_ID='CARPET' / 02-Floor
&OBST XB=6.2,10.1, 3.4,3.5, 2.8,2.9, SURF_ID='CARPET' / 02-Floor
&OBST XB=6.2,15.2, 3.5,5.3, 2.8,2.9, SURF_ID='CARPET' / 02-Floor
&OBST XB=11.2,15.2, 0.1,3.5, 2.8,2.9, SURF_ID='CARPET' / 02-Floor
&OBST XB=0.1,6.2, 0.1,5.3, 2.8,2.9, SURF_ID='CARPET' / 02-Floor
&OBST XB=0.1,6.2, 5.3,10.3, 2.6,2.8, SURF_ID='CARPET' / 02-Floor
&OBST XB=0.1,6.2, 5.3,10.3, 2.8,2.9, SURF_ID='CARPET' / 02-Floor
&OBST XB=7.0,10.1, 3.4,3.4, 2.9,3.7 / 02-Railing Above Stairs
&OBST XB=0.0,15.3, 0.0,10.4, 5.7,5.8, COLOR='INVISIBLE' / Roof
&OBST XB=2.3,2.4, 4.3,4.3, 2.9,4.9, COLOR='GRAY 40' / 02- Master Bath Door
&OBST XB=2.4,2.5, 4.2,4.2, 2.9,4.9, COLOR='GRAY 40' / 02- Master Bath Door
&OBST XB=2.5,2.6, 4.1,4.1, 2.9,4.9, COLOR='GRAY 40' / 02- Master Bath Door
&OBST XB=2.6,2.7, 4.0,4.0, 2.9,4.9, COLOR='GRAY 40' / 02- Master Bath Door
&OBST XB=2.7,2.8, 3.9,3.9, 2.9,4.9, COLOR='GRAY 40' / 02- Master Bath Door
&OBST XB=2.8,2.9, 3.7,3.7, 2.9,4.9, COLOR='GRAY 40' / 02- Master Bath Door
&OBST XB=2.3,2.3, 4.3,4.4, 2.9,4.9, COLOR='GRAY 40' / 02- Master Bath Door
&OBST XB=2.4,2.4, 4.2,4.3, 2.9,4.9, COLOR='GRAY 40' / 02- Master Bath Door
&OBST XB=2.5,2.5, 4.1,4.2, 2.9,4.9, COLOR='GRAY 40' / 02- Master Bath Door
&OBST XB=2.6,2.6, 4.0,4.1, 2.9,4.9, COLOR='GRAY 40' / 02- Master Bath Door
&OBST XB=2.7,2.7, 3.9,4.0, 2.9,4.9, COLOR='GRAY 40' / 02- Master Bath Door
&OBST XB=2.8,2.8, 3.7,3.9, 2.9,4.9, COLOR='GRAY 40' / 02- Master Bath Door
&OBST XB=12.3,12.3, 4.1,4.8, 2.9,4.9, COLOR='GRAY 40' / 02-Bath 2 Door
OBST XB=11.6,11.7, 6.4,6.4, 2.9,4.9, COLOR='GRAY 40' / 02-B2 Door
OBST XB=11.7,11.8, 6.3,6.3, 2.9,4.9, COLOR='GRAY 40' / 02-B2 Door
OBST XB=11.8,11.9, 6.2,6.2, 2.9,4.9, COLOR='GRAY 40' / 02-B2 Door
OBST XB=11.9,12.0, 6.1,6.1, 2.9,4.9, COLOR='GRAY 40' / 02-B2 Door
OBST XB=12.0,12.1, 6.0,6.0, 2.9,4.9, COLOR='GRAY 40' / 02-B2 Door
OBST XB=12.1,12.2, 5.9,5.9, 2.9,4.9, COLOR='GRAY 40' / 02-B2 Door
OBST XB=11.7,11.7, 6.3,6.4, 2.9,4.9, COLOR='GRAY 40' / 02-B2 Door
OBST XB=11.8,11.8, 6.2,6.3, 2.9,4.9, COLOR='GRAY 40' / 02-B2 Door
OBST XB=11.9,11.9, 6.1,6.2, 2.9,4.9, COLOR='GRAY 40' / 02-B2 Door
OBST XB=12.0,12.0, 6.0,6.1, 2.9,4.9, COLOR='GRAY 40' / 02-B2 Door
OBST XB=12.1,12.1, 5.9,6.0, 2.9,4.9, COLOR='GRAY 40' / 02-B2 Door
OBST XB=12.2,12.2, 5.8,5.9, 2.9,4.9, COLOR='GRAY 40' / 02-B2 Door
OBST XB=1.3,2.0, 5.1,5.1, 2.9,4.9, COLOR='GRAY 40' / 02-Master Bath Toilet Door
&OBST XB=2.1,2.1, 6.3,7.1, 2.9,4.9, COLOR='GRAY 40' / 02-MB WIC Door

```

```

&OBST XB=0.0,15.3, 0.0,10.4, 0.0,0.1, COLOR='FOREST GREEN' / Floor Slab

```

```

&ZONE XB = 0.1,15.2,0.1,10.3,0.1,5.7 /

```

```

&DUMP DT_HRR=15, DT_DEVC=1, SIG_FIGS=4, SIG_FIGS_EXP=2 /

```

```

&PROP ID='THCP', BEAD_DIAMETER=1.3E-3, BEAD_EMISSIVITY=0.9 /

```

```

&DEVC XB=0.75,0.75,5.55,5.55,0.405,2.195, ID='10PT', QUANTITY='PRESSURE', POINTS=3, TIME_HISTORY=.TRUE. / Kitchen
&DEVC XB=13.15,13.15,1.85,1.85,0.46,2.59, ID='10TC', PROP_ID='THCP', QUANTITY='THERMOCOUPLE', POINTS=8, TIME_HISTORY=.TRUE. / LR
&DEVC XB= 8.65, 8.65,4.15,4.15,0.46,2.59, ID='11TC', PROP_ID='THCP', QUANTITY='THERMOCOUPLE', POINTS=8, TIME_HISTORY=.TRUE. / Under Hall
&DEVC XB= 8.45, 8.45,1.95,1.95,5.69,1.12, ID='12TC', PROP_ID='THCP', QUANTITY='THERMOCOUPLE', POINTS=16, TIME_HISTORY=.TRUE. / FOYER
&DEVC XB= 4.75, 4.75,2.25,2.25,0.46,2.59, ID='13TC', PROP_ID='THCP', QUANTITY='THERMOCOUPLE', POINTS=8, TIME_HISTORY=.TRUE. / DR
&DEVC XB= 1.55, 1.55,1.35,1.35,0.46,2.59, ID='14TC', PROP_ID='THCP', QUANTITY='THERMOCOUPLE', POINTS=8, TIME_HISTORY=.TRUE. / Laundry Room
&DEVC XB= 2.55, 2.55,7.90,7.90,0.46,2.59, ID='15TC', PROP_ID='THCP', QUANTITY='THERMOCOUPLE', POINTS=8, TIME_HISTORY=.TRUE. / Kitchen
&DEVC XB= 7.85, 7.85,0.05,0.05,0.45,1.85, ID='1BDPT', QUANTITY='THERMOCOUPLE', POINTS=5, TIME_HISTORY=.TRUE. / Front Door
&DEVC XB= 7.85, 7.85,0.05,0.05,0.45,1.85, ID='1BDPV', QUANTITY='V-VELOCITY', CONVERSION_FACTOR=-1.0, POINTS=5, TIME_HISTORY=.TRUE. / Front Door
&DEVC XB= 2.35, 2.35,4.85,4.85,3.56,5.39, ID='1PT', QUANTITY='PRESSURE', POINTS=3, TIME_HISTORY=.TRUE. / MBR
&DEVC XB= 3.91, 3.91,5.97,5.97,5.69,3.53, ID='1TC', PROP_ID='THCP', QUANTITY='THERMOCOUPLE', POINTS=8, TIME_HISTORY=.TRUE. / MBR
&DEVC XB=13.65,13.65,10.35,10.35,4.07,5.13 ID='2BDPT', QUANTITY='THERMOCOUPLE', POINTS=5, TIME_HISTORY=.TRUE. / BR2
&DEVC XB=13.65,13.65,10.35,10.35,4.07,5.13 ID='2BDPV', QUANTITY='V-VELOCITY', POINTS=5, TIME_HISTORY=.TRUE. / BR2
&DEVC XB=13.35,13.35,5.75,5.75,3.565,5.395 ID='2PT', QUANTITY='PRESSURE', POINTS=3, TIME_HISTORY=.TRUE. / BR2
&DEVC XB=13.45,13.45,7.25,7.25,5.69,3.53 ID='2TC', PROP_ID='THCP', QUANTITY='THERMOCOUPLE', POINTS=8, TIME_HISTORY=.TRUE. / BR2
&DEVC XB=13.15,13.15,0.05,0.05,4.05,5.05 ID='3BDPT', QUANTITY='THERMOCOUPLE', POINTS=5, TIME_HISTORY=.TRUE. / BR3
&DEVC XB=13.15,13.15,0.05,0.05,4.05,5.05 ID='3BDPV', QUANTITY='V-VELOCITY', CONVERSION_FACTOR=-1.0, POINTS=5, TIME_HISTORY=.TRUE. / BR3
&DEVC XB=12.65,12.65,3.05,3.05,3.565,5.395 ID='3PT', QUANTITY='PRESSURE', POINTS=3, TIME_HISTORY=.TRUE. / BR3
&DEVC XB=12.45,12.45,1.45,1.45,5.69,3.53 ID='3TC', PROP_ID='THCP', QUANTITY='THERMOCOUPLE', POINTS=8, TIME_HISTORY=.TRUE. / BR3
&DEVC XB=4.65,4.65,0.05,0.05,4.05,5.05 ID='4BDPT', QUANTITY='THERMOCOUPLE', POINTS=5, TIME_HISTORY=.TRUE. / BR4
&DEVC XB=4.65,4.65,0.05,0.05,4.05,5.05 ID='4BDPV', QUANTITY='V-VELOCITY', CONVERSION_FACTOR=-1.0, POINTS=5, TIME_HISTORY=.TRUE. / BR4
&DEVC XB=3.25,3.25,3.15,3.15,3.565,5.395 ID='4PT', QUANTITY='PRESSURE', POINTS=3, TIME_HISTORY=.TRUE. / BR4
&DEVC XB=5.55,5.55,1.75,1.75,5.69,3.53 ID='4TC', PROP_ID='THCP', QUANTITY='THERMOCOUPLE', POINTS=8, TIME_HISTORY=.TRUE. / BR4
&DEVC XB=13.05,13.05,0.05,0.05,0.95,1.95 ID='5BDPT', QUANTITY='THERMOCOUPLE', POINTS=5, TIME_HISTORY=.TRUE. / LR
&DEVC XB=13.05,13.05,0.05,0.05,0.95,1.95 ID='5BDPV', QUANTITY='V-VELOCITY', POINTS=5, TIME_HISTORY=.TRUE. / LR
&DEVC XB=8.55,8.55,0.25,0.25,0.405,2.195 ID='5PT', QUANTITY='PRESSURE', POINTS=3, TIME_HISTORY=.TRUE. / FRONT CORRIDOR
&DEVC XB=11.55,11.55,4.35,4.35,5.69,3.53 ID='5TC', PROP_ID='THCP', QUANTITY='THERMOCOUPLE', POINTS=8, TIME_HISTORY=.TRUE. / EH
&DEVC XB=0.75,0.75,10.35,10.35,1.5,1.9 ID='6BDPT', QUANTITY='THERMOCOUPLE', POINTS=3, TIME_HISTORY=.TRUE. / Kitchen
&DEVC XB=0.75,0.75,10.35,10.35,1.5,1.9 ID='6BDPV', QUANTITY='V-VELOCITY', POINTS=3, TIME_HISTORY=.TRUE. / Kitchen
&DEVC XB=11.65,11.65,0.25,0.25,0.405,2.195 ID='6PT', QUANTITY='PRESSURE', POINTS=3, TIME_HISTORY=.TRUE. / LR
&DEVC XB=8.65,8.65,4.15,4.15,5.69,3.53 ID='6TC', PROP_ID='THCP', QUANTITY='THERMOCOUPLE', POINTS=8, TIME_HISTORY=.TRUE. / MH
&DEVC XB=6.75,6.75,9.75,9.75,5.69,1.12 ID='7TC', PROP_ID='THCP', QUANTITY='THERMOCOUPLE', POINTS=16, TIME_HISTORY=.TRUE. / FAMILY ROOM CORNER
&DEVC XB=12.45,12.45,10.15,10.15,0.405,2.195 ID='8PT', QUANTITY='PRESSURE', POINTS=3, TIME_HISTORY=.TRUE. / Den
&DEVC XB=8.95,8.95,8.25,8.25,5.69,1.12 ID='8TC', PROP_ID='THCP', QUANTITY='THERMOCOUPLE', POINTS=16, TIME_HISTORY=.TRUE. / FAMILY ROOM CENTER
&DEVC XB=11.65,11.65,10.15,10.15,1.125,5.395 ID='9PT', QUANTITY='PRESSURE', POINTS=3, TIME_HISTORY=.TRUE. / FR
&DEVC XB=13.65,13.65,7.95,7.95,0.46,2.59 ID='9TC', PROP_ID='THCP', QUANTITY='THERMOCOUPLE', POINTS=8, TIME_HISTORY=.TRUE. / Den

```

```
&SLCF PBZ=2.5, QUANTITY='TEMPERATURE', CELL_CENTERED=.TRUE. /  
&SLCF PBZ=5.6, QUANTITY='TEMPERATURE', CELL_CENTERED=.TRUE. /  
&SLCF PBZ=2.5, QUANTITY='PRESSURE_ZONE', CELL_CENTERED=.TRUE. /  
&SLCF PBZ=5.6, QUANTITY='PRESSURE_ZONE', CELL_CENTERED=.TRUE. /  
&SLCF PBZ=3.0, QUANTITY='PRESSURE_ZONE', CELL_CENTERED=.TRUE. /  
&SLCF PBZ=7.0, QUANTITY='PRESSURE_ZONE', CELL_CENTERED=.TRUE. /  
&SLCF PBZ=2.5, QUANTITY='PRESSURE', CELL_CENTERED=.TRUE. /  
&SLCF PBZ=5.6, QUANTITY='PRESSURE', CELL_CENTERED=.TRUE. /
```

&TAIL